Dissecting the interconnection of Ca^{2+} and pH signaling in plants with a novel biosensor for dual imaging

Doctoral thesis for a doctoral degree

at the Julius-Maximilians-Universität Würzburg

Submitted by

Kunkun Li

from

Anhui, China

Würzburg, 2021

Submitted on: ……..……..

Members of the Promotions committee:

Chairperson:

Primary Supervisor: Prof. Dr. Dirk Becker

Secondary Supervisor: PD. Dr. Frank Waller

Third Supervisor: Dr. Kai Robert Konrad

Date of Public Defence: ……..……

Date of Receipt of Certificates: ……

Table of Contents

Abstract

Calcium ion (Ca^{2+}) and protons (H^+) are both regarded as second messengers, participating in plant growth and stress mechanisms. However, H^+ signals in plant physiology are less well investigated compared to Ca^{2+} signals. If interconnections between these two second messengers exist remains to be uncovered because appropriate imaging tools to monitor Ca^{2+} and H^+ simultaneously in the same cell as well as accurate bioinformatics analysis remain to be developed. To overcome this problem and unravel the role and possible interconnection of Ca^{2+} and H^+ in plants, a new biosensor named CapHensor was developed and optimized to visualize intracellular Ca^{2+} and H^+ changes simultaneously and ratiometrically in the same cell. The CapHensor consisted of an optimized green fluorescent pH sensor (PRpHluorin) and an established red fluorescent Ca^{2+} sensor (R-GECO1) that were combined in one construct via a P2A sequence. A P2A self-cleavage site between the two sensors allowed to express equal amounts but spatially separated sensors, which enabled artifact-free and ratiometric imaging of cellular Ca^{2+} and pH side-by-side. The function of the CapHensor was verified in pollen tubes, since they possess standing Ca^{2+} and pH gradients. We found better imaging quality and the signal-to-noise ratio to be enhanced in live-cell imaging when two R-GECO1 proteins were fused in tandem within the CapHensor construct. To guarantee exclusive subcellular localization and avoid mixed signals from different compartments, Nuclear Export Sequence (NES) and Nuclear Localization Sequence (NLS) were used to target PRpHluorin and R-GECO1 to distinct compartments. After optimization and verification its function, CapHensor was successfully expressed in different cell types to investigate the role of Ca^{2+} and H^+ signals to control polar growth of pollen tube, stomatal movement or leaf defense signaling.

Results obtained in the past indicated both Ca^{2+} gradients and pH gradients in pollen tubes play roles in polar growth. However, the role and temporal relationship between the growth process and changes in Ca^{2+} and pH have not been conclusively resolved. Using CapHensor, I found cytosolic acidification at the tip could promote and alkalization to suppress growth velocity in *N. tabacum* pollen tubes, indicating that cytosolic H^+ concentrations ($[H^+]_{cyt}$) play an important role in regulation pollen tubes growth despite the accompanied changes in cytosolic Ca^{2+} concentrations ($[Ca^{2+}]_{cyt}$). Moreover, growth correlated much better with the tip $[H^+]_{cyt}$ regime than with the course of the tip $[Ca^{2+}]_{cyt}$ regime. However, surprisingly, tip-focused $[Ca^{2+}]_{cyt}$ and

$[H^+]_{cyt}$ oscillations both lagged behind growth oscillations approximately 33 s and 18 s, respectively, asking for a re-evaluation of the role that tip $[Ca^{2+}]_{cyt}$ may play in pollen tube growth. Live-cell CapHensor imaging combined with electrophysiology uncovered that oscillatory membrane depolarization correlated better with tip $[H^+]_{cyt}$ oscillations than with tip $[Ca^{2+}]_{cyt}$ oscillations, indicative for a prominent role of $[H^+]_{cyt}$ to also control electrogenic membrane transport. Using CapHensor, reading out cellular movement at the same time enabled to provide a precise temporal and spatial resolution of ion signaling events, pointing out a prominent role of $[H^+]_{cyt}$ in pollen tube tip growth.

For leaf cells, a special CapHensor construct design had to be developed, containing additional NES localization sequences to avoid overlapping of fluorescense signals from the nucleus and the cytosol. Once this was achieved, the role of Ca^{2+} and pH changes in guard cells, another typical single-cell system was investigated. Cytosolic pH changes have been described in stomatal movement, but the physiological role of pH and the interaction with changing Ca^{2+} signals were still unexplored. Combining CapHensor with the here developed technique to monitor stomatal movement in parallel, the role of Ca^{2+} and H^+ in stomatal movement was studied in detail and novel aspects were identified. The phytohormone ABA and the bacterial elicitor flagellin (flg22) are typical abiotic and biotic stresses, respectively, to trigger stomatal closure. What kind of Ca^{2+} and H^+ signals by ABA and flg22 are set-off in guard cells and what their temporal relationship and role for stomatal movement is were unknown. Similar $[Ca^{2+}]_{cyt}$ increases were observed upon ABA and flg22 triggered stomatal closure, but $[H^+]_{cyt}$ dynamics differed fundamentally. ABA triggered pronounced cytosolic alkalization preceded the $[Ca^{2+}]_{cyt}$ responses significantly by 57 s while stomata started to close ca. 205 s after phytohormone application. With flg22, stomatal closure was accompanied only with a mild cytosolic alkalization but the $[Ca^{2+}]_{cyt}$ response was much more pronounced compared to the ABA effects. Where the cytosolic alkalization originates from was unclear but the vacuole was speculated to contribute in the past. In this thesis, vacuolar pH changes were visualized by the dye BCECF over time, basically displaying exactly the opposite course of the concentration shift in the vacuole than observed in the cytosol. This is indicative for the vacuolar pH dynamics to be coupled strongly to the cytosolic pH changes. In stomatal closure signalling, reactive oxygen species (ROS) were proposed to play a major role, however, only very high concentration of H_2O_2 (> 200 µM), which resulted in the loss of membrane integrity, induced stomatal closure. Unexpectedly, physiological concentrations of ROS led to cytosolic acidification

which was associated with stomatal opening, but not stomatal closure. To study the role of $[H^+]_{cyt}$ to steer stomatal movement in detail, extracellular and intracellular pH variations were evoked in *N. tabacum* guard cells and their behaviour was followed. The results demonstrated cytosolic acidification stimulated stomatal opening while cytosolic alkalization triggered stomatal closure accompanied by $[Ca^{2+}]_{cyt}$ elevations. This demonstrated pH regulation to be an important aspect in stomatal movement and to feed-back on the Ca^{2+}-dynamics. It was remarkable that cytosolic alkalization but not $[Ca^{2+}]_{cyt}$ increase seemed to play a crucial role in stomatal closure, because more pronounced cytosolic alkalization, evoked stronger stomatal closure despite similar $[Ca^{2+}]_{cyt}$ increases. Increases in $[Ca^{2+}]_{cyt}$, which are discussed as an early stomatal closure signal in the past, could not trigger stomatal closure alone in my experiments, even when extremely strong $[Ca^{2+}]_{cyt}$ signals were triggered. Regarding the interaction between the two second messengers, $[Ca^{2+}]_{cyt}$ and $[H^+]_{cyt}$ were negatively correlated most of the times, which was different from pollen tubes showing positive correlation of $[Ca^{2+}]_{cyt}$ and $[H^+]_{cyt}$ regimes. $[Ca^{2+}]_{cyt}$ elevations were always associated with a cytosolic alkalization and this relationship could be blocked by the presence of vanadate, a plasma membrane H^+-pump blocker, indicating plasma membrane H^+-ATPases to contribute to the negative correlation of $[Ca^{2+}]_{cyt}$ and $[H^+]_{cyt}$. To compare with guard cells, cytosolic and nuclear versions of CapHensor were expressed in *N. benthamiana* mesophyll cells, a multicellular system I investigated. Mesophyll cell responses to the same stimuli as tested in guard cells demonstrated that ABA and H_2O_2 did not induce any $[Ca^{2+}]_{cyt}$ and $[H^+]_{cyt}$ changes while flg22 induced an increase in $[Ca^{2+}]_{cyt}$ and $[H^+]_{cyt}$, which is different from the response in guard cells. I could thus unequivocally demonstrate that guard cells and mesophyll cells do respond differently with $[Ca^{2+}]_{cyt}$ and $[H^+]_{cyt}$ changes to the same stimuli, a concept that has been proposed before, but never demonstrated in such detail for plants.

Spontaneous Ca^{2+} oscillations have been observed for a long time in guard cells, but the function or cause is still poorly understood. Two populations of oscillatory guard cells were identified according to their $[Ca^{2+}]_{cyt}$ and $[H^+]_{cyt}$ phase relationship in my study. In approximately half of the oscillatory cells, $[H^+]_{cyt}$ oscillations preceded $[Ca^{2+}]_{cyt}$ oscillations whereas $[Ca^{2+}]_{cyt}$ was the leading signal in the other half of the guard cells population. Strikingly, natural $[H^+]_{cyt}$ oscillations were dampened by ABA but not by flg22. This effect could be well explained by dampening of vacuolar H^+ oscillations in the presence of ABA, but not through flg22. Vacuolar pH contributes to spontaneous $[H^+]_{cyt}$ oscillations and ABA but not flg22 can block the interdependence of natural

$[Ca^{2+}]_{cyt}$ and $[H^+]_{cyt}$ signals. To study the role of $[Ca^{2+}]_{cyt}$ oscillations in stomatal movement, solutions containing high and low KCl concentrations were applied aiming to trigger $[Ca^{2+}]_{cyt}$ oscillations. The triggering of $[Ca^{2+}]_{cyt}$ oscillations by this method was established two decades ago leading to the dogma that $[Ca^{2+}]_{cyt}$ increases are the crucial signal for stomatal closure. However, I found stomatal movement by this method was mainly due to osmotic effects rather than $[Ca^{2+}]_{cyt}$ increases. Fortunately, through this methodology, I found a strong correlation between cytosolic pH and the transport of potassium across the plasma membrane and vacuole existed. The plasma membrane H^+-ATPases and H^+-coupled K^+ transporters were identified as the cause of $[H^+]_{cyt}$ changes, both very important aspects in stomata physiology that were not visualized experimentally before. Na^+ transport is also important for stomatal regulation and leaves generally since salt can be transported from the root to the shoot. Unlike well-described Ca^{2+}-dependent mechanisms in roots, how leaves process salt stress is not at all understood. I applied salt on protoplasts from leaves, mesophyll cells and guard cells and combined live-cell imaging with V_m recordings to understand the transport and signaling for leaf cells to cope with salt stress. In both, mesophyll and guard cells, NaCl did not trigger Ca^{2+}-signals as described for roots but rather triggered Ca^{2+} peaks when washing salt out. However, membrane depolarization and pronounced alkalinization were very reliably triggered by NaCl, which could presumably act as a signal for detoxification of high salt concentrations. In line with this, I found the vacuolar cation/H^+ antiporter NHX1 to play a role in sodium transport, $[H^+]_{cyt}$ homeostasis and the control of membrane potential. Overexpression of AtNHX1 enabled to diminish $[H^+]_{cyt}$ changes and resulted in a smaller depolarization responses druing NaCl stress. My results thus demonstrated in contrast to roots, leaf cells do not use Ca^{2+}-dependent signalling cascades to deal with salt stress. I could show Na^+ and K^+ induced $[H^+]_{cyt}$ and V_m responses and Cl^- transport to only have a minor impact.

Summing all my results up briefly, I uncovered pH signals to play important roles to control pollen tube growth, stomatal movement and leaf detoxification upon salt. My results strongly suggested pH changes might be a more important signal than previously thought to steer diverse processes in plants. Using CapHensor in combination with electrophysiology and bioinformatics tools, I discovered distinct interconnections between $[Ca^{2+}]_{cyt}$ and $[H^+]_{cyt}$ in different cell types and distinct $[Ca^{2+}]_{cyt}$ and $[H^+]_{cyt}$ signals are initiated through diverse stimuli and environmental cues. The CapHensor will be very useful in the future to further investigate the coordinated role of Ca^{2+} and pH changes in controlling plant physiology.

Zusammenfassung

Kalziumionen (Ca^{2+}) und Protonen (H^{+}) werden beide als Botenstoffe angesehen, die am Pflanzenwachstum und an Mechanismen zur Stressbewältigung beteiligt sind. In der Pflanzenphysiologie sind H+-Signale jedoch im Vergleich zu Ca^{2+}-Signalen weniger gut untersucht. Die Frage, ob zwischen diesen beiden Botenstoffen Zusammenhänge bestehen, muss noch geklärt werden, da geeignete bildgebende Verfahren zur gleichzeitigen Aufzeichnung von Ca^{2+} und H^{+} Signalen sowie eine genaue bioinformatische Analyse noch entwickelt werden müssen. Um dieses Problem zu überwinden und die Rolle und möglichen Zusammenhang von Ca^{2+} und H^{+} Signalen in Pflanzen zu entschlüsseln, wurde ein neuer Biosensor namens CapHensor entwickelt und optimiert, um intrazelluläre Ca^{2+}- und H^{+}-Veränderungen gleichzeitig und ratiometrisch zu untersuchen. Der CapHensor bestand aus einem optimierten grün fluoreszierenden pH-Sensor (PRpHluorin) und einem etablierten rot fluoreszierenden Ca^{2+}-Sensor (R-GECO1), die über eine P2A-Sequenz in einem Konstrukt kombiniert wurden. Eine sogenannte P2A-„self-cleavage site“ zwischen den beiden Sensoren ermöglichte die Expression gleicher Mengen, aber räumlich getrennter Sensoren, was eine artefaktfreie und ratiometrische Darstellung von zellulärem Ca^{2+} und pH nebeneinander ermöglichte. Die Funktion des CapHensors wurde in Pollenschläuchen verifiziert, da diese einen ständigen Ca^{2+}- und pH-Gradienten aufweisen. Wir stellten fest, dass die Qualität der Bildaufnahmen und das Signal-Rausch-Verhältnis bei der Bildgebung in lebenden Zellen verbessert wurden, wenn zwei R-GECO1-Proteine innerhalb des CapHensor-Konstrukts translational fusioniert wurden. Um eine ausschließliche zytosolische Lokalisierung zu gewährleisten und gemischte Signale aus verschiedenen Kompartimenten zu vermeiden, wurden sogenannte „Nuclear Export Sequence“ (NES) und die „Nuclear Localization Sequence“ (NLS) verwendet, um PRpHluorin und R-GECO1 in unterschiedlichen Kompartimente zu lokalisieren. Nach der Optimierung und Überprüfung seiner Funktionsweise wurde CapHensor erfolgreich in verschiedenen Zelltypen exprimiert, um die Rolle von Ca^{2+}- und H^{+}-Signalen bei der Kontrolle des polaren Wachstums von Pollenschläuchen, die Stomabewegung oder Abwehrmechanismen der Blätter zu untersuchen.

Die in der Vergangenheit erzielten Ergebnisse deuten darauf hin, dass sowohl der Ca^{2+}-Gradient als auch der pH-Gradient in Pollenschläuchen eine Rolle beim polaren Wachstum spielen, wobei dem Ca^{2+}-Gradient zum Teil die Hauptrolle zugesprochen wird. Die Rolle und die zeitliche

Beziehung zwischen dem Wachstumsprozess und den Veränderungen von Ca^{2+} und pH sind jedoch noch nicht abschließend geklärt. Mit Hilfe von CapHensor fand ich heraus, dass eine zytosolische Ansäuerung an der Spitze die Wachstumsgeschwindigkeit in *N. tabacum*-Pollenschläuchen fördern und eine Alkalisierung die Wachstumsgeschwindigkeit unterdrücken kann, was darauf hindeutet, dass die zytosolische H^+-Konzentration ($[H^+]_{cyt}$) trotz der damit einhergehenden Veränderungen der zytosolischen Ca^{2+}-Konzentration ($[Ca^{2+}]_{cyt}$) eine wichtige Rolle bei der Regulierung des Wachstums von Pollenschläuchen spielt. Außerdem korrelierte das Wachstum viel besser mit dem $[H^+]_{cyt}$-Verlauf an der Spitze als mit dem Verlauf des $[Ca^{2+}]_{cyt}$-Signals. Überraschenderweise hinkten jedoch sowohl die $[Ca^{2+}]_{cyt}$- als auch die $[H^+]_{cyt}$-Oszillationen an der Spitze den Wachstumsoszillationen um etwa 33 s bzw. 18 s hinterher, so dass die Rolle von $[Ca^{2+}]_{cyt}$ an der Spitze für das Wachstum des Pollenschlauchs neu bewertet werden muss. Die CapHensor-Bildgebung an lebenden Zellen in Kombination mit Elektrophysiologie ergab, dass die oszillierende Membrandepolarisation besser mit den $[H^+]_{cyt}$-Oszillationen an der Spitze korrelierte als mit den $[Ca^{2+}]_{cyt}$-Oszillationen, was darauf hindeutet, dass $[H^+]_{cyt}$ auch eine wichtige Rolle bei der Kontrolle des elektrogenen Membrantransports spielt. Mit Hilfe des CapHensors und dem gleichzeitigen Auslesen der Zellbewegungen konnte eine präzise zeitliche und räumliche Auflösung der Ereignisse erzielt werden, was auf eine herausragende Rolle von $[H^+]_{cyt}$ beim Wachstum der Pollenschlauchspitze hinweist.

Für den Einsatz des CapHensors in Blattzellen musste ein spezielles CapHensor-Konstrukt entwickelt werden, das zusätzliche NES-Lokalisierungssequenzen enthielt, um eine Überlappung der Fluoreszenzsignale aus dem Zellkern und dem Zytosol zu vermeiden. Nachdem dies erreicht war, wurde die Rolle von Ca^{2+}- und pH-Änderungen in Schließzellen, einem gut beschriebenen Einzelzellsystem, untersucht. Veränderungen des zytosolischen pH-Werts wurden bei der Bewegung von Stomata in früheren Studien beschrieben, aber die physiologische Rolle dieser Veränderungen und die Interaktion mit sich verändernden Ca^{2+}-Signalen waren noch unerforscht. Der Einsatz von CapHensor zusammen mit der von mir entwickelten Technik zur parallelen Erfassung der Stomatabewegung hat unser Verständnis der Rolle von Ca^{2+} und H^+ bei der Stomatabewegung erheblich verbessert. Das Phytohormon ABA und der bakterielle Elicitor Flagellin (flg22) sind typische abiotische bzw. biotische Stressfaktoren, die das Schließen der Stomata auslösen. Welche Art von Ca^{2+}- und H^+-Signalen in den Schließzellen durch ABA und flg22 ausgelöst werden und in welchem zeitlichen Zusammenhang sie stehen und welche Rolle sie

für die Bewegung der Stomata spielen, war bisher unbekannt. Bei der durch ABA und flg22 ausgelösten Schließung der Stomata wurde ein Anstieg von $[Ca^{2+}]_{cyt}$ beobachtet, aber die Dynamik von $[H^+]_{cyt}$ unterschied sich grundlegend und zeigte eine andere Dynamik. ABA löste eine ausgeprägte zytosolische Alkalisierung aus, die der $[Ca^{2+}]_{cyt}$-Antwort um 57 s deutlich vorausging, während die Spaltöffnungen erst ca. 205 s danach anfingen zu schliessen. Bei Flg22 ging das Schließen der Spaltöffnungen nur mit einer leichten zytosolischen Alkalisierung einher, aber die Ca^{2+}-Reaktion war im Vergleich zur ABA-Reaktion viel ausgeprägter. Woher die zytosolische Alkalisierung stammt, war unklar, aber in der Vergangenheit wurde spekuliert, dass die Vakuole dazu beiträgt. In dieser Arbeit wurden vakuoläre pH-Änderungen mit Hilfe des Farbstoffs BCECF über die Zeit verfolgt, wobei die Konzentrationsverschiebung in der Vakuole im Grunde genommen genau den umgekehrten Verlauf aufwies als im Zytosol beobachtet. Dies deutet darauf hin, dass die Dynamik des vakuolären pH-Wertes stark an die Änderungen des zytosolischen pH-Wertes gekoppelt ist. Aus der Literatur ist bekannt, dass reaktive Sauerstoffspezies (ROS) bei der Signalgebung für das Schließen der Stomata eine wichtige Rolle spielen. Als ich jedoch definierte H_2O_2-Mengen auf die Zellen applizierte, führten nur unphysiologosch hohe H_2O_2-Konzentrationen (> 200 µM), die zu einem Verlust der Membranintegrität führten, zum Schließen der Stomata. Unerwarteterweise führten physiologische Konzentrationen von ROS zu einer Ansäuerung des Zytosols, die mit der Öffnung der Stomata, aber nicht mit der Schließung der Stomata in Verbindung gebracht wurde. Um die Rolle von $[H^+]_{cyt}$ bei der Steuerung der stomatären Bewegung im Detail zu untersuchen, wurden extrazelluläre und intrazelluläre pH-Änderungen in *N. tabacum*-Schließzellen hervorgerufen um deren Verhalten bei pH-Änderungen zu untersuchen. Die Ergebnisse zeigten, dass eine zytosolische Ansäuerung die Öffnung der Stomata stimuliert, während eine zytosolische Alkalisierung die Schließung der Stomata auslöst, begleitet von einem Anstieg von $[Ca^{2+}]_{cyt}$. Dies beweist, dass die pH-Regulierung ein wichtiger Aspekt der stomatären Bewegung darstellt und auf die Ca^{2+}-Dynamik einwirkt. Bemerkenswert war, dass die zytosolische Alkalisierung und nicht der Ca^{2+}-Anstieg eine entscheidende Rolle bei der Schließung der Stomata zu spielen schien, da eine stärkere zytosolische Alkalisierung trotz eines ähnlichen $[Ca^{2+}]_{cyt}$ -Anstiegs eine stärkere Schließung der Stomata hervorrief. Erhöhungen von $[Ca^{2+}]_{cyt}$, die in der Vergangenheit als frühes Stomataschließungssignal diskutiert wurden, konnten in meinen Experimenten den Stomataschluß nicht allein auslösen, selbst wenn extrem starke Ca^{2+}-Signale ausgelöst wurden. Was die Interaktion zwischen den beiden Botenstoffen anbelangt, so waren

$[Ca^{2+}]_{cyt}$ und $[H^+]_{cyt}$ meist negativ miteinander korreliert, was sich von den Pollenschläuchen unterschied, die eine positive Korrelation zwischen $[Ca^{2+}]_{cyt}$ und $[H^+]_{cyt}$ aufwiesen. Ca^{2+}-Erhöhungen waren immer mit einer Alkalisierung des Zytosols verbunden, und diese Beziehung konnte durch die Anwesenheit von Vanadat, ein H^+-Pumpen Blocker blockiert werden, was darauf hindeutet, dass die H^+-ATPasen der Plasmamembran zu der negativen Korrelation von $[Ca^{2+}]_{cyt}$ und $[H^+]_{cyt}$ beitragen. Im Vergleich zu den CapHensor-Reaktionen bei Schließzellen wurden zytosolische und Zellkern-lokalisierende Versionen von CapHensor in Mesophyllzellen von *N. benthamiana*, einem von uns untersuchten multizellulären System, exprimiert. Die Reaktionen der Mesophyllzellen auf die gleichen Stimuli wie bei den Schließzellen zeigten, dass ABA und H_2O_2 keine Veränderungen von $[Ca^{2+}]_{cyt}$ und $[H^+]_{cyt}$ hervorrufen, während flg22 einen Anstieg von $[Ca^{2+}]_{cyt}$ und $[H^+]_{cyt}$ bewirkt, der sich von der Reaktion in Schließzellen unterscheidet. Damit konnte ich eindeutig nachweisen, dass Schließ- und Mesophyllzellen in Bezug auf $[Ca^{2+}]_{cyt}$- und $[H^+]_{cyt}$-Änderungen sehr unterschiedlich auf dieselben Stimuli reagieren, ein Konzept, das zwar schon früher vorgeschlagen, aber noch nie so detailliert für Pflanzen nachgewiesen wurde.

Ein Phänomen, das seit langem in Schließzellen beobachtet wird, dessen Funktion oder Ursache aber noch nicht verstanden ist, sind regelmäßige Ca^{2+}-Oszillationen, die spontan auftreten. Interessanterweise wurden zwei Populationen von oszillierenden Schließzellen anhand ihrer $[Ca^{2+}]_{cyt}$- und $[H^+]_{cyt}$-Phasenbeziehung identifiziert. Bei etwa der Hälfte der oszillierenden Zellen gingen die $[H^+]_{cyt}$-Oszillationen den $[Ca^{2+}]_{cyt}$-Oszillationen voraus, während in der anderen Hälfte der Schließzellenpopulation $[Ca^{2+}]_{cyt}$ das vorangehende Signal war. Auffallend ist, dass die natürlichen $[H^+]_{cyt}$-Oszillationen durch ABA gedämpft wurden, nicht aber durch flg22. Dieser Effekt lässt sich gut durch die Dämpfung der vakuolären H^+-Oszillationen in Gegenwart von ABA erklären, aber nicht durch flg22, das ich mit BCECF sichtbar gemacht habe. Es zeigte sich, dass sowohl der vakuoläre pH-Wert zu spontanen $[H^+]_{cyt}$-Oszillationen beiträgt als auch, dass ABA, nicht aber flg22, den Zusammenhang der natürlichen $[Ca^{2+}]_{cyt}$- und $[H^+]_{cyt}$-Signale blockieren kann. Um die Rolle der $[Ca^{2+}]_{cyt}$-Oszillationen bei der Bewegung der Stomata zu untersuchen, wurden Lösungen mit hohen und niedrigen KCl-Konzentrationen verwendet, um $[Ca^{2+}]_{cyt}$-Oszillationen auszulösen. Das Auslösen von Ca^{2+}-Oszillationen nach dieser Methode wurde in Studien vor zwei Jahrzehnten etabliert, und die Ergebniss daraus haben zu dem Dogma geführt, dass der Anstieg von $[Ca^{2+}]_{cyt}$ das entscheidende Signal für die Schließung von Stomata ist. Ich habe jedoch herausgefunden, dass die Bewegung der Stomata mit dieser Methode hauptsächlich auf osmotische

Effekte und nicht auf die Auswirkungen der $[Ca^{2+}]_{cyt}$-Erhöhungen zurückzuführen waren. Glücklicherweise fand ich mit dieser Methode heraus, dass es eine starke Korrelation zwischen dem zytosolischen pH-Wert und dem Kaliumtransport über die Plasmamembran und die Vakuole gibt. Die H^+-ATPasen der Plasmamembran und die H^+-gekoppelten K^+-Transporter wurden als Ursache für die pH-Änderungen identifiziert, beides sehr wichtige Aspekte in der Stomaphysiologie, die zuvor nicht experimentell sichtbar gemacht werden konnten. Der Transport von Natriumionen (Na^+) ist für die Regulierung der Stomata und der Adaption von Blättern bei Salzstress wichtig, da Salz von der Wurzel zum Spross transportiert werden kann. Im Gegensatz zu den gut beschriebenen Ca^{2+}-abhängigen Na^+-Transportmechanismen in den Wurzeln ist überhaupt nicht bekannt, wie Blätter Salzstress verarbeiten. Ich habe Salz auf Protoplasten von Blättern, Mesophyllzellen und Schießzellen appliziert und „Live-Cell-Imaging“ mit Aufzeichnungen der Membranspannung kombiniert, um den Transport und die Signalreizweiterleitung bei Salzstress in Blättern zu verstehen. Sowohl in Mesophyll- als auch in Schließzellen löste NaCl keine Ca^{2+}-Signale aus, wie sie für Wurzeln beschrieben wurden, sondern führte beim Auswaschen von Salz zu $[Ca^{2+}]_{cyt}$-Transienten. Eine Membrandepolarisation und eine ausgeprägte Alkalisierung wurden jedoch sehr zuverlässig durch NaCl ausgelöst, was vermutlich als Signal für die Entgiftung von hohen Salzkonzentrationen dienen könnte. Im Einklang damit konnte ich zeigen, dass der vakuoläre Kationen/H^+-Antiporter NHX1 eine Rolle beim Natriumtransport, der zytosolischen pH-Homöostase und der Kontrolle des Membranpotenzials spielt. Die Überexpression von AtNHX1 ermöglichte es, $[H^+]_{cyt}$-Veränderungen zu vermindern und führte zu einer geringeren Depolarisationsreaktion unter NaCl-Stress. Meine Ergebnisse zeigen somit, dass Blattzellen im Gegensatz zu Wurzeln keine Ca^{2+}-abhängigen Signalkaskaden nutzen, um mit Salzstress umzugehen, und ich konnte zeigen, dass Na^+ und K^+ die $[H^+]_{cyt}$- und Membranspannungs-Reaktionen auslöst und der Cl^--Transport nur einen geringen Einfluss hat.

Zusammenfassend habe ich festgestellt, dass pH-Signale eine wichtige Rolle bei der Kontrolle des Wachstums von Pollenschläuchen spielen, sowie bei der Bewegung der Stomata und der Entgiftung der Blätter durch Salz beteiligt sind. Meine Ergebnisse deuten stark darauf hin, dass pH-Änderungen ein wichtigeres Signal für die Steuerung verschiedener Prozesse in Pflanzen sein könnten als bisher angenommen. Durch den Einsatz des CapHensors in Kombination mit elektrophysiologischen und bioinformatischen Methoden konnte ich feststellen, dass in verschiedenen Zelltypen unterschiedliche Zusammenhänge zwischen $[Ca^{2+}]_{cyt}$ und $[H^+]_{cyt}$ bestehen

und dass unterschiedliche $[Ca^{2+}]_{cyt}$- und $[H^{+}]_{cyt}$-Signale durch verschiedene Stimuli und Umweltreize ausgelöst werden. Der CapHensor wird in Zukunft sehr nützlich sein, um die koordinierte Rolle von Ca^{2+}- und pH-Änderungen bei der Steuerung der Pflanzenphysiologie weiter zu untersuchen.

1 Introduction

1.1 Stresses in plants

Plants as sessile organisms live in constantly dynamic environments facing abiotic stresses such as drought, salinity and biotic stresses like pathogen attack. These major environmental stresses result in economic loss because of reduction in yield and food security. Improving plants resistance to stress is a major goal to promote agricultural productivity and environmental sustainability. Hence, how plants sense different stresses and initiate processes to adapt to the environment are fundamentally important questions, but many scientific questions remain unresolved. Answering those would help to identify signaling mechanisms for targeted breeding programs in the future.

1.1.1 Drought stress

With global warming, water consumption for agriculture is estimated to rise continuously, already over 70 % of the fresh water worldwide is used in agriculture nowadays [1]. Under drought stress, increasing ion concentrations triggers osmotic effects in plants. Therefore, plants need to re-establish the osmotic equilibrium to survive under drought stress. Ca^{2+}-permeable channels have been proposed to be activated by mechanical forces under osmotic stress, which contributes to transient cytosolic Ca^{2+} ($[Ca^{2+}]_{cyt}$) increases [2-4]. Several proteins responsible for sensing osmotic stress have been identified recently. For instance, OSCA1 which localizes at the plasma membrane was identified as a putative hyper-osmotic sensor responsible for $[Ca^{2+}]_{cyt}$ increases during osmotic stress [4]. Besides osmotic effects, abscisic acid (ABA), a phytohormone associated with drought stress, has been extensively reported to steer plant responses to low water availability [5-7].

1.1.2 Salt stress

Salinity is one of the most severe global problems limiting crop production and land usage [8]. Over 6 % of the world's land area [9] and more than 20 % of the irrigated lands are affected by salinity [10]. A better understanding of the mechanisms how plants adapt to high-salinity stress could help researchers develop appropriate approaches to enhance crops performance.

High salinity is commonly mimicked by applying high salt (NaCl) concentrations resulting in three adaptive processes including cellular osmotic stress, ionic stress and secondary stresses to accomplish salt detoxification in plants [2]. Osmotic stress functions as the primary signal and triggers compatible osmolyte synthesis to maintain stability of cellular structures and protein

functions [9,11,12]. The osmolytes which are accumulated under salt or osmotic stress include sugars like sucrose and mannitol, charged metabolites including proline and ions such as K^+ and Na^+ [13]. High concentration of Na^+ and Cl^- are both regarded as toxic ions for plants [9]. The classic Salt Overly Sensitive (SOS) pathway, described to counteract salt stress was demonstrated to involve Ca^{2+}-signaling. High cytosolic Na^+ loads are thought to trigger $[Ca^{2+}]_{cyt}$ increases which activate Salt Overly Sensitive 1 (SOS1) a plasma membrane Na^+/H^+ exchanger to export Na^+ out of the cytosol or to sequester Na^+ into the vacuole through Na^+/H^+ antiporters at the tonoplast [2,14].

1.1.3 Pathogen stress

Plants have conserved microbial molecules-detecting receptors to perceive potentially harmful microbes in terms of conserved microbe or pathogen-associated molecular patterns (MAMPs or PAMPs). Perception of the elicitors consequently initiates a sequence of defense responses to trigger innate immunity [15,16]. Knowledge about the mechanisms of plants dealing with various pathogen elicitors will provide the possibility to develop strategies to cope with pathology problems of plants in the context of agriculture.

Summary

Even though plants handle with the complex environmental conditions via integrated or overlapping signaling pathways, they ultimately need to balance plant growth and establishment of defense and detoxification. Some of these response pathways share common features such as Ca^{2+} oscillations, pH effects and/or ROS homeostasis, which function as 'second messenger' in many abiotic and biotic stresses [17]. However, species and cell types dependent differences in defense strategies and/or in the sources of signals exist to regulate the developmental processes [18,19], some of them, however, received less attention in the past. In plants, typical single-cell systems such as pollen tubes and guard cells are used to investigate the signaling pathways with distinct features because physiological parameters like cell motion can be quantified particularly well. However, plants react to stresses on the multicellular level, and it is essential to understand how plants cope with multi-changing information by coordinating second messenger systems on organ level. It is thus important to investigate common, but also different signaling pathways on the single-cell level for instance in pollen tubes and guard cells and compare them with multicellular systems like mesophyll cells to understand the mechanisms of information processing in plants in general. The role of ion signaling has already been discovered through work on single

cell systems, but how exactly Ca^{2+} and pH signaling control plant responses in these cells or at the organ level is still poorly understood, especially how both signals are interconnected.

1.2 Generation of $[Ca^{2+}]_{cyt}$ and $[H^+]_{cyt}$ signals

1.2.1 Generation of $[Ca^{2+}]_{cyt}$ signals

Ca^{2+} functions as a universal second messenger in many stress responses such as osmotic stress, drought, salt and pathogen infections. $[Ca^{2+}]_{cyt}$ is maintained approximately at 100-200 nM while Ca^{2+} in intracellular organelles and the appoplast is in the millimolar range [20,21]. It is known that transient Ca^{2+} increases may be elicited by various stimuli and these are sensed by Ca^{2+}-binding proteins including Ca^{2+}-dependent protein kinases (CDPKs or CPKs), calmodulins (CaMs), CaM-like proteins (CaMLs or CMLs), and the CBL (calcineurin B-like proteins)/CIPK (CBL-interacting protein kinases) system [22-27] to either directly (CPKs) or indirectly (CBL/CIPK, CAM) relayed the information encoded by the Ca^{2+} signal. $[Ca^{2+}]_{cyt}$ dynamics with different frequency, duration or amplitude are thought to encode distinct physiological outputs, which are known as "Ca^{2+} signatures" [28-32]. The ability of specific cell types or tissues to relay direct Ca^{2+} signals into defined responses primarily depends on the cellular localization, concentration and Ca^{2+} binding affinity of signaling components, which can sense and convert Ca^{2+} signatures into specific outputs [33]. $[Ca^{2+}]_{cyt}$ homeostasis is regulated by Ca^{2+} influxes via Ca^{2+}-permeable channels as well as Ca^{2+} effluxes through Ca^{2+}-ATPases and Ca^{2+}/H^+ transporters [34-37].

1.2.1.1 Influx of Ca^{2+}

Many Ca^{2+}-permeable channels or transporters exist in different cellular membranes in order to regulate $[Ca^{2+}]_{cyt}$ homeostasis [38-42] (Fig. 1) based on their expression profiles. According to the activation mechanisms, Ca^{2+} permeable channels can be divided into voltage-dependent, ligand-gated and stretch-activated Ca^{2+} channels [35,43-45]. These different activation mechanisms are thought to shape Ca^{2+} fluxes to generate different Ca^{2+} signatures to regulate physiological activities in plants [31,35,44,46] (Fig. 1). Hyperpolarization-activated Ca^{2+}-permeable channels in the plasma membrane were identified to regulate intracellular Ca^{2+} concentration [43,47,48] such as sustained Ca^{2+} influx upon ABA administration [48,49]. Cyclic nucleotide-gated channels (CNGCs) and glutamate receptor-like channels (GLRs) are typical ligand-gated cation channels that received considerable attention as important regulators of Ca^{2+} fluxes. CNGC18 was implicated to regulate

apical growth of pollen tubes by maintaining tip-focused $[Ca^{2+}]_{cyt}$ gradient [50]. CNGC4, CNGC11 and CNGC12 have been identified to function in response to pathogens [51,52] while GLR1.1 in *Arabidopsis* regulated ABA biosynthesis [53]. Stretch-activated Ca^{2+} channels are related to pressure or mechanical changes. Mechanical sensing channels were identified in guard cells to be permeable to Ca^{2+} [4,45,54-56].

1.2.1.2 Efflux of Ca^{2+}

To avoid toxic effects of high $[Ca^{2+}]_{cyt}$ and to maintain standing $[Ca^{2+}]_{cyt}$ gradients in pollen tubes, $[Ca^{2+}]_{cyt}$ needs to be maintained at low concentration via Ca^{2+} efflux [57]. The coordinated regulation of the cellular extrusion systems is still not fully understood. P-type Ca^{2+}-ATPases and Ca^{2+}/H^+ antiporters are two main systems identified so far to extrude Ca^{2+} from the cytosol [35,42,43] (Fig. 1).

Ca^{2+}-H^+ Antiporters

In *Arabidopsis*, 6 putative Ca^{2+}/H^+ antiporters (CAXs) were proposed to regulate Ca^{2+} but also other cation homeostasis [35,42,58-60]. Ca^{2+}/H^+ antiporters were reported to have high-affinity low capacity of Ca^{2+} efflux to establish $[Ca^{2+}]_{cyt}$ levels in the nanomolar range [35] (Fig. 1). However, members of CAXs express in different tissues and function differently upon stresses [35,60]. For instance, the *cax3* mutant was more sensitive to salt and low pH whereas no phenotype was observed in the *cax1* mutant [35,60]. This might result from differential expression of CAX1 and CAX3 because the former mainly expresses in leaves while the latter prominently expresses in roots [60].

Ca^{2+}-ATPases

Ca^{2+}-ATPases are the major Ca^{2+} efflux way to regulate $[Ca^{2+}]_{cyt}$ homeostasis by pumping Ca^{2+} out of the cytosol to the apoplast and/or organelles [57,61] (Fig. 1). In contrast to Ca^{2+}/H^+ antiporters, Ca^{2+}-ATPases display low-affinity but high capacity of Ca^{2+} efflux [35]. *Arabidopsis* P-type Ca^{2+}-ATPases were classified as PIIA Ca^{2+}-ATPases and PIIB Ca^{2+}-ATPases [35,61,62]. PIIA Ca^{2+}-ATPases include 4 genes in *Arabidopsis* and locate at the endoplasmic reticulum (ER) and endosomes named ECA1-4, but their contribution to $[Ca^{2+}]_{cyt}$ homeostasis is largely unknown. PIIB type Ca^{2+} pumps are also named autoinhibited Ca^{2+} ATPases (ACAs) (Fig. 1) with variable localizations [57] such as the ER (ACA2) [63], vacuolar membrane (ACA4 and ACA11) [64], plasma membrane (ACA7-10, 12 ,13) [65-67], just to name a few. When calmodulin binds to the regulatory domain of ACAs, the autoinhibitory domain is relieved to subsequently activate the pump [63].

1.2.2 Generation of $[H^+]_{cyt}$ signals

Although Ca^{2+} as a second messenger is widely accepted, $[H^+]_{cyt}$ as a second messenger is still controversially discussed [68]. In plants, the cytosol is around pH 7-8 while the appoplast and the vacuole are acid about pH 5-5.5 [69-71]. The mobility of H^+ within the cell is high, for Ca^{2+} it is much lower and thus the role of H^+ in plants upon stresses is probably different from Ca^{2+} [68,72]. $[H^+]_{cyt}$, in other words cytosolic pH is manipulated by various processes including H^+ transport across membranes, cytosolic buffering and H^+ consumption or release through metabolisms [68,72,73] (Fig. 1). $[H^+]_{cyt}$ homeostasis was important in plant physiology such as apical growth [74-77]. However, the demonstration of $[H^+]_{cyt}$ to function as a second messenger in plants and which molecular components participate in $[H^+]_{cyt}$ homeostasis remain to be uncovered. Potential mechanisms such as H^+ efflux via H^+-ATPases and H^+-PPases [61,78,79] or H^+ influx through proton transporters [40,80-82] await to be ascertained (Fig. 1).

1.2.2.1 Efflux of H^+

The H^+-ATPases as well as H^+-PPases at the vacuolar membrane are characterized to build up and maintain the apoplastic, cytosolic and vacuolar pH by ATP-driven H^+ pumping [68,78,79,83]. Plasma membrane H^+-ATPases are electrogenic ion pumps that extrude H^+ from the cytosol thereby hyperpolarizing the plasma membrane [84]. Given the electrochemical gradients of H^+, plasma membrane H^+-ATPases are regarded as important regulators for plant growth, and have recently been characterized in pollen tubes [61,68,75,85]. Although the structure of these pumps has been revealed and genetic evidence has been provided [77,86-89], the redundancy of plasma membrane H^+-ATPases makes it difficult to clearly identify their specific functions since 12 autoinhibited H^+-ATPases (AHAs) were found in *Arabidopsis* [90]. The single loss-of-function mutant of the major AHAs *aha1* or *aha2* grew normally whereas the double knockout mutant was lethal [91,92]. As most chemical inhibitors are not specific for plasma membrane H^+-ATPases, the physiological roles of plasma membrane H^+-ATPases remain to be uncovered. AHA expression levels depend on cell types, for example AHA6-9 specifically express in pollen tube while AHA1, 2, 5 highly express in guard cells [75,83,93].

1.2.2.2 Influx of H^+

Except H^+ efflux out of the cytosol via H^+-ATPases or H^+-PPases, various transporters such as cation/H^+ antiporters (CAXs, NHXs or CHXs), H^+/Cl^- symporters and other H^+-coupled transporters were identified to use the pH gradient across the plasma membrane and the vacuolar

membrane while changing H^+ homeostasis [11,94,95] (Fig. 1). Because the H^+-pumps constantly pump H^+ out of the cytosol, H^+-coupled transporters result in either a temporary charge imbalance leading to a transient membrane potential change or do compensate intracellular pH gradients until the new equilibrium is obtained. For example, SOS1, a Na^+/H^+ antiporter in the plasma membrane and NHX1 in the vacuolar membrane play a critical role by exporting Na^+ out of the cytosol by using the H^+-motive force [1,2,11]. Ca^{2+}/H^+ antiporters (CAXs) and K^+/H^+ antiporters (CHXs) were identified or speculated to regulate $[H^+]_{cyt}$ homeostasis [35,42,61,96]. Some genetic evidence as well as modeling approaches have been provided to show the existence of cation/H^+ antiporters in plants [35,42,97,98], but cation/H^+ transporters function to regulate cytosolic pH is rarely discussed (Fig. 1). How H^+ co-transporters are coordinated along with the H^+-ATPases to regulate physiological processes while maintaining pH homeostasis awaits to be characterized in the future.

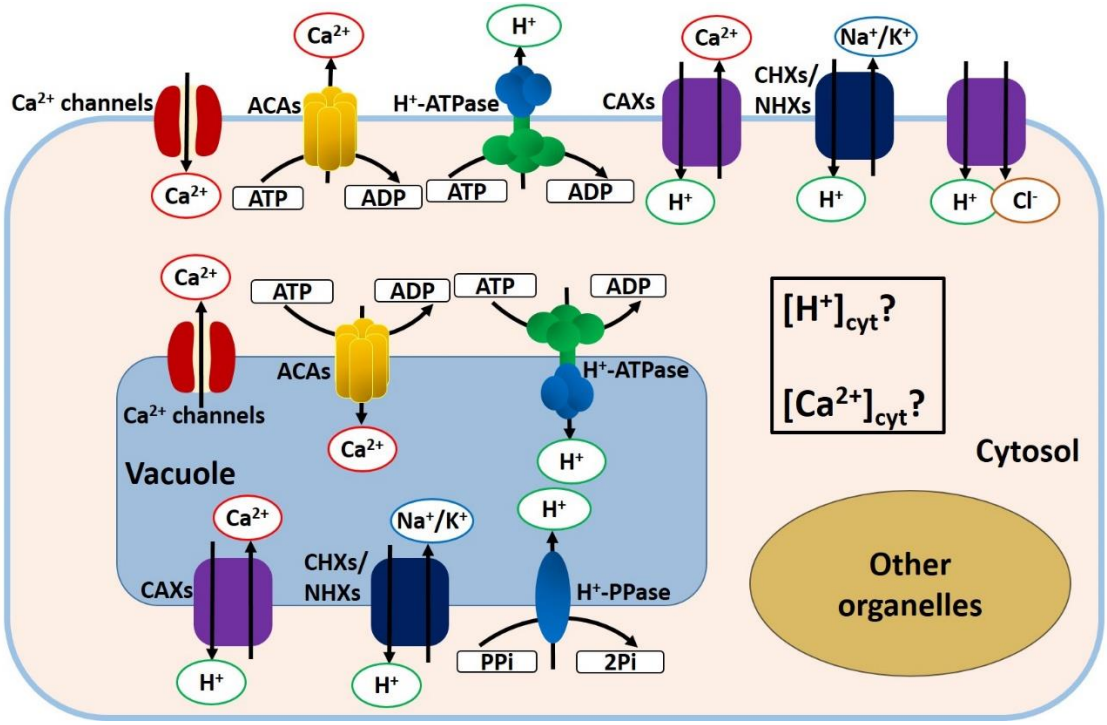

Figure 1. Main components for $[Ca^{2+}]_{cyt}$ and $[H^+]_{cyt}$ homeostasis in plant cells.

A scheme of $[Ca^{2+}]_{cyt}$ and $[H^+]_{cyt}$ homeostasis through channels, transporters and pumps at the plasma membrane and the vacuolar membrane is described. Ca^{2+} influx can be achieved by Ca^{2+} permeable channels (red) while Ca^{2+} effluxes via Ca^{2+}-ATPases (ACAs, yelow) and/or Ca^{2+}/H^+ antiporters (CAXs, purple) at the plasma membrane and the vacuolar membrane. $[H^+]_{cyt}$ homeostasis is regulated by H^+-ATPases and H^+-PPases constantly pumping H^+ out of the cytosol and maintain the H^+ motive force at the membrane. The reverse effect is mediated by H^+-coupled transporters (CHXs/NHXs/CAXs, H^+/Cl^- symporters, dark blue and purple) that co-transport H^+ into the cytosol. Contributions by other organelles to $[Ca^{2+}]_{cyt}$ and $[H^+]_{cyt}$ homeostasis are not shown in this scheme.

1.3 Biosensors for Ca^{2+} and H^+ visualization

To monitor cellular $[Ca^{2+}]_{cyt}$ and $[H^+]_{cyt}$, fluorescent dyes with high brightness can be used, however chemical indicators were shown to have toxic side-effects [99,100]. To overcome these limitations, genetically encoded fluorescent indicators or luminescent biosensors were developed and optimized to visualize Ca^{2+} and H^+ in living cells [101-103]. Genetically encoded probes widely used nowadays have the advantage of less toxic effects and stable expression levels and to be targeted to specific cellular locations. However, due to different sensitivities and brightness of biosensors one needs to choose appropriate biosensors according to the requirement of the scientific project.

1.3.1 Ca^{2+} biosensors

The sensitivity and signal-to-noise ratio are important factors to consider when applying genetically encoded indicators. A variety of fluorescent Ca^{2+} sensors have been developed and optimized in recent years [102,104]. Two main designs for genetically encoded Ca^{2+} sensors have been proven useful. One is based on two fluorescent proteins (FP) performing Förster Resonance Energy Transfer (FRET). The other strategy is based on a single FP that is fused to a Ca^{2+}-binding protein structure called CaM/M13 [100,105].

The Ca^{2+} sensors based on a single FP include the series of GCaMPs [106,107] and GECO sensors [101]. In these Ca^{2+}-biosensors, fusion of sensory modules to a circularly permutated FPs provided significantly enhanced brightness and fluorescence change when binding with Calmodulin (CaM) and M13 [100,105]. Single FP Ca^{2+} sensors were developed to display higher signal-to-noise ratio and higher sensitivity compared with FRET-based Ca^{2+} sensors. For instance, R-GECO1 is more sensitive to detect $[Ca^{2+}]_{cyt}$ changes compared with NES-YC3.6 [108]. Originally for the use in deep tissue experiments, red variants of the Ca^{2+} sensors were developed to also combine with sensors or actuators in a lower wavelength spectrum enabling multicolor approaches [101,109,110].

1.3.2 H^+ biosensors

Since all proteins basically harbor amino acids that are able to bind H^+, pH homeostasis is important for protein stability and enzyme activity. H^+ is the substrate for secondary active transport processes and many physiological processes such as growth were reported to be controlled by $[H^+]_{cyt}$ homeostasis [73,83], suggesting pH dynamics as a key signaling element in physiology. Chemical pH indicators, such as 2,7-bis-(2-carboxyethyl)-5-(and-6)-

carboxyfluorescein (BCECF) [111,112] or genetically encoded fluorescent biosensors for $[H^+]_{cyt}$ detection were employed to monitor cellular pH dynamics [99,100,103,113,114]. A pH-sensitive GFP variant, named 'ratiometric pHluorin' was used to quantify the absolute pH values and exhibited a reversible excitation ratio facing either pH 5.5 or 7.5 [113]. Ratiometric pHluorin can be used as a dual-excitation (395 nm and 475 nm) and one-emission (508 nm) wavelength probe with pKa of 6.9 [103,113], desirable for monitoring changes in cellular pH.

Although many optimized biosensors for both $[Ca^{2+}]_{cyt}$ and $[H^+]_{cyt}$ have been developed and a whole palette of fluorescent proteins with different colors are available, probes for simultaneously measuring $[Ca^{2+}]_{cyt}$ and $[H^+]_{cyt}$ are rarely reported. In recent years, though, the interest in pH changes together with $[Ca^{2+}]_{cyt}$ changes has emerged and studies using either Ca^{2+} or pH sensors [115,116] were performed, the interconnection between $[Ca^{2+}]_{cyt}$ and $[H^+]_{cyt}$ remains to be addressed in physiological processes.

1.4 The role of $[Ca^{2+}]_{cyt}$ and $[H^+]_{cyt}$ in pollen tubes

In plants, pollen grains germinate and grow in a polarized manner to form pollen tubes. Pollen tubes elongate rapidly within the pistil, trying to reach the ovules to release their sperm cells to accomplish plant sexual reproduction.

Pollen tubes growth occurs in the apex of the tube in a pronounced oscillatory pattern, where growth speed is alternating between a rapid and a slow phase [75,117,118] (Fig. 2, blue color). Tip-focused $[Ca^{2+}]_{cyt}$ and $[H^+]_{cyt}$ gradients were extensively described in pollen tubes and were assumed to be crucial for the growth process [75,76,119] (Fig. 2). Oscillatory parameters such as frequency or period, duration and amplitude were analyzed to some extent, but conclusive results on causal relationships between growth, $[Ca^{2+}]_{cyt}$ and $[H^+]_{cyt}$ could not be drawn [120]. Researches in the past focused on the regulatory mechanisms in the apex during polar growth, however pollen tubes are structurally divided into regions called apex, apical flank, subapical region and the shank (50-100 µm far from the tip) [118,121] (Fig. 2). Particularly, changes in $[Ca^{2+}]_{cyt}$ have been extensively studied in the context of pollen tube growth [19,122,123] at the extreme apex and sometimes even considered to be the main regulator [124]. However, an acidic cytosol in the tip seems to play fundamental roles in pollen tubes growth as well [75,77,123]. Other ions such as K^+ and Cl^- are also

involved in pollen tubes polar growth [117] and affected by membrane potential and tip-focused $[Ca^{2+}]_{cyt}$ and $[H^{+}]_{cyt}$ gradients [123,125].

1.4.1 The role of $[Ca^{2+}]_{cyt}$ in pollen tubes

Elongating pollen tubes show a steep tip-focused $[Ca^{2+}]_{cyt}$ gradients between the tip and the shank (Fig. 2) with a tip-directed Ca^{2+} influx and efflux at the shank [117,126] (Fig. 2, red color). Pollen tube growth is diminished when the $[Ca^{2+}]_{cyt}$ gradient is inhibited or altered indicating $[Ca^{2+}]_{cyt}$ to play a key role in polar growth [127-130]. To investigate the role of $[Ca^{2+}]_{cyt}$ in steering pollen tube growth and orientation, dyes and fluorescent proteins were used to monitor $[Ca^{2+}]_{cyt}$ [125,126,129,131,132]. $[Ca^{2+}]_{cyt}$ at the apex oscillated in the range of 750-3000 nM, which was in phase with oscillations of growth rate [117,131,133] but delayed by 10-15 s, which was attributed to the limitation of the technique used to detect Ca^{2+} changes (extracellular vibrating ion selective microelectrodes techniques) [117,131]. Later time-lapse imaging using genetically encoded biosensors still exhibited peaks of growth oscillations preceding that of the tip $[Ca^{2+}]_{cyt}$ by 1-4 s [134,135]. Furthermore, pollen tubes growth was characterized to lag behind exocytosis of vesicles by 5-10 s [136,137]. Based on these results, a polar growth mechanism driven by Ca^{2+}-dependent exocytosis seemed to be unlikely [138,139]. Another mismatch of the hypothesis that Ca^{2+} is the main regulator for exocytosis-driven tip growth is that $[Ca^{2+}]_{cyt}$ oscillations with high amplitude start to occur when pollen tube growth ceases [140-142]. This asks for re-evaluation of the role of $[Ca^{2+}]_{cyt}$ in pollen tube growth and asks to answer what physiological meaning distinct $[Ca^{2+}]_{cyt}$ oscillations really have. Ca^{2+} influx by Ca^{2+} permeable channels [35,43,45] (Fig. 2) like CNGCs and GLRs was reported to be responsible for generating Ca^{2+} gradients in pollen tubes, being important for tip growth [143,144]. For example, the *cngc18* mutant exhibited a pollen tube bursting phenotype whereas overexpression of CNGC18 inhibited pollen tube growth *in vitro* [50,144]. Besides, some mechanosensitive Ca^{2+}-permeable channels were assumed to highly express in *Arabidopsis* pollen tubes and to be involved in tip-focused $[Ca^{2+}]_{cyt}$ gradients [37,56,119,145], but up until now few data based on genetic evidence is reported so far. Thus, $[Ca^{2+}]_{cyt}$ oscillations lagging behind growth oscillations were proposed to originate from stretch-activated Ca^{2+} channels in the pollen tubes tip [55]. Moreover, the autoinhibited Ca^{2+}-ATPases (ACAs) are reported to regulate $[Ca^{2+}]_{cyt}$ homeostasis [35,43]. For instance, ACA9 contributed to generate Ca^{2+} gradients by exporting Ca^{2+} at the shank [65] (Fig. 2, red lines). Still, the physiological function of many other members from the ACAs family has not

been addressed in detail. High spatial and temporal resolution of $[Ca^{2+}]_{cyt}$ dynamics would help to understand the role of Ca^{2+} in pollen tubes growth.

1.4.2 The role of $[H^+]_{cyt}$ in pollen tubes

H^+ has been proposed to play an important role in pollen tubes growth as well [68,75,77]. Pollen tubes exhibit an acidic cytosol at the tip. The alkalized region behind the tip (Fig. 2) in pollen tubes of lily species might regulate actin organization [76,117,123]. $[H^+]_{cyt}$ gradients were established by membrane-localized H^+-ATPases, which regulate H^+ efflux at the shank [146] (Fig. 2). pH gradients were observed when applying low concentrations of the pH indicator dye, BCECF-dextran [76] only in growing pollen tubes. Extracellular H^+ flux profiles displayed a current loop localized in the apical domain fitting the $[H^+]_{cyt}$ distribution [76] (Fig. 2, green color). Based on this finding, it was claimed that H^+ currents might play a primary role in pollen tube polar growth [75,76,119].

Previous studies reported that growth is influenced when changing extracellular pH from 5.5 to 4.5 or 6.5 accompanied with abolished $[Ca^{2+}]_{cyt}$ oscillations in *Lilium longiflorum* pollen tubes [140]. The slightly acidic cell wall matches with the acid growth theory, facilitating cell expansion through loosening of the cell wall and arranging cytoskeleton organization [147]. Linked through extracellular pH changes, oscillations of cell wall thickness, membrane trafficking and cytoskeleton organization were supposed to contribute to oscillatory growth as well [118,123,148-150]. However, the exact role of $[H^+]_{cyt}$ oscillations and their association with growth still remain to be demonstrated.

1.4.3 Membrane potential in pollen tubes

Pollen tubes growth relies on osmotically driven cell expansion at the tip, a result of coordinated ion transporter across the plasma membrane [123]. Ca^{2+}, H^+ and voltage-regulation of membrane transport suggest tip-focused $[Ca^{2+}]_{cyt}$ and $[H^+]_{cyt}$ gradients to be an important regulator of turgor driven cell elongation [68,117]. Membrane potential can be regulated by anion fluxes, which are important for pollen tubes growth via anion channels. For example, two groups of Ca^{2+}-dependent anion channels (Rapid- and Slow- type) were found to positively regulate pollen tubes growth [125,130] and light-gated anion channels ACR1 activation can trigger anion efflux to depolarize the cell and inhibit pollen tubes growth [151]. In addition to anions, K^+ homeostasis is also important for pollen tubes growth especially based on findings that outward K^+ channels SKOR and inward K^+ channels SPIK (Fig. 2) were regulated by $[Ca^{2+}]_{cyt}$ and $[H^+]_{cyt}$ [152-156]. However, it should be

mentioned that the polarity of pollen tubes was lost in the protoplasts system thus tip-focused $[Ca^{2+}]_{cyt}$ and $[H^+]_{cyt}$ gradients were lost when measuring ion currents by patch-clamp and the results from these studies should be seen critically.

Then previous studies using intracellular electrodes could record electric signals in intact pollen tubes preserving cell polarity [157,158], but these were never correlated to intracellular changes in ion concentrations. Time-resolved changes in membrane potential together with ion imaging could uncover the link between ion signaling, membrane transport and growth but this technique has not yet been applied in pollen tubes to study their interconnection.

1.4.4 Integrating ion dynamics and ion signaling with growth in pollen tubes

Although $[Ca^{2+}]_{cyt}$ and $[H^+]_{cyt}$ were identified to oscillate in phase with growth with slight delays, Cl^- seems to be the only ion to oscillate exactly in antiphase [117,123,159] (Fig. 2, purple lines). Given that observed tip-focused $[Ca^{2+}]_{cyt}$ oscillations lag behind the growth and exist in non-growing pollen tubes [160], Ca^{2+} might not be a prerequisite for the growth mechanism. However, growth speed is associated with high tip Ca^{2+} concentrations while moderate or slow growth speed is associated with reduced $[Ca^{2+}]_{cyt}$ gradients [127-130]. A similar correlation can be found for $[H^+]_{cyt}$ gradients. Pollen tubes usually show an acid tip whereas dissipation of this gradient diminishes growth [76]. Recent genetic and imaging results indicated $[H^+]_{cyt}$ gradients between the tip and the shank were important for pollen tubes growth [75,77,161].

Fluorescent biosensors are powerful probes to correlate pollen tubes growth speed with tip-focused $[Ca^{2+}]_{cyt}$ and $[H^+]_{cyt}$ gradients. The link between $[Ca^{2+}]_{cyt}$, $[H^+]_{cyt}$ and growth oscillations from the same pollen tube has never been simultaneously recorded to perform correlation analysis to precisely quantify their interrelation. Quantitative methods to analyze parameters of oscillations in pollen tubes growth were developed only recently [75,159,160,162].

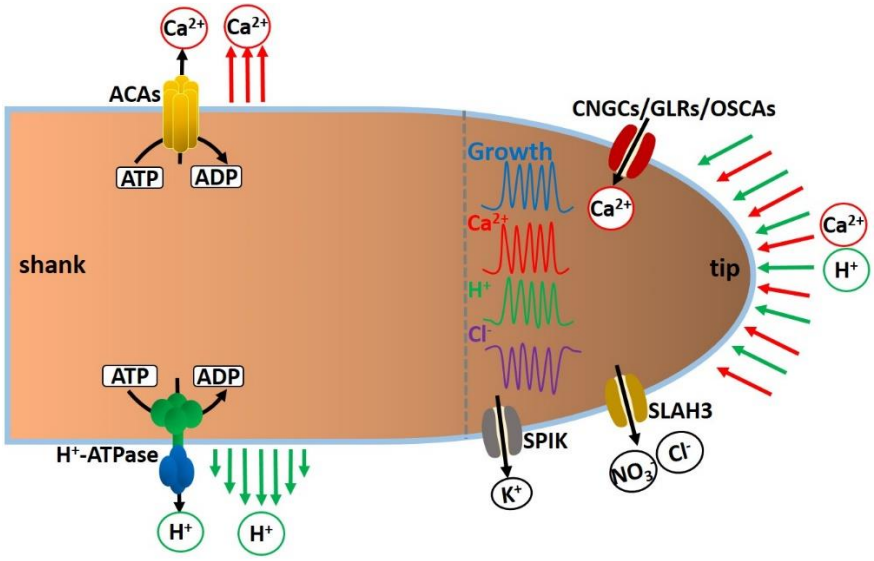

Figure 2. Ion homeostasis and growth oscillations in pollen tubes.

Ca^{2+} (red) and H^+ (green) enter the cell at the tip through Ca^{2+} permeable channels such as CNGCs/GLRs/OSCAs and yet unknown H^+ channels, respectively. Ca^{2+} and H^+ efflux occurs at the shank via Ca^{2+}-ATPases (ACAs) and H^+-ATPases, respectively. The growth oscillations are shown by the blue trace, while Ca^{2+}, H^+ and Cl^- oscillations are shown in red, green and purple colors, respectively. Some ions transporters integrated in membrane potential changes such as K^+ and anion (Cl^- and NO_3^-) channels are exemplified via SPIK (shaker pollen inward K^+ channel) and SLAH3 (slow anion channel 3), respectively, which are reported to function in pollen tube growth regulation.

1.5 The physiological role of $[Ca^{2+}]_{cyt}$ and $[H^+]_{cyt}$ in guard cells

Stomata are pores surrounded by a pair of guard cells mostly localized in epidermal layers of leaves. Variations in guard cells turgor pressure can cause changes of the pore size [163-167]. Stomatal aperture is fine-tuned through different stimuli to control water loss and gas exchange. Elements that control stomatal movement via osmotic changes include ion channels, transporters, pumps and alterations in metabolisms (Fig. 3).

1.5.1 $[Ca^{2+}]_{cyt}$ oscillations in guard cells

Ca^{2+} is the best characterized second messenger to regulate stomatal movement. $[Ca^{2+}]_{cyt}$ oscillations in guard cells may occur after specific stimuli to close stomata, but often already occur spontaneously in the ground-state.

1.5.1.1 Imposed $[Ca^{2+}]_{cyt}$ oscillations

Stimuli triggered $[Ca^{2+}]_{cyt}$ oscillations have been extensively investigated to study the role of Ca^{2+} in guard cells responses to ABA, pathogen, hydrogen peroxide (H_2O_2) and high external Ca^{2+}

[6,36,168-170] (Fig. 3). It revealed that $[Ca^{2+}]_{cyt}$ signals with different frequency, duration, amplitude and transient numbers are triggered by different stimuli [19,31,35,171,172]. A defined range of $[Ca^{2+}]_{cyt}$ transients encodes for stomatal closure [171,172]. Furthermore, 1-10 mM external Ca^{2+} triggered stomatal closure whereas low external Ca^{2+} was recognized to open stomata [168,173].

1.5.1.2 Spontaneous $[Ca^{2+}]_{cyt}$ oscillations

Spontaneously occurring repetitive $[Ca^{2+}]_{cyt}$ oscillations have been observed by live-cell imaging [34,174,175] (Fig. 3), but these cells are usually discarded from any analysis since it is difficult to discriminate the stimuli-induced $[Ca^{2+}]_{cyt}$ response from the spontaneous $[Ca^{2+}]_{cyt}$ oscillations. However, some groups observed 45 % guard cells exhibited spontaneous $[Ca^{2+}]_{cyt}$ oscillations, which were distinct from some specific stimuli induced $[Ca^{2+}]_{cyt}$ oscillations [34,175]. In comparison to $[Ca^{2+}]_{cyt}$ oscillations induced by ABA, it may also inhibit spontaneous $[Ca^{2+}]_{cyt}$ oscillations [175]. The physiological role of spontaneous $[Ca^{2+}]_{cyt}$ oscillations observed in guard cells or other cell types is still completely unknown.

1.5.2 The role of $[Ca^{2+}]_{cyt}$ and $[H^{+}]_{cyt}$ in ABA induced stomatal movement

Due to increasing global climate changes and water usage, ABA is the most widely studied hormone concerning stomatal movement. ABA synthesis is triggered under drought and salt stress [2,9,176]. ABA is perceived intracellularly by receptors of the PYR/PYL/RCAR family to trigger the ABA signaling pathway [177-182] (Fig. 3). Transient $[Ca^{2+}]_{cyt}$ increases were considered for a long time to be essential in stomatal closure regulated by ABA, especially because genetic evidence for the involvement of CPKs and Ca^{2+}-dependent anion channels activation were described [168,183-185] (Fig. 3). However, ABA evoked $[Ca^{2+}]_{cyt}$ elevations were only observed in 30-70 % of guard cells in *Arabidopsis thaliana, Commelina communis* or *Nicotiana tabacum.* Stomatal closure may also occur without any $[Ca^{2+}]_{cyt}$ rise [5,112,186-188]. Considering the timing of ABA induced stomatal closure and the occurrence of $[Ca^{2+}]_{cyt}$ increases, many times they do not match [5,168,189,190]. These observations also imply Ca^{2+}-independent mechanisms to be present in the regulation of stomatal movement and the underlining membrane transport processes [5,188,189,191,192] (Fig. 3). Therefore, which regulatory mechanism underlies the Ca^{2+}-independent stomatal movements still remains to be resolved.

1.5.2.1 Ca^{2+} dependent guard cell signaling mechanisms

A Ca^{2+}-dependent signaling pathway has been proposed in ABA induced stomatal movement (Fig. 3). After ABA binding, the receptors binds with clade A protein phosphatases type 2C (PP2Cs) to form a complex [179,193] to inhibit PP2Cs activity such as ABA-insensitive 1 (ABI1) or ABA-insensitive 2 (ABI2) [178,194,195] (Fig. 3). The *abi1-1* and *abi2-1* mutant exhibited diminished $[Ca^{2+}]_{cyt}$ rise, ROS production and S-type anion currents and loss of sensitivity to ABA, suggesting a $[Ca^{2+}]_{cyt}$ rise to be important in ABA signaling [174,196-198]. ABI1 interacts with and functions as a negative regulator of sucrose non-fermenting 1 related protein kinase 2 (SnRK2s) such as open stomata1 (OST1/SnRK2.6) [198,199] (Fig. 3). Besides OST1, other SnRKs especially SnRK2.2, SnRK2.3 can interact with PP2Cs as well. The triple *snrk2.2/snrk2.3/snrk2.6* mutant was insensitive to ABA [200,201]. The cellular events often described to occur in guard cells under ABA treatment include $[Ca^{2+}]_{cyt}$ elevations, cytosolic alkalization, production of ROS and nitric oxide along with a series of phosphorylation and dephosphorylation events to steer cation and anion channel activation [202]. For example, NADPH oxidase respiratory burst homolog (Rbohs) at the plasma membrane such as RbohD and RbohF can be phosphorylated by SnRK2s to produce ROS, a second messenger mediating a variety of stress pathways [48,112,163,164,188,203-212] (Fig. 3). ROS activates hyperpolarization-activated Ca^{2+}-permeable channels in *Arabidopsis* guard cells [48] (Fig. 3). Based on Ca^{2+} encoding and decoding proteins, CPKs are considered as one of main regulators and are identified to activate anion channels, the initial step in stomatal closure [213,214] (Fig. 3). The quadruple *cpk5/6/11/23* mutant exhibited deactivated S-type anion channel activity and was defective to ABA induced stomatal closure [191]. The *slac1* mutant showed impaired stomatal closure upon ABA and largely reduced S-type anion channel currents [215]. S-type anion channels are activated by ABA to depolarize the membrane potential followed by inhibited inward-rectifying K^+ channels and activated voltage-dependent K^+ outward rectifying channel GORK to export K^+ out of the cell which increases the water potential in the cell to close stomata [6,45,213,214,216-219] (Fig. 3).

1.5.2.2 Ca^{2+} independent guard cell signaling mechanisms

Although a Ca^{2+}-independent mechanism in ABA induced stomatal closure is accepted to exist, its importance and exact mechanism have been much less studied (Fig. 3). In *Arabidopsis*, OST1, a Ca^{2+}-independent protein kinase is activated to trigger numerous downstream responses [195,198,199,220-224] such as activation of R- and S- type anion channels while the *ost1* mutant displayed

opened stomata phenotype [224]. Thus Ca^{2+}-dependent and independent mechanisms seemed to connect at OST1 in the ABA signaling cascade [5,191,225] (Fig. 3).

Cytosolic alkalization by 0.3 to 0.4 pH units is one typical feature in ABA induced stomatal closure [68,173]. Intracellular and extracellular pH changes were discussed to play a crucial role in Ca^{2+}-independent mechanism since cytosolic alkalization seemed to be essential in stomatal closure induced by ABA [5,112,226] (Fig. 3). The cytosolic alkalization was observed to facilitate outward-rectifying K^+ channels, which were activated during ABA induced stomatal closure [227,228]. Surprisingly, not only the cytosol, but also the apoplast is alkalized in response to ABA [229,230]. This indicates both sides of the plasma membrane alkalize, which cannot be established by H^+ transport across the plasma membrane only. The regulation of apoplastic pH is still controversially discussed [230,231] and proposed to be caused by binding of H^+ to organic anions [229], which are released from guard cells during stomatal closure. The pH gradient of most plant cells is generated by plasma membrane H^+-ATPases which also generate the negative membrane potential [232]. To study the role of plasma membrane H^+-ATPases in stomatal movement, chemicals such as vanadate and fusicoccin were used to inhibit or activate plasma membrane H^+-ATPases activity [233-236], respectively, to regulate stomatal movement [237,238]. Furthermore, three out of 12 members of the H^+-ATPases called AHAs (AHA1, AHA2 and AHA5) highly express in *Arabidopsis* guard cells [239]. The single *ost2-2D* mutant carries a single point mutation in AHA1 to have constitutively activated H^+-ATPases resulting in stomata insensitivity to ABA [240]. Except proton gradients between the cytosol and the apoplast established by plasma membrane H^+-ATPases, pH gradients between the cytosol and the tonoplast are established by V-type ATPases and H^+-pumping pyrophosphatases (H^+-PPases) at the vacuolar membrane (Fig. 1). The double *vha-a2/vha-a3* mutant lacking V-type ATPase activity displayed more alkalized vacuoles and delayed stomatal closure in response to ABA [239,241]. H^+-PPases were activated in the vacuolar membrane of guard cells [242] to participate in generating the proton motive force and the electrochemical gradient over the tonoplast [79,83]. ABA induced stomatal closure and vacuolar acidification were delayed in the *avp1* mutant (vacuolar proton pyrophosphatase1) [243]. Thus, the cytosolic alkalization initially induced by ABA in guard cells might result from vacuolar acidification [96,112,244,245].

Whether and how cytosolic pH signals control stomatal movement in a Ca^{2+}-independent pathway remains to be shown. How $[Ca^{2+}]_{cyt}$ and $[H^+]_{cyt}$ interact to regulate stomatal movement is also unknown, but studies on $[Ca^{2+}]_{cyt}$ and $[H^+]_{cyt}$ interconnections could provide conclusive ideas how

the Ca^{2+}-dependent and independent mechanisms are integrated in ABA signaling pathway to control guard cells motion.

1.5.3 The role of $[Ca^{2+}]_{cyt}$ and $[H^+]_{cyt}$ in flg22 induced stomatal movement

Stomata not only function to control transpiration, but are important gates for pathogen entry [246,247]. Pathogens can be sensed by guard cells autonomously and stomatal closure is induced after perception of elicitors like PAMPs such as flagellin (flg22) [16,248,249].

Flagellin is one of the best investigated PAMPs in *Arabidopsis*. Flagellin is perceived by plants through pattern recognition receptors (PRRs) named Flagellin sensitive 2 (FLS2) at the plasma membrane [250-252] (Fig. 3). The *fls2* mutant showed impaired stomatal closure in response to flg22 [246,251,253], which indicated FLS2 is essential in flg22 triggered stomatal closure. FLS2 binds flg22 to form a complex with another receptor like kinase called BRI1-associated kinase 1 (BAK1) [254] which does not bind flg22 directly [255] (Fig. 3). It was hypothesised that BAK1 might regulate the interplay between FLS2 and OST1, since BAK1 is supposed to be a positive regulator of OST1 [256] (Fig. 3). Flg22 induced $[Ca^{2+}]_{cyt}$ increases, apoplastic alkalization, K^+ efflux, ROS generation and activation of MPKs [16,249,253,257-261] (Fig. 3). $[Ca^{2+}]_{cyt}$ increases by CNGCs are considered as one of the initial and essential signals in pathogen induced immunity [170,259,261].

In *Arabidopsis*, H_2O_2 production is detected upon flg22 treatment and NADPH oxidases, RbohD and RbohF contribute to this ROS generation [202,209,249] (Fig. 3). AtRbohD can be phosphorylated and activated by CPKs under flg22 treatment [262,263] linking ROS and Ca^{2+} signaling. ROS production upon flg22 is reduced in the double *cpk5/cpk6* mutant [264,265], suggesting that CPKs are necessary for PAMP induced ROS production. However, AtRbohD was proposed to interact with FLS2 and was phosphorylated by Botrytis-induced kinase 1 (BIK1) in a Ca^{2+}-independent manner [167,266,278]. Therefore, Ca^{2+}-dependent (CPKs) and Ca^{2+}-independent (BIK1) control of AtRbohD are both associated with ROS production in response to flg22 [267-269] (Fig. 3). Genetic reprogramming after pathogen invasion depends on activation of mitogen-activated protein kinase (MAPKs) and CPKs (CPK4/5/6/11) [264,270,271]. ROS production and $[Ca^{2+}]_{cyt}$ increases regulated outward K^+ currents in PAMPs [250,258,259,272]. SLAC1 was also proposed to be activated to close stomata in response to PAMPs [261]. This activation was regulated by OST1. However, how OST1 connects with FLS2 is still unknown. Stomatal closure of the double *slac1/slah3* mutant was impaired in response to flg22 whereas the closure phenotype was not or only partially impaired in the single *slah3* or *slac1* mutant, respectively [261].

Plasma membrane H^+-ATPases were also involved in flg22 induced stomatal closure [273-275]. In *Arabidopsis*, AHA1 and AHA2 were inhibited by phosphorylation in the autoinhibitory C-terminal domain during flg22 induced stomatal closure [84,273]. Stomatal closure in the *ost2* mutant was impaired under flg22 treatment [276]. Moreover, inhibition or activation of plasma membrane H^+-ATPases activity can regulate cellular membrane potential [259,275].

1.5.4 Stomatal opening

Stomatal opening is necessary to maintain the transpiration stream and guarantee gas exchange. A $[Ca^{2+}]_{cyt}$ increase was also observed in stomatal opening [112,277]. How the same second messenger controls opening and closing of stomata, two opposite physiological processes, is still unclear.

During stomatal opening, plasma membrane H^+-ATPases were identified to pump H^+ out of the cytosol to hyperpolarize the membrane potential and drive K^+ into the cell to open stomata [5,278]. Genetic evidence supports two H^+-ATPases functioning in *Arabidopsis* stomata control [240]. The *Arabidopsis ost2* mutants exhibited a stomatal opening phenotype [240] while inhibition of the H^+-ATPase isoform (PMA4) identified in tobacco guard cells showed impaired stomata opening [279].

In *Arabidopsis*, inwardly rectifying K^+ channels such as KAT1 and KAT2 participated in K^+ influx during stomatal opening, activated by external acidification [280-282]. Uptake of K^+ was balanced by uptake of inorganic anions such as Cl^- and NO_3^-, and malate orginating from starch [5,283,284]. Accordingly, decreases in water potential and passive water influx subsequently result in turgor increase and stomatal opening. GORK is the only outwardly rectifying K^+ channels in guard cells identified so far and activated by membrane depolarization which is induced by many stress signals such as drought and salt [217,285]. Surprisingly, the full loss-of-function GORK mutant (*gork1*) lacked the charcteristic of slow-activating outward currents but stomatal closure upon ABA is only partially impaired, indicating other K^+-efflux mechanisms to exist [286]. Indeed, the triple *kup6/kup8/gork* mutant displayed impaired stomatal closure in response to ABA [287]. Besides, several signals also influenced GORK channel activity such as external K^+ [217] and pH [217] and Ca^{2+} [288]. In addition to K^+ transported by channels, cation/H^+ antiporters (NHXs) and cation/H^+ exchangers (CHXs) participated in K^+-transport [95,289-292] (Fig. 1). For instance, NHX1 and NHX2 highly express in *Arabidopsis* guard cells [81,290]. The double *nhx1/nhx2* mutant showed impaired stomatal opening and closure, and a more acidic vacuole compared to wild-type [290,293].

1.5.5 Distinct and common signaling mechanisms in guard cells by ABA and flg22

How Ca^{2+} as the second messenger is supposed to trigger the contrary stomatal reactions (closing and opening) remains to be explained. The distinct pH responses may imply that pH changes could be an essential regulator in stoma physiology, however, data on the physiological role of pH changes is rare. How $[Ca^{2+}]_{cyt}$ signals or different signatures are sensed and relayed to regulate distinct downstream components is still not well characterized. Whether $[H^+]_{cyt}$ changes function to control ABA, salt and flg22 in addition to $[Ca^{2+}]_{cyt}$ requires further studies. Second messengers like ROS were already reported to be involved in PAMP and ABA induced stomatal closure [6,167,203,209,294] while $[Ca^{2+}]_{cyt}$ and ROS were known to influence plasma membrane H^+-ATPases activity in guard cells [5]. The PAMP and ABA signaling pathway in guard cells seemed to branch into different downstream mechanisms at OST1 [248], the Ca^{2+}-independent kinase. What the shared or independent spatio-temporal dynamics of second messenger Ca^{2+}, ROS and pH signals are to make the physiological decision in stomatal movement remains to be shown (Fig. 3).

Precise time-resolved analysis of $[Ca^{2+}]_{cyt}$ and $[H^+]_{cyt}$ in the process of rapid stomatal movement was rarely considered in the past. Even though stomatal closure responses are commonly observed within 5-15 min in response to various stresses such as ABA [187] and bacteria [261], apertures are mostly recorded 0.5-2 h after stimuli application. A detailed description of $[Ca^{2+}]_{cyt}$ and $[H^+]_{cyt}$ dynamics during stomatal movement still awaits to be performed, but would shed light on the temporal relationship between these two second messengers and their role for stomatal movement.

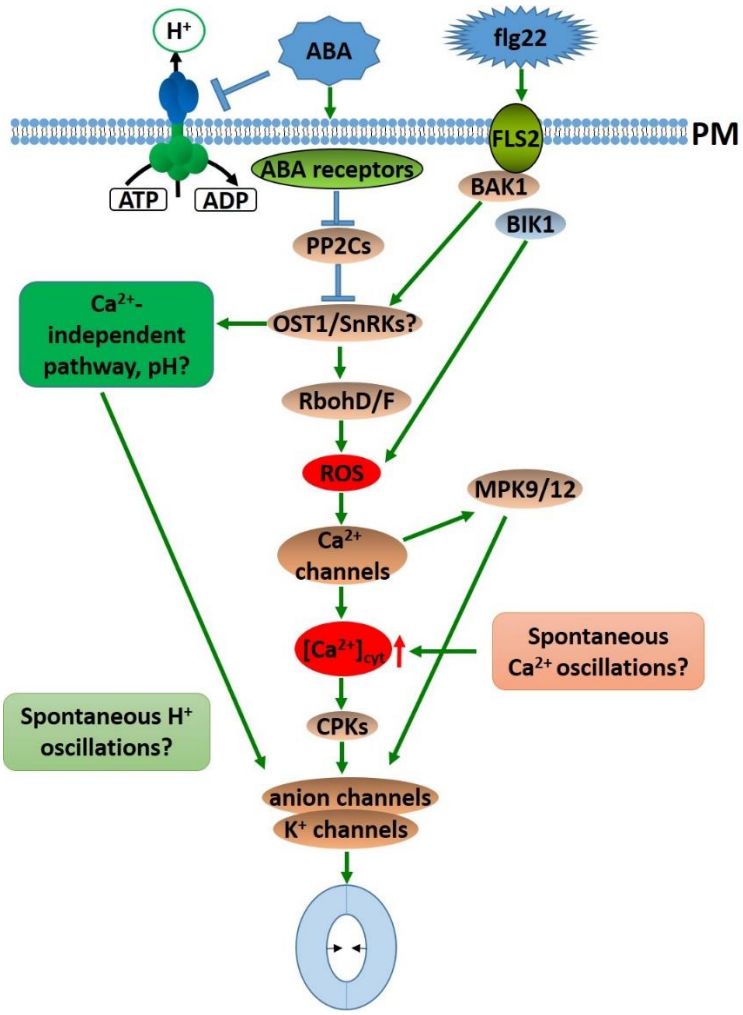

Figure 3. ABA and flg22 pathway to close stomata.

The scheme represents the sequence of events proposed in ABA and flg22 induced stomatal closure. ABA perception terminates the inhibition of PP2Cs activity by the ABA-receptors. Inhibition of PP2Cs activity may activate SnRKs such as OST1, the Ca^{2+}-independent kinase. In the Ca^{2+}-dependent pathway in the presence of ABA, RbohD/F can be activated by OST1 to generate ROS. ROS production activates Ca^{2+} channels to increase cytosolic Ca^{2+} ($[Ca^{2+}]_{cyt}$) which can be sensed by CPKs to further activate anion channels and K^+ channels which result in stomatal closure. Ca^{2+}-independent pathway in ABA triggered stomatal closure is shown but its components are not known. Plasma membrane H^+-ATPases are inhibited by ABA. Therefore, pH is regarded as the possible candidate to function in the Ca^{2+}-independent pathway in ABA induced stomatal closure. Except ABA, flg22 can be recognized by Flagellin sensitive 2 (FLS2) receptor and then associated with BRI1-associated kinase 1 (BAK1) to interact with OST1 and trigger similar downstream events compared with ABA including ROS generation, $[Ca^{2+}]_{cyt}$ increases and anion and K^+ channels activation or deactivation. However, another kinase Botrytis-induced kinase 1 (BIK1) is proposed to be directly phosphorylate by RbohD regardless of OST1 in a Ca^{2+}-independent manner to produce ROS in the presence of flg22. Flg22 invasion depends on activation of MAPKs such as MPK9/12 and CPKs to regulate anion and K^+ channels. Therefore, how pH functions in stomatal closure and whether pH functions in a Ca^{2+}-independent manner in ABA and/or flg22 mechanism are both unknown. In addition, whether spontaneous $[H^+]_{cyt}$ and/or $[Ca^{2+}]_{cyt}$ oscillations participate in stomtal movement in ABA and flg22 mechanisms is unknown. Hence, how $[Ca^{2+}]_{cyt}$, $[H^+]_{cyt}$ and genes such as OST1 function as distinct or

overlapping signals in ABA and flg22 induced stomatal closure remains to be addressed as well. More details are described in the text.

1.6 The role of Ca^{2+} and pH changes in leaf physiology

1.6.1 How do leaves cope with salt and drought stress – is there a difference to roots?

Osmotic effects are identified as very early signals under drought and salt stress [9] that result in cell shrinkage for example in root tips and young leaves. When plants suffer from drought, ABA synthesis occurs and the phytohormone can be transported from the roots to the shoots [176,295,296] or its synthesis occurs in guard cells autonomously [297]. ABA concentration in *Arabidopsis* guard cells increases in drought stress and thus stomata close in soil salinity [298]. The K^+ uptake was impaired under drought stress to cause K^+ deficiency since ABA induced depolarization [94,291,295,299]. K^+ homeostasis was typically de-regulated in response to drought stress and apoplastic H^+ transiently reduced after ABA application [107,229,234,300,301]. However, whether leaves have similar mechanisms upon drought stress compared with roots remains to be investigated.

Salt stress is extensively investigated in roots and Na^+ and Cl^- ions can translocate from the root to the shoot via the xylem to trigger reactions in leaves including stomatal closure. Salt detoxification mechanisms were uncovered to mainly depend on the SOS pathway in roots [11,302,303] (Fig. 4). This pathway encompasses several elements to maintain ionic homeostasis by sequestration of Na^+ from the cytosol to the apoplast and the vacuole [2,304]. In roots, Na^+ enters the cell through non-selective cation channels (NSCCs) and/or Na^+ transporters such as HKTs and thus induces transient $[Ca^{2+}]_{cyt}$ increases [11,305-308] (Fig. 4). The increased $[Ca^{2+}]_{cyt}$ can be sensed by SOS3 (CBL4) that binds to SOS2 (CIPK24) to mediate SOS1 (Na^+/H^+ antiporter) activation at the plasma membrane to extrude Na^+ out of the cytosol [2,309-311] (Fig. 4). The SOS1 antiport activity led to an increase of $[H^+]_{cyt}$, which was compensated by activated plasma membrane H^+-ATPases activity upon salt and/or osmotic stresses [312-314]. Plasma membrane H^+-ATPases activity is stimulated to establish steeper proton gradients to promote SOS1 function [315]. The importance of plasma membrane H^+-ATPases in this context is reflected by a consitutively active H^+-ATPase mutant called *ost2-2D* and an AHA overexpressing mutant that displayed a salt tolerant phenotype [316,317]. Similar to plasma membrane H^+-ATPases, vacuolar membrane H^+-ATPases and/or vacuolar membrane H^+-PPases are also activated by SOS2, in order to generate steeper proton gradients

across the vacuolar membrane that drive vacuolar NHXs activity [311,318,319] (Fig. 4). Overexpression of AtAVP1 in the tonoplast exhibited elevated salt and drought resistance by enhanced cations uptake such as Na^+ and/or K^+ [318,320,321]. To reduce Na^+ accumulation in the cytosol, some NHXs, putative Na^+/H^+ exchangers located at the tonoplast transport Na^+ from the cytosol to the vacuole [95] (Fig. 4). In addition, CBL10 interacts with SOS2 to form the complex CBL10/CIPK24 to sequestrate Na^+ into the vacuole by NHXs at the vacuolar membrane [319,322-324] (Fig. 4). However, it is under debate if NHXs contribute to the salt detoxification via detoxifying Na^+ or by increasing vacuolar osmolality [95,325]. Different from salt tolerance in roots, an alternative SOS-pathway was reported to transport Na^+ out of the cell including two different CIPK/CBL modules in shoots, SCABP8/CBL10 and CIPK8/CBL10 [323,326]. They found SOS3-like calcium binding protein 8 (SCABP8) overexpression only partially rescued salt-sensitive phenotype in single *sos3* mutant [323] while CIPK8 regulation of SOS1 was independent on SOS3 in shoots under salt stress [326]. This suggests different tissues could deal with salt stress by distinct salt mechanisms. Under non-stressed conditions, K^+ regulates turgor pressure in guard cells, but how Na^+ influences stomatal movement is still obscure. Early experiments showed stomata can use Na^+ as primary ions to maintain the turgor pressure [327]. However, K^+ homeostasis is interrupted by NaCl resulting in lowering the K^+/Na^+ ratio which has negative effects on plant growth [328-332]. Na^+ can be sequestered into vacuoles and thus K^+ is released to maintain cytosolic K^+/Na^+ ratio.

Except the toxic effects of cations during salinity, Cl^- was considered as toxic ions as well in some species [230,333,334] (Fig. 4). Cl^- accumulation in roots leads to increased ABA concentrations, reduced stomatal conductance and transient alkalization in the apoplast of leaves [82,94,230]. Salt tolerance mechanisms are mainly investigated in roots but the transport and signaling machineries characterized from root experiments are believed to take place in leaves without in-depth studies. However, how leaf tissues respond to salt stress and if cations or chloride trigger toxic effects in leaves are unclear. It is also not clear if Ca^{2+} and H^+ signals in leaves take place upon salinity. Moreover, salt triggered mechanisms to regulate stomatal movement also remain to be shown.

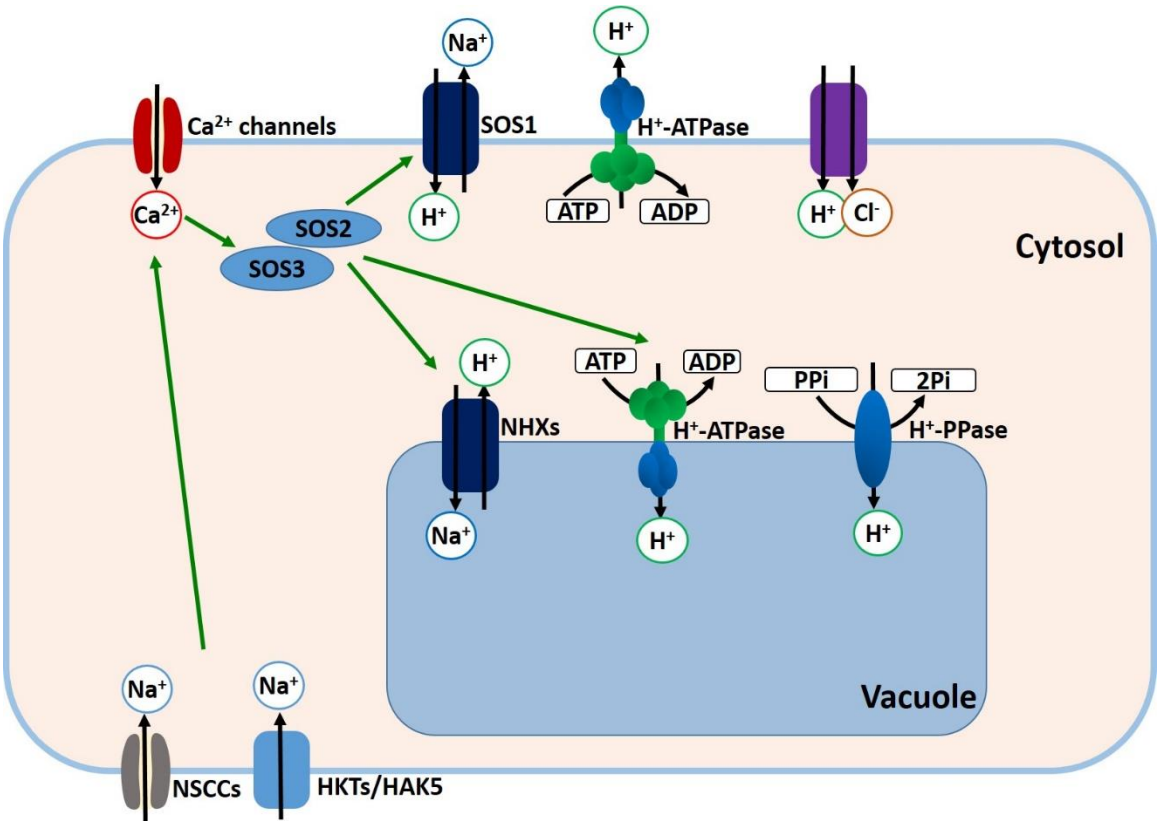

Figure 4. Salt mechanisms in roots.

A scheme of salt mechanisms in roots is displayed. Na^+ enters the cells via non-selective cation channels (NSCCs, grey) and Na^+ transporters such as HKTs/HAK5 (light blue) or others to activate Ca^{2+}-permeable channels (red) to induce $[Ca^{2+}]_{cyt}$ elevations. The increased $[Ca^{2+}]_{cyt}$ can be sensed by SOS3 and combined with SOS2 to form the complex to activate SOS1 (dark blue) at the plasma membrane to export Na^+ out of the cytosol and activate NHXs (dark blue) at the vacuolar membrane to sequester Na^+ into the vacuole. Cl^- also can be transported into the cell via H^+/Cl^- (purple) symporters under salt stress. Except H^+-coupled transporters, $[H^+]_{cyt}$ homeostasis is also regulated by plasma membrane H^+-ATPases and vacuolar membrane H^+-ATPases and H^+-PPases. V-type H^+-ATPases activity also can be activated by SOS2.

1.6.2 Pathogen infection triggers leaf ion signaling

Similar to ABA in guard cells, pathogen effectors like flg22 also induce membrane depolarization and extracellular alkalization [16,259,275,335]. In mesophyll cells, pathogen induced $[Ca^{2+}]_{cyt}$ increases trigger anion channels activation to cause the membrane depolarization. However, this response seems to be independent of ROS [45,259,336]. La^{3+}, a calcium channel blocker can abolish flg22 induced membrane potential depolarization [259] still suggesting a Ca^{2+}-dependent mechanism to be set off. It is proposed that CPK3, 5, 6 and 11 are required for ROS production in leaves in response to flg22 [261,262,264]. However, flg22 triggered depolarization in mesophyll cells of the quadruple

cpk3/5/6/11 mutant was not influenced and stomatal closure was not impaired either by ABA or flg22 in this quadruple mutant [261]. If cytosolic pH changes are associated with responses to flg22 in a similar fashion than in the ABA induced stomatal closure is not known. How Ca^{2+} and H^+ participate in the flg22 pathway in mesophyll cells remains to be investigated and compared to guard cells.

In general, ion signalings via Ca^{2+} and H^+ occurred under different stress conditions in guard cells await to be compared with multicellular systems like mesophyll cells to clarify the function of these second messengers there. Studies with mesophyll tissues would also provide the possibilities to study cell-to-cell signal transmission and long distance signaling.

1.7 Interaction of Ca^{2+} and H^+ in plants: does it take place?

As mentioned above, the signature of $[Ca^{2+}]_{cyt}$ signals upon different stimuli may differ between cells and tissues due to cell-type specific expression of Ca^{2+} channels and specific responses to distinct stimuli. Possible correlations between Ca^{2+} and H^+ are emerging recently. It was reported Ca^{2+} changes are not influenced by changes in cytosolic pH from 7.8 to 7.2 in *Vicia faba* guard cells whereas Ca^{2+} channel activity relies on cytosolic pH lower than 7.0 [337]. Many hints suggest possible links between Ca^{2+} and H^+ homeostasis based on Ca^{2+} and pH dependent regulation of ion channels and transporters [68,72,173,338]. A general link between Ca^{2+} and pH dynamics was revealed recently in plants [115,116,339].

In polar growing cells such as pollen tubes, tip-focused $[Ca^{2+}]_{cyt}$ and $[H^+]_{cyt}$ gradients are required for apical growth. A temporal sequence of Ca^{2+}, H^+, Cl^- and growth changes in growing pollen tubes was proposed [117] (Fig. 2), mainly based on extracellular ion fluxes, which were later discussed to be strongly influenced by buffer capacities of Ca^{2+} and H^+ of the cell wall [340]. A detailed quantitative characterization with a good spatial resolution of these second messengers with growth awaits to be performed to clearly propose causal relationships between them.

In guard cells, $[Ca^{2+}]_{cyt}$ elevation and cytosolic alkalization occur in ABA induced stomatal closure [68,112,173], but quantitative analysis on the sequence of events has not been performed yet. Blocking $[Ca^{2+}]_{cyt}$ elevation or cytosolic alkalization both interrupted stomatal closure triggered by ABA or other stimuli [172,173]. $[Ca^{2+}]_{cyt}$ increases and alterations in plasma membrane H^+-ATPases in guard cells and mesophyll cells during stress signals occurred side-by-side. However only $[Ca^{2+}]_{cyt}$

changes and extracellular pH changes were reported upon flg22 treatment in mesophyll cells so far [16,259,274,275]. In leaves, $[Ca^{2+}]_{cyt}$ and ROS waves were proposed to co-incide during long distance defense signaling [341,342] and plasma membrane H^+-ATPases also contributed to wounding induced traveling of membrane potential waves in leaves [343,344].

Because of the nearly parallel appearance of Ca^{2+}, pH and ROS signals with voltage changes during stress signals in guard cells and mesophyll cells, these signals might be related [341,344,345]. For example, Ca^{2+} and ROS waves were associated with systemic electric signals involving Ca^{2+}-permeable channels such as GLRs [341,345,346]. A direct link between Ca^{2+} and H^+ are cation/H^+ transporters, which were supposed to contribute to intracellular Ca^{2+} and H^+ homeostasis [40,42,78] (Fig. 1). In whole seedlings, a link between pH and Ca^{2+} was revealed, where an extracellular acidification mediated $[Ca^{2+}]_{cyt}$ elevation [347]. More evidence for such a link between Ca^{2+} and H^+ was provided by biochemical means, showing high external Ca^{2+} to inhibit plasma membrane H^+-ATPases activity [348]. Recently, GLRs were activated by extracellular alkalization causing Ca^{2+} influx [344]. Therefore, whether different $[Ca^{2+}]_{cyt}$ and $[H^+]_{cyt}$ interrelations exist in defined cell types remains to be identified. Even though not many reports document a pH contribution on electric signals, pH effects have been proven to feed-back on electric signals through plasma membrane H^+-ATPases [343,344]. Of special note is that electric waves were found to precede Ca^{2+} waves, suggesting possible roles of other second messenger to accompany or trigger the voltage waves [349]. In pollen tubes (Fig. 2) [125,130,152,154-156] or guard cells [6,45,213,214,216-219] (Fig. 3), anion channels and potassium channels can be regulated by Ca^{2+} and/or H^+ and thus to trigger membrane potential changes. Hence, how Ca^{2+} and H^+ regulate plant physiology together with electric signals upon different stimuli remains largely unknown.

2 Aims of the study

Given that the role of pH changes in plant physiology is poorly understood and conflicting results have been described for the role of Ca^{2+}, I aimed to understand the specific and interconnected role of Ca^{2+} and H^+ in plant physiology. In the past it was difficult to analyze the interconnection of these two signals accurately since biosensors for monitoring Ca^{2+} and pH were optimized recently. Furthermore, up until now, biosensors for Ca^{2+} and H^+ were only applied in separate experiments in plants. Reading out both signals in parallel in the same cell would be extremely valuable. Hence, I aimed to develop a genetically encoded biosensor called CapHensor by combining a Ca^{2+} sensor (R-GECO1) and a pH sensor (PRpHluorin) into one multicistronic vector enabling to monitor Ca^{2+} and H^+ simultaneously in the same cell. I wanted to verify the functioning of CapHensor in different plant model cell systems including pollen tubes, guard cells and mesophyll cells to study the interconnected role of ion signaling in these cell types.

In pollen tubes, the existence of standing $[Ca^{2+}]_{cyt}$ and $[H^+]_{cyt}$ gradients is well known and their association with oscillatory growth has been recognized for quite some time. However, whether $[Ca^{2+}]_{cyt}$ or/and $[H^+]_{cyt}$ oscillations contribute to oscillatory growth pattern and how they are interconnected have not yet been conclusively resolved. Due to the standing $[Ca^{2+}]_{cyt}$ and $[H^+]_{cyt}$ gradients, I aimed to make use of the pollen tube system to test and optimize the CapHensor design. After setting up the design of the sensor and a newly developed imaging technique to resolve Ca^{2+} and pH dynamics spatially and temporally, my first task was to investigate what the interconnection between $[Ca^{2+}]_{cyt}$, $[H^+]_{cyt}$ and growth oscillations in pollen tubes is and then ask whether $[Ca^{2+}]_{cyt}$ and $[H^+]_{cyt}$ oscillations are essential for growth. I also wanted to clarify the long-standing question whether there is a causal relationship between $[Ca^{2+}]_{cyt}$ and $[H^+]_{cyt}$ on the one hand and between $[Ca^{2+}]_{cyt}$ or $[H^+]_{cyt}$ and growth on the other. My objective was to use quantitative methods and algorithms for this purpose that could be applied to growing cells in order to perform quantitative biology. The relationship between cell growth and the membrane potential as an integrating factor of membrane transport should also be investigated and quantified via a combination of CapHensor live-imaging and electrophysiology.

Guard cells are another well-studied cells with respect to Ca^{2+} signaling. However, some conflicting models and results question whether Ca^{2+} functions as the main second messenger responsible for controlling stomatal aperture. To address the question of Ca^{2+}-dependent and Ca^{2+}-

independent mechanisms to control guard cell motion, the responses of different stimuli to control stomatal movement were investigated. Quantitative readouts of stomatal aperture with simultaneous determination of $[Ca^{2+}]_{cyt}$ and $[H^+]_{cyt}$ response-times should be compared to elucidate the contribution and role of these two signals for stomatal movement. For this purpose, I also aimed to apply a technique for inducing $[Ca^{2+}]_{cyt}$ oscillations to investigate whether defined $[Ca^{2+}]_{cyt}$ signals can trigger stomatal closure and what role of $[H^+]_{cyt}$ changes might play in this context. In addition to the imposed $[Ca^{2+}]_{cyt}$ oscillations, spontaneous $[Ca^{2+}]_{cyt}$ oscillations exist in guard cells as well, but their physiological role is unknown. Therefore, I asked whether there are interactions between spontaneous $[Ca^{2+}]_{cyt}$ and $[H^+]_{cyt}$ signatures in guard cells and whether these natural oscillations have an impact on guard cell physiology. Furthermore, the role and influence on $[Ca^{2+}]_{cyt}$ and $[H^+]_{cyt}$ dynamics of K^+, the ion that is significantly involved in the osmotically driven turgor pressure changes, should be investigated. In a final step, live-cell CapHensor imaging should be supplemented with a pH imaging techniques to measure vacuolar pH, combined with a pharmacological approach to identify the transport mechanisms involved in H^+-coupled K^+ and $[Ca^{2+}]_{cyt}$ homeostasis.

In contrast to the two single cell systems, guard cells and pollen tubes, mesophyll cells should be employed as a multicellular system to investigate the control of stress responses by Ca^{2+} and pH signaling in leaves. Therefore, I compared Ca^{2+} and H^+ dynamics in the cytosol and in the nuclei of mesophyll cells with the same stimuli (ABA, flg22, H_2O_2 and salt) as in guard cells to understand how different cell types within the leaf integrate abiotic and biotic stress information. Are there possible differences in the responses between these cell types was an important question to be solved. Within the framework of this thesis, the role of Ca^{2+} and H^+ and membrane potential signaling in leaves upon salt stress should be investigated and compared to the responses in roots. The question should be answered as to which of the two ions in salt stress, Na^+ or Cl^-, triggers the initiation to start the detoxification transport mechanisms in leaves.

In conclusion, the purpose of this thesis was to develop a technique to monitor signaling networks of chemical (Ca^{2+} and pH) and electrical signals for stress processing and to demonstrate the physiological relevance of such signals in specific stress situations in different plant cell types using quantitative biology methods.

3 Materials and methods

3.1 Molecular biology and cloning

3.1.1 Cloning the different CapHensor constructs

Cloning was performed by the USER cloning technique [350]. To target both the PRpHluorin and the R-GECO1 in the CapHensor into the cytosol or nucleus, nuclear export sequences (NESs) or nuclear localization sequences (NLSs) were used, respectively. The constructs with different promoters for localizing CapHensor in the cytosol contained a NES sequence at the N- and C-terminus of PRpHluorin as well as a NES sequence at the N-terminus of the R-GECO1 tandem (pCambia3300 LeLAT52 NES PRpHluorin P2A NES 2xR-GECO1; pCambia3300 35S NES PRpHluorin NES P2A NES 2xR-GECO1; pCambia1300 35S NES PRpHluorin NES P2A NES 2xR-GECO1 (Hygromycin); pSAT UBQ10 NES PRpHluorin NES P2A NES 2xR-GECO1) (Fig. 5). The NES sequences at the N- or C-terminus of PRpHluorin originated from heat stable inhibitor (PKI) [351,352] and *Xenopus* MAPKK [353], respectively. The amino acid sequence of the short linker between two R-GECO1s was GLNLSGG. The coding sequence of PRpHluorin and R-GECO1 was separated by the sequence of a 'self-cleaving peptide' called P2A [354] which enables to express two proteins simultaneously but spatially separated in the same cell. Within the t-DNA region, the pCambia3300 vectors contained the BASTA resistance gene while the pCambia1300 vector contained the gene for hygromycin resistance. Constructs for nucleus CapHensor localization (pCambia3300 35S NLS NLS PRpHluorin P2A R-GECO1 NLS-linker R-GECO1; pCambia3300 35S long NLS PRpHluorin P2A R-GECO1 NLS-linker R-GECO1; pCambia3300 LeLAT52 NLS NLS PRpHluorin P2A R-GECO1 NLS-linker_R-GECO1; pCambia3300 LeLAT52 long NLS PRpHluorin P2A R-GECO1 NLS-linker R-GECO1; pSAT UBQ10 NLS NLS PRpHluorin P2A R-GECO1 NLS-linker R-GECO1; pSAT UBQ10 long NLS PRpHluorin P2A R-GECO1 NLS-linker R-GECO1) (Fig. 5) contained two nuclear localization sequences (NLSs) or a long NLS sequence at the N-terminus of PRpHluorin and a NLS-linker between two R-GECO1s which were from the *simian virus* 40 (SV40) T-antigen [351,355]. The pSAT vector with the UBQ10 promoter was used to transform *Arabidopsis* protoplasts. The pCambia vectors fused with LeLAT52 promoter [356] and RBC-terminator or 35S promoter or 35S terminator were used for pollen tubes or ubiquitous expression, respectively.

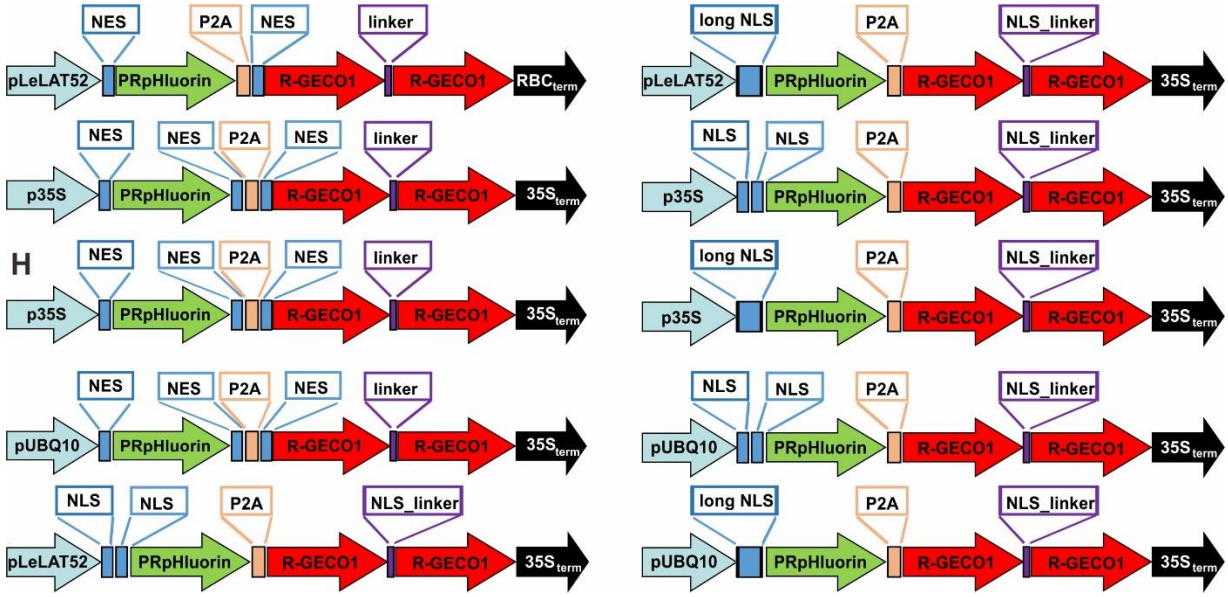

Figure 5. Schemes of CapHensor constructs.

CapHensor versions with different promoters and subcellular localization are elucidated. pLeLAT52, p35S and pUBQ10 are promoters specifically driving expressing in pollen tubes or ubiquitous expressing in plants, respectively. NES is a sequence to target PRpHluorin and R-GECO1 into the cytosol while NLS and long NLS are sequences to express two fluorescent proteins into the nucleus. PRpHluorin and R-GECO1 is a ratiometric pH sensor and a red fluorescence Ca^{2+} sensor, respectively. P2A is a self-cleavage sequence to combine PRpHluorin and R-GECO1 into one construct to simultaneously express in one cell, but spatially separated. Linker and NLS_linker are short sequences to connect two R-GECO1 molecules together. RBC_{term} and $35S_{term}$ are terminators. (H: the construct contains hygromycin resistance gene; others contain BASTA resistance gene).

Primers used to generate the NES and NLS sequences and to clone all CapHensor constructs are listed in Table 1.

Table 1. Primers used to clone CapHensor localized in the cytosol and the nuclei

Cloning Primers	Sequences
CapHensor NLS	
NLSNLS PR User pHluorin fwd	GGCTTAAUATGCCAAAAAAGAAGAGAAAGGTAGAAGACCCCATGCCAAAGAAGAAGCGTAAGGTAAGT
Long NLS PR pHluorin User fwd	GGCTTAAUATGCCAAAAAAGAAGAGAAAGGTAGAAGACCCCAGTAAAGGAGAAGAACTTTTCACTGGAG T
P2A pHluorin User rev	AGCCTGCTUCAGCAGGCTGAAGTTAGTAGCTCCGCTTCCTTTGTATAGTTCATCCATGCCATG
P2A half R-GECO1 fwd	AAGCAGGCUGGAGACGTGGAGGAGAACCCTGGACCTATGGTCGACTCTTCACGTCGTAAG
NLS-linker R-GECO1 rev	ACCTTTCTCUTCTTTTTTGGAGGCTTCGCTGTCATCATTTGTACAAACT
NLS-linker R-GECO1 fwd	AGAGAAAGGUAGAAGACCCCGGGGATCCACCGGTCGCCACCGTCGACTCTTCACGTCGTAAGTGG
RGECO1 User rev	GGTTTAAUCTACTTCGCTGTCATCATTTGTACAAA

CapHensor NES	
pHluorin half NES User rev	AGCTTCTTCUGCAAGGCCACCGCTTTGTATAGTTCATCCATGCCA TGT
NES USER fwd	GGCTTAAUATGCTGCAGAACGAGCTTGC
P2A half NES User fwd	AGAAGAAGCUGGAGGAGCTAGAGCTTGGAAGCGGAGCTACTAA CTTCAGC
RGECO1 RGECO1 User rev	ACTGAGGTTUAATCCCTTCGCTGTCATCATTTGTACAAAC
RGECO1 RGECO1 User fwd	AAACCTCAGUGGTGGAATGGTCGACTCTTCACGTCGT
RGECO1 User rev	GGTTTAAUCTACTTCGCTGTCATCATTTGTACAAA
Half NES pHluorin fwd	ACAAGACUGGAGGAGTCGACTCGAGTGCGGCCGCCACCATGAGT AAAGGAGAAGAACTTTTCACTG
LeLAT half NES rev	AGTCTTGUTAATATCAAGTCCAGCCAACTTAAGAGCAAGCTCGTT CTGCAGCATTTTTTTTTTGGTGTGTGTACTTTTTTTT
UBQ10 half NES rev	AGTCTTGUTAATATCAAGTCCAGCCAACTTAAGAGCAAGCTCGTT CTGCAGCATGATCCCGCACTCGAGCTGT
P2A half NES rev	AGTCTTGUTAATATCAAGTCCAGCCAACTTAAGAGCAAGCTCGTT CTGCAGCATAGGTCCAGGGTTCTCCTCCAC
Half NES R-GECO1 fwd	ACAAGACUGGAGGAGTCGACTCGAGTGCGGCCGCCACCATGGTC GACTCTTCACGTCGTAA
Sequencing primers	
UBQ10 seq fwd	TGTCGAATAATTACTCTTCG
pHluorin CT seq fwd	CGAAAGATCCCAACGAAAAG
R-GECO1 NLS-linker seq fwd	TGACAGCGAAGCCTCCAAAAA
R-GECO1 NLS-linker seq rev	GAGTCGACGGTGGCGACC
pHluorin User rev	GGTTTAAUTTATTTGTATAGTTCATCCATGCCATG
35S Terminator rev	GGTTTAAUGTCACTGGATTTTGGTTTTAGGAATTAG
RGECO1 RGECO1 seq rev	TTCCACCACTGAGGTTTAATCCC
RGECO1 RGECO1 seq fwd	GGGATTAAACCTCAGTGGTGGAA
LeLAT52 seq fwd	CAAGACACACACAAAGAGAAGGAG
R-GECO1 mid seq rev	CCCTCGATCTCGAACTCG TG
RBC seq rev	GTGCGCAATGAAACTGATGC

3.1.2 Cloning NHX1

Arabidopsis gene of NHX1 was cloned into the pCambia3300 vector with 35S promoter and terminator using the USER cloning technique. Primers are listed in Table 2.

Table 2. Primers used to clone *Arabidopsis* NHX1

Cloning Primers	Sequences
AtNHX1 USER fwd	ATGTTGGATTCTCTAGTGTCGAAACT
AtNHX1 USER rev	TCAAGCCTTACTAAGATCAGGAGG
AtNHX1 USER oS rev	AGCCTTACTAAGATCAGGAGGGTTTCTCTC
Sequencing primers	Sequences
AtNHX1 USER fwd	ATGTTGGATTCTCTAGTGTCGAAACT
AtNHX1 USER rev	TCAAGCCTTACTAAGATCAGGAGG
RBC seq rev	GTGCGCAATGAAACTGATGC

3.1.3 Molecular cloning process

3.1.3.1 PCR system

PCR reaction process is shown in Table 3.

Table 3. PCR reaction

Components	Volume
Template	- 1 µg
dNTP	1 µl
5 x Buffer	5 µl
Phusion enzyme	0.5-1 µl
Primes (F+R)	1 + 1 µl
PCR water	to 50 µl

Temperature	Time	
98 °C	2 min	
98 °C	30 s	30-35 cycles
55-58 °C	30 s	
72 °C	30-50 s	
72 °C	3 min	
10 °C	hold	

The PCR products from PCR cyclers (Eppendorf) were used for the agarose gel electrophoresis. After obtaining the target sequence, the right band was cut out, purified and used for cloning. The concentration of the products was measured by a spectrophotometer (NanoDrop, Wilmington, USA). The USER-cloning step is shown in Table 4.

Table 4. USER reaction system

	Volume
PCR product	4 µl
Terminated vector	1.5 µl
USER enzyme	1 µl
TE buffer	To 10 µl

The USER reaction was processed at 37 °C for 30 min and then put at room temperature for 30 min.

3.1.3.2 Plasmids transformation into *E.coli*

Plsamids were transformed to chemically competent *E.coli* cells (MRF) strain by heat shock. Add 10 µl products into competent *E.coli*. Gently mix and put it on ice for 30 min, followed by 42 °C for 90 s, 3-5 min on ice. And then add 200 µl Super Optimal broth with Catabolite repression

(SOC) medium, put on a shaker with 300 rpm at 37 °C for 30-45 min and plate on Lysogeny-Broth (LB) mdium with Agar plates containing relative antibiotics (either Ampicillin or Kanamycin) and spread evenly. Then put the plates at 37 °C overnight.

3.1.4 Plasmid extraction and transformation into *Agrobacterium tumefaciens*

3.1.4.1 Plasmid extraction

Step 1. The transformed *E.coli* were cultivated overnight in LB medium. 1.5 ml cultivated *E.coli* were collected by centrifuging for 45 s with a speed of 14100 rcf.

Step 2. Decant the supernatant and vortex until *E.coli* were resuspended.

Step 3. Firstly add 300 µl P1 (see Table 5) and shake (not vortex), then add 300 µl P2 (see Table 5). Gently mix and wait for 2-3 min.

Step 4. Add 300 µl sodium acetate (NaAc) (pH 5.2) and gently mix. Then centrifuge for 4 min, 14100 rcf.

Step 5. Transfer the supernatant to new 1.5 ml Eppis. Add 600 µl Isopropanol, mix and centrifuge for 4 min, 14100 rcf.

Step 6. Pour away the supernatant. Add 500 µl 70 % ethanol (EtOH) and centrifuge for 2 min, 14100 rcf.

Step 7. Pour away the supernatent. Put the Eppis at 37 °C for 20-30 min, with the lids open to get rid off EtOH completely.

Step 8. The isolated plasmid was diluted in deionized water or Tris-EDTA (TE) buffer. The DNA concentration and quality was measured by a spectrophotometer and stored at -20 °C.

Larger amount of plasmid DNA from *E.coli* was isolated using QIAGEN Plasmid Midi Kit (QIAGEN, Hilden, Germany). Midi extracted plasmids were used for pollen bombardment and transient transformation of protoplasts while mini extracted plasmids were used for cloning experiments.

Table 5. Composition of solutions (add water to 50 ml)

P1 (50 ml)	P2 (50 ml)
0.303 g Tris	1 ml 10 M NaOH
0.186 g EDTA	2.5 ml 20 % SDS
3 ml RNAse (only when using)	

3.1.4.2 Plasmid transformation into *Agrobacterium tumefaciens*

Extracted plasmid DNA was transformed into *Agrobacterium tumefaciens* strain GV3101 through electroporation using an electroporator machine (Electroporator 2510, Eppendorf, Hamburg, Germany) with 2 mm cuvettes under 2500 V. Then the *Agrobacterium tumefaciens* strain GV3101 containing the CapHensor constructs were stored in 50 % glycerin at -80 °C.

3.2 Plant growth condition and transformation

3.2.1 *Nicotiana tabacum*

3.2.1.1 Growth condition

Nicotiana tabacum seeds were sterilized with 6 % sodium hypochlorite (NaClO) for 3-5 min, washed with sterilized water 4-5 times and sown on Murashige and Skoog (MS) medium shown in Table 6 without antibiotics and hormones in 750 ml volume vessels. They were cultivated in the chamber with condition of 26 °C : 22 °C, 14 h light : 10 h dark, light intensity around 300 $\mu mol \cdot m^{-2} \cdot s^{-1}$ for 4-6 weeks.

3.2.1.2 Stable transformation of plants

CapHensors were stably transformed into *Nicotiana tabacum* cultivar (SR1) by following protocol.

Step 1. *Agrobacterium* harboring a pCambia CapHensor vector stored at -80 °C, re-growth was performed on Yeast Extract Beef (YEB) medium agar plates containing 100 mg/L Kanamycin + 50 mg/L Gentamicin + 50 mg/L Rifampicin for 2 days at 28 °C.

Step 2. A single colony was picked and transferred to YEB liquid medium containing the same antibiotics and incubated at 28 °C, 200 rpm overnight. Prior to the leaf inoculation process, *Agrobacterium* were cultivated with 150 µM Acetosyringone for 2 hours.

Step 3. In the clean bench, *Agrobacterium* were spinned down, the medium decanted, bacteria were washed 3-5 times with sterile water and then re-suspended in sterilized MS liquid medium containing 3 % sucrose as shown in Table 6. The OD_{600} values were adjusted to 0.1 with sterilized MS liquid medium (Table 6).

Step 4. The *N. tabacum* leaves were cut into pieces of about 1 cm x 1 cm after removing veins as much as possible. Pieces of leaves were immersed for 15-20 min into *Agrobacterium* MS liquid medium and shook occasionally. Then the leaves were put on sterilized filter papers to remove

remaining *Agrobacterium* medium before putting on MS-plates with co-cultivated medium (Table 6) for 2 days, in darkness.

Step 5. After 2 days in darkness, leaves were transferred to MS agar plates with selective medium containing BASTA (Table 6) as well as hormones to induce calli formation, kept at normal growth conditions in the light. Every 7-10 days, leaves and generated calli were transferred to new medium plates. The generated shoots that appeared after 3-4 weeks were transferred into root medium (see Table 6). Plants with roots were transferred on soil under growth condition 14 h : 10 h, light : dark at 26 °C : 22 °C in the greenhouse with around 60 % humidity.

Table 6. Composition of media for *N. tabacum* transformation (The medium pH was adjusted with KOH to 5.8)

For 500 ml	MS medium	MS liquid medium	Co-cultivated medium	Selection medium	Root medium
MS	2.45g	2.45g	2.45g	2.45g	2.45g
Sucrose	15 g	15 g	15 g	15 g	15 g
Gelzan	4 g	/	4 g	4 g	4 g
Myo-inositol (100 mg/ml)	/	/	/	500 µl (100 mg/L)	500 µl (100 mg/L)
BAP (10 mg/ml)	/	/	/	50 µl (1 mg/L)	/
NAA (4 mg/ml)	/	/	/	12.5 µl (0.1 mg/L)	/
BASTA (40 mg/ml)	/	/	/	250 µl (0.02 mg/L)	250 µl (0.02 mg/L)
Thiamine (1 mg/ml)	/	/	/	500 µl (1 mg/L)	500 µl (1 mg/L)
Ticarcillin (100 mg/ml)	/	/	/	2.5 ml (0.5 mg/L)	2.5 ml (0.5 mg/L)

3.2.2 *Nicotiana benthamiana*

3.2.2.1 Growth condition

Nicotiana benthamiana wild type plants and plants stably expressing the Ca^{2+} reporter GCaMP3 with 35S promoter [106] were grown on soil in a greenhouse with the same condition as *N. tabacum*.

Thanks to Simon Gilroy and Masatsugu Toyota for providing GCaMP3 transgenic *N. benthamiana* plants.

3.2.2.2 Transient expression

The *Agrobacterium* harboring CapHensor constructs stored at -80 °C were re-activated in YEB liquid medium containing 100 mg/L Kanamycin + 50 mg/L Gentamicin + 50 mg/L Rifampicin and grown overnight, and 2 hours before infiltration 150 µM Acetosyringone was added. Before infiltration the *Agrobacterium* were washed and re-suspended with Agromix [321] (see Table 7) to have a final OD_{600} of 0.5.

Leaves of 5-6 week-old plants were infiltrated with *Agrobacterium* containing CapHensor constructs harboring the 35S promoter or co-infiltrated with AtNHX1. The leaves were infiltrated with Agromix containing *Agrobacterium* with a 1 ml syringe. The infiltrated plants were cultivated in the green house for 3 days. Prior to the experiments, the expression level of leaves was checked under a fluorescent stereo-microscope (Leica DFC500, Leica, Switzerland AG) to confirm good expression.

Table 7. Composition of Agromix for leaves infiltration

Components	Stock concentration	Final concentration
$MgCl_2$	1 M	0.01 M
MES pH 5.6 (KOH)	0.5 M	0.01 M
Acetosyringone	10 mM	150 µM

3.2.3 *Arabidopsis thaliana*

3.2.3.1 Growth condition

Arabidopsis thaliana seeds were sown on soil under 14 h : 10 h, light : dark regime at 22 °C : 16 °C, respectively.

3.2.3.2 Stable transformation (floral-dipping method)

Arabidopsis thaliana plants were transformed by the floral-dipping method as described [357]. The cultivation procedure of *Agrobacterium tumefaciens* strain GV3101 was the same as that for *N. benthamiana* infiltration containing constructs (pCambia3300 35S NES PRpHluorin NES P2A NES 2xR-GECO1; pCambia1300 35S NES PRpHluorin NES P2A NES 2xR-GECO1

(Hygromycin); pCambia3300 35S NLS NLS PRpHluorin P2A R-GECO1 NLS-linker R-GECO1). After centrifuging and washing 3-times with water, *Agrobacterium* were re-suspended in dipping solution containing 5 % sucrose, 1.5 µl Silwet in 10 ml H_2O with OD_{600} = 0.5. The plants were immersed in the dipping solution around 30 s and covered by plastic bags under dark conditions around 24-36 h and transformation procedure was repeated 1-2 times every 7-10 days.

3.3 Transgenic plants screening

3.3.1 *Nicotiana tabacum*

Anthers of transgenic *N. tabacum* plants expressing constructs harboring the LeLAT52 promoter were collected from flowering tobacco plants and were stored at -20 °C. Pollen grains were germinated in pollen germination solution (Table 8) and screened with an inverted fluorescent microscope (Zeiss AxioObserver, Carl Zeiss AG) according to the expression level and localization.

Leaves of transformed *N. tabacum* plants expressing constructs driving expression with the 35S promoter were screened using a confocal laser scanning microscope (Leica TCS SP5 II). Plants with good fluorescence were kept for generating seeds. The next generation were screened by putting transgenic *Nicotiana tabacum* seeds on MS medium containing 25 mg/L BASTA. 7-10 days plants were transferred on soil and cultivated in the green house with condition 14 h : 10 h, light : dark at 26 °C : 22 °C with around 60 % humidity. These plants were further screened for good fluorescence with the confocal laser scanning microscope. 5-6 week-old plants were used for all described experiments.

Table 8. Pollen tube germination medium

Components	Stock concentration	Final concentration
H_3BO_4	400 mM	1.6 mM
$CaCl_2.2H_2O$	500 mM	0.2 mM
MES	500 mM	1 mM
HCl	1 M	9.6/19.6 mM
D-Sucrose	/	420 mosmol
Adjust pH to 5.8 with Tris		

3.3.2 *Arabidopsis thaliana*

Arabidopsis thaliana leaves were screened by the procedure described in 3.3.1. *Arabidopsis* seeds were sown on ¼ MS medium containing BASTA or Hygromycin antibiotics. 10-14 day-old plants were transferred on soil and cultivated in a growth chamber (Binder KBWF 720 E5.2, Tuttlingen, Germany) with condition 14 h : 10 h, light : dark at 22 °C : 16 °C with around 60 % humidity. 6-7 week-old plants were used for experiments.

3.4 Preparation of plant tissues

3.4.1 *Nicotiana tabacum* pollen tube transformation and cultivation

3.4.1.1 Pollen biolistic transformation

Constructs were transiently transformed in pollen via biolistic bombardment.

Step 1. Prepare tungston particles

50 mg tungston (Bio-Rad; 1 µm diameter) was weighed and put in 1.5 ml reaction tubes (Eppis). 500 µl 100 % EtOH was added and then vortexed for 5 min to sterilize tungston particles. The EtOH was poured away after centrifugation for 20 min to remove EtOH to let the tungston dry completely. Tungston concentration was adjusted to 50 µg/µl with deionized water.

Step 2. Precipitate DNA to tungston particles

Plasmid DNA (with a total amount of about 8-10 µg) was added into 50 µl tungston (50 µg/µl) and mixed rigorously.

50 µl 2.5 M $CaCl_2$ was put on the side of the Eppi firstly. Then 20 µl spermidine (0.1 M in water) was added and vortex immediately for 3-5 min.

100 µl pre-cooled 100 % EtOH (-20 °C) was quickly added 3 times.

The reaction Eppis were gently mixed and stored at -20 °C for 30 min to precipitate DNA to particles.

Then the reaction Eppis were gently mixed and shortly centrifuged for 2-3 seconds to be able to decant EtOH completely. Particles were mixed with 50 µl water.

Step 3. Bombardment of tungston particles into pollen grains

Either fresh or stored *Nicotiana tabacum* pollen were diluted in pollen tubes germination medium (shown in Table 8). Diluted pollen grains were spread in a thin layer on the surface of Agarose plates containing 2 % low-melt Agarose and dried for several minutes. The self-made machine for bioloistic delivery was used to shoot Tungston particles into pollen grains on the agar plates. The details about the machine and the procedure were described previously [125].

3.4.1.2 Pollen tubes cultivation and solutions used

Step 1. Pollen tube germination medium with 2 % low-melt Agarose was heated to 90 °C, 650 rpm for 15 min, mixed several times in between and cooled to 39 °C.

Step 2. Put 0.01 % Poly-L-Lysin on cleaned growth chambers for 7 min, then dry the chamber and pre-heat it on a heating plate at 39 °C for 5 min.

Step 3. Either frozen or bomarded pollen grains were diluted in pollen tube germination medium. Put 200 µl diluted pollen grains in the chambers, add 230 µl of the low-melt Agarose, and mix with the pipette rigorously the entire medium.

Step 4. Incubate on the heater at 39 °C for 5 min to let the pollen grains sink down on the cover glass, and then remove 130 µl solution from the rim of the chamber. After that, the chamber was gently transferred to room temperature for 15 min to solidify the agarose. When the Agarose solidified, 800 µl germination medium was added on top of the solidified agarose in the chamber.

Step 5. The pollen grains were incubated and germinated at 22 °C for 3-5 hours in darkness until use.

3.4.2 Preparing and handling of *Nicotiana benthamiana* protoplasts

3.4.2.1 Protoplast preparation

Step 1. Enzyme solution and other solutions were prepared (see Table 9) and usually stored at -20 °C for long time use. The enzyme solution was poured into a petri dish. The infiltrated *N. benthamiana* leaves were processed by removing the epidermis of the abaxial side with sand paper. The leaves excluding the veins were cut into pieces and put into the enzyme solution for 1.5-2 h while shaking with low speed.

Step 2. When the mesophyll tissues of the leaves were well digested, enzyme solution was poured through a 100 μm mesh into a 50 ml tube and washed with wash solution B1 (see Table 9) gently twice.

Step 3. Centrifuge the 50 ml tube with 18 *g* without acceleration at 4 °C for 7 min and then carefully remove the supernatant.

Step 4. Add solution C along the tube to 30 ml to dilute the protoplasts and evenly separate them into two 50 ml tubes.

Step 5. Carefully add 5 ml solution D1 using pipetting tips with cut tips into each 50 ml tube and then add 5 ml solution B2 very gently in the same way.

Step 6. Centrifuge 50 ml tubes under 300 *g* without acceleration and deacceleration at 4 °C for 5 min. The protoplasts in the middle layer were carefully taken out using cut pipette tips and transferred them into a new 50 ml tube.

Step 7. Carefully add solution B1 with cut pipette tips to 20 ml and gently mix by swirling the tube by hand. Centrifuge the 50 ml tube for 7 min at 4 °C, 18 *g* without acceleration.

Step 8. Remove the supernatant and add appropriate amounts of solution B1 to dilute the clean protoplasts.

Table 9. Solutions for protoplast extraction and purification

	A Enzyme solution	B1 Standard scrubbing solution	B2 Wash solution	C	D1
BSA	1 %	/	/	/	/
Pectolyase Y23	0.05 %	/	/	/	/
Cellulase R-10	0.5 %	/	/	/	/
Mazerozym R-10	0.5 %	/	/	/	/
$CaCl_2$	1 mM	1 mM	1 mM	1 mM	1 mM
MES	10 mM	/	5 mM	5 mM	5 mM
Sucrose	/	/	/	500 mM	400 mM
D-Sorbitol	500 mM	500 mM	500 mM	/	100 mM
pH	5.6 with Tris	/	6.0 with KOH		

3.4.2.2 Perfusion solutions

Solution B1 was used as control solution. 50 mM NaCl, 50 mM KCl or 50 mM HCl were added into the perfusion solution containing 1 mM $CaCl_2$ and the osmolality was adjusted to 500 mosmol, the same applies for B1 with D-sorbitol.

3.4.3 Leave discs for *Nicotiana benthamiana* mesophyll cell observation

3.4.3.1 Preparation

Infiltrated leaves were screened under a fluorescent microscope. Good expressing leaves were selected and the abaxial epidermis of leaf discs (cut into approximately 1 cm x 1 cm) was gently removed by twizzers while the adaxial side was rapidly glued to the cover slip mounted in custom made chambers with Medical Adhesive B (Ulrich Swiss, St Gallen, Switzerland). The leaves bathed in standard leaf solution (**1 mM $CaCl_2$, 1 mM KCl and 10 mM MES**) adjusted to pH 5.8 with bis-tris propane (BTP) and recovered overnight at room temperature in darkness.

3.4.3.2 Solutions

N. benthamiana leaves were perfused with a standard solution for leaves. Either acetic acid (HAc; Applichem, Darmstadt, Germany), ABA (diluted in 100 % ethanol; SigmaAldrich, St Louis, MO, USA), flg22 (diluted in water; Genscript, Piscataway, NJ, USA), hydrogen peroxide (H_2O_2, Sigma-Aldrich), NaCl (diluted in water) were added to the respective concentrations as indicated in the legends to figures. In mesophyll cells under 50 mM NaCl experiments, control solution (75 mM MES, 1 mM $CaCl_2$, adjusted pH = 5.8 with Tris) was used in experiments to balance osmolality. All experiments were performed under permanent perfusion with speed around 700 µl min^{-1}.

3.4.4 *Nicotiana tabacum* and *Arabidopsis thaliana* epidermal strips

3.4.4.1 Preparation

The epidermal strips were peeled from leaves of 5-6 week-old tobacco plants or 6-7 week-old *Arabidopsis* plants and glued with Medical Adhesive B to cover slips with adaxial side down. Epidermal strips from *N. tabacum* leaves recovered in standard leaf solution containing 1 mM $CaCl_2$ while epidermal strips from *Arabidopsis thaliana* leaves recovered in *Arabidopsis* standard solution (50 µM $CaCl_2$, 1 mM KCl, 10 mM MES with pH = 5.8 adjusted by BTP) for 3-6 h under a white light lamp (ca. 20-25 µmol m^{-2} s^{-1}) at room temperature before experiments.

For monitoring vacuolar pH, *N. tabacum* epidermal strips were firstly incubated with a vacuolar pH indicator 2,7-bis-(2-carboxyethyl)5-(and-6)-carboxyfluorescein (BCECF) acetoxymethyl ester (AM) (15 µM) (Invitrogen, diluted in DMSO) for 2 h before starting the experiments and then washed BCECF dye out with leaves standard solution and recovered for another 2-4 h. After the BCECF dye entered into the vacuole, following experiments were performed.

3.4.4.2 Solutions

Guard cells were perfused with a solution (0.1/1 mM KCl, 0.01/1 mM $CaCl_2$, 10 mM MES, pH 5.8 adjusted with BTP) very often used to incubate *N. tabacum* or *Arabidopsis thaliana* leaves as it mimicks the apoplast conditions for specific experiments. The effectors used including ABA, flg22, H_2O_2, butyric acid (BTA; SigmaAldrich), sodium vanadate (Na_3VO_4), NaCl, KCl, mannitol (diluted in water, SigmaAldrich) were added into control solutions, respectively, and pH of the solutions were corrected with BTP if required. For guard cells experiments upon 50 mM NaCl

treatment, control solution (75 mM MES, 1 mM $CaCl_2$, adjusted pH = 5.8 with Tris) was used to balance osmolality. The perfusion procedure was the same as that in leaves.

3.5 Confocal imaging

Subcellular localization of CapHensor in plants, screening and expression level verification of transgenic lines and CapHensor imaging in *N. tabacum* roots were performed on a Leica TCS SP5 II confocal laser scanning microscope equipped with a HCX IRAPO 25x/0.95 objective. The excitation laser line for PRpHluorin and R-GECO1 was 476 nm and 561 nm, respectively, while emission fluorescence was captured at 530 ± 30 nm and 617 ± 26 nm, respectively. The autofluorescence derived from chlorophyll was captured at 680 ± 37 nm. The details were described previously [339].

3.6 Live-cell imaging

Live-cell fluorescence imaging of pollen tubes, guard cells and leaves expressing CapHensor were performed on an inverted Zeiss microscope AxioObserver (Carl Zeiss). The details were described previously [339]. The imaging hardware and settings were controlled by VisiView software (Visitron Systems). The microscope was equipped with the VisiChrome High-Speed Polychromator System (Visitron Systems) for fluorophore excitation and an EMCCD camera (Photometrics) to capture fluorescence with a 512 X 512 pixel chip. Based on the different size of cells, 20x, 40x and 60x objectives (Carl Zeiss) were used for *N. benthamiana* mesophyll cells, *N. tabacum* guard cells & pollen tubes and *Arabidopsis thaliana* guard cells, respectively. To record PRpHluorin and R-GECO1 fluorescence simultaneously, a dual-band dichroic mirror (ET, Chroma 59001bs) was used and combined with a high-speed filter wheel (Ludl Electronic Products Ltd.) equipped with bandpass filters (AF Analysentechnik, Chroma Technology Corporation) for PRpHluorin (ET 525 ± 25 nm) and R-GECO (ET 605 ± 26 nm) (Semrock Inc.), respectively. For BCECF imaging on *N. tabacum* guard cells, the excitation spectra were 440 nm and 500 nm while a YFP (ET 535 ± 15 nm) bandpass filter was used to capture the fluorescence. For plants expressing GCaMP3, a YFP (ET 535 ± 15 nm) bandpass filter was used to capture the fluorescence under 10x objective. The ratiometric PRpHluorin was excited at 400 nm and 470 nm for H^+ ratio calculation while R-GECO1 was excited at 540 nm. To identify the isosbestic point, 400, 405, 410, 415, 420, 425, 435

nm were used to excite PRpHluorin. The live-cell imaging protocol for CapHensor imaging contained the illumination of R-GECO1 at 540 nm and PRpHluorin at 400, 415 and 470 nm. A brightfield image was generated with a white LED illumination using the (ET 525 ± 25 nm) filter in the filterwheel. In case of pollen tube recording, the time intervals for each series of exposure were 2 s and 3 s, when combined with or without electrical recordings, respectively. The time intervals in live-cell imaging of guard cells and leaves were 5 s and 3 s, respectively. Image processing was performed on personal computer with FIJI/IMAGEJ v.1.50. For guard cells, a custom-made Fiji macro (Table 10) was used to detect and quantify the aperture area, indicative for stomatal movement. Data were further processed and plotted by specific R-scripts (see below) and IGOR PRO 5.02 software (Wavemetrics Inc., Portland, OR, USA).

Table 10. Macros for aperture area detection

```
        run("Duplicate...", "duplicate");
        run("Set Scale...", "distance=250 known=100 pixel=1 unit=um global");
        setAutoThreshold("Default dark");
        //run("Threshold...");
        setOption("BlackBackground", false);
        run("Convert to Mask", "method=Default background=Dark calculate");

        //setTool("wand");
        //run("Wand Tool...", "tolerance=2 mode=Legacy");

        {               frames=nSlices;

                for(i=0; i<frames; i++){
                        currentslice=i+1;
                        setSlice(currentslice);
                        run("Set Scale...", "distance=2.5 known=1 pixel=1
        unit=µm");
                        run("Select None");
                        //setTool("wand");
                        doWand(xx, xx, 2, "Legacy");
                        roiManager("Add");
                        run("Measure");
                        run("Select None");
                }
}
```

3.7 Membrane potential recordings

3.7.1 Voltage recordings in pollen tubes

Glass-microelectrodes (Hilgenberg, 1 mm outer diameter and 0.58 mm inner diameter) were pulled on a horizontal laser puller (P2000; Sutter Instruments), which was described in detail before [358]. Then, the electrode was filled with 300 mM KCl and connected with a silver wire to the pre-amplifier of a TEC-05X amplifier (npi electronic, Tamm, Germany). The ground electrode was filled with 300 mM KCl and 2 % low-melt agarose at the tip as the reference. The current clamp protocols were performed by WINEDR software (University of Strathclyde, Glasgow, UK). The electrode positions were controlled by a micromanipulator (Sensapex SMX, Finland).

N. tabacum pollen grains were germinated and grown for 3-4 h under dark conditions prior to electrode impalement. The microelectrode was put along the growing pollen tubes and then the live-cell imaging and free running membrane potential recordings were started at the same time. Several minutes later, the microelectrode was gently impaled into the pollen tube at either the shank. The resistance of electrodes used was usually between 60-120 MΩ.

3.7.2 Voltage recordings in mesophyll cells

The same microelectrodes as described in 3.7.1 were used to record membrane potentials in *N. benthamiana* mesophyll cells that recovered overnight in darkness. The electrode was impaled in the mesophyll until the values were stable and then the live-cell imaging and membrane potential recording were started simultaneously. All experiments were performed in the presence of a perfusion system with a speed of 700 µl min^{-1}.

3.8 Quantitative analysis

3.8.1 Image J

FIJI/IMAGEJ was used to extract the fluorescent intensity over time of the image-stacks from VisiView. In detail, fluorescence intensity of guard cells and mesophyll cells was extracted. The PRpHluorin was excited at two wavelengths to image H^+ change and at a wavelength called the isosbestic point at which the fluorescence does not change upon pH changes shown in Fig. 6d. Thus relative H^+ and Ca^{2+} concentrations were calculated by the fluorescent intensity of

PRpHluorin at 470 nm and 400 nm which were divided (H^+ ratio = PRpHluorin470nm/PRpHluorin400nm) and the fluorescent intensity of R-GECO1 divided by the fluorescence of PRpHluorin at the isosbestic point which was proven to be at 415 nm excitation (Ca^{2+} ratio = R-GECO1/PRpHluorin415nm), respectively. The vacuolar H^+-ratio of guard cells transiently expressing BCECF dye was calculated by fluorescent intensity at 440 nm dividing fluorescent intensity at 500 nm (H^+ ratio = F_{440}/F_{500}). These ratio calculations were done by the 'image calculator' tool in FIJI/IMAGEJ. The aperture of guard cells were detected using the 'Wand' tool in FIJI/IMAGEJ with the fluorescent image at 470 nm wavelength (Table 10). Subsequent phase analysis, correlation and wavelet transforms were performed with the open source software R (GNU software project) v.3.6 (see 'R scripts'). The fluorescence intensity from *N. benthamiana* leaves stably expressing GCaMP3 was extracted in FIJI/IMAGEJ.

Ca^{2+}- and H^+-ratio analysis of pollen tubes fluorescence was done by the 'image calculator' tool in FIJI/IMAGEJ as described for guard cells and mesophyll cells. Kymographs were generated in FIJI/IMAGEJ by the 'multiple kymograph' plugin and quantification of H^+ ratio (PRpHluorin470nm/PRpHluorin400nm), Ca^{2+} ratio (RGECO1/PRpHluorin415nm), Ca^{2+} raw (R-GECO1) at the tip (1–5 µm behind the tip) and at the shank (35–40 µm behind the tip) and polar growth velocity were performed with R-scripts based on the CHUKNORRIS algorithm [160]. Subsequent coherence analysis on pollen tubes was performed with R v.3.6 (see 'R scripts').

3.8.2 R scripts

The quantification analysis for periodic signals was performed by cross-wavelet and cross-correlation methodology. I would like to show great gratitude to our collaborator Juan Prada providing us these R-scripts and explaining to use these R-scripts. In pollen tubes, the interrelation between Ca^{2+}, H^+, growth rate and V_m were quantified by R-scripts named 'experiments_auto_analysis', 'phase_analysis', 'CrossWaveGraph_pollen', 'pollen_voltage_script' and 'phase_analysis_voltage'. For spontaneous oscillations in guard cells, two R-scripts called 'Guard_excelfile_analysis_new' and 'phase_analysis_guard' were used to analyze the phase relationship between Ca^{2+} and H^+. For some signals without periodic oscillations, only one big transient was observed. Thus, for the time and values of the onset and the peak of Ca^{2+}, H^+ and aperture in guard cells and Ca^{2+}, H^+ and V_m in leaves were both quantified by the

same R-script ‘leaves_analysis’. The onset time point was identified with the package ‘baseline’ [359], which indicates the constant increase compared to the baseline in the control solutions. The wavelet analysis was interpreted with the help of the package WaveletComp [360] to identify the frequency of different signals and the phase relationships between Ca^{2+} and H^{+}, Ca^{2+} and growth as well as H^{+} and growth. A running window correlation was performed to verifiy correlations between two oscillatory signals such as spontaneous oscillations between Ca^{2+} and H^{+}. All analysis was performed with R version 3.6. All the analysis in this thesis was done in personal computer.

3.9 Statistical analysis

Traces are demonstrated by means ± standard errors (SEs). An unpaired t-test and one-way ANOVA were performed by GRAPHPAD software (GraphPad Software Inc.) and ORIGINPRO software (OriginLab, Northampton, MA, USA), respectively. Significant differences were compared with p values (*, $p < 0.05$; **, $p < 0.01$; ***, $p < 0.001$; ****, $p < 0.0001$).

4 Results

4.1 Design and functional verification of CapHensor

4.1.1 Design scheme of CapHensor

To monitor intracellular Ca^{2+} and H^+ dynamics and possible interactions of both second messengers simultaneously in the same cell, I designed a construct combining a pH biosensor and a Ca^{2+} biosensor, we named CapHensor. I generated constructs with two spectral distinct genetically encoded indicators: PRpHluorin, a pH-sensitive ratiometric green fluorescent protein [113] which was optimized for application in plants [361] and the red fluorescent Ca^{2+} sensor R-GECO1 with high sensitivity to Ca^{2+} changes [101]. Since proton gradients between the tip and the shank exist in pollen tubes, ratiometric detection of relative cytosolic H^+ concentrations ($[H^+]_{cyt}$) was performed with PRpHluorin after transient expression in pollen tubes, shown as the pseudocolored image (Fig. 6a). PRpHluorin has a bi-phasic excitation spectra with two peaks (400 nm and 470 nm) shifting reciprocally with changes in cellular pH and an isosbestic point which is insensitive to pH changes (Fig. 6b). Thus the ratiometric H^+ ratio (rel. H^+) was calculated in the way that the PRpHluorin fluorescent intensity when excited at 470 nm was divided by the fluorescent intensity when excited at 400 nm (Fig. 6c). The isosbestic point of PRpHluorin, the wavelength which shows pH insensitive characteristics, was used to perform the calculations for detecting Ca^{2+} ratiometrically (Fig. 6c). The isosbestic point has been monitored *in vitro* [113], however, I visualized the isosbestic point *in vivo* in living cells under biological conditions to exclude spectral shifts in different cell types including mesophyll cells, pollen tubes and guard cells (Fig. 6d, S1). To precisely verify the isosbestic point, seven excitation wavelengths were chosen from 400 nm to 435 nm in mesophyll cells transiently expressing CapHensor, in pollen tubes and guard cells stably expressing CapHensor. Acetate (HAc), a weak acid, was used here to acidify the cytosol while the extracellular medium was adjusted to normal medium condition with pH 5.8 to vary cellular pH while monitoring the fluorescence over time at the different wavelengths close to the isosbestic point (Fig. 6d, S1). The protonated form of HAc was reported to permeate membranes and release protons inside to acidify the cytosol [362]. The PRpHluorin intensity at 415 nm showed insensitivity to pH changes by HAc treatment because there were no fluorescence changes upon cytosolic acidification while fluorescence at other wavelengths (higher or lower than 415 nm) either increased or decreased upon cytosolic acidification (Fig. 6d, S1). The characteristics of the CapHensors' isosbestic point were extremely important to set up the proper imaging technique to

allow ratiometric Ca^{2+} detection. Thereby ratiometric Ca^{2+} values (rel. Ca^{2+}) were calculated by dividing the fluorescent intensity of R-GECO1 at 540 nm by that of PRpHluorin at the isosbestic point (PRpHluorin 415 nm) (Fig. 6c).

To monitor Ca^{2+} and H^+ in the same cell, pH sensor PRpHluorin and Ca^{2+} sensor R-GECO1 were combined into one construct by a self-cleavage P2A sequence [354] to possibly obtain equal expression of both biosensors under LeLAT52 promoter in pollen tubes (Fig. 6e, f). A spatial separation of the two fluorescent proteins prevent FRET events to occur that would cause the two fluorophores to influence each other. By using the P2A sequence, the direct fluorescence intensity changes from each biosensor can be used to calculate the H^+ ratio and Ca^{2+} ratio according to the formula provided in Fig. 6c. The fluorescent intensity of PRpHluorin could be well visualized whereas the red fluorescence of R-GECO1 was comparably low (Fig. 6e) because of a relatively lower quantum yield of red fluorescent protein compared with green fluorescent protein [363]. To overcome the low fluorescence level, CapHensor was optimized by fusing two R-GECO1 open reading frames (ORFs) (Fig. 6f) in tandem to double the amount of R-GECO1 proteins being expressed in the cell to improve the intensity of red fluorescence and thus to impove the signal-to-noise ratio for high quality imaging. Since fluorescent proteins tend to accumulate in the nuclei [364], the nuclear export sequence (NES) was used to target CapHensor exclusively into the cytosol to monitor $[Ca^{2+}]_{cyt}$ and $[H^+]_{cyt}$ signals avoiding mixed signals from other compartments in pollen tubes (Fig. 6e, f). Quantitative Ca^{2+} ratio measurements in pollen tubes showed CapHensor with two R-GECO1 to result in the double amount of fluorescent intensity compared with one R-GECO1 (Fig. 6g). The optimized design of the CapHensor construct (Fig. 6f) was used to stably transform in *Nicotiana tabacum* plants driving CapHensor expression under the pollen specific promoter.

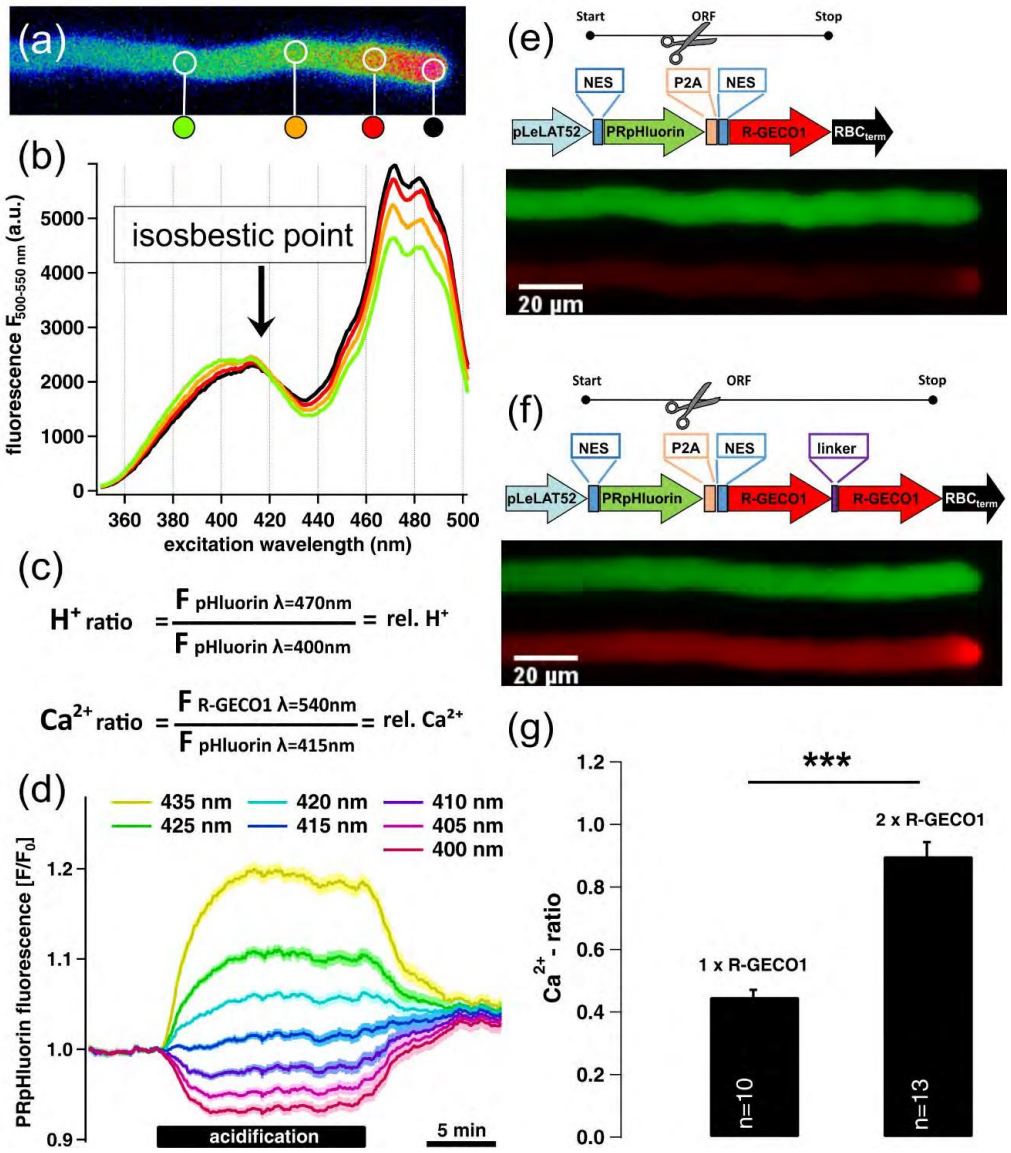

Figure 6. Design, verification and optimization of CapHensor.

The design and concept of CapHensor constructs in *Nicotiana tabacum* pollen tubes. (a) False colored $[H^+]_{cyt}$ ratio from pollen tube transiently expressing PRpHluorin. The color from the red to the blue stands for higher H^+ concentrations (tip, low pH) and lower H^+ concentration (shank, high pH). (b) The excitation spectra of PRpHluorin are displayed in the same color as colors marked by circles in (a). The isosbestic point of excitation spectrum at 415 nm has the property of being insensitive to pH (indicated by the black arrow), which is verified in (d). (c) Formulas of calculation of Ca^{2+} and H^+ ratios representing relative Ca^{2+} and H^+ concentrations, respectively. (d) Mean fluorescence of PRpHluorin in *N. benthamiana* mesophyll cells (n = 67) at seven different wavelengths under 5 mM acetate (HAc). The PRpHluorin fluorescence is unaltered at 415 nm in spite of effective responses excited at other wavelengths. (e and f) The design scheme of CapHensor containing PRpHluorin (pH sensor, green emission) and R-GECO1 (Ca^{2+} sensor, red emission) with single (e) or double (f) R-GECO1 in pollen tubes stably expressing the CapHensor version shown above. The self-cleavage P2A sequence is used to separate the two sensors in the ORF marked by the scissors. (g) Mean values of Ca^{2+} ratio from the shank of pollen tubes expressing constructs shown in (e) and (f). t-test was used in g. ***, $p < 0.001$.

4.1.2 Verification of CapHensor in *Nicotiana tabacum* pollen tubes

To further verify PRpHluorin and R-GECO1 in the CapHensor approach to function as pH and Ca^{2+} sensor, respectively, extracellular medium pH was varied and a hypo-shock was applied via a perfusion system on pollen tubes (Fig. 7a) to evoke changes in cellular $[Ca^{2+}]_{cyt}$ and $[H^+]_{cyt}$, respectively. Dynamics of $[H^+]_{cyt}$ ratio, $[Ca^{2+}]_{cyt}$ ratio and growth rate of pollen tubes were displayed by false colored kymographs, a graphical representation to visualize the dynamics in growth, $[Ca^{2+}]_{cyt}$ and $[H^+]_{cyt}$ along the pollen tube (Fig. 7a). The treatments were applied from the time point marked by white arrows and washed out until the next treatment was applied. The fluorescent intensity of tip $[H^+]_{cyt}$ ratio (green line), tip $[Ca^{2+}]_{cyt}$ ratio (red line) and growth rate (blue line) were extracted from kymographs similar to the representative example in Fig. 7a using the CHUKNORRIS algorithm, a set of statistical tools [160] to quantify signal intensity and growth rate over time. The average data from 12 cells extracted by the CHUKNORRIS was illustrated in Fig. 7b. According to the fact that H^+ influx likely mediated by H^+-channel occurs at the pollen tube tip [76] (Fig. 2), external medium with pH 5.0 acidified while pH 6.8 alkalized the cytosol at the tip (Fig. 7a, b), indicating that PRpHluorin functions well as a pH sensor in pollen tubes. A hypo-osmotic shock was reported to induce intracellular Ca^{2+} transients [4] by activating mechanosensitive Ca^{2+}-permeable channels. Since mechanosensitive Ca2+-permeable channels such as MSL8 exist in pollen tubes [37,56,145]. This type of stimulus was applied on pollen tubes to confirm the Ca^{2+} sensor R-GECO1 functioning in CapHensor since tip $[Ca^{2+}]_{cyt}$ increases occured upon hypoosmotic shock (Fig. 7a, b). R-GECO1 fluorescence was reported to increase upon elevated pH [101,108], however this was not observed in my study, since $[Ca^{2+}]_{cyt}$ increases and decreases in case of a cytosolic acidification or alkalization, respectively (Fig. 7a, b). Therefore, $[Ca^{2+}]_{cyt}$ and $[H^+]_{cyt}$ changes can be manipulated by extracellular stimuli and were used to show here that the two biosensors in CapHensor do not interfere with each other.

4.2 The role of $[Ca^{2+}]_{cyt}$ and $[H^+]_{cyt}$ in pollen tube growth

4.2.1 Tip $[H^+]_{cyt}$ correlates better with growth than does tip $[Ca^{2+}]_{cyt}$

After verifying functioning of the CapHensor to spatially and temporally monitor $[Ca^{2+}]_{cyt}$ and $[H^+]_{cyt}$, the roles of these two signals for pollen tubes growth were studied by applying a series of extracellular treatments (Fig. 7). Since changes in $[H^+]_{cyt}$ had physiological significance during pollen tube growth [75,77,365], but, its exact role is unknown, I quantified and compare the correlation

of $[H^+]_{cyt}$ and growth as well as $[Ca^{2+}]_{cyt}$ and growth. For this purpose, CapHensor imaging was performed side-by-side with growth velocity analysis when extracellular pH was modified to change cytosolic pH (Fig. 7a, b). In case the medium with pH 5.8 was exchanged to the same medium with pH 5.0 apical growth was stimulated whereas the growth was arrested upon extracellular alkalization condition with pH 6.8 (Fig. 7a, b). The ceased growth was restored while switching back to normal growth medium (Fig. 7a, b). Hypo-osmotic shock resulted in transient $[Ca^{2+}]_{cyt}$ and $[H^+]_{cyt}$ increases at the tip (Fig. 7a, b). The results from this experiment indicated $[H^+]_{cyt}$ accentuation or dissipation at the tip by extracellular pH alterations were involved in regulating growth speed (Fig. 7a, b). To reveal if this effect is based on extracellular or intracellular pH changes, 2 mM HAc was used to acidify the cytosol while the extracellular medium remained unchanged at pH 5.8 (Fig. 7c). By exclusive cytosolic acidification through 2 mM HAc at the tip, the growth rate was stimulated as well (Fig. 7c), which suggested cytosolic pH changes to play a crucial role in apical growth and probably $[H^+]_{cyt}$ to have signaling function. Another interesting phenomenon was that cytosolic acidification was always accompanied by $[Ca^{2+}]_{cyt}$ elevation (Fig. 7a-c). Hence I wanted to study the role of $[Ca^{2+}]_{cyt}$ rise in pollen tube growth. Caffeine was identified to inhibit pollen tubes growth by dissipation of tip $[Ca^{2+}]_{cyt}$ gradients [129,131,133]. Therefore, 3 mM caffeine was applied to pollen tubes for 10 min and then washed out (Fig. 7d and 7e). Pollen tubes growth was indeed suppressed by 3 mM caffeine, accompanied by tip $[Ca^{2+}]_{cyt}$ reduction but also fast and strong dissipation of the $[H^+]_{cyt}$ gradient (Fig. 7d, e, n = 8). Surprisingly, tip $[H^+]_{cyt}$ almost returned to the basic level after washing caffeine out whereas tip $[Ca^{2+}]_{cyt}$ only slightly recovered (Fig 7d, e, triangle, t = 20-30 min). During re-gain of growth velocity, only the $[H^+]_{cyt}$ gradient, but barely the $[Ca^{2+}]_{cyt}$ gradient re-established (Fig. 7d, e). To further investigate and quantify if either tip $[Ca^{2+}]_{cyt}$ or tip $[H^+]_{cyt}$ regulates pollen tubes growth, correlation coefficient between growth and apical $[Ca^{2+}]_{cyt}$ ratio as well as growth and apical $[H^+]_{cyt}$ ratio during promoted growth or regrowth were quantified in selected time windows marked by symbols in Fig. 7a-e (Fig. 7f). The correlation coefficient of 0 symbolizes no correlation while correlation coefficient equals to 1 symbolizes identical signals. In detail, correlation coefficients between growth and tip $[H^+]_{cyt}$ ratio regimes (green bars) were 0.51 ± 0.03 and 0.30 ± 0.07 while the cross-correlation value between growth and $[Ca^{2+}]_{cyt}$ ratio was 0.33 ± 0.03 and -0.01 ± 0.06 when the cytosol was acidified with pH 5.0, respectively (Fig. 7b, square, t = 15-25 min; Fig. 7c, white circle, t = 50-60 min). When pollen tubes started to re-grow after a growth arrest (Fig. 7b, diamond, t = 55-75 min; Fig.

7e, triangle, t = 20-30 min), correlations between growth and tip $[H^+]_{cyt}$ ratio were 0.36 ± 0.05 and 0.41 ± 0.03 while the values for growth and $[Ca^{2+}]_{cyt}$ ratio were 0.05 ± 0.05 and 0.27 ± 0.04, respectively. Except HAc treatment (Fig. 7c, black circle, t = 15-25 min) with correlation coefficient at the level of 0.18 ± 0.07 between growth and tip $[Ca^{2+}]_{cyt}$ and 0.27 ± 0.06 between growth and tip $[H^+]_{cyt}$, significantly better correlation values were observed for growth and $[H^+]_{cyt}$ (green bars) than for growth and $[Ca^{2+}]_{cyt}$ ratio (red bars) (Fig. 7f). In conclusion, better correlation between growth and tip $[H^+]_{cyt}$ rather than tip $[Ca^{2+}]_{cyt}$ revealed tip $[H^+]_{cyt}$ gradients probably are more important than tip $[Ca^{2+}]_{cyt}$ gradients to promote growth (Fig. 7f), which is consistent with recent genetic and pharmacological studies revealing the importance of $[H^+]_{cyt}$ gradients in regulation of pollen tubes growth [75,366].

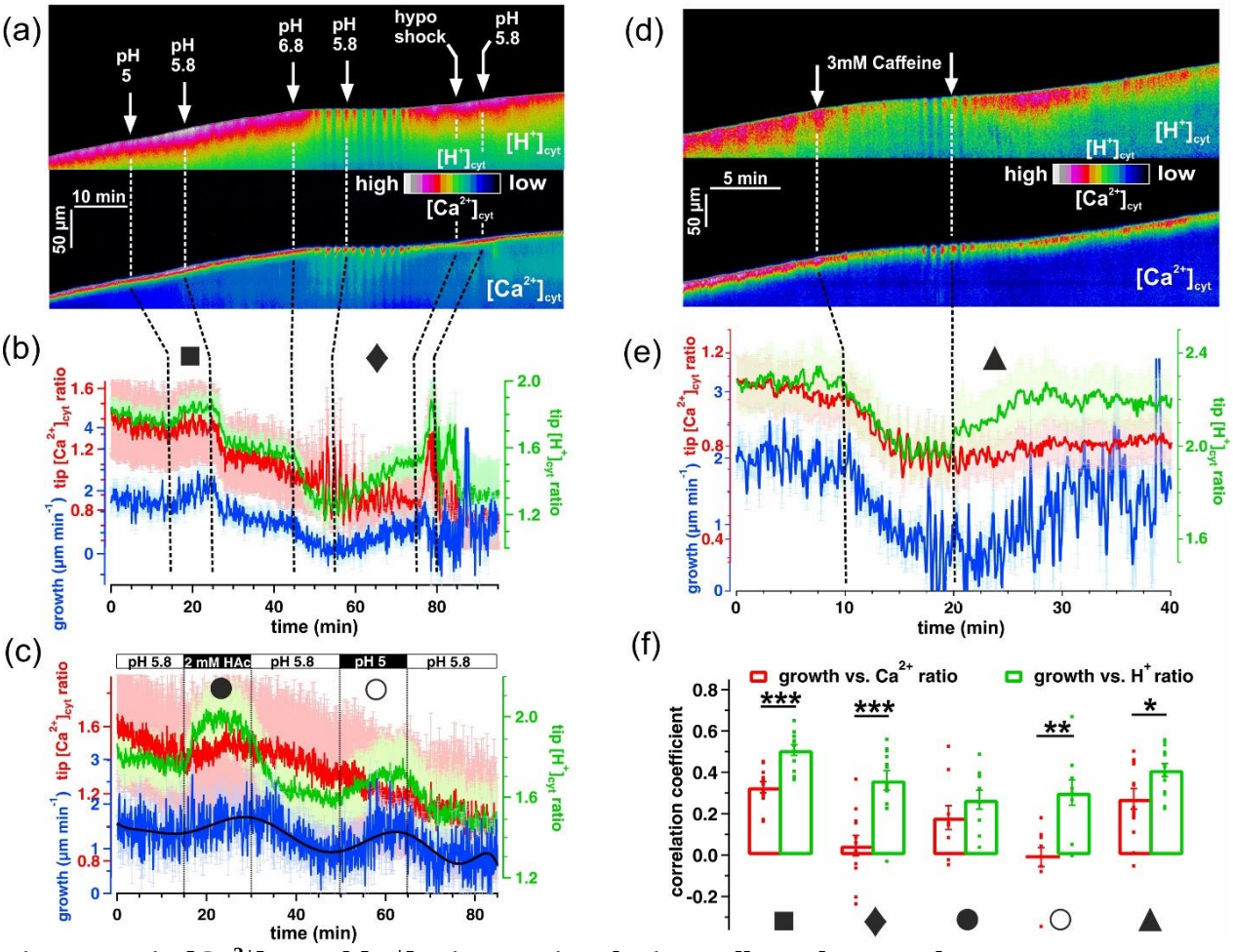

Figure 7. Tip $[Ca^{2+}]_{cyt}$ and $[H^+]_{cyt}$ interaction during pollen tube growth.

Live-cell imaging of *N. tabacum* pollen tubes stably expressing CapHensor to quantify spatio-temporal $[Ca^{2+}]_{cyt}$, $[H^+]_{cyt}$ at the tip with apical growth during different treatments. (a) False colored $[H^+]_{cyt}$ ratio (top)

and $[Ca^{2+}]_{cyt}$ ratio (bottom) kymographs from a representative pollen tube stably expressing CapHensor in time-lapse imaging with a sequence of external solution exchanges with different pH or low osmolality (hypo shock) marked by white arrows and washed out by the next treatment. (b) Quantification of mean $[Ca^{2+}]_{cyt}$- (red), $[H^+]_{cyt}$- (green) ratio at the tip and growth rate (blue) from measurements (n = 12) with the same experimental design shown in (a). (c) Quantification of mean $[Ca^{2+}]_{cyt}$- (red), $[H^+]_{cyt}$- (green) ratio at the tip and growth rate (blue) from measurements (n = 8) under 2 mM HAc treatment or extracellular acid medium (pH 5) to acidify the cytosol. (d) False colored $[H^+]_{cyt}$ ratio (top) and $[Ca^{2+}]_{cyt}$ ratio (bottom) kymographs from a representative pollen tube stably expressing CapHensor in time-lapse imaging perfusion with 3 mM caffeine (marked by white arrows). (e) Quantification of mean tip $[Ca^{2+}]_{cyt}$- (red), $[H^+]_{cyt}$- (green) ratio and growth rate (blue) from measurements (n = 15) with the same sequence of treatment as in (d). (f) Quantification of correlation coefficient between growth rate (blue traces) and tip $[Ca^{2+}]_{cyt}$ ratio (red traces), growth and tip $[H^+]_{cyt}$ ratio (green traces) changes in the phase of stimulated growth or regrowth from measurements in (b, ■, 15–25 min; ♦, 55–75 min), (c, ●, 15–25 min; ○, 50-60 min) and (e, ▲, 20–30 min). Error bars = SE. Dots in (f) represent individual experiments and t-test was used. *, $p < 0.05$; **, $p < 0.01$; ***, $p < 0.001$.

4.2.2 Oscillatory patterns of $[Ca^{2+}]_{cyt}$, $[H^+]_{cyt}$ and growth in pollen tubes

Pollen tubes growth displays an oscillatory mode while $[Ca^{2+}]_{cyt}$ and $[H^+]_{cyt}$ oscillations are also reported [75,117,134]. However, how oscillatory growth velocity is associated with $[Ca^{2+}]_{cyt}$ and $[H^+]_{cyt}$ still remains obscure. To verify coherence between $[Ca^{2+}]_{cyt}$, $[H^+]_{cyt}$ and growth in pollen tubes, extracellular medium with high Cl^- concentration was applied, known to often cause oscillatory behavior [125,130]. The fluorescent intensity of tip $[H^+]_{cyt}$, tip $[Ca^{2+}]_{cyt}$ and growth rate of a representative pollen tube of Fig. 8a were extracted and illustrated (Fig. 8b). Indeed, high extracellular Cl^- induced more pronounced tip $[Ca^{2+}]_{cyt}$-, $[H^+]_{cyt}$- ratio and growth oscillations (Fig. 8a, b). Interestingly, higher frequency of tip $[Ca^{2+}]_{cyt}$ and $[H^+]_{cyt}$ oscillations was triggered when the extracellular medium was switched to pH 6.8 in spite of abrogated growth (Fig. 8a, b). To compare the properties of oscillations among the three parameters, phase analysis was performed through wavelet and cross-wavelet analysis on representative sequences (Fig. 8a, b). The dynamics of oscillatory power and period of $[Ca^{2+}]_{cyt}$ and $[H^+]_{cyt}$ ratio were displayed in the wavelet spectra (Fig. 8c). The periods of tip $[Ca^{2+}]_{cyt}$ ratio and tip $[H^+]_{cyt}$ ratio oscillations over time in pollen tubes during growth or non-growth states were quantified, showing the oscillatory frequency in growing pollen tubes was approximately one-third compared with that when pollen tubes stopped growth (Fig. 8d). Monitoring $[Ca^{2+}]_{cyt}$ and $[H^+]_{cyt}$ in the same cell simultaneously provided the possibility to compare the interconnection between tip $[Ca^{2+}]_{cyt}$, tip $[H^+]_{cyt}$ and growth in a highly accurate way. The cross-correlation of two signals between tip $[Ca^{2+}]_{cyt}$ ratio and growth, tip $[H^+]_{cyt}$ ratio and growth, tip $[Ca^{2+}]_{cyt}$ ratio and tip $[H^+]_{cyt}$ ratio was quantified in growing and non-growing

pollen tubes (Fig. 8e). The results displayed both apical $[Ca^{2+}]_{cyt}$ and $[H^+]_{cyt}$ oscillations lagged behind growth oscillations (Fig. 8e) since $[Ca^{2+}]_{cyt}$ and $[H^+]_{cyt}$ oscillations both shifted to the right side of the dotted lines. However, apical $[H^+]_{cyt}$ oscillations preceded tip $[Ca^{2+}]_{cyt}$ oscillations in growing pollen tubes while the relationship was reversed in non-growing pollen tubes (Fig. 8e).

Due to the fact that cross-correlation analysis tends to analyze signals with constant oscillatory parameters and thus lacks any temporal information or dynamics [160], wavelet transformation analysis was performed and used to quantify not only the correlations but the order and the time shift between two signals over time we called phase analysis [367] (Fig. 8f). The wavelet analysis uses decomposing the time-series into a window with time frequency to identify the main patterns of oscillatory variations and displays how these patterns vary over time by providing wavelet spectra and phase analysis [367]. Phase shifts of two oscillations are converted into radians (π, $-\pi$) in order to compare better between different experiments and even between species through normalizing for the period of oscillations [117]. The phase analysis can be quantified in terms of radians with signs and time of phase shifts (n = 10, Fig. 8f) of the experimental data. The phase shifts from cross-wavelet analysis displayed similar coherence between the growth rate and apical $[Ca^{2+}]_{cyt}$ ratio or $[H^+]_{cyt}$ ratio (Fig. 8f) compared with cross-correlation analysis (Fig. 8e), demonstrating the ability of both methods to display the correct phase relationships that tip $[Ca^{2+}]_{cyt}$ and $[H^+]_{cyt}$ both lagged behind growth (Fig. 8e, f). Tip $[H^+]_{cyt}$ oscillations lagged behind growth oscillations by 17.87 ± 0.46 s, but preceded tip $[Ca^{2+}]_{cyt}$ oscillations by 14.55 ± 0.60 s (Fig. 8f), which was different from previous reports in terms of H^+ oscillations lagging behind Ca^{2+} oscillations, despite that $[Ca^{2+}]_{cyt}$ was observed also to lag behind growth [117,134]. When the signals are put in a temporal context, growth occurs first, followed by tip $[H^+]_{cyt}$ oscillations and finally by tip $[Ca^{2+}]_{cyt}$ oscillations (Fig. 8e, f). In agreement with the cross-correlation analysis (Fig. 8e), phase relationships between tip $[Ca^{2+}]_{cyt}$ and $[H^+]_{cyt}$ oscillations were inverted in non-growing oscillating pollen tubes, in which tip $[Ca^{2+}]_{cyt}$ oscillations preceded tip $[H^+]_{cyt}$ oscillations by 14.36 ± 1.42 s in alkalized media with pH 6.8 (Fig. 8f).

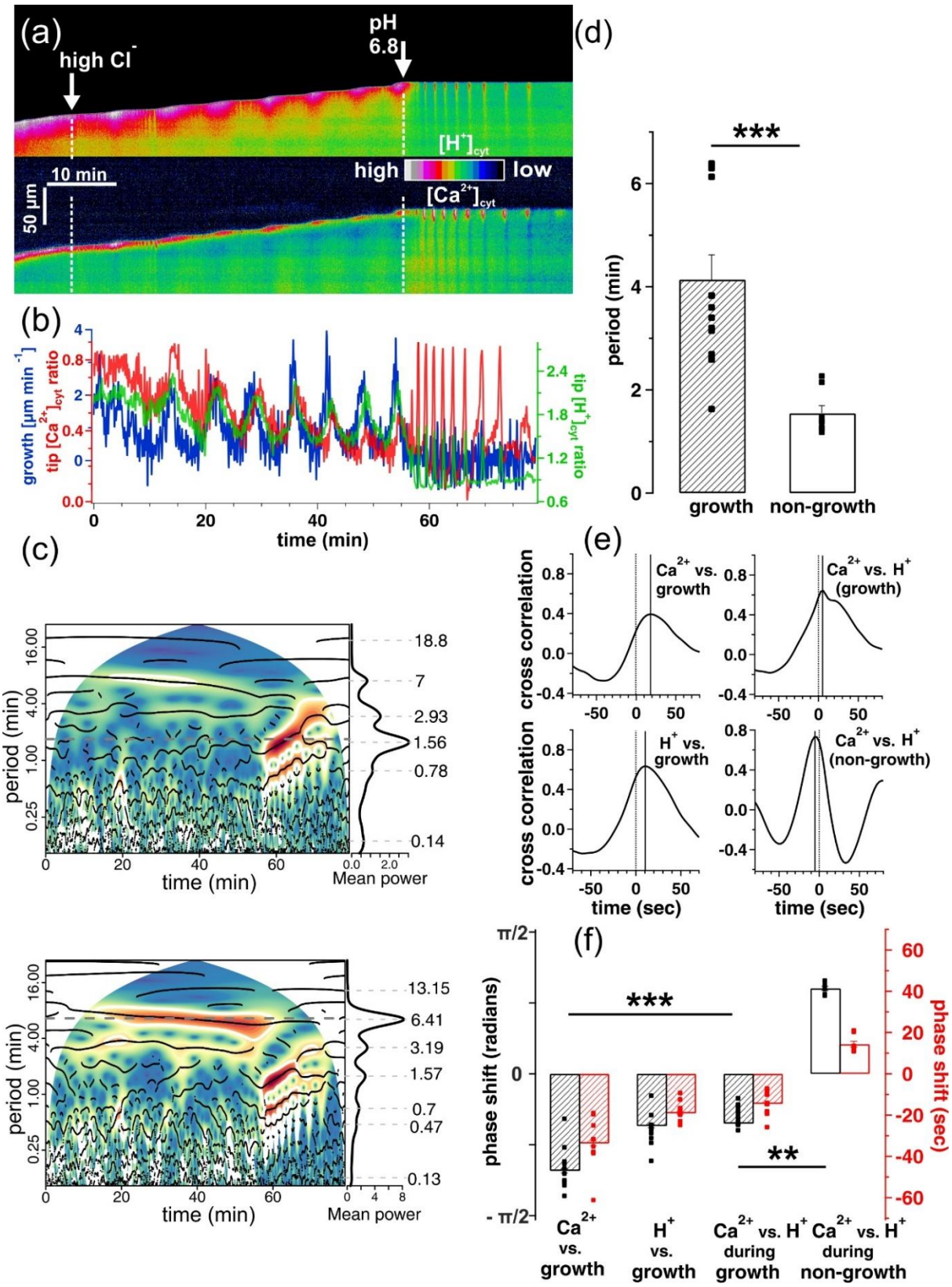
(a)
high Cl-
pH 6.8
[H+]cyt
high
low
[Ca2+]cyt
10 min
50 µm
(b)
growth [µm min-1]
tip [Ca2+]cyt ratio
tip [H+]cyt ratio
time (min)
(c)
period (min)
time (min)
Mean power
18.8
7
2.93
1.56
0.78
0.14
13.15
6.41
3.19
1.57
0.7
0.47
0.13
(d)
***
period (min)
growth
non-growth
(e)
Ca2+ vs. growth
Ca2+ vs. H+ (growth)
H+ vs. growth
Ca2+ vs. H+ (non-growth)
cross correlation
time (sec)
(f)
phase shift (radians)
phase shift (sec)
***
**
Ca2+ vs. growth
H+ vs. growth
Ca2+ vs. H+ during growth
Ca2+ vs. H+ during non-growth

Figure 8. Phase relations between $[Ca^{2+}]_{cyt}$, $[H^+]_{cyt}$ and growth in oscillating pollen tubes.

Live-cell imaging of oscillating *N. tabacum* pollen tubes stably expressing CapHensor to quantify spatio-temporal interactions of $[Ca^{2+}]_{cyt}$ and $[H^+]_{cyt}$ with growth. (a) False colored $[H^+]_{cyt}$ ratio (top) and $[Ca^{2+}]_{cyt}$ ratio (bottom) kymographs from a representative pollen tube in response to extracellular medium containing 20 mM chloride (Cl^-) and followed by both 20 mM Cl^- and pH 6.8 medium at the time point marked by white arrows. (b) Quantification of tip $[Ca^{2+}]_{cyt}$- (red), $[H^+]_{cyt}$- (green) ratio and growth rate (blue) from the experiment in (a). (c) Wavelet spectra of period dynamics (vertical axis) and mean power of tip $[Ca^{2+}]_{cyt}$- (top) and $[H^+]_{cyt}$- (bottom) ratio oscillations over time of a representative pollen tube upon extracellular medium with high Cl^- and pH 6.8. The significant phase correlations are displayed by the area ($p < 0.05$) borded with white lines shown as the red color. (d) Bar diagram of mean period of $[Ca^{2+}]_{cyt}$- and $[H^+]_{cyt}$- ratio oscillations in growing (shadow, n = 13) and non-growing (white, n = 8) pollen tubes in high Cl^- solution with pH 5.8 or pH 6.8 medium. (e, f) Quantification of phase-relations between three parameters through cross-correlation (e) and cross-wavelet analysis (f) from growing (n = 10) and non-growing (n = 8) pollen tubes in the same experiments as in (b). Time between the vertically solid and dotted lines represents the lagging (shift to right side) or leading (shift to left side) signals in (e). Phase relationships of $[Ca^{2+}]_{cyt}$ vs. growth, $[H^+]_{cyt}$ vs. growth, $[Ca^{2+}]_{cyt}$ vs. $[H^+]_{cyt}$ in growing and non-growing pollen tubes are displayed in radians (black, showing the lagging or leading phase) and then interpreted as shifts in seconds (red) in (f). It is important to point out the time delay or leading in correlation analysis shown in (e) is in line with time shifts in the wavelet analysis (f) in despite of the opposite sign. Error bars = SE. t-test was used in (d) while one-way ANOVA was used in (f). **, $p < 0.01$; ***, $p < 0.001$.

When pollen tubes were switched from an extracellular medium from optimal pH 5.8 to pH 6.8, pollen tubes growth ceased and this was accompanied by pronounced tip $[Ca^{2+}]_{cyt}$ and tip $[H^+]_{cyt}$ oscillations (Fig. 9a, b). This abrogated growth and higher frequency oscillations even remained in media with pH 5.8 demonstrating that this type of oscillatory behavior is not specific to the extracellular pH of 6.8 (Fig. 9a, b). Interestingly, tip $[Ca^{2+}]_{cyt}$ and tip $[H^+]_{cyt}$ oscillations may not change after shifting extracellular pH changes since the wavelet spectra showed similar period (Fig. 9c, d) which was quantified in Fig. 8d. In conclusion, this phase relation of tip $[Ca^{2+}]_{cyt}$ proceding tip $[H^+]_{cyt}$ signals may occur independently of the medium as long as pollen tubes growth was abrogated (Fig. 9). This phenomenon of tip $[Ca^{2+}]_{cyt}$ to lead $[H^+]_{cyt}$ regime relationship might be a general feature of pollen tubes that stopped growth or be the cause for pollen tube growth arrests, but these two scenarios could not be distinguished within our experiments.

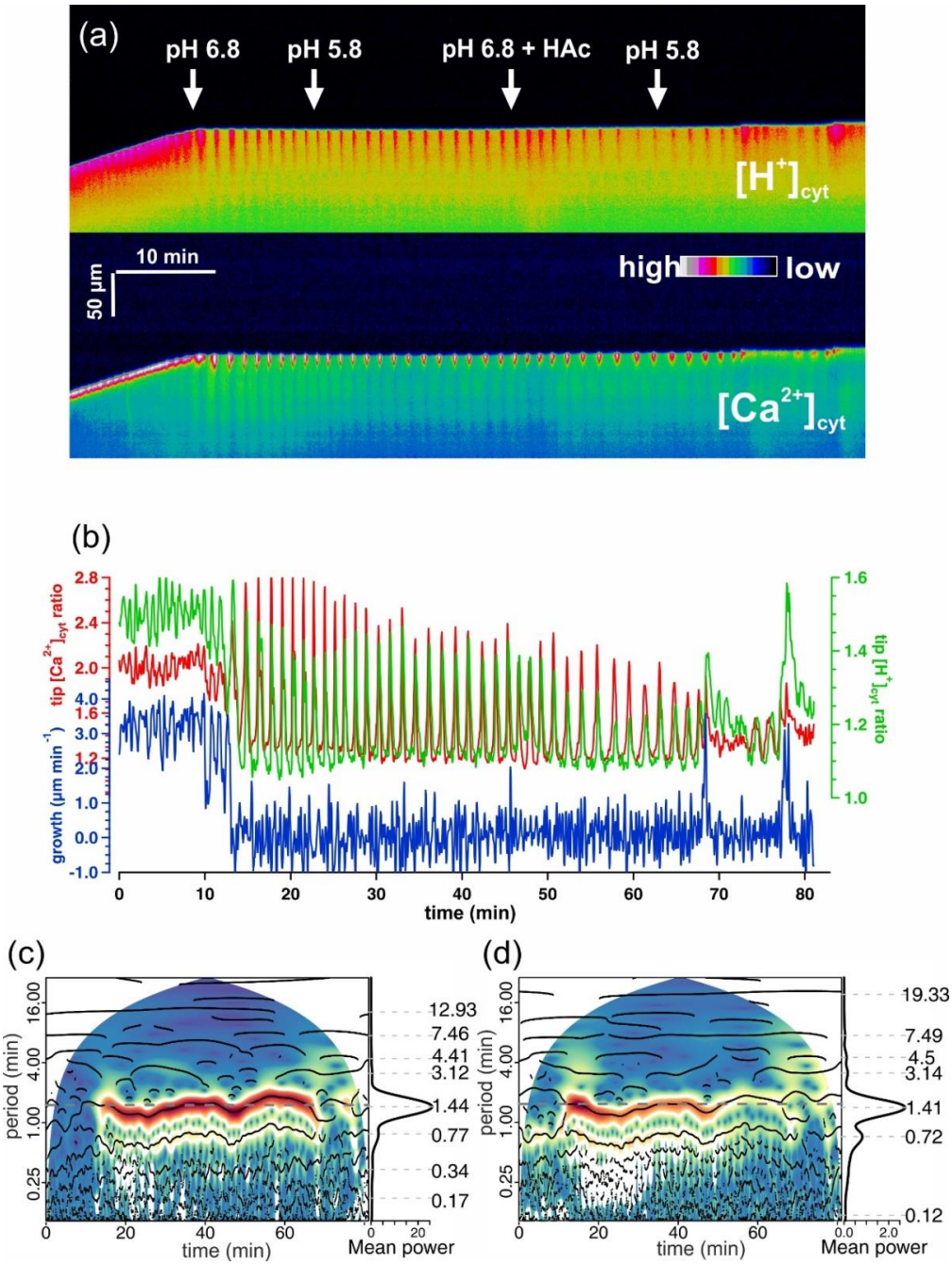

Figure 9. Tip $[Ca^{2+}]_{cyt}$ oscillations precede $[H^+]_{cyt}$ oscillations in non-growing pollen tubes independent of the extracellular pH as long as growth is arrested.

Live-cell imaging of a representative pollen tube stably expressing CapHensor upon extracellular medium with different pH aiming to change tip $[H^+]_{cyt}$ gradients. (a) False colored kymographs of tip $[H^+]_{cyt}$ (top) and $[Ca^{2+}]_{cyt}$ (bottom) dynamics when a pollen tube is challenged by different treatments shown by white arrows. (b) Tip $[Ca^{2+}]_{cyt}$- (red) and $[H^+]_{cyt}$- (green) ratio and growth rate (blue) over time are extracted from (a). (c, d) Wavelet spectra of period dynamics (vertical axis) and mean power of tip $[Ca^{2+}]_{cyt}$ ratio (c) and $[H^+]_{cyt}$ ratio (d) oscillations over time from (a). The significant phase correlations are displayed by the area ($p < 0.05$) bordered with white lines shown as the red color.

4.2.3 Tip $[H^+]_{cyt}$ correlates better than tip $[Ca^{2+}]_{cyt}$ with membrane potential changes

Since $[Ca^{2+}]_{cyt}$ and $[H^+]_{cyt}$ gradients between the tip and the shank were important for pollen tubes growth [75,76]. To ask whether these two signals have interactions between the tip and the shank, I quantified both $[Ca^{2+}]_{cyt}$ and $[H^+]_{cyt}$ signals from Fig. 8a at the tip (1-5 µm behind the tip) and the shank (35-40 µm behind the tip) (Fig. 10a, b). Interestingly, $[Ca^{2+}]_{cyt}$ oscillations between the tip (red line) and the shank (purple line) were almost in antiphase (with absolute phase shift in radians values bigger than half π) (Fig. 10a, b). The time shift of $[Ca^{2+}]_{cyt}$ oscillations between the tip and the shank was 126.48 ± 7.96 s and 30.96 ± 1.86 s in growing and non-growing pollen tubes, respectively (Fig. 10a, b). In contrast, $[H^+]_{cyt}$ oscillations between the tip and the shank were in-phase (with absolute phase shift in radians values smaller than half π) regardless of pollen tubes growing or not with the time shift 5.56 ± 0.57 s in growing pollen tubes and 6.00 ± 0.17 s in non-growing pollen tubes (Fig. 10a, b). Differences of phase shifts between $[Ca^{2+}]_{cyt}$ at the tip and the shank were significantly distinct from that between $[H^+]_{cyt}$ at the tip and the shank (Fig. 10b), indicating different roles of $[Ca^{2+}]_{cyt}$ and $[H^+]_{cyt}$ changes between the tip and the shank.

Given that apical $[Ca^{2+}]_{cyt}$ and $[H^+]_{cyt}$ oscillations both lagged behind growth oscillations (Fig. 8e, f), it implies that other signals might also play a role in controlling pollen tube growth. The transport of ions across the plasma membrane was consequently associated with variations in the membrane potential [97,117,368]. The membrane potential was regarded as a good candidate to control oscillatory pollen tubes growth [75,117,157,369]. I made use of sharp glass microelectrodes, combined with live-cell imaging of $[Ca^{2+}]_{cyt}$, $[H^+]_{cyt}$ and growth to correlate the four parameters (Fig. 10c). The kymographs of a representative pollen tube were aligned with time-lapse tip $[Ca^{2+}]_{cyt}$- (upper side) and tip $[H^+]_{cyt}$- (lower side) ratio signals (Fig. 10d). Unfortunately, tobacco pollen tubes growth was interrupted when the microelectrodes were impaled at the shank (Fig. 10c, d). Therefore the fluorescent intensity of $[Ca^{2+}]_{cyt}$ ratio (dark red trace) and $[H^+]_{cyt}$ ratio (dark green trace) at the tip was extracted and plotted side-by-side with membrane potential recordings at the shank (V_m, black trace) of non-growing pollen tubes (Fig. 10e). Although pollen tube growth was abolished after impalement, which limited studies on regulators in growth, the relationship between oscillations of tip $[Ca^{2+}]_{cyt}$ ratio, tip $[H^+]_{cyt}$ ratio and V_m after the impalement was quantified by cross-wavelet analysis and displayed in phase shifts (Fig. 10f) and correlation coefficient (Fig. 10g). Apical $[Ca^{2+}]_{cyt}$ and $[H^+]_{cyt}$ oscillations were associated with transient depolarizations (Fig. 10e) and both were in phase (Fig. 10f). Tip $[Ca^{2+}]_{cyt}$ oscillations preceded tip

$[H^+]_{cyt}$ oscillations and shank V_m depolarization transients by 18.76 ± 2.34 sec and 25.29 ± 2.66 sec, respectively (Fig. 10f). Correlations between two signals of $[Ca^{2+}]_{cyt}$, $[H^+]_{cyt}$ and V_m were performed with a running window correlation approach. Based on the fact that higher correlation coefficient represents better synchronization of the signals, V_m correlated much better with tip $[H^+]_{cyt}$ having a correlation coefficient value of 0.62 ± 0.04 while quantification of the correlation coefficient between V_m and tip $[Ca^{2+}]_{cyt}$ displayed a value of 0.13 ± 0.09 (n = 6) (Fig. 10g). Tip $[Ca^{2+}]_{cyt}$ and tip $[H^+]_{cyt}$ correlated at the level of 0.46 ± 0.04 (n = 6) (Fig. 10g). These correlations indicated a tight coupling between V_m and tip $[H^+]_{cyt}$ and much less correlation between V_m and tip $[Ca^{2+}]_{cyt}$. This result strongly indicates that tip $[H^+]_{cyt}$ was mainly responsible for the control of electrogenic ion transport under these experimental conditions.

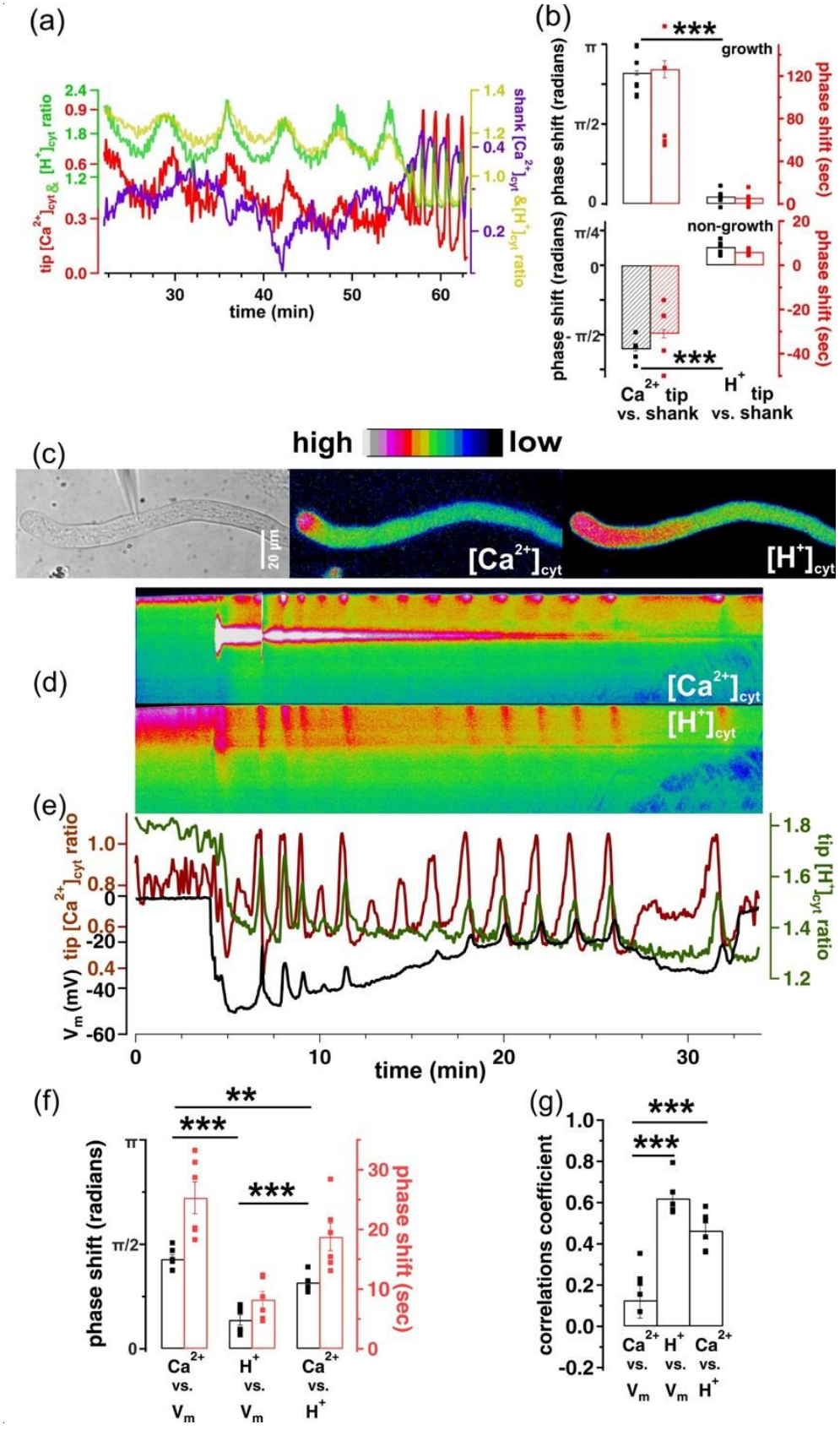
(a)
tip [Ca2+]cyt & [H+]cyt ratio
shank [Ca2+]cyt &[H+]cyt ratio
time (min)
(b)
***
growth
non-growth
phase shift (radians)
phase shift (sec)
Ca2+ tip vs. shank
H+ tip vs. shank
(c)
high
low
20 µm
[Ca2+]cyt
[H+]cyt
(d)
[Ca2+]cyt
[H+]cyt
(e)
Vm (mV)
tip [Ca2+]cyt ratio
tip [H+]cyt ratio
time (min)
(f)
**
***
***
phase shift (radians)
phase shift (sec)
Ca2+ vs. Vm
H+ vs. Vm
Ca2+ vs. H+
(g)
***
***
correlations coefficient
Ca2+ vs. Vm
H+ vs. Vm
Ca2+ vs. H+

Figure 10. Phase relations of tip $[Ca^{2+}]_{cyt}$, $[H^+]_{cyt}$ and V_m in pollen tubes impalement.

Live-cell imaging of *N. tabacum* pollen tubes stably expressing CapHensor to quantify spatio-temporal interrelation of $[Ca^{2+}]_{cyt}$ and $[H^+]_{cyt}$ at the tip and the shank along membrane potential (V_m) recordings at the shank via impalement. (a) Dynamics of $[Ca^{2+}]_{cyt}$ and $[H^+]_{cyt}$ ratio at the tip (left axis) and shank (right axis) from the cell in (Fig. 8a, b). (b) Bar diagrams of phase relationships via cross-wavelet analysis between $[Ca^{2+}]_{cyt}$ and $[H^+]_{cyt}$ oscillations at the tip (1–5 µm from tip) and shank (35–40 µm from tip) from growing (upper) and non-growing (lower) pollen tube as exemplified in (Fig. 8a). (c) Brightfield and false colored $[Ca^{2+}]_{cyt}$- and $[H^+]_{cyt}$- ratio image from a representative pollen tube expressing CapHensor combined with simultaneous V_m recording at the shank. Note the electrode in the brightfield image right before impalement. (d) $[Ca^{2+}]_{cyt}$- (upper) and $[H^+]_{cyt}$- (lower) ratio kymographs from a representative recording. (e) The corresponding $[Ca^{2+}]_{cyt}$- (dark red), $[H^+]_{cyt}$- (dark green) ratio and V_m (black) from (d). (f) Bar diagram of the mean phase relations between $[Ca^{2+}]_{cyt}$-, $[H^+]_{cyt}$- ratio and V_m in radians (black, n = 7) and shifts in seconds (red, n = 7). (g) Mean correlation coefficient of pairs of tip $[Ca^{2+}]_{cyt}$-, tip $[H^+]_{cyt}$- ratio and V_m signals (n = 7). Error bars = SE. t-test was used in (b) while one-way ANOVA was used in (f, g). **, $p < 0.01$ or ***, $p < 0.001$.

4.2.4 Quantitative assessment of the link between $[Ca^{2+}]_{cyt}$ and $[H^+]_{cyt}$ in pollen tubes

Overall, $[Ca^{2+}]_{cyt}$ and $[H^+]_{cyt}$ at the tip and the shank could be monitored via CapHensor imaging and quantified via bioinformatics approaches in two different cell states (growing and non-growing pollen tubes) (Fig. 11). Cross-correlation, phase shift and time shift quantifications after time-resolved CapHensor imaging are a powerful tool to dissect the interrelation of chemo-electric signaling when CapHensor imaging is even combined with electrophysiology. Strikingly, growth preceded tip $[H^+]_{cyt}$ regimes and tip $[Ca^{2+}]_{cyt}$ signals even lagged behind the $[H^+]_{cyt}$ signal (Fig. 11, upper), indicating other signals to initiate growth. An important phenomenon I uncovered is apical growth or membrane potential both correlated better with tip $[H^+]_{cyt}$ than with $[Ca^{2+}]_{cyt}$ (Fig. 10g), suggesting tip $[H^+]_{cyt}$ to harbor a prominent function in pollen tubes growth and regulation of ion transport. In addition, shank $[H^+]_{cyt}$ (yellow line) and tip $[H^+]_{cyt}$ oscillations were in phase whereas shank $[Ca^{2+}]_{cyt}$ (orange line) oscillations were in antiphase with tip $[Ca^{2+}]_{cyt}$ (Fig. 11), which might relay a $[Ca^{2+}]_{cyt}$ signal with a time-shift to the back of the pollen tube. One of the most obvious phenomena between growing and nongrowing pollen tubes was that tip $[Ca^{2+}]_{cyt}$ lagged behind tip $[H^+]_{cyt}$ (Fig. 11, upper side) whereas the order of these two signals was opposite when pollen tubes stopped growing (Fig. 11, lower side) (Fig. 10a, 10b). Although a higher frequency of tip $[Ca^{2+}]_{cyt}$ and $[H^+]_{cyt}$ oscillations occurred as long as pollen tube growth stopped (Fig. 11, lower side) compared with that in growing PTs (Fig. 11, upper side), tip $[Ca^{2+}]_{cyt}$ and $[H^+]_{cyt}$ always oscillate synchronously. Membrane potential (black lines) was synchronous with tip $[Ca^{2+}]_{cyt}$ and $[H^+]_{cyt}$ oscillations as well (Fig. 11, lower side), and better correlated with tip $[H^+]_{cyt}$ (Fig. 10g). The

properties of oscillations and the order of growth, membrane potential, $[Ca^{2+}]_{cyt}$ and $[H^+]_{cyt}$ indicate a strong coupling of these signals in pollen tubes growth.

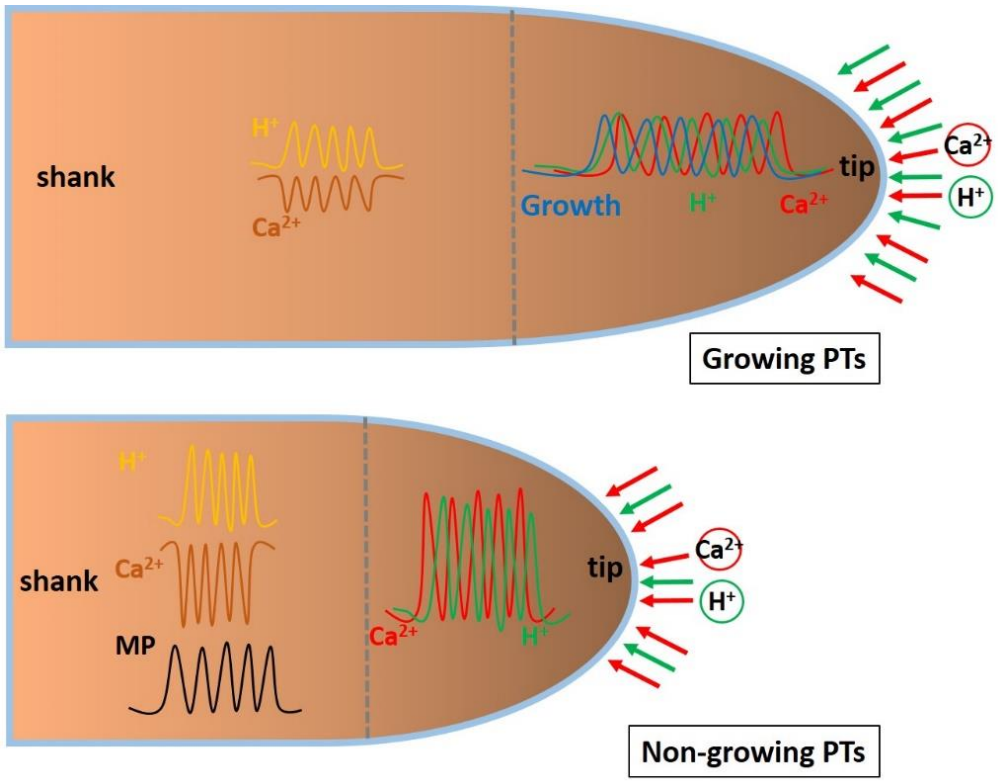

Figure 11. Interactions of $[Ca^{2+}]_{cyt}$ and $[H^+]_{cyt}$ oscillations in growing and non-growing pollen tubes.

The scheme of a growing (top) and non-growing pollen tube (PT) (bottom) is shown. The sequence of events in growth, $[Ca^{2+}]_{cyt}$ and $[H^+]_{cyt}$ is as follows: growth > tip $[H^+]_{cyt}$ > tip $[Ca^{2+}]_{cyt}$. Growth oscillations (blue) precede tip $[H^+]_{cyt}$ (green) and tip $[Ca^{2+}]_{cyt}$ (red) oscillations (top). The shank $[Ca^{2+}]_{cyt}$ oscillations (orange) are in anti-phase with tip $[Ca^{2+}]_{cyt}$ oscillations while the shank $[H^+]_{cyt}$ oscillations (yellow) and tip $[H^+]_{cyt}$ oscillations (green) are in-phase (top). Tip $[Ca^{2+}]_{cyt}$ and $[H^+]_{cyt}$ oscillations are in higher frequency and the sequence between them is reversed in non-growing pollen tubes compared to growing pollen tubes, meaning tip $[Ca^{2+}]_{cyt}$ oscillations precede tip $[H^+]_{cyt}$ oscillations. The shank $[Ca^{2+}]_{cyt}$ and $[H^+]_{cyt}$ oscillations are in similar higher frequency but with similar phase relation (bottom) compared with growing pollen tubes. The membrane potential (V_m) (black) during the impalement at the shank is also in oscillatory patterns, and lags behind tip $[Ca^{2+}]_{cyt}$ and $[H^+]_{cyt}$ oscillations, but correlates better with tip $[H^+]_{cyt}$.

4.3 Distinct roles of $[Ca^{2+}]_{cyt}$ and $[H^+]_{cyt}$ in guard cells upon different stimuli

4.3.1 Subcellular localization of optimized CapHensor expressing in leaves

Guard cells are model cells extensively characterized in terms of ion signaling triggered cellular movement upon biotic and abiotic stresses. Ca^{2+} as a second messenger is thought to encode information to trigger stomatal movement whereas the role of H^+ received much less attention in

the past. To study the role of $[Ca^{2+}]_{cyt}$ and $[H^{+}]_{cyt}$ in guard cells, CapHensor was stably expressed in the cytosol of *Nicotiana tabacum* guard cells. Despite replacing the promoter, the CapHensor version used for pollen tubes exhibited good expression in guard cells (Fig. 12a). However, PRpHluorin expressed not only in the cytosol but in the nuclei (Fig. 12a, green) although R-GECO1 was exclusively targeted in the cytosol (Fig. 12a, red, upper left side). Therefore, to prevent an overlapping signal from the nuclei and study $[Ca^{2+}]_{cyt}$ and $[H^{+}]_{cyt}$ signals only in the cytosol, I had to optimize the construct to eliminate the nucleus distribution. Therefore, I generated an optimized version of CapHensor with another NES in the C-terminal of PRpHluorin (Fig. 12b) and stably expressed optimized CapHensor in tobacco guard cells, displaying PRpHluorin fluorescence exclusively in the cytosol, as desired (Fig. 12b).

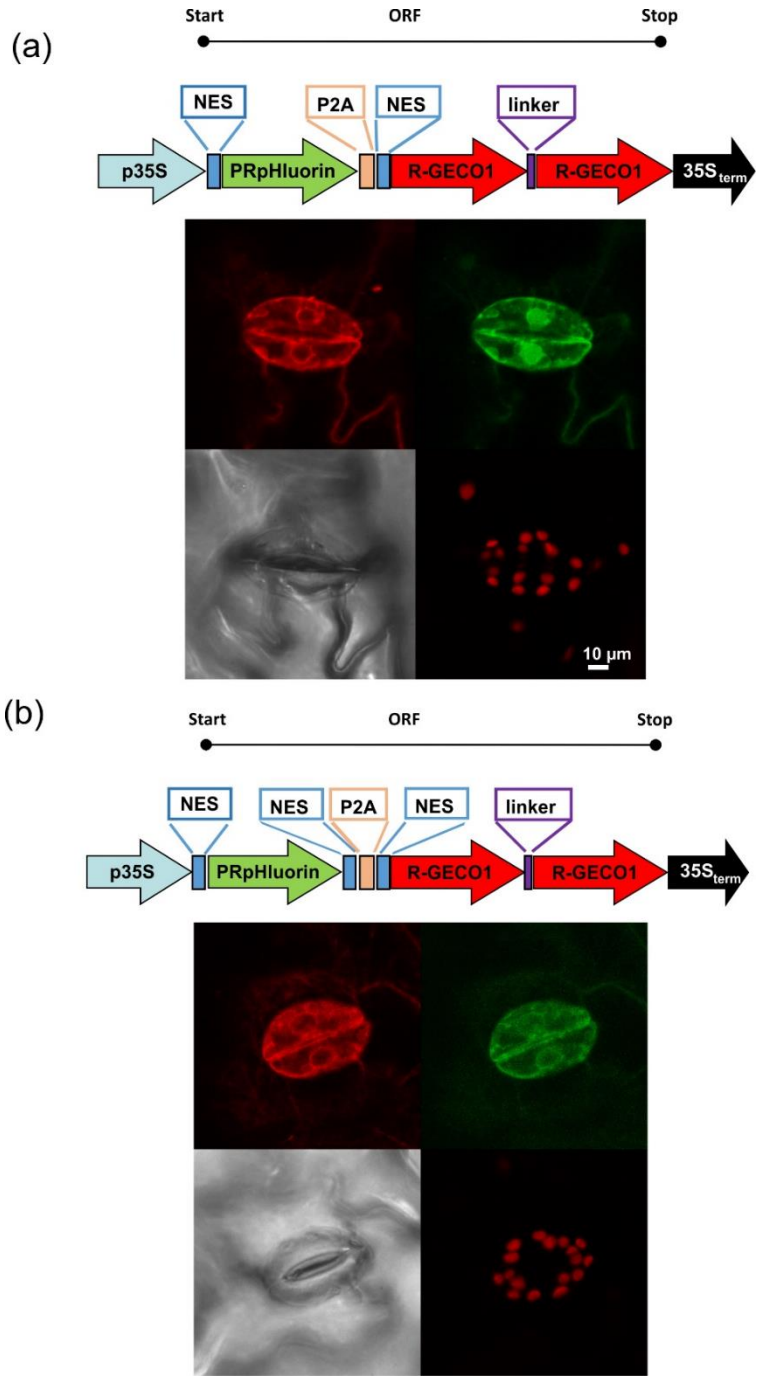

Figure 12. Subcellular localization of CapHensor in the cytosol of guard cells.

Confocal images of *N. tabacum* guard cells stably expressing multicistronic vectors harboring CapHensor targeting in the cytosol. The scheme of vector design is shown in the upper part. The difference between a and b is another nuclear excluding sequence (NES) is fused in the C-terminus of PRpHluorin in (b). The lower part is subcellular localization image of R-GECO1 (red), PRpHluorin (green), and chlorophyll (red) fluorescent images and brightfield (gray) image. The PRpHluorin in (a) is not only expressed in the cytosol but in the nuclei, but exclusively expressed in the cytosol in (b). The R-GECO1 is successfully only expressed in the cytosol (a, b). The CapHensor version exclusively located at the cytosol in b is used for following experiments in guard cells and mesophyll cells.

It is worth mentioning that all these transgenic tobacco plants did not develop any pleiotropic effects related to growth retardation, as reported for other genetically encoded biosensors [116,370], and no phenotypic differences were observed in comparison to wild type (SR1) plants (Fig. 13).

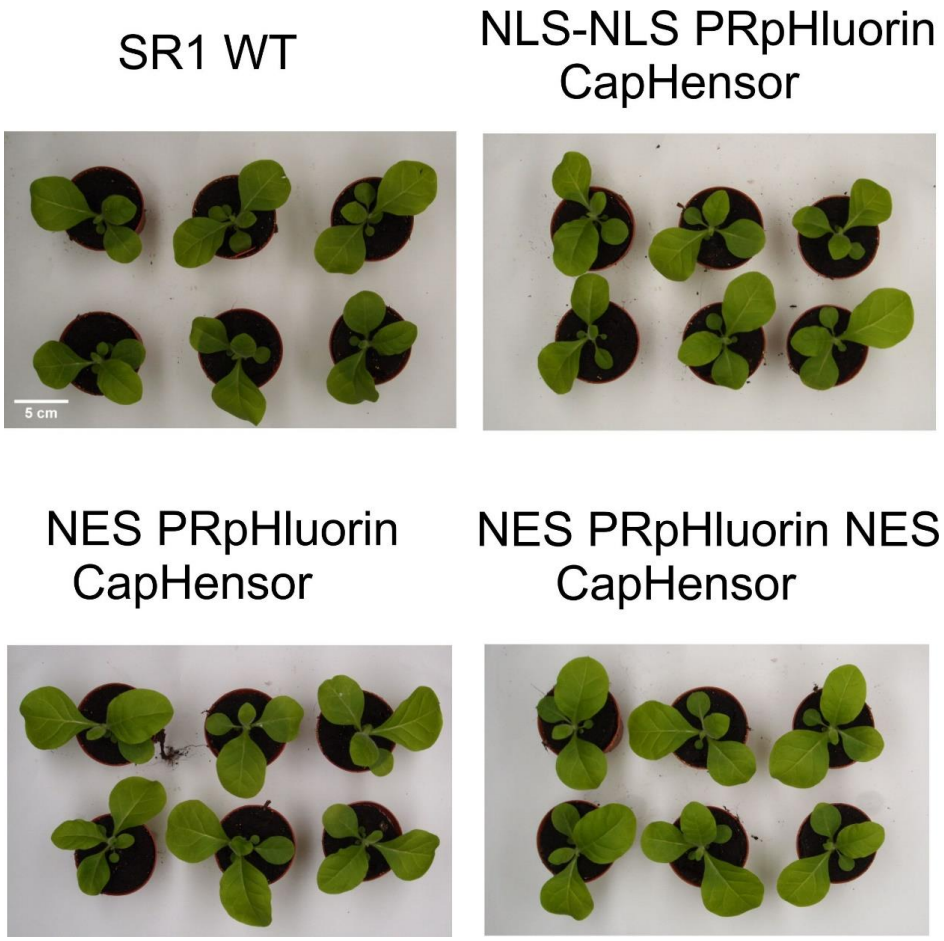

Figure 13. Transgenic *N. tabacum* plants expressing CapHensor grow normal.

Phenotype of 5 weeks old *N. tabacum* wild type plants and transgenic plants expressing CapHensor grown in the green house under the same condition. Six plants of each group are shown with wild type (SR1) (upper left), CapHensor located at the nuclei (upper right), CapHensor located at the cytosol with PRpHluorin harboring N-terminal NES (lower left) or PRpHluorin harboring N- and C-terminal NES (lower right).

4.3.2 Unique $[Ca^{2+}]_{cyt}$ and $[H^+]_{cyt}$ regimes in different stress pathways to control guard cell movement

Osmotically driven stomatal movement is very important for the control of water loss during drought and is vital to prevent microbes from entering leaves. How different stimuli induced

stomatal closure via second messengers is extremely important for understanding distinct signaling processes, and thus for breeding plants that can better cope with drought stress or pathogen invasion. Therefore simultaneous $[Ca^{2+}]_{cyt}$, $[H^+]_{cyt}$ and stomatal movement upon different stimuli were visualized. ABA is best studied phytohormone to induce stomatal closure [211,218,371-373]. $[Ca^{2+}]_{cyt}$ and $[H^+]_{cyt}$ responses to ABA have been reported but the sequence and role of both second messengers remained unresolved [68,112,173]. The time-lapse images of stomatal movement (upper, Brightfield, black trace), $[H^+]_{cyt}$ (middle, green trace) and $[Ca^{2+}]_{cyt}$ (bottom, red trace) were recorded before (15 min), during (15-45 min) and after removing (45-75 min) 10 µM ABA (Fig. 14a, b). Transient $[Ca^{2+}]_{cyt}$ elevation and $[H^+]_{cyt}$ reduction (cytosolic alkalization) were observed in guard cells and stomatal closed (Fig. 14a, b, S2b) by ABA while there was no effects upon an equivalent amount of EtOH in the control experiment (Fig. S2a). Quantification of the onset and peak times of the $[Ca^{2+}]_{cyt}$ and $[H^+]_{cyt}$ responses after ABA application demonstrated pH responses to occur earlier than $[Ca^{2+}]_{cyt}$ increase (Fig. 14c). On average, cytosolic alkalization was the earliest initiated signal with an onset time of 32.78 ± 6.13 s, followed by a $[Ca^{2+}]_{cyt}$ increase starting 80 ± 15.70 s after ABA application (Fig. 14c). Stomatal closure set in around 205 ± 14.36 s after ABA application and thus followed both ion signaling events (Fig. 14c). The peak of the cytosolic alkalization response occurred at 190 ± 18.63 s and recovered slowly while maximum $[Ca^{2+}]_{cyt}$ elevation reached the peak at 302.22 ± 13.47 s after ABA application (Fig. 14a-c). I can conclude that the pH response was identified as the initial signal in guard cells upon ABA treatment. To reveal whether the pH effects in ABA induced stomatal closure exist in other stimuli, $[Ca^{2+}]_{cyt}$ and $[H^+]_{cyt}$ in stomatal closure triggered by pathogen such as a bacterial elicitor 1 µM flg22 were investigated (Fig. 14d, S2c). Even though similar but stronger $[Ca^{2+}]_{cyt}$ increases during stomatal closure were monitored upon flg22, only a very minor cytosolic alkalization was observed (Fig. 14d). The quantitative temporal analysis indicated $[Ca^{2+}]_{cyt}$ elevations were the first signal in response to flg22, followed by a slight cytosolic alkalization and stomatal closure, but the peaks of $[Ca^{2+}]_{cyt}$ and $[H^+]_{cyt}$ occurred at similar time points (Fig. 14e), indicating $[Ca^{2+}]_{cyt}$ and $[H^+]_{cyt}$ might play distinct roles in different stimuli.

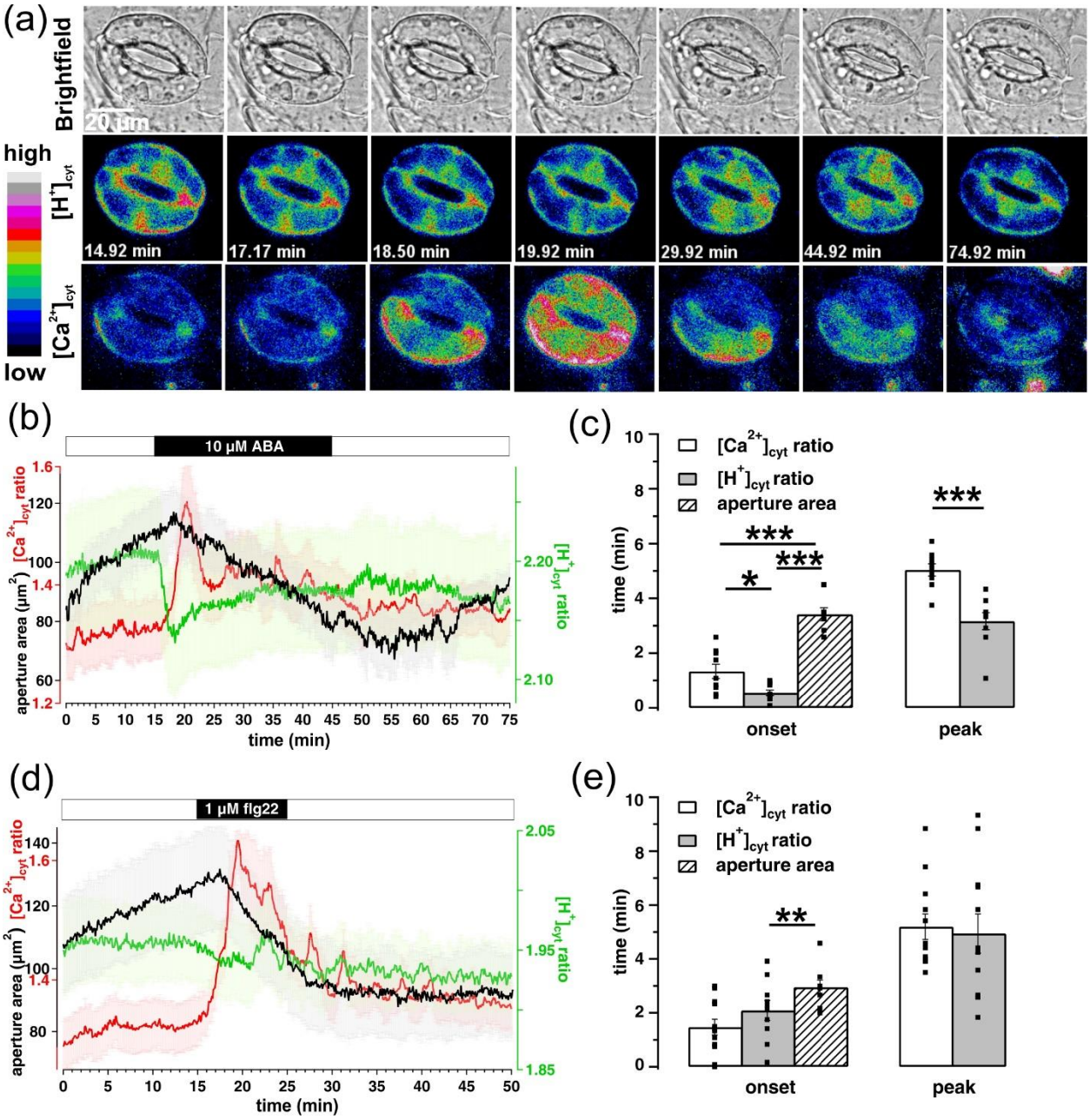

Figure 14. Distinct $[Ca^{2+}]_{cyt}$ and $[H^+]_{cyt}$ in guard cells in response to different stimuli.

Time-lapse CapHensor imaging and monitoring stomata aperture in guard cells of *N. tabacum* epidermal strips stably expressing CapHensor. (a) Brightfield (top), false colored $[H^+]_{cyt}$- (middle) and $[Ca^{2+}]_{cyt}$- (bottom) ratio images of a representative measurement upon 10 µM ABA application. (b, d) Mean $[Ca^{2+}]_{cyt}$ ratio (red), $[H^+]_{cyt}$ ratio (green) and stomatal aperture area (black) over time upon application of (b) 10 µM ABA (n = 10), (d) 1 µM flg22 (n = 12). Bars above the mean traces indicate the time of treatments. (c, e) The average time of the onset and peak response to 10 µM ABA (b, n = 10) or 1 µM flg22 (d, n = 12) are displayed in bar diagrams in (c) and (e), respectively. Error bars = SE. t-test and one-way ANOVA were used in (c) and (e). *, $p < 0.05$, **, $p < 0.01$ or ***, $p < 0.001$.

4.3.3 Vacuolar acidification under ABA and flg22 treatment in guard cells

The vacuole is the biggest organelle with a pH around 5-5.5 known to play a crucial role in cytosolic pH regulation in plants [62,71,243]. To study whether the vacuolar H^+-transport mechanisms contribute to cytosolic pH changes induced by ABA and flg22 in guard cells, I measured the dynamics of vacuolar H^+ changes upon 10 µM ABA and 1 µM flg22 (Fig. 15) using the pH indicator BCECF-AM, known to accumulate in the vacuole in plants [69,321,374]. Right after the application of ABA the vacuole acidified and remained acidified in the presence of ABA (Fig. 15a, b). Differently, the vacuole only acidified transiently upon flg22 treatment (Fig. 15c, d), which fits a marginal alkalization in the cytosol I recorded earlier upon flg22 treatment (Fig. 14b, d). The sustained vacuolar acidification upon ABA (Fig. 15a, b) also well matched the observed temporal dynamics of $[H^+]_{cyt}$ regime (Fig. 14 a, b). My results are consistent with previous reports using mutants of the vacuolar H^+-ATPase [96,112,244,245]. For example, the vacuole of the double V-H^+-ATPases (*vha-a2/a3*) mutant was less acidic after ABA treatment and stomatal closure was delayed [239,241]. The results from CapHensor imaging and BCECF imaging demonstrated the vacuolar acidification was very likely to contribute to the cytosolic alkalization upon ABA and flg22 treatment as they had more or less identical dynamics, but opposite directions (compare Fig. 14 and Fig. 15).

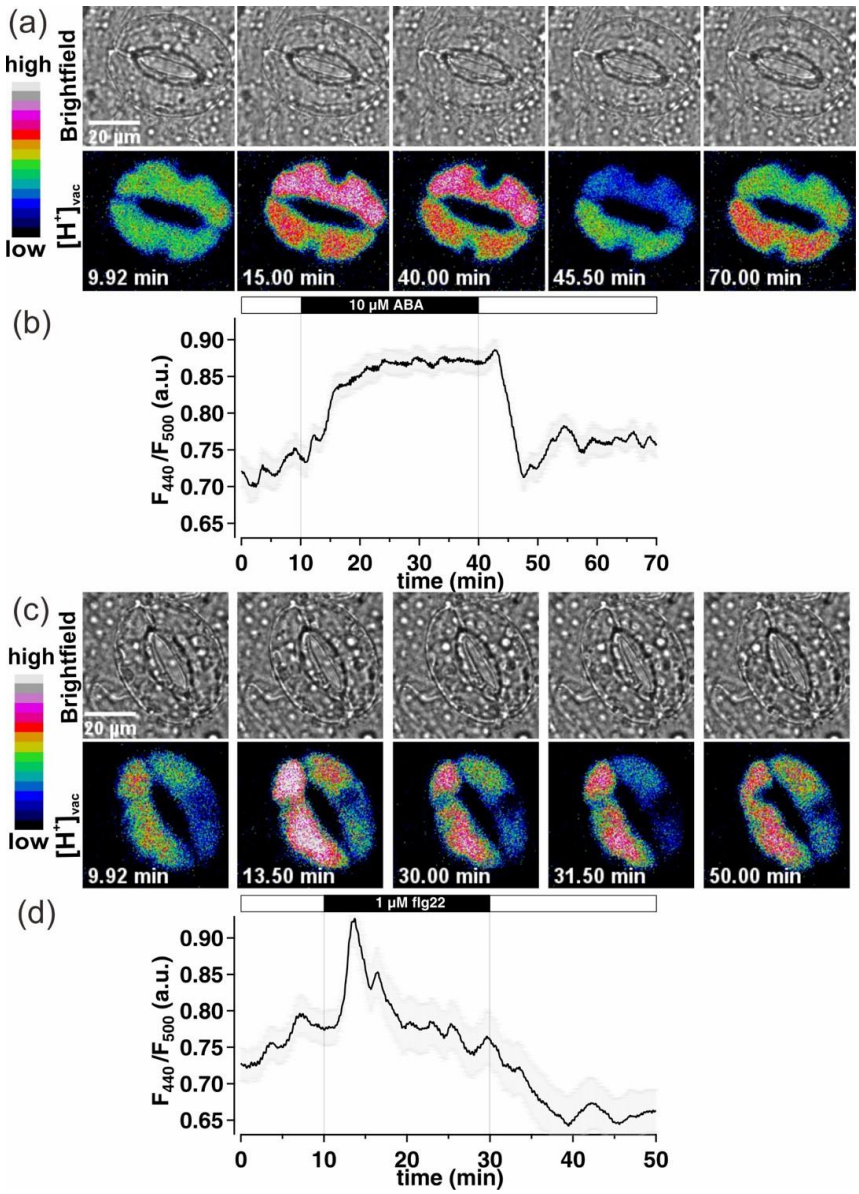

Figure 15. Vacuolar acidification in guard cells upon ABA and flg22 treatment.

(a, c) Brightfield images (top) and false-colored fluorescent images (bottom) of *N. tabacum* wild-type guard cells (SR1) incubated with 15 µM BCECF for 2 h before starting measurements upon application of 10 µM ABA (a) or 1 µM flg22 (c). (b, d) Mean vacuolar H^+ concentration ($[H^+]_{vac}$ ratio) (black, F_{440}/F_{500}) upon 10 µM ABA (b, n = 24) or 1 µM flg22 (d, n = 22). Bars above indicated the time of treatments. Error bars = SE.

4.3.4 $[Ca^{2+}]_{cyt}$ and $[H^+]_{cyt}$ in guard cells upon different H_2O_2 concentrations

In addition to Ca^{2+} and H^+, ROS was proposed as another important messenger participating in both ABA and flg22 induced stomatal closure [175,209]. For example, 0.1-1 mM H_2O_2 was reported to induce $[Ca^{2+}]_{cyt}$ oscillations or elevations accompanied by stomatal closure [48,375,376]. When I

applied 20 µM or 200 µM H_2O_2, regarded as physiological concentrations of H_2O_2 [261], $[Ca^{2+}]_{cyt}$ was not affected and stomatal aperture was not altered but a pronounced cytosolic acidification was observed in *N. tabacum* guard cells (Fig. 16a, b), which is contrary to previous study in *Vicia faba* guard cells [375]. A higher concentration of H_2O_2 at 1 mM triggered steady-increasing $[Ca^{2+}]_{cyt}$ and $[H^+]_{cyt}$ rises and resulted in mild stomatal closure (Fig. 16c). This stomatal movement as observed here fits recent studies that showed stomata opened upon low concentration of H_2O_2 while stomata closed under high concentration of H_2O_2 [284,377].

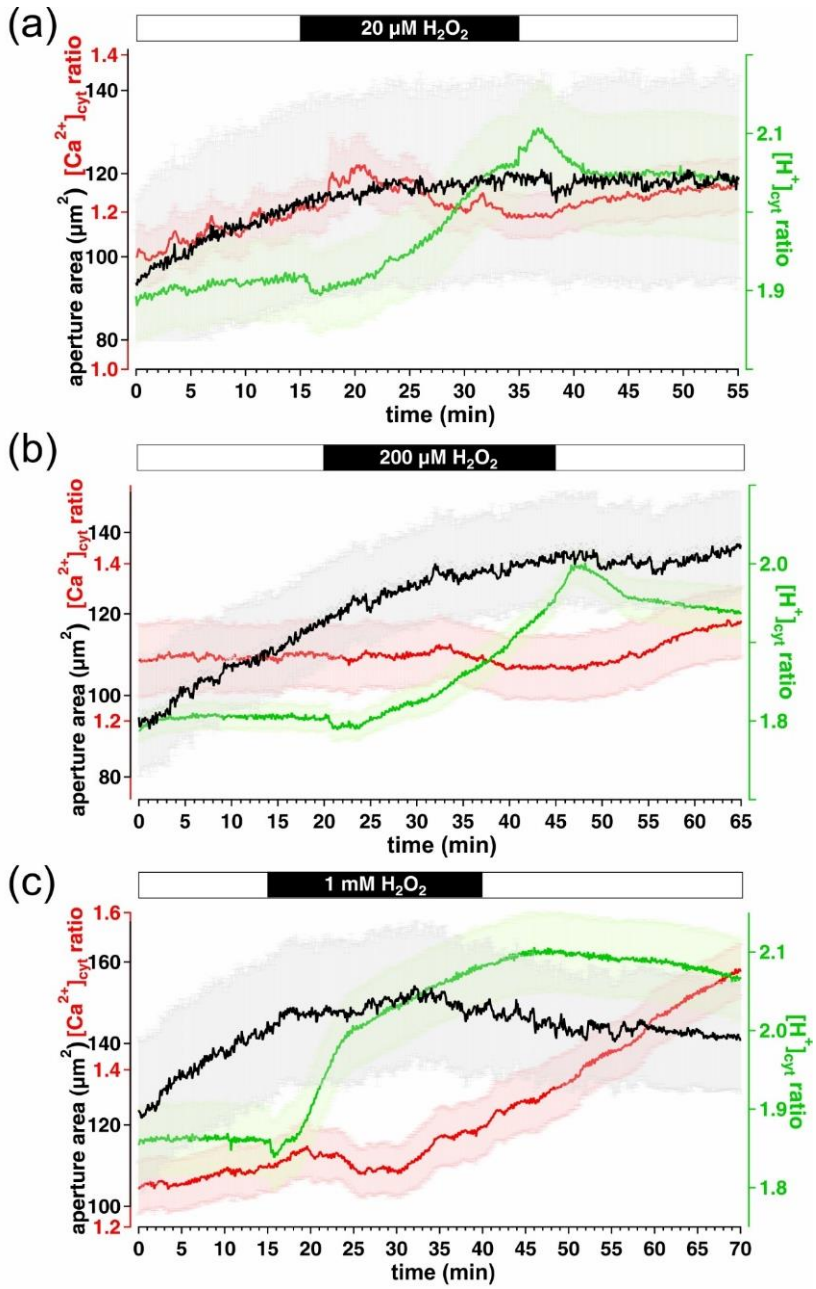

Figure 16. Physiological concentrations of H_2O_2 in guard cells induce cellular acidification without a $[Ca^{2+}]_{cyt}$ signal.

Time-lapse CapHensor imaging and monitoring stomata aperture in guard cells of *N. tabacum* epidermal strips stably expressing CapHensor. (a-c) Mean $[Ca^{2+}]_{cyt}$ ratio (red), $[H^+]_{cyt}$ ratio (green) and stomatal aperture area (black) challenged with (a) 20 µM H_2O_2 (n = 10), (b) 200 µM H_2O_2 (n = 22) and (c) 1 mM H_2O_2 (n = 18). Error bars = SE.

To investigate the effects of different concentrations of H_2O_2 on guard cells and to investigate if high H_2O_2 concentrations have a negative impact on cells' integrity, the cytosolic streaming in

guard cells was monitored by kymographs within the brightfield images. The nosier pattern of the kymograph under lower concentration of H_2O_2 represents normal cytosolic streaming (Fig. 17a-b). The loss of cell integrity is indicated by non-mobile cytosolic structures and abrogated cytosolic streaming which indicated by a kymograph with an unchanged pattern (Fig. 17a-c). Exactly this was seen when guard cells were treated with 1 mM H_2O_2 but not with 20-200 µM H_2O_2 (Fig. 17a-c). This indicates unphysiologically high H_2O_2 concentrations are toxic since membrane integrity is lost, which might be the reason for the $[Ca^{2+}]_{cyt}$ and $[H^+]_{cyt}$ increases in guard cells monitored after 1 mM H_2O_2 application.

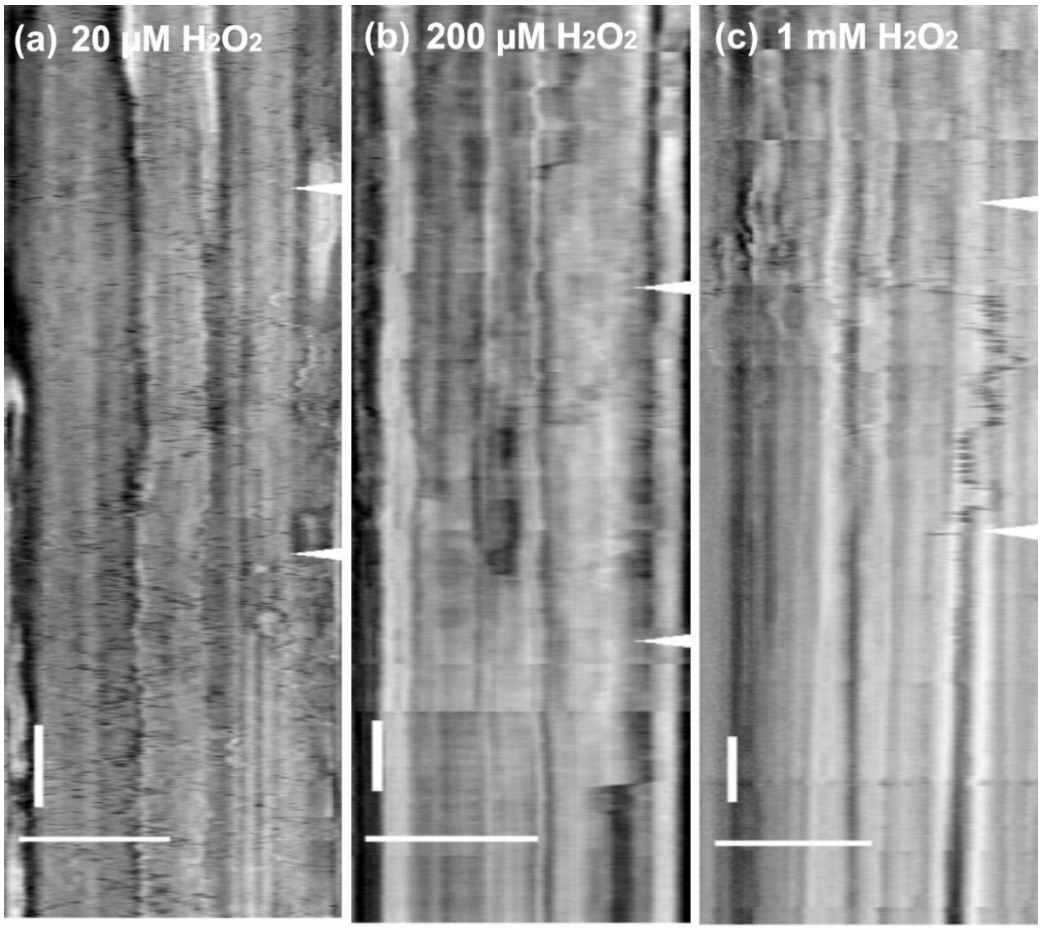

Figure 17. *Nicotiana tabacum* guard cells are killed by 1 mM H_2O_2.

(a-c) Brightfield kymographs of a representative guard cell treated with (a) 20 µM H_2O_2, (b) 200 µM H_2O_2 and (c) 1 mM H_2O_2. The time of H_2O_2 treatment and wash out is marked by white marks on the right side of the kymographs. A noisy pattern shown in the kymograph represents cytosolic streaming. The loss of cell integrity is indicated by distinct and constant patterning of the kymograph, which was observed under 1 mM H_2O_2 treatment.

4.3.5 pH changes play a prominent role in stomatal movement

My previous results demonstrated guard cells responses to different stimuli displayed distinct $[Ca^{2+}]_{cyt}$ and $[H^+]_{cyt}$ signals during stomatal closure (Fig. 14, 16). I wondered whether cytosolic alkalization is essential for stomatal closure induced by ABA or flg22 and if the pH response affects the dynamics of $[Ca^{2+}]_{cyt}$ increases. Therefore, butyric acid (BTA), a weak acid was applied to exclusively acidify the cytosol [173,375,378] aiming to block cytosolic alkalization induced by ABA or flg22 (Fig. 18a-c). Making use of BTA in combination with ABA or flg22, I studied if the alkalization is essential for stomatal closure and if cytosolic acidification can influence the ABA or flg22 pathway in guard cells (Fig. 18a-c). Despite ABA being the known strongest stomatal closure signal, stomatal opening was induced by BTA even in the presence of ABA (Fig. 18a, b). Through BTA administration, $[Ca^{2+}]_{cyt}$ increases upon ABA treatment were strongly reduced (Fig. 18a-b) compared to the experiment in the absence of BTA (Fig. 14b). However, stomatal closure in response to ABA was immediately set in after removing BTA (n = 22, Fig. 18a). In line with these BTA effects on diminishing the ABA response in guard cells, ABA pre-incubated closed stomata opened immediately when BTA was applied (n = 22, Fig. 18b). BTA effects on stomatal closure induced by flg22 were similar to ABA, but with higher $[Ca^{2+}]_{cyt}$ increases (n = 24, Fig. 18c). These results suggested cytosolic acidification to promote stomatal opening via a yet unknown mechanism. Additionally, it indicates that cytosolic alkalization is important for ABA and flg22 triggered stomatal closure. Not only stomatal closure induced by ABA and flg22 was altered in the presence of BTA, $[Ca^{2+}]_{cyt}$ elevations were partially inhibited as well (Fig. 18a-c), demonstrating that pH can change stimulus triggered $[Ca^{2+}]_{cyt}$ increases. But why was Ca^{2+} influenced by BTA? Does $[H^+]_{cyt}$ act on the signaling mechanisms to activate Ca^{2+}-permeable channels, or do pH changes influence the channels directly? What is the interrelation between $[Ca^{2+}]_{cyt}$ and $[H^+]_{cyt}$ homeostasis? Does Ca^{2+} also act on the pH homeostasis?

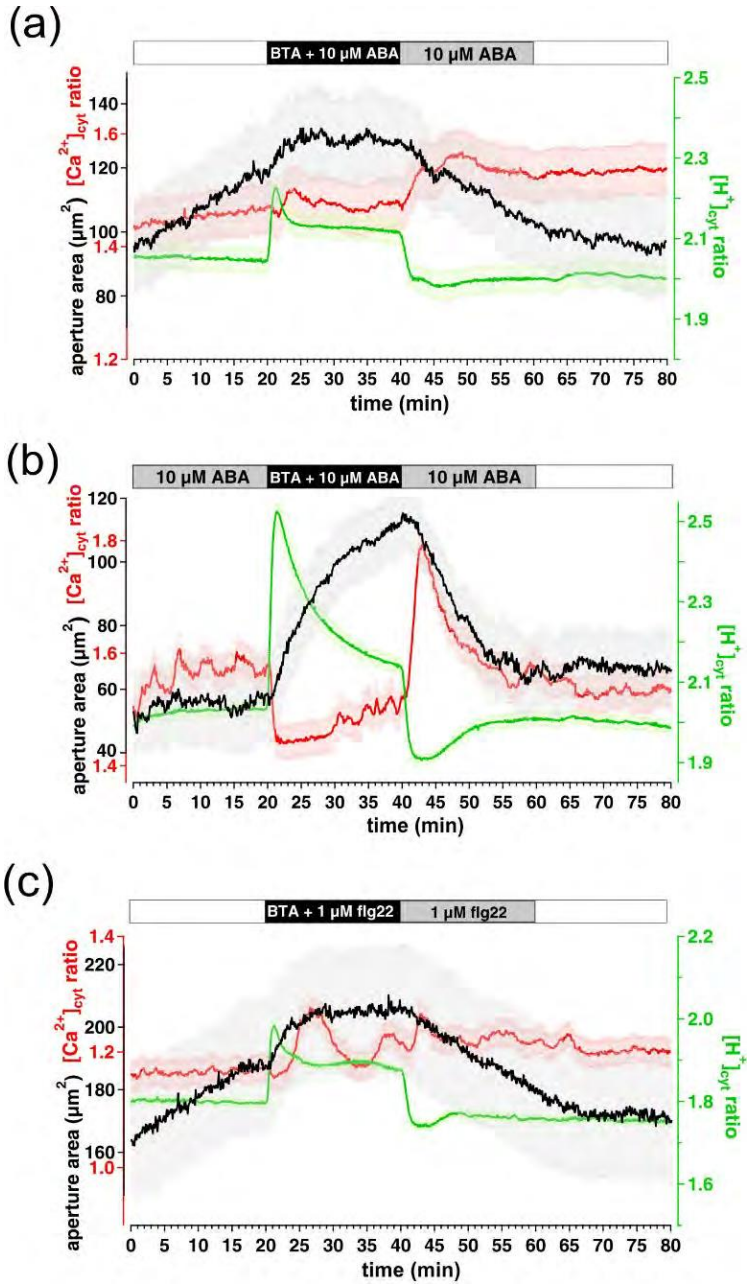

Figure 18. The cytosolic alkalization in guard cells is important for stomatal closure.

Time-lapse CapHensor imaging together with monitoring stomata aperture in guard cells of *N. tabacum* epidermal strips stably expressing CapHensor. Mean $[Ca^{2+}]_{cyt}$ ratio (red), $[H^{+}]_{cyt}$ ratio (green) and stomata aperture area (black) time-course experiments are displayed. (a) Guard cells are challenged by 10 µM ABA plus 3 mM BTA followed by exclusive ABA (n = 22). (b) 10 µM ABA pre-incubated guard cells are treated with simultaneous 10 µM ABA and 3 mM BTA followed by only 10 µM ABA (n = 22). (c) Guard cells are treated with simultaneous application of 3 mM BTA plus 1 µM flg22 followed by flg22 treatment only (n = 24). Bars above indicate time of relative treatments. Error bars = SE.

To answer these questions, I performed experiments to alter external pH or $CaCl_2$ concentration of the medium, looked at the $[Ca^{2+}]_{cyt}$ and $[H^+]_{cyt}$ signals and quantitatively compared the guard cell responses (Fig. 19). Based on an extracellular medium with pH 5.8, which is mimicking the physiological conditions, I lowered or lifted the extracellular pH by one pH unit first. After that I induced Ca^{2+} signals by increasing the extracellular $CaCl_2$ concentration from 10 µM to 1 mM in the media (Fig. 19a, b, n = 24). An experimental design like this has the advantage of comparing the $[Ca^{2+}]_{cyt}$, $[H^+]_{cyt}$ and aperture dynamics from the same guard cell in one experiment. When exchanging the medium pH from 5.8 to 4.8, a cytosolic acidification and a small transient $[Ca^{2+}]_{cyt}$ decrease were observed, which led to an increase in aperture with the opening speed from 0.8143 μm^2/min to 1.190 μm^2/min (Fig. 19a, b, f). This result confirmed the results from Fig. 18a-c that cytosolic acidification promoted stomatal opening. Switching back to pH 5.8 medium reduced the velocity of aperture opening back to 0.2317 μm^2/min (Fig. 19b, f). When switching from pH 5.8 to pH 6.8 medium, I observed cytosolic alkalization, $[Ca^{2+}]_{cyt}$ transients and pronounced stomatal closure (Fig. 19a-f). Although pronounced $[Ca^{2+}]_{cyt}$ transients were also induced when I elevated the medium $CaCl_2$ concentration from 10 µM to 1 mM, only slight stomatal closure occurred, which was accompanied by a small transient cytosolic alkalization (Fig. 19a-f). Probably the most interesting aspect of this experiment is that very obvious stomatal closure was induced by pH 6.8 treatment when pronounced cytosolic alkalization was triggered while similar $[Ca^{2+}]_{cyt}$ increases but small alkalization upon 1 mM $CaCl_2$ treatment did not lead to stomatal closure (Fig. 19a, b, c, f). Therefore I hypothesized the magnitude of cytosolic alkalization probably is important to control stomatal closure.

To determine the role of $[Ca^{2+}]_{cyt}$ transients and/or $[H^+]_{cyt}$ changes in the regulation of stomatal closure, I performed quantitative analysis and compared the amplitude of $[Ca^{2+}]_{cyt}$ increases and $[H^+]_{cyt}$ decreases in response to pH 6.8 and 1 mM $CaCl_2$ (Fig. 19c-e). Similar amplitude of $[Ca^{2+}]_{cyt}$ ratio ($\Delta[Ca^{2+}]_{cyt}$ ratio) was induced upon pH 6.8 or high $CaCl_2$ (Fig. 19c) whereas cytosolic alkalization induced by pH 6.8 (white) was significantly higher than the high external $CaCl_2$ (1 mM) induced cytosolic alkalization (grey) (Fig. 19d, e), which was in line with a significant difference in aperture closing speed (Fig. 19f). Stomata closed with approximately 2.099 μm^2/min under pH 6.8 treatment, significantly faster than that in response to high $CaCl_2$ (0.8186 μm^2/min) (Fig. 19b, f). Thus, high external Ca^{2+} only induced slightly, but pH 6.8 induced more effectively stomatal closure (Fig. 19f), which prompted me to compare the aperture speed with the ratio of

$[H^+]_{cyt}$ and $[Ca^{2+}]_{cyt}$ signals. The regression analysis between aperture changes was positively correlated with $\Delta[H^+]_{cyt}/\Delta[Ca^{2+}]_{cyt}$ ratio (Fig. 19g), pointing out that the higher the alkalization is with equal $[Ca^{2+}]_{cyt}$ signals, the faster stomatal closure occurred. This again demonstrated that $[H^+]_{cyt}$ plays a dominant role in stomatal movement.

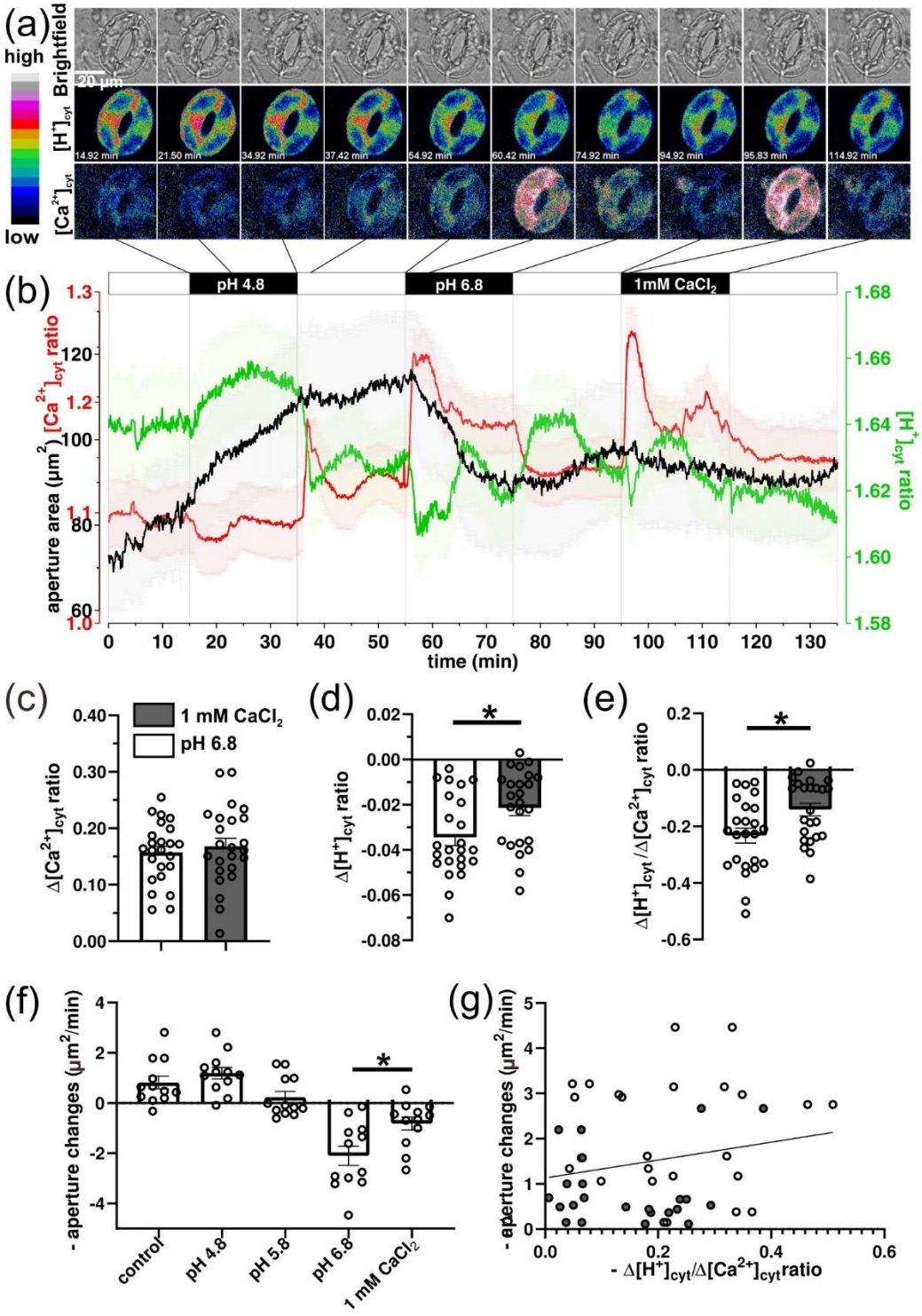

Figure 19. The cytosolic pH in guard cells has a prominent role for stomatal movement.

Time-lapse CapHensor imaging in guard cells of *N. tabacum* epidermal strips stably expressing CapHensor together with stomata aperture monitoring. (a) Time-lapse brightfield (top), $[H^+]_{cyt}$ ratio (middle) and $[Ca^{2+}]_{cyt}$ (bottom) images from a representative stomata under sequential treatments of extracellular acid (pH 4.8) and alkalized (pH 6.8) or high $CaCl_2$ concentration (1 mM) medium. (b) Mean $[Ca^{2+}]_{cyt}$ ratio (red), $[H^+]_{cyt}$ ratio (green) and stomata aperture area (black) time-course live-cell imaging in guard cells upon different treatments indicated by bars above (n = 24). The optimal medium contains 10 µM $CaCl_2$ with pH 5.8. (c-e) Quantification of amplitude changes of $[Ca^{2+}]_{cyt}$ ratio ($\Delta[Ca^{2+}]_{cyt}$ ratio, c), $[H^+]_{cyt}$ ratio ($\Delta[H^+]_{cyt}$ ratio, d) and ratiometric H^+/Ca^{2+} ($\Delta[H^+]_{cyt}$ ratio/$\Delta[Ca^{2+}]_{cyt}$ ratio, e) upon pH 6.8 and 1 mM $CaCl_2$ from (b) (n = 24). (f) Quantification and comparison of aperture responses (Δaperture changes (µm²/min)) to different treatments shown in (b) (n = 24). (g) Regression line between Δaperture changes (µm²/min) and $\Delta[H^+]_{cyt}$ ratio/$\Delta[Ca^{2+}]_{cyt}$ ratio. Dots represent individual guard cells. Error bars = SE. t-test was used in (c-f). *, $p < 0.05$.

4.4 Flg22 but not ABA and H_2O_2 evoke Ca^{2+}, H^+ and V_m signals in mesophyll cells

Signals from the mesophyll are also important for controlling the width of the stoma, actually apoplastic alkalization was reported in the substomatal cavity after ABA application [68]. How does that fit cytosolic alkalization in guard cells during ABA responses? Therefore, I monitored mesophyll cells as a multicellular system to possibly generate chemo-electric signals which can be sensed by guard cells. $[Ca^{2+}]_{cyt}$, $[H^+]_{cyt}$ and membrane potential changes have been reported to play physiological roles to different stresses [115,259,344]. To study the dynamics of Ca^{2+}, pH and voltage changes during different stimuli in the mesophyll, I set up an approach to monitor these parameters simultaneously. In CapHensor expressing leaves of *N. benthamiana* transformed by infiltration, the membrane voltage was recorded with sharp glass microelectrodes (Fig. 20a). The sharp microelectrode was gently inserted as close as possible to the imaging region with great care. Contrary to the flg22 response in guard cells (Fig. 14d), $[H^+]_{cyt}$- and $[Ca^{2+}]_{cyt}$- ratio in mesophyll cells exhibited a single pronounced increase (acidification) under 100 nM flg22 treatment (Fig. 20b). Intriguingly, a depolarization occurred on average 125.72 ± 15.68 s in all cases (n = 9, Fig. 20b, i) and preceded the onset of $[Ca^{2+}]_{cyt}$ and $[H^+]_{cyt}$ response by 121.61 ± 22.04 s and 145.12 ± 20.13 s upon flg22 application, respectively (both p-values < 0.001) (Fig. 20b, 20i). On average, the maximum depolarization was 54 mV from a resting membrane potential of 114 ± 6.84 mV (Fig. 20b, k). Different from the guard cells responses, $[Ca^{2+}]_{cyt}$, $[H^+]_{cyt}$ and V_m responses to 10 µM ABA or 200 µM H_2O_2 were not observed (Fig. 20c, d). However, drought stress and pathogen invasion related to ROS generation are found to result in genetic reprogramming [264,379-381]. Hence, I developed a CapHensor version with both the PRpHluorin and the R-GECO1 localized in the

nucleus to monitor nuclear Ca^{2+} concentrations ($[Ca^{2+}]_{nuc}$) and nuclear H^+ concentrations ($[H^+]_{nuc}$) (Fig. 6, 20e). Similar to the responses in the cytosol, $[Ca^{2+}]_{nuc}$ and $[H^+]_{nuc}$ transiently increased upon 100 nM flg22 treatment together with a membrane depolarization (Fig. 20ef, k). The onset of membrane potential changes significantly preceded $[Ca^{2+}]_{nuc}$ and $[H^+]_{nuc}$ elevations by approximately 141.01 ± 22.09 and 117.51 ± 17.15 s after flg22 application, respectively (Fig. 20f, j). The onset of $[Ca^{2+}]_{nuc}$ and $[H^+]_{nuc}$ occurred around 226.29 ± 16.94 and 202.79 ± 12.59 s (Fig. 20j), similar to the time of $[Ca^{2+}]_{cyt}$ and $[H^+]_{cyt}$ responses. In line with the cytosolic response (Fig. 20c, d), no responses of V_m, $[Ca^{2+}]_{nuc}$ and $[H^+]_{nuc}$ were observed upon 10 µM ABA and 200 µM H_2O_2 administration (Fig. 20g, h).

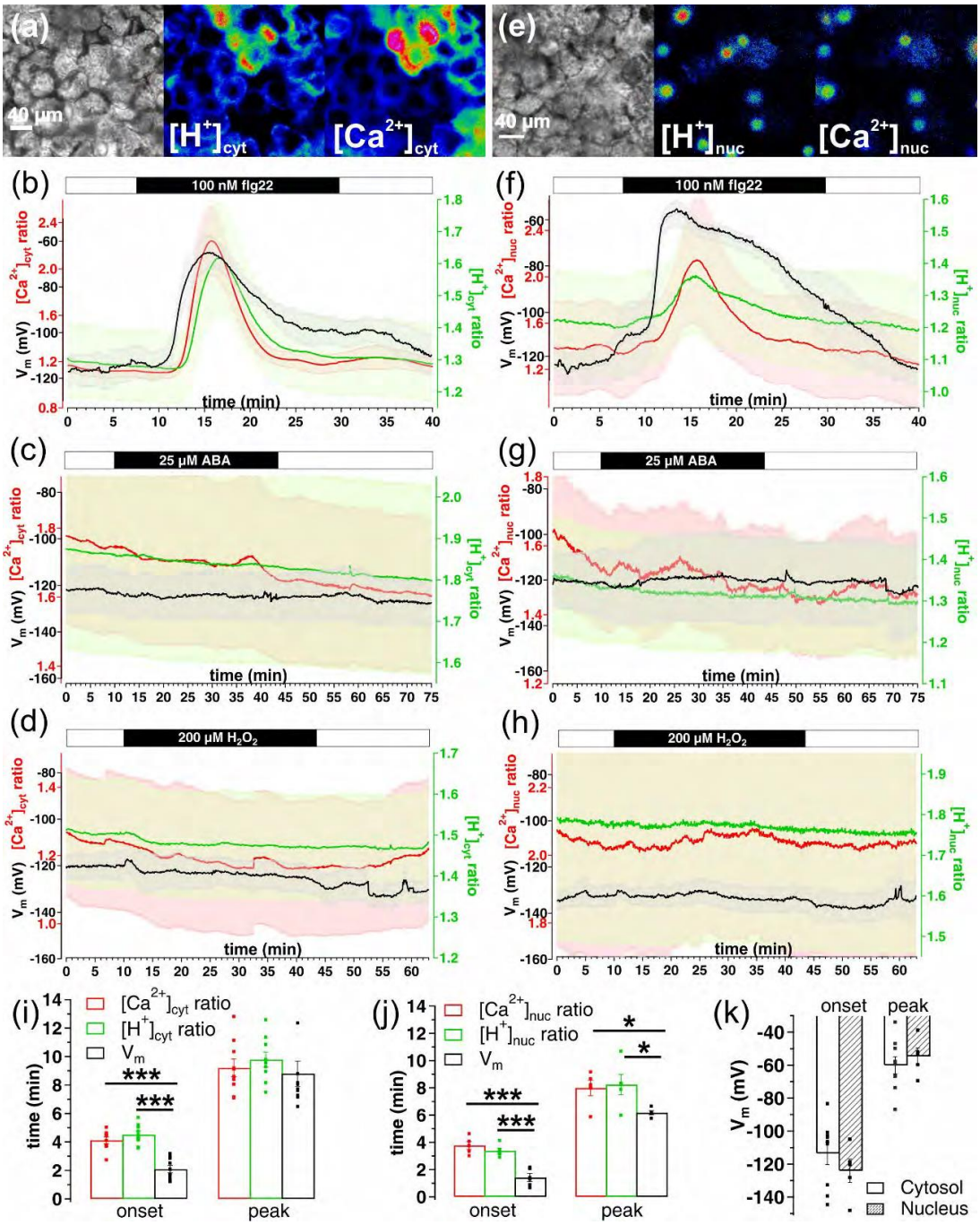

Figure 20. Distinct Ca^{2+} and H^+ signatures in the cytosol and nuclei of mesophyll cells under different stimuli.

Simultaneous Ca^{2+}, H^+ ratio imaging and V_m recordings in mesophyll cells of *N. benthamiana* leaves transiently expressing CapHensor in the cytosol or nucleus. (a, e) Representative brightfield (left), false colored H^+ ratio (middle) and Ca^{2+} ratio (right) images of mesophyll cells expressing CapHensor in the cytosol (a) and nucleus (e). (b–d) Mean $[Ca^{2+}]_{cyt}$ ratio (red), $[H^+]_{cyt}$ ratio (green) and membrane potential (V_m, black) responses to (b) 100 nM flg22 (n = 9), (c) 25 µM ABA (n = 6) and (d) 200 µM H_2O_2 (n = 5). (f–h) Mean $[Ca^{2+}]_{nuc}$ ratio (red), $[H^+]_{nuc}$ ratio (green) and V_m (black) responses to (f) 100 nM flg22 (n = 6), (g) 25 µM ABA (n = 4) and (h) 200 µM H_2O_2 (n = 5). (i, j) Mean values of the onset and peak time of Ca^{2+}

ratio (red), H^+ ratio (green) and V_m after 100 nM flg22 in the cytosol (i) and nucleus (j). (k) Bar diagram of mean membrane potential (V_m) in mesophyll cells at the onset (left) and peak (right) response to flg22 expressing CapHensor in the cytosol (blank, n = 9) or nucleus (shadow, n = 6). Dots in (i–k) indicate individual experiments. Error bars = SE. One-way ANOVA was used in (i) and (j). *, $p < 0.05$; ***, $p < 0.001$.

Ca^{2+} and H^+ changes in the cytosol or in the nucleus were monitored and combined with V_m recording on mesophyll cells transiently expressing CapHensor without any treatment as control recordings (Fig. 21). There were no significant changes of Ca^{2+}, H^+ and V_m demonstrating that without any treatment, the fluorescence and membrane voltage signals remained unchanged.

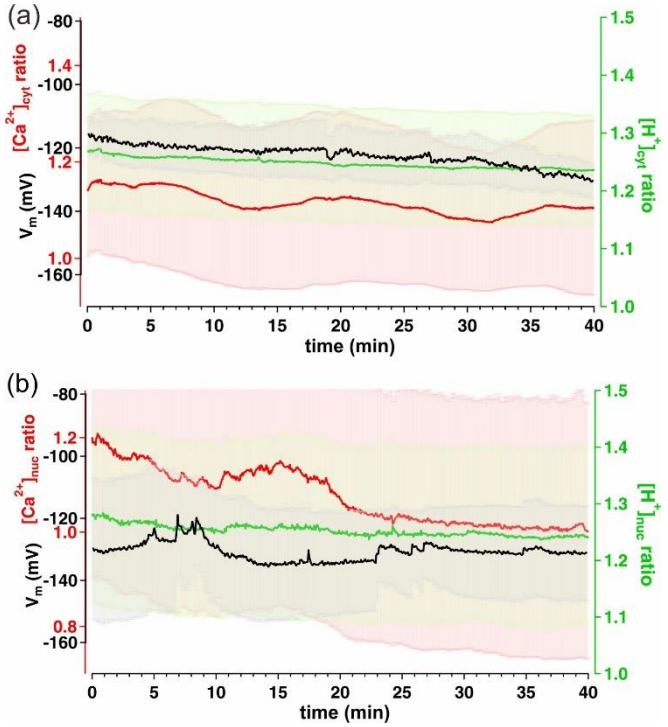

Figure 21. Ca^{2+}, H^+ and V_m in mesophyll cells under control conditions.

Simultaneous live-cell imaging of Ca^{2+} and H^+ together with membrane potential (V_m) recordings in mesophyll cells of *N. benthamiana* leaves transiently expressing CapHensor in the cytosol or in the nucleus. (a) Mean $[Ca^{2+}]_{cyt}$ ratio (red), $[H^+]_{cyt}$ ratio (green) and V_m (black) over time under control conditions (n = 4). (b) Mean $[Ca^{2+}]_{nuc}$ ratio (red), $[H^+]_{nuc}$ ratio (green) and V_m (black) over time under control conditions (n = 3). Error bars = SE.

4.5 Distinct Ca^{2+} and H^+ responses to various stimuli in different cell types

Up to this point, I have examined the Ca^{2+} and pH responses of different cell systems and in different subcellular locations, sometimes even together with membrane potential recordings, to

different stress stimuli. In pollen tubes, tip $[H^+]_{cyt}$ and $[Ca^{2+}]_{cyt}$ oscillations correlated positively with oscillatory growth velocity (Fig. 11, 22 shown in the left side) and I demonstrated tip $[H^+]_{cyt}$ regime to correlate better with growth than does tip $[Ca^{2+}]_{cyt}$ (Fig. 7, 8). In guard cells, $[Ca^{2+}]_{cyt}$ elevation and cytosolic alkalization were responsible for stomatal closure induced by ABA (Fig. 14b, 22 shown at the bottom on the right side) whereas the same phytohormone did not induce any $[Ca^{2+}]_{cyt}$, $[H^+]_{cyt}$ and membrane potential responses in mesophyll cells (Fig. 20c, g). On the contrary, flg22 induced similar Ca^{2+} in the cytosol and nucleus of mesophyll cells but accompanied with cytosolic and nuclear acidification together with a depolarization (Fig. 20b, 20f, 22 shown in the middle on the right side). The stomatal closure signals after flg22 were also very different from that of ABA, since flg22 induced a more pronounced $[Ca^{2+}]_{cyt}$ transient but no pH response in guard cells (Fig. 14d). As a resume from these experiments, my results demonstrated that Ca^{2+} and H^+ signals are not only distinct under different stimuli, but specific in different cell types, which might relay distinct information in plants (Fig. 22).

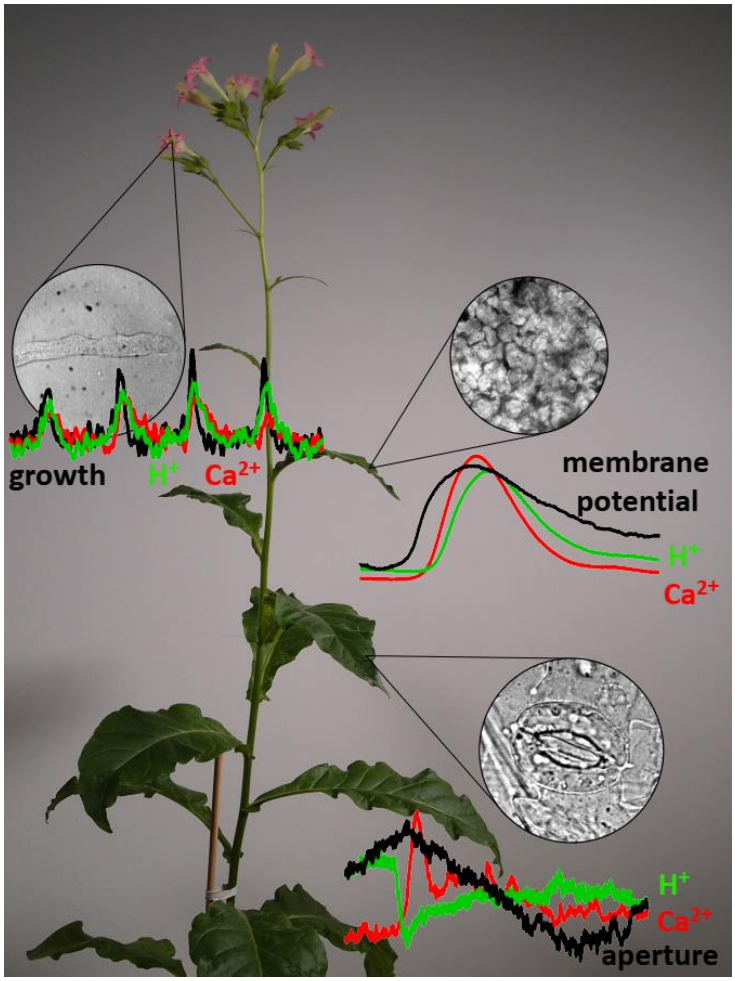

Figure 22. Distinct $Ca^{2+}$and H^+ signatures in different cell types in *Nicotiana tabacum*.

Disctinct Ca^{2+} (red line) and H^+ (green line) signatures participate in specific physiological processes in different cell types. In pollen tubes, $[Ca^{2+}]_{cyt}$, $[H^+]_{cyt}$ and growth oscillations are positively correlated with slightly shifted phase (left side). A single Ca^{2+} and H^+ peak and membrane depolarization were triggered by flg22, but not by ABA or H_2O_2 in mesophyll cells (right side, top). Cytosolic alkalization and $[Ca^{2+}]_{cyt}$ transients are accompanied with ABA induced stomatal closure (right side, bottom).

4.6 Spontaneous $[Ca^{2+}]_{cyt}$ and $[H^+]_{cyt}$ oscillations in guard cells - description of the parameters to trace their physiological role

4.6.1 Interplay between spontaneous $[Ca^{2+}]_{cyt}$ and $[H^+]_{cyt}$ oscillations in guard cells

In contrast to the imposed $[Ca^{2+}]_{cyt}$ oscillations I sometimes evoked in guard cells (Fig. S2b, c), spontaneous $[Ca^{2+}]_{cyt}$ oscillations have been often described in the literature [34,175]. In this thesis, 38.31 % of observed guard cells (n = 95 out of 248 cells) displayed naturally occurring $[Ca^{2+}]_{cyt}$ oscillations at control conditions. The spontaneous $[Ca^{2+}]_{cyt}$ transients were accompanied by synchronized $[H^+]_{cyt}$ oscillations, which prompted me to study their relationship, by using the wavelet transformation technique I used before to quantify the correlation, phase shift and interrelation between the two signals according to the package WaveletComp [360]. These synchronized $[Ca^{2+}]_{cyt}$ and $[H^+]_{cyt}$ oscillations are generally grouped into two populations (n = 32, Fig. 23a and 23b). Approximately 56.25 % oscillatory cells exhibited in-phase $[Ca^{2+}]_{cyt}$ and $[H^+]_{cyt}$ dynamics (Fig. 23a) whereas 43.75 % of the guard cells displayed antiphase behavior of $[Ca^{2+}]_{cyt}$ and $[H^+]_{cyt}$ (Fig. 23b). After cross-wavelet analysis, the period of synchronicity of $[Ca^{2+}]_{cyt}$ and $[H^+]_{cyt}$ oscillations at the significant level from a representative measurement of Fig. 23a and 23b is illustrated by regions bordered with white lines in the cross-wavelet spectra in Fig. 23c and 23d, respectively. The direction and angle of black arrows in Fig. 23c and 23d represent the temporal relationship between $[Ca^{2+}]_{cyt}$ and $[H^+]_{cyt}$ oscillations, which fits the models of synchronization of sine wave oscillations in the top of Fig. 23a and 23b and were converted into phase shifts from $-\pi$ to π. Therefore, the coherence of $[Ca^{2+}]_{cyt}$ and $[H^+]_{cyt}$ oscillations was characterized to be in-phase or antiphase based on the absolute values lower or higher than half π, respectively [360] as indicated by the scheme at the top in Fig. 23a, b. The arrows in the wavelet spectra (Fig. 23c, d) and the distribution in circular phase plot (Fig. 23, 24a) represent leading and lagging signals. This means that the sign of the phase shift suggested the sequence of $[Ca^{2+}]_{cyt}$ or $[H^+]_{cyt}$ oscillations, demonstrating which signal is leading or lagging (Fig. 23a, b).

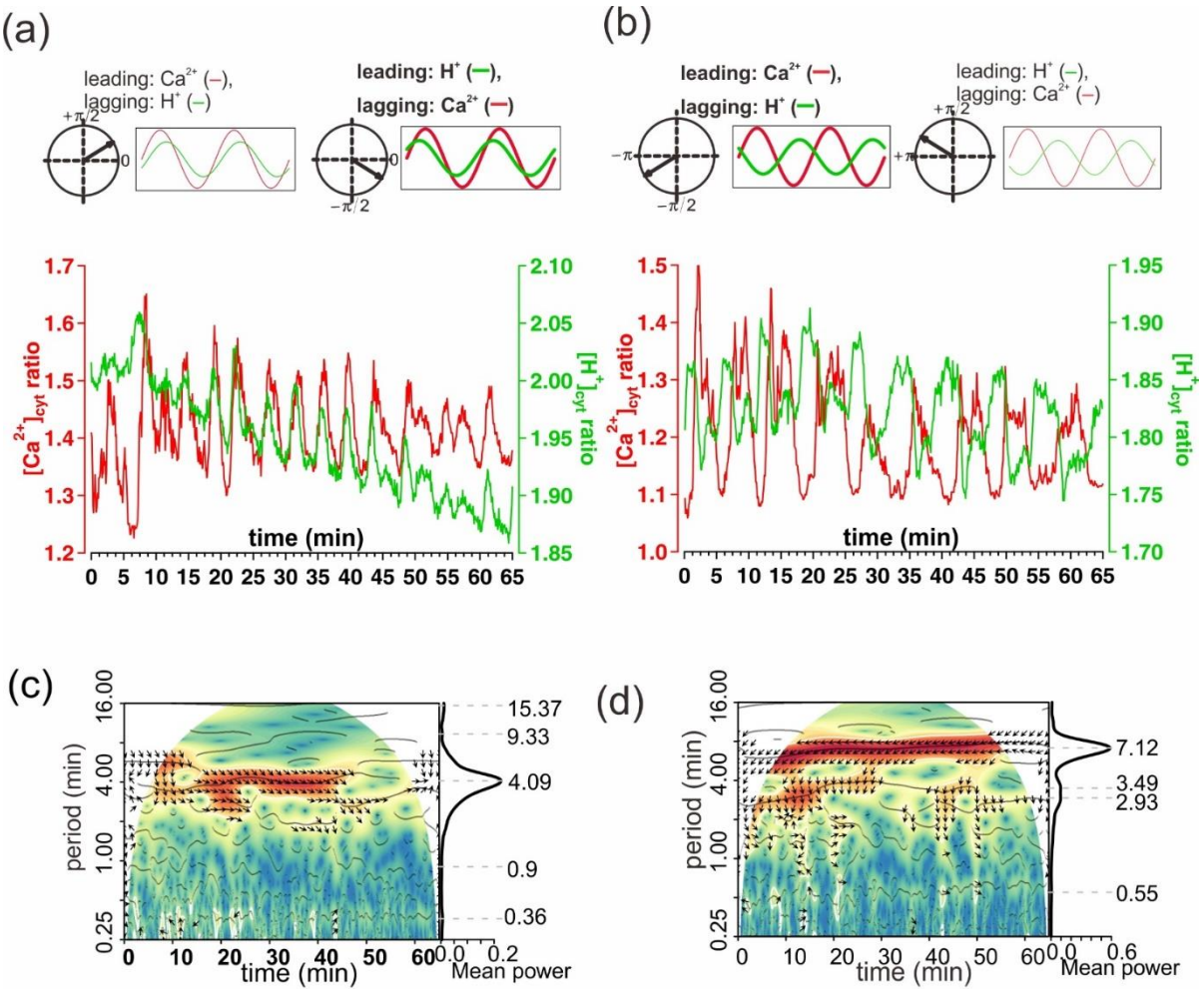

Figure 23. Two populations of guard cells with spontaneous $[Ca^{2+}]_{cyt}$ and $[H^+]_{cyt}$ oscillations.

Spontaneous $[Ca^{2+}]_{cyt}$ and $[H^+]_{cyt}$ oscillations in *N. tabacum* guard cells stably expressing CapHensor under normal conditions. (a, b) Representative spontaneous $[Ca^{2+}]_{cyt}$ ratio (red) and $[H^+]_{cyt}$ ratio (green) in guard cell indicated in-phase correlation (a) and antiphase correlation (b). The circles on the top of the trace in a and b are used to demonstrate the leading and lagging signal of Ca^{2+} or H^+ according to the package [360]. (c, d) Wavelet spectra are performed by wavelet transformation of $[Ca^{2+}]_{cyt}$ and $[H^+]_{cyt}$ oscillations from experiments in (a) and (b), respectively. The red color represents the power of oscillations over time with the significant area ($p < 0.05$) surrounded by white lines. The directions of arrows in c and d fit the circle in a and b, respectively, representing the leading or lagging signal. The periods of $[Ca^{2+}]_{cyt}$ and $[H^+]_{cyt}$ oscillations are shown in vertical axis (left side) and the most significant and stable period is read out with the peak in vertical axis (right side).

The phase distribution of each guard cell was displayed in a circular phase plot (Fig. 24a), where white colored bars represent the in-phase guard cell (Fig. 23a) while the antiphase guard cells (Fig. 23b) are represented by the grey color bars (Fig. 24a). The circular phase plot indicated that $[H^+]_{cyt}$

was leading $[Ca^{2+}]_{cyt}$ in the in-phase guard cells whereas $[Ca^{2+}]_{cyt}$ was the leading signal in guard cells having antiphase $[Ca^{2+}]_{cyt}$ and $[H^+]_{cyt}$ regime (Fig. 24a). The averaged correlation coefficient of $[Ca^{2+}]_{cyt}$ and $[H^+]_{cyt}$ oscillations in in-phase and antiphase guard cells was 0.41 ± 0.05 and -0.45 ± 0.04, respectively (Fig. 24b), meaning the correlation level was similar in opposite phase relations in the two populations of guard cells. The magnitude of the correlation coefficients indicates a very good correlation of $[Ca^{2+}]_{cyt}$ and $[H^+]_{cyt}$ signals. The average phase values of in-phase and antiphase guard cells were quantified between 0.56 ± 0.19 and -2.53 ± 0.11 radians with a significant difference, respectively (Fig. 24c). Moreover, $[H^+]_{cyt}$ oscillations preceded $[Ca^{2+}]_{cyt}$ oscillations by 13.10 ± 4.94 s in in-phase guard cells whereas $[Ca^{2+}]_{cyt}$ transients led $[H^+]_{cyt}$ transients by 25.67 ± 1.91 s in antiphase guard cells (Fig. 24c). In respect to the period of $[Ca^{2+}]_{cyt}$ and $[H^+]_{cyt}$ oscillations, similar wavelet power spectra in Fig 23c and 23d were received and only the most significant period in the vertical axis on the right side was used to read out and quantify the main period (Fig. 24d). $[Ca^{2+}]_{cyt}$ and $[H^+]_{cyt}$ oscillations in the same cell displayed similar period with a mean period of 4.48 ± 0.18 min ranging from 3.44-5.82 min in in-phase guard cells whereas the mean period was around 8.89 ± 1.35 min in antiphase guard cells (Fig. 24d). These spontaneous $[Ca^{2+}]_{cyt}$ and $[H^+]_{cyt}$ oscillations showed a tight coupling of these two signals, even in different oscillatory regimes. However, what the exactly physiological role of these naturally occurring $[Ca^{2+}]_{cyt}$ and $[H^+]_{cyt}$ oscillations might be and what kind of information, if any, they encode still remains to be shown.

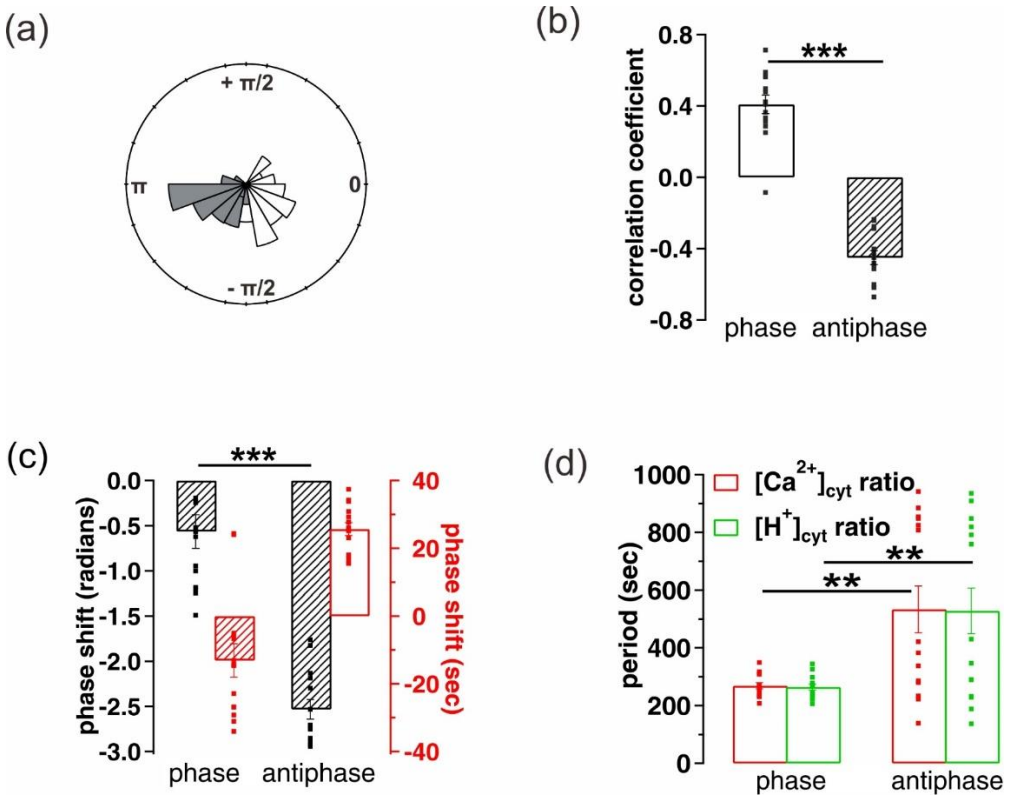

Figure 24. Two populations of guard cells with different $[Ca^{2+}]_{cyt}$ and $[H^+]_{cyt}$ phase-relations.
Quantification of phase analysis and correlations between natural $[Ca^{2+}]_{cyt}$ and $[H^+]_{cyt}$ oscillations of the two populations of *N. tabacum* guard cells. (a) Mean phase shift in radians of guard cells in phase (white, n = 18, a) and guard cells in antiphase (grey, n = 14, b) based on the values and sign of circular plots. Note: $[Ca^{2+}]_{cyt}$ and $[H^+]_{cyt}$ oscillations are in phase or in antiphase when the absolute phase in radians is lower or higher than half π, respectively. (b) Correlation coefficient of inphase (white, n = 18) and antiphase (shadow, n = 14) $[Ca^{2+}]_{cyt}$ and $[H^+]_{cyt}$ oscillations in guard cells. (c) Phase relations in radians (black) and shifts in seconds (red) in (c) between $[Ca^{2+}]_{cyt}$- and $[H^+]_{cyt}$- ratio oscillations of two populations of guard cells. (d) Period quantification of $[Ca^{2+}]_{cyt}$ (red) and $[H^+]_{cyt}$ (green) oscillations from inphase and antiphase guard cells. Dots in (b-d) represent datapoints of individual guard cells. Error bars = SE. t-test was used in (b-d). **, $p < 0.01$; ***, $p < 0.001$.

4.6.2 Natural $[H^+]_{cyt}$ oscillations are blocked by ABA but not by flg22

The possible role of Ca^{2+} oscillations in the coding of information is discussed extensively [31,32,171,345,346,382,383], but whether the spontaneously occurring oscillations are related to signaling pathways is not clear. To study whether these oscillations could represent part of the ABA or flg22 signaling pathway, I applied 10 µM ABA and 1 µM flg22 on oscillatory guard cells (Fig. 25). Stomatal closure induced by 10 µM ABA and 1 µM flg22 seen in non-oscillatory guard cells (Fig. 14b, 14d) was partially suppressed in oscillatory guard cells (Fig. 25a, b, e, f). Interestingly, $[Ca^{2+}]_{cyt}$ oscillations were not altered by either ABA or flg22 whereas $[H^+]_{cyt}$ oscillations were

abolished by ABA but not by flg22 (Fig. 25a, b, e, f). The cross-wavelet spectra, as exemplified in Fig. 25c and Fig 25d also displayed the interruption of $[H^+]_{cyt}$ oscillations, since the significant area shown in red color surrounded with white lines disappeared during the application of ABA but not after flg22 treatment (Fig. 25c, d). The disappearing significant area (red) and arrows during ABA but not flg22 treatment suggested the link between spontaneous $[Ca^{2+}]_{cyt}$ and $[H^+]_{cyt}$ oscillations to be diminished in the presence of ABA (Fig, 25c, d). This was confirmed by cross-correlation analysis showed ABA significantly interrupted the link between natural $[Ca^{2+}]_{cyt}$ and $[H^+]_{cyt}$ oscillations by dampening $[H^+]_{cyt}$ oscillations (Fig. 25g) whereas this was not the case with flg22 (Fig. 25h). This interesting phenomenon questions how natural $[H^+]_{cyt}$ oscillations were blocked by ABA.

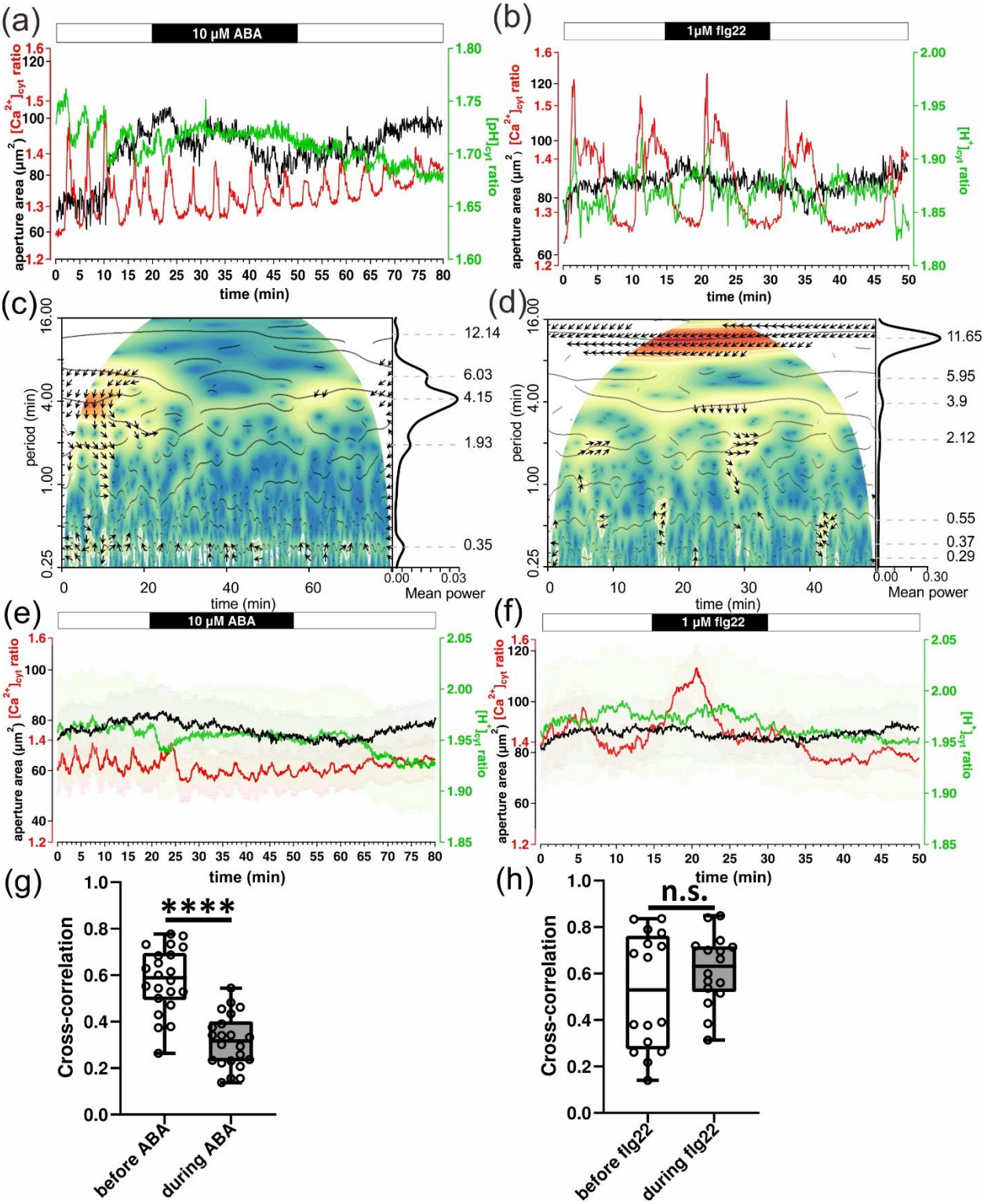

Figure 25. Correlation between spontaneous $[Ca^{2+}]_{cyt}$ and $[H^+]_{cyt}$ oscillations in guard cells is interrupted by ABA but not by flg22.

Interaction between spontaneous $[Ca^{2+}]_{cyt}$ and $[H^+]_{cyt}$ oscillations in response to ABA and flg22 in *N. tabacum* guard cells stably expressing CapHensor. (a, b) A representative measurement of $[Ca^{2+}]_{cyt}$ (red),

$[H^+]_{cyt}$ (green) and aperture area (black) upon 10 µM ABA (a) and 1 µM flg22 (b). (c, d) Wavelet spectra of the entire measurement of 10 µM ABA from (a) and 1 µM flg22 from (b), respectively. The significant oscillations are shown in the red area borded with white lines. The arrow directions indicate the lagging or leading signals of $[Ca^{2+}]_{cyt}$ or $[H^+]_{cyt}$ according to the scheme in Fig. 23a, 23b. (e, f) Mean traces of spontaneous $[Ca^{2+}]_{cyt}$ (red) oscillations, $[H^+]_{cyt}$ (green) oscillations and aperture area (black) of oscillatory *N. tabacum* guard cells stably expressing CapHensor upon 10 µM ABA (e) and 1 µM flg22 (f). (g, h) Bar diagrams of quantification of cross-correlation between spontaneous $[Ca^{2+}]_{cyt}$ and $[H^+]_{cyt}$ oscillations before (white) and during (grey) ABA (g, n = 22) or flg22 (h, n = 16) treatment. Error bars = SE. Dots indicate individual guard cells. Error bars = SE. t-test was used in (g, h). ****, $p < 0.0001$; n.s.: no significant difference.

4.6.3 Vacuolar H^+ homeostasis is blocked by ABA but not by flg22

Given the pH difference between the cytosol and the vacuole of almost two pH units, I hypothesized that vacuolar H^+ homeostasis could feed-back on $[H^+]_{cyt}$. I tested if vacuolar pH is responsible for spontaneous $[H^+]_{cyt}$ oscillations in guard cells under normal conditions and contributes to the blocked spontaneous $[H^+]_{cyt}$ oscillations by ABA (Fig. 25). The BCECF dye was used on oscillatory guard cells to monitor changes in vacuolar H^+ concentrations ($[H^+]_{vac}$, F_{440}/F_{500}) after the application of ABA and flg22 (Fig. 26). I found vacuolar H^+ dynamics also to display oscillations under normal conditions (Fig. 26). Interestingly, the vacuole became acidified sustainly upon ABA treatement and transiently by flg22 (Fig. 15, 26) whereas vacuolar H^+ oscillations were dampened by ABA, but not by flg22 (Fig. 26). Moreover, vacuolar H^+ oscillations restarted to occur when removing ABA, which is more visible in single cell recordings (Fig. 26a). I could conclude that dampening of the spontaneous cytosolic and vacuolar H^+ oscillations by ABA are coupled. Therefore, cytosolic pH alterations are suggested to be caused by changes in vacuolar H^+ translocation to finally regulate $[H^+]_{cyt}$ oscillations.

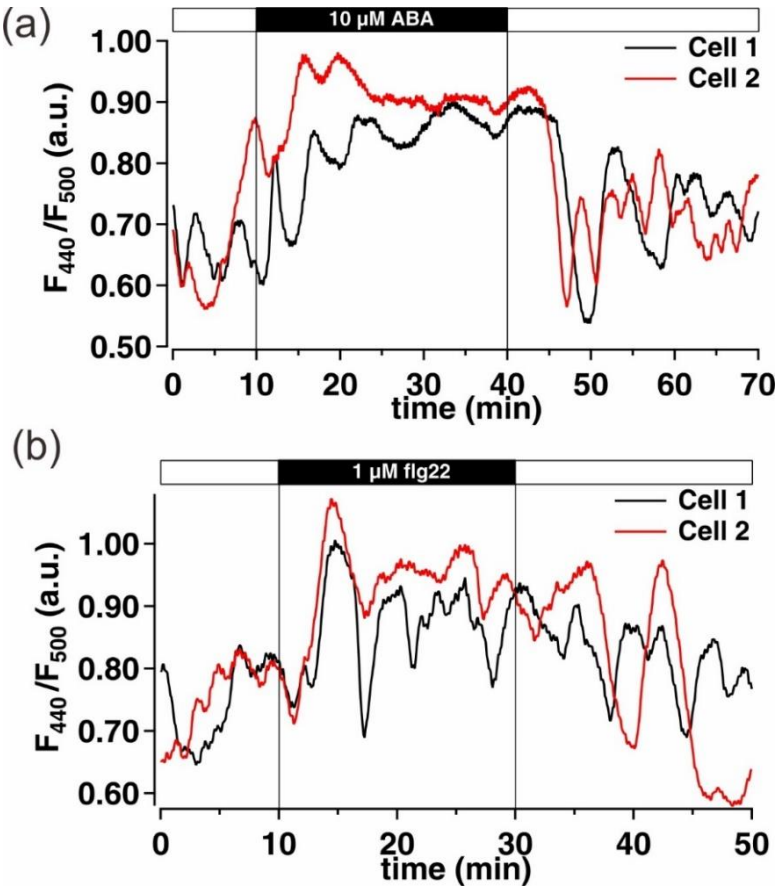

Figure 26. Vacuolar acidification is triggered by ABA or flg22 in individual guard cells.
Guard cells of *N. tabacum* (SR1) epidermal strips are incubated in solutions containing 15 µM BCECF dye and washed out before starting measurements. (a, b) Ratiomatric fluorescences from BCECF dye (F_{440}/F_{500}) represent vacuolar H^+ concentrations ($[H^+]_{vac}$) of representative individual guard cells upon 10 µM ABA (a) and 1 µM flg22 (b) over time. Vacuolar acidification in guard cells is induced by ABA and flg22 and dampening of oscillations is triggrered by ABA, but not by flg22.

4.7 Interconnection between Ca^{2+}, H^+ and K^+ dynamics in regulating stomatal movement

4.7.1 Imposed $[Ca^{2+}]_{cyt}$ transients are accompanied by reduced $[H^+]_{cyt}$ in guard cells

My previous results (Fig. 19) showed that, high external Ca^{2+} only induced slowly and slightly stomatal closure but $[H^+]_{cyt}$ and $[Ca^{2+}]_{cyt}$ homeostasis is reversely connected with each other in guard cells. Furthermore, my data on active pH change has shown a pH signal in the cytosol seems to be a signal superimposed on the Ca^{2+} signal and the level of alkalization controls the stomatal closure rate (Fig. 19). To investigate $[Ca^{2+}]_{cyt}$ and $[H^+]_{cyt}$ correlations in guard cells and a possible role of $[Ca^{2+}]_{cyt}$ oscillations in stomatal regulation, I evoked repetitive $[Ca^{2+}]_{cyt}$ increases by

increasing the medium Ca^{2+} concentration from 10 µM to 1 mM. Regular $[Ca^{2+}]_{cyt}$ oscillations could be induced this way every 5 min four times in a row (Fig. 27a, S3). The imposed $[Ca^{2+}]_{cyt}$ oscillations were always accompanied by cytosolic alkalization (Fig. 27a, S3), however pronounced stomatal closure was not observed with this experimental design, despite the huge Ca^{2+} changes could be evoked (Fig. 27a, b). These results showed a reproducible antiphase relation between $[Ca^{2+}]_{cyt}$ and $[H^+]_{cyt}$ in guard cells (Fig. 27a, b) and demonstrated that $[Ca^{2+}]_{cyt}$ increases per se are not essentially inducing stomatal closure responses. To identify which membrane transport component in guard cells possibly participates in high $CaCl_2$ induced cytosolic alkalization, sodium orthvanadate (Na_3VO_4) was applied (Fig. 27a, b). Na_3VO_4 was used in previous studies as a potent H^+-ATPase inhibitor to block H^+-pump activity [233,234,236]. The negative correlations between $[Ca^{2+}]_{cyt}$ and $[H^+]_{cyt}$ induced by extracellular high $CaCl_2$ were switched into positive correlations and stomata started to close in the presence of Na_3VO_4 (Fig. 27a-c). This suggested plasma membrane H^+-ATPases are responsible for the antiphase correlation between $[Ca^{2+}]_{cyt}$ and $[H^+]_{cyt}$ under high $CaCl_2$ treatment. Quantification of the onset and the peak times of $[Ca^{2+}]_{cyt}$ and $[H^+]_{cyt}$ upon 1 mM $CaCl_2$ treatment (Fig. 27d) in the absence of vanadate since vanadate altered the negative correlations between the two signals. $[Ca^{2+}]_{cyt}$ started to increase 0.52 ± 0.07 min after high $CaCl_2$ application while $[H^+]_{cyt}$ took 1.19 ± 0.08 min to response (Fig. 27d). Relatively, the peak of $[Ca^{2+}]_{cyt}$ transients still significantly preceded maximum cytosolic alkalization (Fig. 27d). These timing analysis suggests $[Ca^{2+}]_{cyt}$ could regulate plasma membrane H^+-ATPases leading to this negative correlations between $[Ca^{2+}]_{cyt}$ and $[H^+]_{cyt}$ (Fig. 27d). To study in more detail the negative correlation between $[Ca^{2+}]_{cyt}$ and $[H^+]_{cyt}$ in previous guard cells experiments that I performed up until now (Fig. 14, 19), I again made use of BTA to study the interconnection of $[Ca^{2+}]_{cyt}$ and $[H^+]_{cyt}$ homeostasis. I asked if Ca^{2+} permeable channels responsible for $[Ca^{2+}]_{cyt}$ homeostasis could be regulated by intracellular pH. Therefore, BTA was applied to guard cells with spontaneous $[Ca^{2+}]_{cyt}$ oscillations (Fig. 27e), which enabled me to compare the effect of cytosolic acidification on the regularly occurring $[Ca^{2+}]_{cyt}$ transients. Pronounced stomatal opening was triggered by BTA but $[Ca^{2+}]_{cyt}$ oscillations were hardly affected by cellular acidification, they were only slightly dampened in the first 5 to 10 min when cytosolic pH was not yet at equilibrium (Fig. 27e). Especially in the individual traces (Fig. 27e, upper figure), it was evident that cytosolic acidification did not alter at all $[Ca^{2+}]_{cyt}$ oscillations, pointing to a pH-insensitivity of the Ca^{2+} channels involved. Overall, the negative correlation between $[Ca^{2+}]_{cyt}$ and

$[H^+]_{cyt}$ in guard cells provided solid experimental evidence for defined cross-links in $[Ca^{2+}]_{cyt}$ and $[H^+]_{cyt}$ homeostasis, which partially involved plasma membrane H^+-ATPases activity.

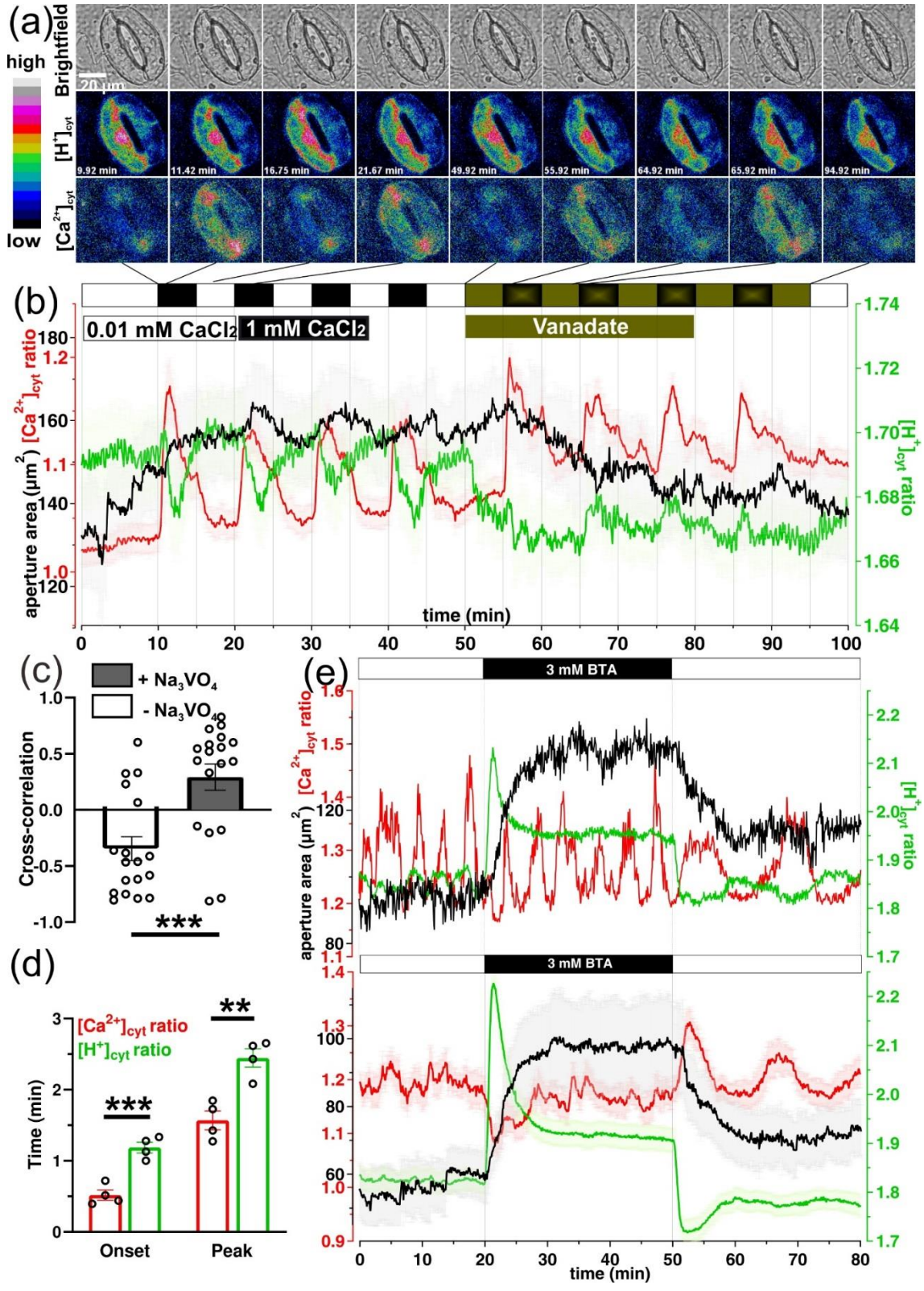

Figure 27. Interactions of $[Ca^{2+}]_{cyt}$ and $[H^+]_{cyt}$ in guard cells upon different stimuli.

Live-cell imaging of $[Ca^{2+}]_{cyt}$, $[H^+]_{cyt}$ together with stomatal movement in *N. tabacum* guard cells from epidermal strips stably expressing CapHensor. (a) Representative brightfield (top), false colored $[H^+]_{cyt}$ ratio (middle) and $[Ca^{2+}]_{cyt}$ ratio (bottom) images of a stomata in response to high $CaCl_2$ in the absence or presence of vanadate (Na_3VO_4). (b) Mean $[Ca^{2+}]_{cyt}$ ratio (red), $[H^+]_{cyt}$ ratio (green) and aperture area (black) dynamics over time when perfusing from 10 µM $CaCl_2$ to 1 mM $CaCl_2$ and then combine with 100 µM vanadate (Na_3VO_4) (n = 18). (c) Bar diagram of quantification of cross-correlation between $[Ca^{2+}]_{cyt}$ and $[H^+]_{cyt}$ without and with vanadate from (b, n=18). (d) Bar diagram of quantification of onset and peak time of $[Ca^{2+}]_{cyt}$ ratio and $[H^+]_{cyt}$ ratio after application of 1 mM $CaCl_2$ in the phase of without vanadate from (b, n = 18). (e) $[Ca^{2+}]_{cyt}$ (red), $[H^+]_{cyt}$ (green) and aperture area (black) from a representative oscillatory *N. tabacum* guard cell stably expressing CapHensor in the cytosol upon 3 mM BTA application (top) and mean values (n = 20, bottom). The cytosolic pH is clamped to be more acid and stomata open whereas $[Ca^{2+}]_{cyt}$ oscillations are not interrupted by BTA. Bars above indicate the time of treatments and different treatments are marked with different colors. Dots in (c) indicate individual measurements from (b). Dots in (d) indicate the average point of each 1 mM $CaCl_2$ treatment from individual measurements from (b). Error bars = SE. t-test was used in (c and d). ***, $p < 0.001$; **, $p < 0.01$.

4.7.2 Osmotic effects are the main cause for stomatal movement and $[Ca^{2+}]_{cyt}$ changes induced by high and low KCl solutions

Oscillations in $[Ca^{2+}]_{cyt}$ with distinct signatures such as variable amplitude or frequency are discussed to encode specific information in guard cells [31,35,384]. Stomatal closure was hypothesized to be associated with a defined range of $[Ca^{2+}]_{cyt}$ oscillations by challenging guard cells with a combination of high/low KCl buffers that elicit depolarization and hyperpolarization of the plasma membrane to evoke $[Ca^{2+}]_{cyt}$ rises [171,172]. However, from my previous results (Fig. 19, 27), $[Ca^{2+}]_{cyt}$ increases did not induce pronounced stomatal closure. Hence, to modify defined $[Ca^{2+}]_{cyt}$ oscillations and stomatal movement as reported by high/low KCl buffer exchanges, I used stably expressing tobacco CapHensor lines and evoked by a similar manner oscillatory $[Ca^{2+}]_{cyt}$ increases in guard cells to monitor stomatal behavior (Fig. 28a, b). This enabled me to test the hypothesis whether defined $[Ca^{2+}]_{cyt}$ oscillations do steer guard cells behavior as it was particularly interesting especially I found cytosolic pH changes control stomatal movement more efficiently than $[Ca^{2+}]_{cyt}$ (Fig. 14, 18 and 19). In addition, by using high and low K^+-solutions I could investigate the role of K^+ in stomatal movement since K^+ is the main inorganic cation to be uptaken by guard cells to build up the turgor pressure. I used a hyperpolarization solution (0.1 mM KCl, 1 mM $CaCl_2$, 10 mM MES with pH 5.8 adjusted with BTP) and depolarization solution (50.1 mM KCl, 1 mM $CaCl_2$, 10 mM MES, pH 5.8) with equal $CaCl_2$ concentrations (Fig. 28, 29a). Stomatal closure induced by high KCl solution was accompanied with a cytosolic alkalization but without a $[Ca^{2+}]_{cyt}$ increase,

when this was repeated four times (Fig. 28, 29a). However, a cytosolic acidification and a $[Ca^{2+}]_{cyt}$ peak occurred when switching back to the low KCl solutions (n = 30, Fig. 28, 29a). Curiously, when alternating high/low potassium concentrations were applied, I observed that opening but not closing was associated with a $[Ca^{2+}]_{cyt}$ signal, which is contrary to the general opinion on stomata regulation. Because the tight interrelation between $[Ca^{2+}]_{cyt}$ and $[H^{+}]_{cyt}$ homeostasis has been investigated (Fig. 27b, c), whether $[Ca^{2+}]_{cyt}$ rises could be altered in stomatal opening was tested using 3 mM BTA (Fig. 28a, b). The results (Fig. 28b, 29a) showed $[Ca^{2+}]_{cyt}$ peaks associated with stomatal opening were not influenced by BTA (Fig. 28c). This results further confirmed that cytosolic acidification led to stomatal opening as I have shown in previous studies, where BTA could block stomatal closure induced by ABA and flg22 (Fig. 18) [339].

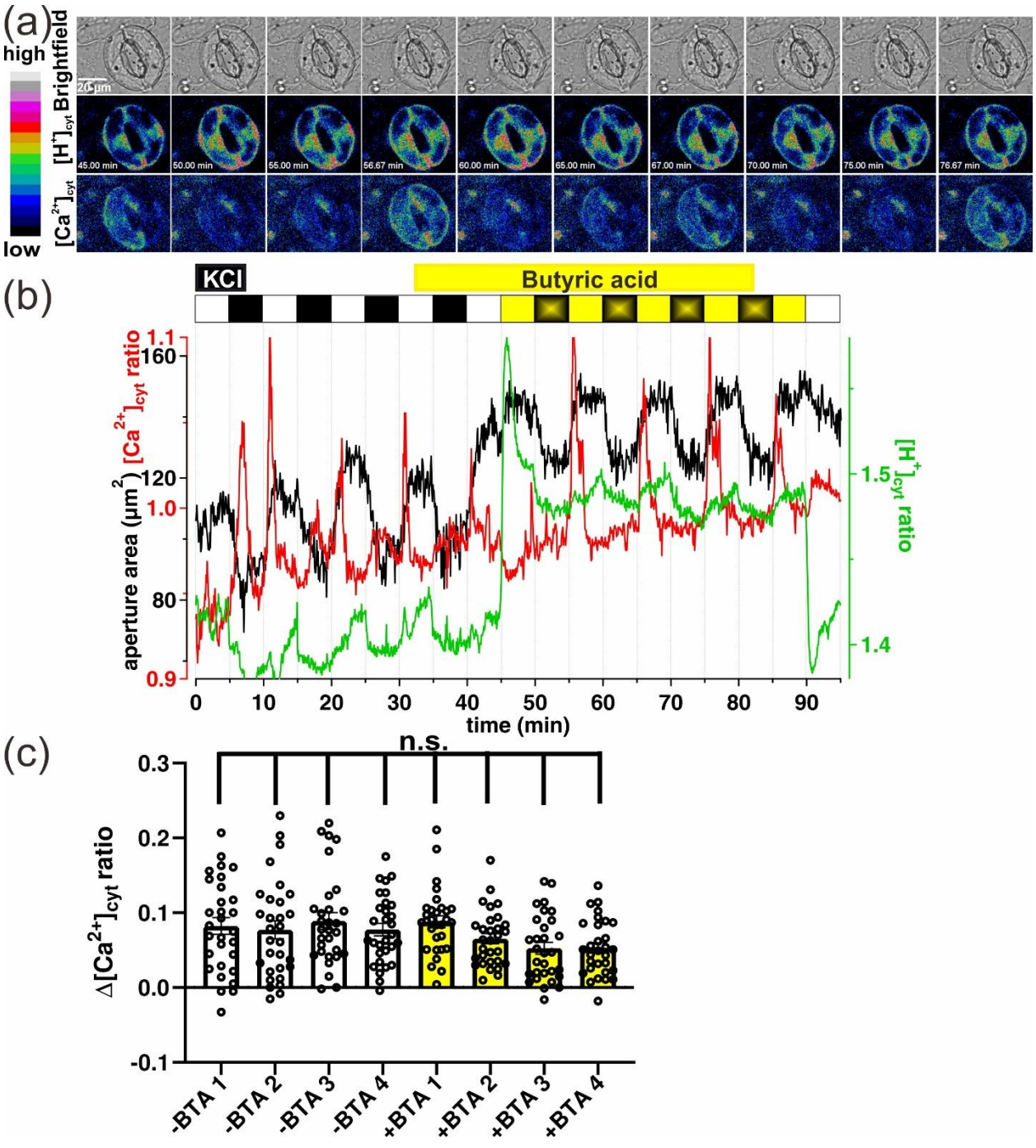

Figure 28. $[Ca^{2+}]_{cyt}$, $[H^+]_{cyt}$ and stomatal movement under different KCl concentrations in individual guard cells.

Live-cell imaging of CapHensor stably expressed in a representative *N. tabacum* guard cell together with aperture monitoring upon different KCl concentrations. (a) Time-lapse brightfield (upper), false colored $[H^+]_{cyt}$ ratio (middle) and $[Ca^{2+}]_{cyt}$ ratio (bottom) images of a representative stomata. (b) $[Ca^{2+}]_{cyt}$- (red), $[H^+]_{cyt}$- (green) ratio and aperture area (black) upon different KCl concentrations without (-) and with (+) 3 mM BTA from (a). (c) Amplitude of $[Ca^{2+}]_{cyt}$ changes ($\Delta[Ca^{2+}]_{cyt}$ ratio) when switching back to solutions containing 0.1 mM KCl without (-) and with (+) BTA (n = 30). The presence of BTA does not influence

$[Ca^{2+}]_{cyt}$ transients significantly. Error bars = SE. One-way ANOVA was used in (c). n.s.: no significant difference.

4.7.3 $[H^+]_{cyt}$ homeostasis is modulated by potassium transport in guard cells

To investigate if the closing and opening of the stomata by switching high/low KCl solutions was rather related to an osmotic effect, I made use of approximately 100 mM mannitol with equal osmolality to replace 50 mM KCl (n = 24, Fig. 29b). A rigorous comparison of repetitive changes in high/low KCl and mannitol treatments was performed in the presence and absence of BTA. Stomatal movement and $[Ca^{2+}]_{cyt}$ responses to 100 mM mannitol and 50 mM KCl (Fig. 29a, b) were very similar, indicating that stomatal movement and $[Ca^{2+}]_{cyt}$ changes when switching between low and high KCl solutions were mainly a result of osmotic imbalance (Fig. 29a, b). Stomatal movement and $[Ca^{2+}]_{cyt}$ changes were not influenced much in the presence of BTA (Fig. 28c, 29a, 29b, 29e). Interestingly, cytosolic acidification and alkalization occurred when switching low/high KCl solution and these changes in $[H^+]_{cyt}$ homeostasis became more pronounced in the presence of BTA (Fig. 28b, 29a, 29d). Contrary to that, no changes in $[H^+]_{cyt}$ homeostasis were observed upon treatment with the mannitol solution (Fig. 29b, 29d), pointing out that $[H^+]_{cyt}$ changes are based on changes in ions rather induced by the osmotic shock. However, where the alterations in $[H^+]_{cyt}$ during high KCl application originate from was unclear, but I always saw an alkalization upon high KCl concentration. I assumed KCl rather than Ca^{2+} to be responsible for changes in the $[H^+]_{cyt}$ homeostasis. Thus, I made use of the effective K^+ channel blocker Cs^+ [385,386], and exchanged the 50 mM KCl solution with 50 mM CsCl to test if K^+-channels were involved in the pH changes. Similar stomatal movement and $[Ca^{2+}]_{cyt}$ responses were observed with 50 mM CsCl treatment, but $[H^+]_{cyt}$ changes were largely reduced but still occurred obviously (n = 26, Fig. 29c, d, e). Stomatal opening always occurred in hyperpolarization solution (0.1 mM KCl) while stomatal closure was induced in solution regardless of 50 mM KCl, 100 mM mannitol or 50 mM CsCl (Fig. 29a-c, 29e), which demonstrated the osmolality changes to be the main factor for stomatal movement. But the KCl was associated with the changes in $[H^+]_{cyt}$ homeostasis (Fig. 29a-c, e).

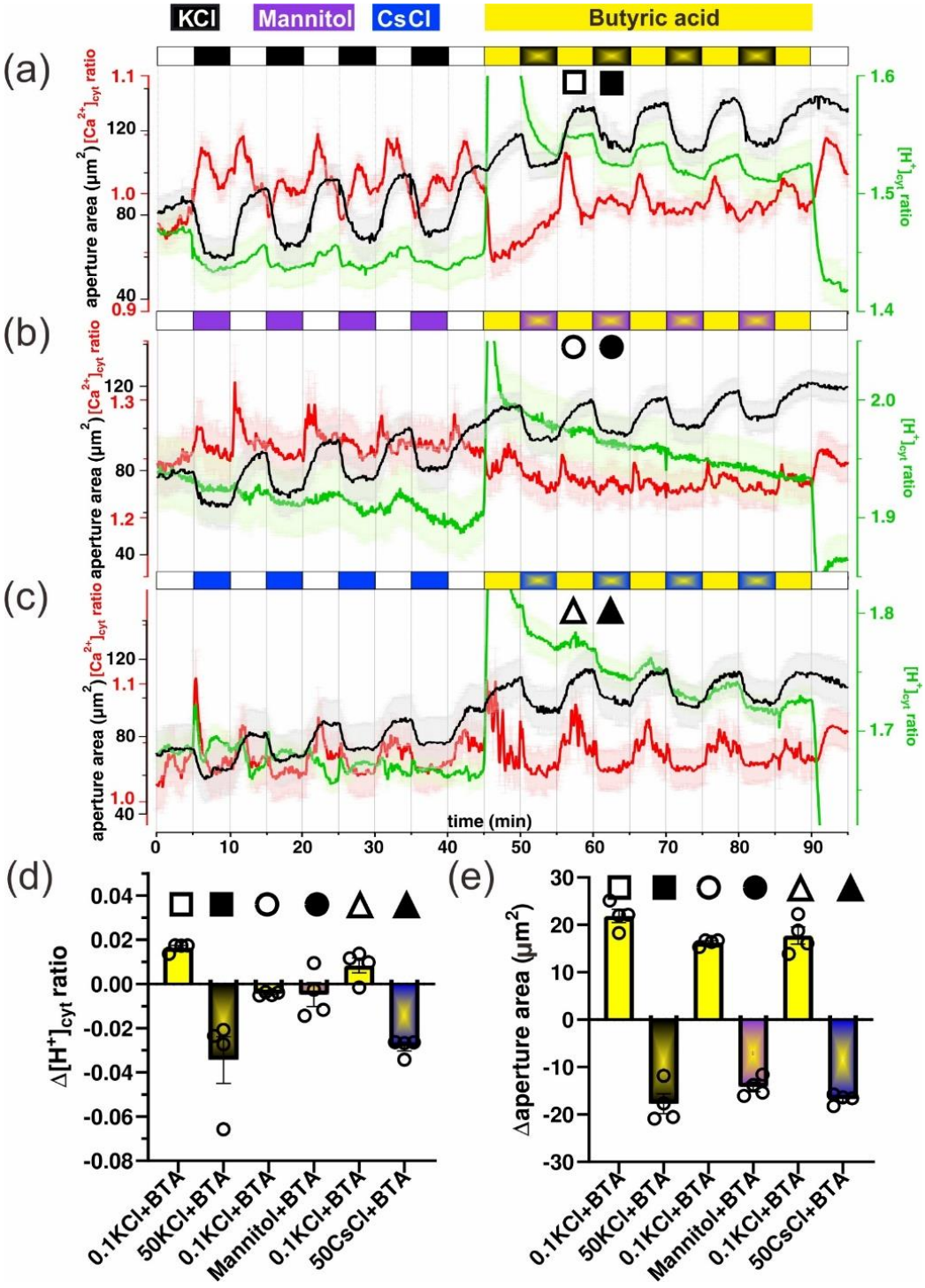

Figure 29. $[Ca^{2+}]_{cyt}$ and $[H^+]_{cyt}$ responses and stomatal movement upon different KCl concentrations.

Live-cell imaging of $[Ca^{2+}]_{cyt}$ ratio and $[H^+]_{cyt}$ ratio and monitoring aperture area under different stimuli. (a) Mean $[Ca^{2+}]_{cyt}$ (red), $[H^+]_{cyt}$ (green) and aperture area (black) perfusion from 0.1 mM KCl to 50.1 mM KCl repeated for four times and then combined with 3 mM BTA (n = 30). (b, c) Mean $[Ca^{2+}]_{cyt}$ (red), $[H^+]_{cyt}$ (green) and aperture area (black) response to 100 mM mannitol (b, n = 24) or 50 mM CsCl (c, n = 26) four

times and then both combined with 3 mM BTA. (d, e) Quantification of $[H^+]_{cyt}$ changes ($\Delta[H^+]_{cyt}$ ratio, d) and aperture changes (Δaperture area, e) from the experiments in (a-c). Bars above indicate the time of treatments and different treatments are marked with different colors. Dots in (d, e) indicate average values of each repeat marked by symbols of individual measurements in (a-c). Error bars = SE.

4.7.4 $[H^+]_{cyt}$ homeostasis is regulated by plasma membrane potassium transport and H^+-ATPases activity in guard cells

Based on the smaller $[H^+]_{cyt}$ dynamics with the CsCl solution compared with the low/high KCl solution (Fig. 29a, c, d), two possible H^+-transport scenarios can be imagined to induce $[H^+]_{cyt}$ homeostasis including plasma membrane H^+-ATPases and/or H^+-coupled transporters. Plasma membrane H^+-ATPases usually pump H^+ out of the cytosol to maintain the chemical-electric gradient. To investigate whether plasma membrane H^+-ATPases function in low/high KCl induced $[H^+]_{cyt}$ homeostasis, vanadate, a H^+-ATPases blocker was combined with applications of the low/high KCl solution in the presence of BTA (Fig. 30a). In the presence of vanadate, high/low KCl solutions triggered stomatal movement remained (Fig. 30a, d), but significantly less pronounced $[H^+]_{cyt}$ reduction (alkalization) was monitored (Fig. 30a, c), which was suggestive for plasma membrane H^+-ATPases to partially function in $[H^+]_{cyt}$ response to KCl application (n = 26, Fig. 30a, c, d). The other possible factor to modulate $[H^+]_{cyt}$ homeostasis under KCl conditions was K^+ and/or Cl^- in co-transport with H^+. Given that the changes in $[H^+]_{cyt}$ were only partially reduced by CsCl solution (Fig. 29c, d) or KCl solutions containing vanadate (Fig. 30a, c), I asked whether Cl^- was associated with $[H^+]_{cyt}$ changes in low/high KCl solutions. I used 50 mM Tris-Cl (Fig. 30b) to monitor the effect of Cl^- on a possible pH regulation. The application of 50 mM Tris-Cl did not change $[H^+]_{cyt}$ homeostasis to the same extent as KCl did, while stomatal movement was similarly regulated (n = 26, Fig. 30b-d). Interestingly, in contrast to a cytosolic alkalization, a slight cytosolic acidification was observed upon Tris-Cl application, indicative for the existence of H^+/Cl^- symporters at the plasma membrane.

In conclusion, these results suggested $[H^+]_{cyt}$ homeostasis was mainly attributed to transport of potassium and plasma membrane H^+-ATPases activity, and chloride transport had a minor role in the observed KCl-driven alkalization (Fig. 29-30).

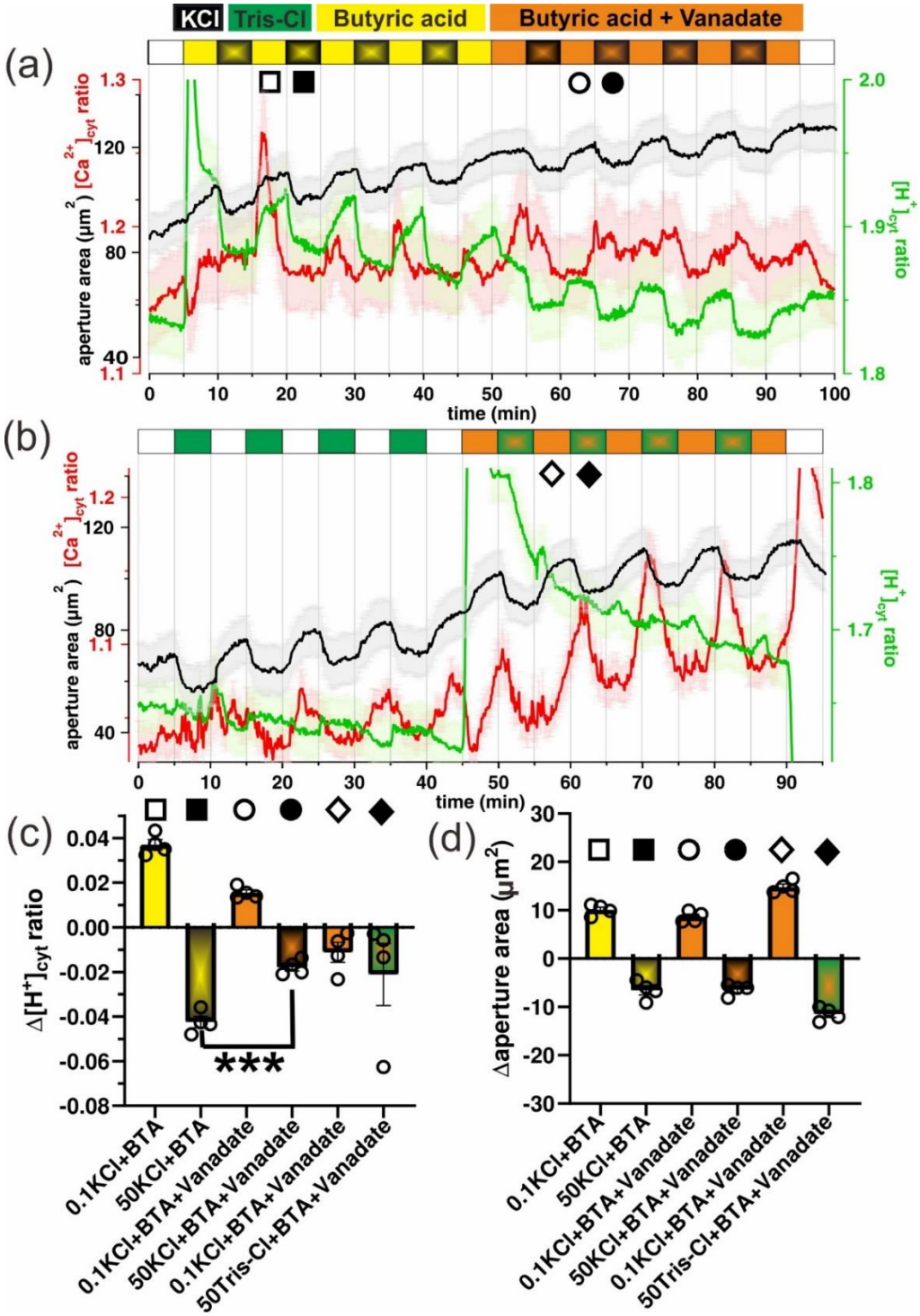

Figure 30. H^+-ATPases and K^+ are responsible for $[H^+]_{cyt}$ homeostasis in guard cells upon different KCl concentrations.

Live-cell imaging of $[Ca^{2+}]_{cyt}$ ratio and $[H^+]_{cyt}$ ratio and monitoring aperture area under different stimuli. (a) Mean $[Ca^{2+}]_{cyt}$ (red), $[H^+]_{cyt}$ (green) and aperture area (black) perfusion from 0.1 mM KCl to 50.1 mM KCl together with 3 mM BTA firstly for four repeats and then combined with 1 mM vanadate (Na_3VO_4) (n = 26). (b) Mean $[Ca^{2+}]_{cyt}$ (red), $[H^+]_{cyt}$ (green) and aperture area (black) response to 50 mM Tris-Cl for four

times and then combined with 3 mM BTA and 1 mM vanadate (Na_3VO_4) (n = 26). (c, d) Quantification of $[H^+]_{cyt}$ changes ($\Delta[H^+]_{cyt}$ ratio, c) and aperture changes (Δaperture area, d) from experiments in (a and b). Bars above indicate the time of treatments and different treatments are marked with different colors. Dots in (c, d) indicate average values of each repeat marked by symbols of individual measurements in (a, b). Error bars = SE. t-test was used in (c). ***, $p < 0.001$.

4.7.5 External KCl affects vacuolar H^+ homeostasis

Based on the vacuolar pH recordings with the BCECF dye, I learned that cytosolic pH changes could be well regulated by H^+-translocation by the tonoplast in ABA and flg22 induced responses (Fig. 15, 26). To ask, whether the 50.1 mM KCl induced cytosolic alkalization could originate from the transport of H^+ from the cytosol to the vacuole, wild-type *N. tabacum* epidermal strips were incubated with the BCECF dye to monitor vacuolar H^+ changes under low/high KCl solutions (Fig. 31a, b). Stomata opened in 0.1 mM KCl solution while stomata closed when switching to 50.1 mM KCl solution (Fig. 31a), which was in line with my previous experiments (Fig. 28a, 28b, 29a). Interestingly, vacuolar acidification (increased F_{440}/F_{500}) and alkalization (decreased F_{440}/F_{500}) occurred in low and high KCl solution, respectively, which was not influenced by vanadate (Fig. 31b, c). It indicates vacuolar H^+ homeostasis could be regulated by KCl. However, since both $[H^+]_{vac}$ and $[H^+]_{cyt}$ decreased upon high KCl application, cytosolic alkalization was unlikely to result from H^+ translocation into the vacuole (Fig. 29a, 31), which further suggested K^+ triggered $[H^+]_{cyt}$ homeostasis to rely on plasma membrane H^+ translocation. Using vanadate to block plasma membrane H^+-ATPases did not influence the BCECF signal much (Fig. 31b, c) indicating plasma membrane H^+-ATPases to have little effect on vacuolar pH but to contribute in part to the cytosolic alkalization induced by high K^+ (Fig. 30a, 30c, 31).

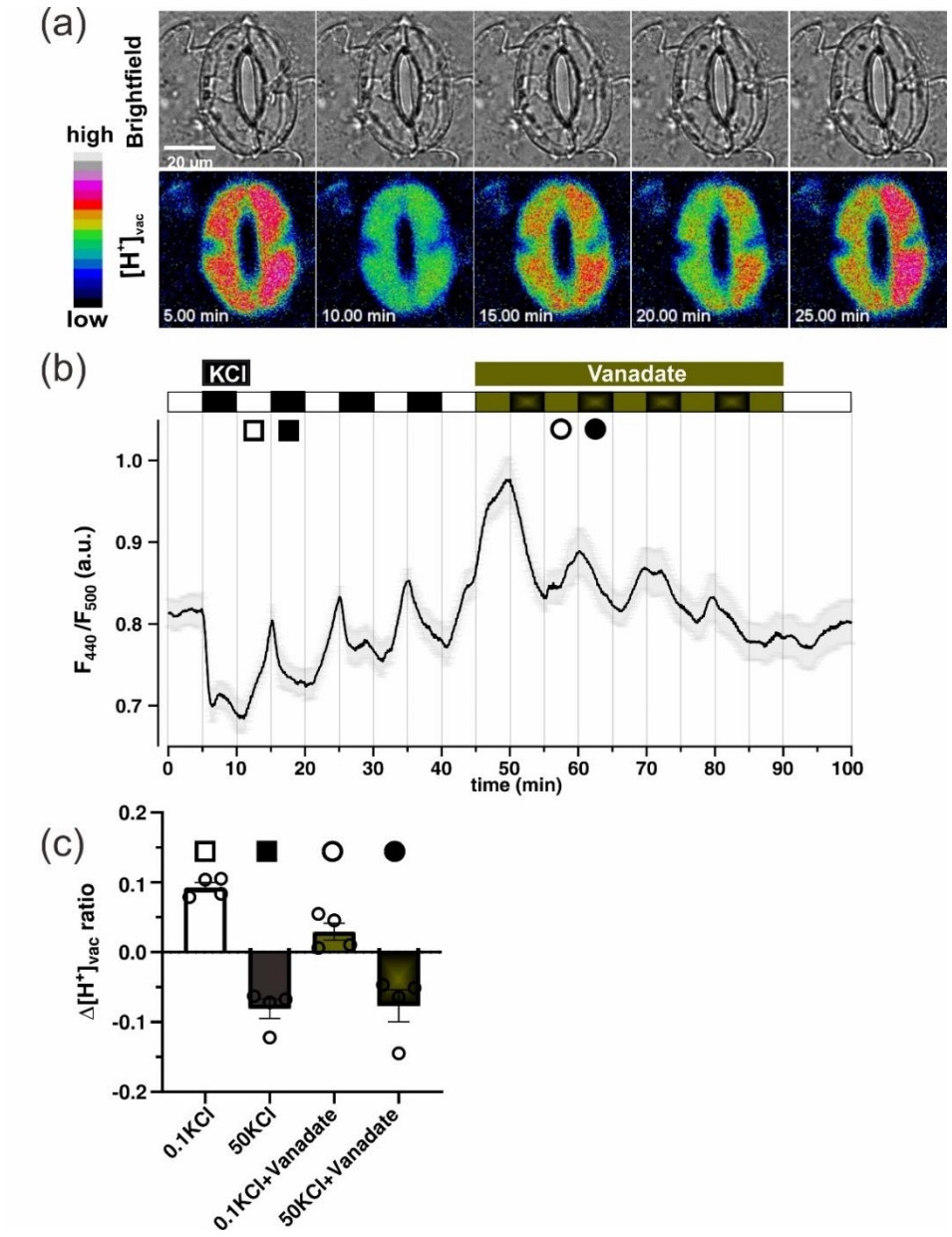

Figure 31. Vacuolar H^+ in guard cells responses to different KCl concentrations.

(a) Representative brightfield (top) and false colored $[H^+]_{vac}$ ratio (bottom) images in *N. tabacum* wild type (SR1) guard cells incubated with 15 µM BCECF for 2 h before starting the treatments with different KCl concentrations. (b) Mean $[H^+]_{vac}$ ratio (black, shown by F_{440}/F_{500}) responses to 0.1 mM KCl and 50.1 mM KCl for four times without (-) and with (+) 1 mM vanadate (Na_3VO_4) (n = 28). (c) Quantification of $[H^+]_{vac}$ ($\Delta[H^+]_{vac}$ ratio) responses of the experiments in (b). Bars above the trace indicate the time of treatments and different treatments are marked with different colors. Dots in (c) indicate the average values of each repeat marked by symbols of individual measurements. Error bars = SE.

4.7.6 Summary of Ca^{2+} and H^+ regulations in stomatal closure upon different stimuli

Summarizing my results and combing with others studies about the transport events at the plasma membrane and tonoplast (see introduction 1.2) (Fig. 1), a scheme is presented to propose possible transport components contributing to $[Ca^{2+}]_{cyt}$ and $[H^+]_{cyt}$ homeostasis in guard cells responses to either flg22, ABA or extracellular alkalization (pH 6.8) (Fig. 32). $[Ca^{2+}]_{cyt}$ increases and cytosolic alkalization were observed to be associated with stomatal closure under flg22, ABA and pH 6.8 treatment (Fig. 14, 19). A negative correlation between $[Ca^{2+}]_{cyt}$ increases and $[H^+]_{cyt}$ decreases exists in high external $CaCl_2$ or pH 6.8 treatment but more pronounced stomatal closure was associated with stronger alkalization (Fig. 19). Ca^{2+} influx might be regulated via Ca^{2+} permeable channels at the plasma membrane such as OSCAs and GLRs, while putative Ca^{2+}/H^+ exchangers (CAXs) and/or Ca^{2+}-ATPases (ACAs) [34-37] and H^+-ATPases or H^+-PPases [61,78,79] are suggested to function in $[Ca^{2+}]_{cyt}$ and $[H^+]_{cyt}$ interactions (Fig. 1, 32). The vacuole became more acid during ABA or flg22 treatments (Fig. 15, 26), which might be one of the origins of the cytosolic alkalization but the molecular mechanisms that couple cytosolic and vacuolar pH remain to be ascertained.

It was shown here that $[H^+]_{cyt}$ dynamics play an important role in regulation of stomatal movement (Fig. 14, 16, 18, 19b, 27e), which might be related to CAXs and K^+/H^+ transporters (NHXs) reported to be associated with intracellular H^+ homeostasis (see introduction 1.2) [1,2,11,35,42,61,96] (Fig. 1, 32). I found, K^+ fluxes not only to be important for turgor pressure to regulate stomatal movement through inward- and outward- K^+ channels, but I uncovered a strong link between K^+ and $[H^+]_{cyt}$ and $[H^+]_{vac}$ homeostasis in guard cells (Fig. 28-32). To sum up, cytosolic alkalization is a general feature in stomatal closure observed in this thesis and Ca^{2+}, H^+ and K^+ homeostasis could be identified to be strongly interconnected in guard cells.

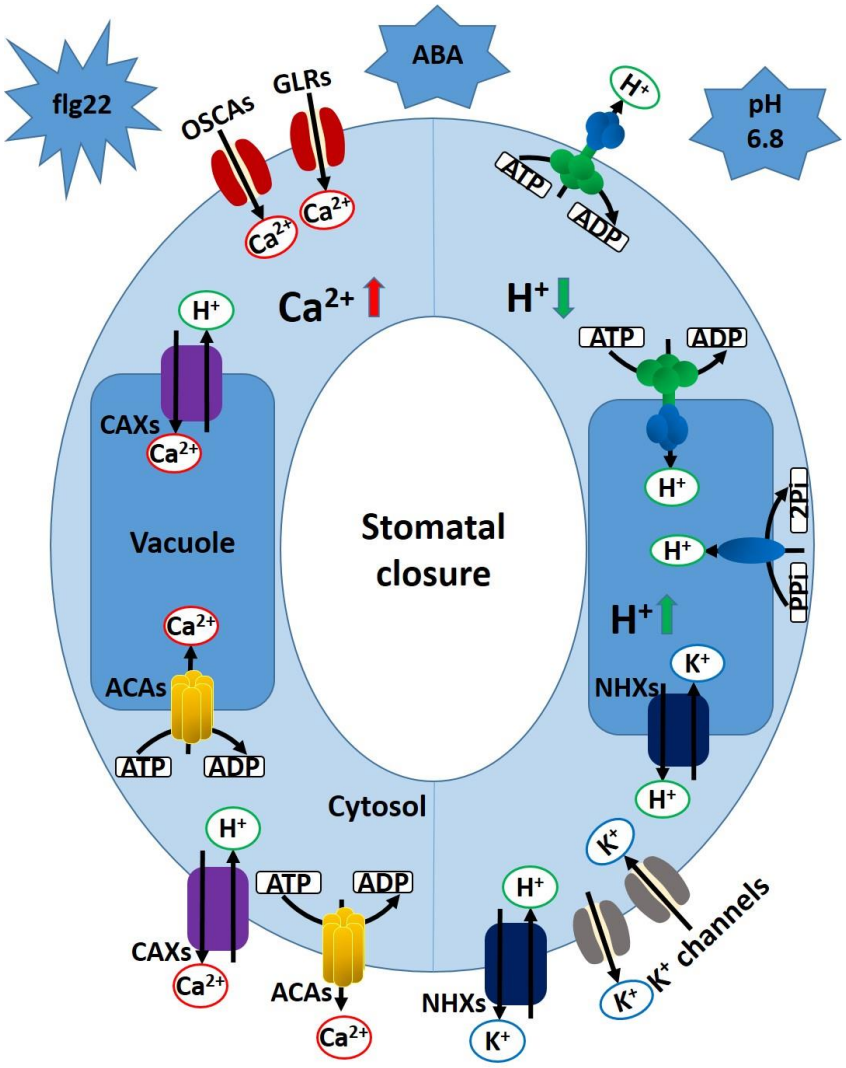

Figure 32. A scheme of Ca^{2+}, H^+, K^+ and transports regulation in stomatal closure induced by different stimuli.

A scheme to summarize possible components contributing to Ca^{2+}, H^+ and K^+ homeostasis in guard cells responses upon signaling cues such as flg22, ABA and extracellular alkalization (pH 6.8). $[Ca^{2+}]_{cyt}$ increases (red arrow up) and alkalization (green arrow down) occur in flg22, ABA and pH 6.8 induced stomatal closure. The vacuole became more acid upon ABA or flg22 treatment. Plasma membrane H^+-ATPases, vacuolar membrane H^+-ATPases and vacuolar membrane H^+-PPases both constantly pump H^+ out of the cytosol either to the apoplast or to the vacuole. The negative correlation between $[Ca^{2+}]_{cyt}$ increases and $[H^+]_{cyt}$ decreases is observed in stimuli such as high external $CaCl_2$ or pH 6.8 treatment. Ca^{2+} influxes via Ca^{2+} permeable channels (OSCAs, GLRs, etc.), some putative Ca^{2+}/H^+ exchangers (CAXs), Ca^{2+}-ATPases (ACAs), H^+-ATPases and H^+-PPases are proposed to contribute to the interconnection of $[Ca^{2+}]_{cyt}$ and $[H^+]_{cyt}$. K^+ transport through inward- and outward- K^+ channels as well as K^+/H^+ transporters are proposed not only to contribute to K^+ homeostasis, but steer $[H^+]_{cyt}$ and $[H^+]_{vac}$ homeostasis.

4.8 The role of Ca^{2+} and H^+ in salt adaptation mechanisms in leaves

4.8.1 Link of Ca^{2+}, H^+ and membrane potential in leave cells during salt stress

It is known that in salt stress enormous amounts of Na^+ and Cl^- are stored in the leaves and during acute salt stress Ca^{2+} signals from the root to the above ground parts were observed [9,327,387]. Apoplastic pH waves were also observed in leaves due to the administration of salt to the roots [230,300]. Whether Ca^{2+} and pH signals are involved in controlling salt detoxification in leaves and how they control salt processing or detoxification can be nicely investigated by direct administration of salt to leaves.

To study the responses on the single cell level first, I transiently expressed CapHensor including the cytosolic and nuclear version in *N. benthamiana* leaves and extracted protoplasts from the mesophyll. It allowed me to precisely perfuse with osmolality-balanced solutions containing 50 mM NaCl, 50 mM KCl and 50 mM Tris-Cl with pH 5.8 adjusted with Tris (Fig. 33a-c, 34) to study Ca^{2+} and pH reactions of the cells with respect to different ion conditions in one experiment. The results showed $[Ca^{2+}]_{cyt}$ decreased and the cytosol alkalized in response to 50 mM NaCl and KCl whereas slight $[Ca^{2+}]_{cyt}$ reduction and minor cytosolic acidification occurred upon 50 mM Tris-Cl treatment (Fig. 33b). This demonstrated that Na^+ and K^+ were equally effective to induce more pronounced Ca^{2+} and pH changes than Cl^- in the mesophyll cells. The results for the pH regime were very similar to those observed in guard cells, where I observed a pronounced alkalization upon high K^+ treatment (Fig. 29a). Also very similar to the results obtained with guard cell (Fig. 29a-c), I saw a pronounced transient $[Ca^{2+}]_{cyt}$ increase and cytosolic acidification after washing 50 mM NaCl and KCl out while no $[Ca^{2+}]_{cyt}$ and $[H^+]_{cyt}$ changes occurred when removing 50 mM Tris-Cl (Fig. 33b). Consistently, nuclear Ca^{2+} concentrations ($[Ca^{2+}]_{nuc}$) and nuclear H^+ concentrations ($[H^+]_{nuc}$) displayed a similar regime to 50 mM NaCl, KCl and Tris-Cl treatment (Fig. 33c) compared with changes in the cytosol but were just less pronounced. Ions transport across the plasma membrane is consequently having an impact on the membrane potential. Hence, I used a membrane voltage dye bis-(1,3-dibutylbarbituric acid)-trimethine oxonol ($DiBAC_4(3)$) to monitor membrane potential changes side-by-side with R-GECO1 fluorescence (Fig. 33a, d), since I could not monitor fluorescences of CapHensor and $DiBAC_4(3)$ together because of the spectral overlap. The fluorescence increases of $DiBAC_4(3)$ do represent membrane potential depolarization while fluorescence decreases mean membrane hyperpolarization indicated by the black trace (Fig. 33d). 50 mM NaCl and 50 mM KCl induced mesophyll cell depolarization since $DiBAC_4(3)$

fluorescence increased whereas almost no $DiBAC_4(3)$ fluorescence changes were observed in response to 50 mM Tris-Cl (Fig. 33a, d). These results demonstrated intracellular decreases in Ca^{2+} and H^+ accompanied by a depolarization were more likely to be a result of cation transport, rather than chloride transport across the plasma membrane in leaf cells upon salt.

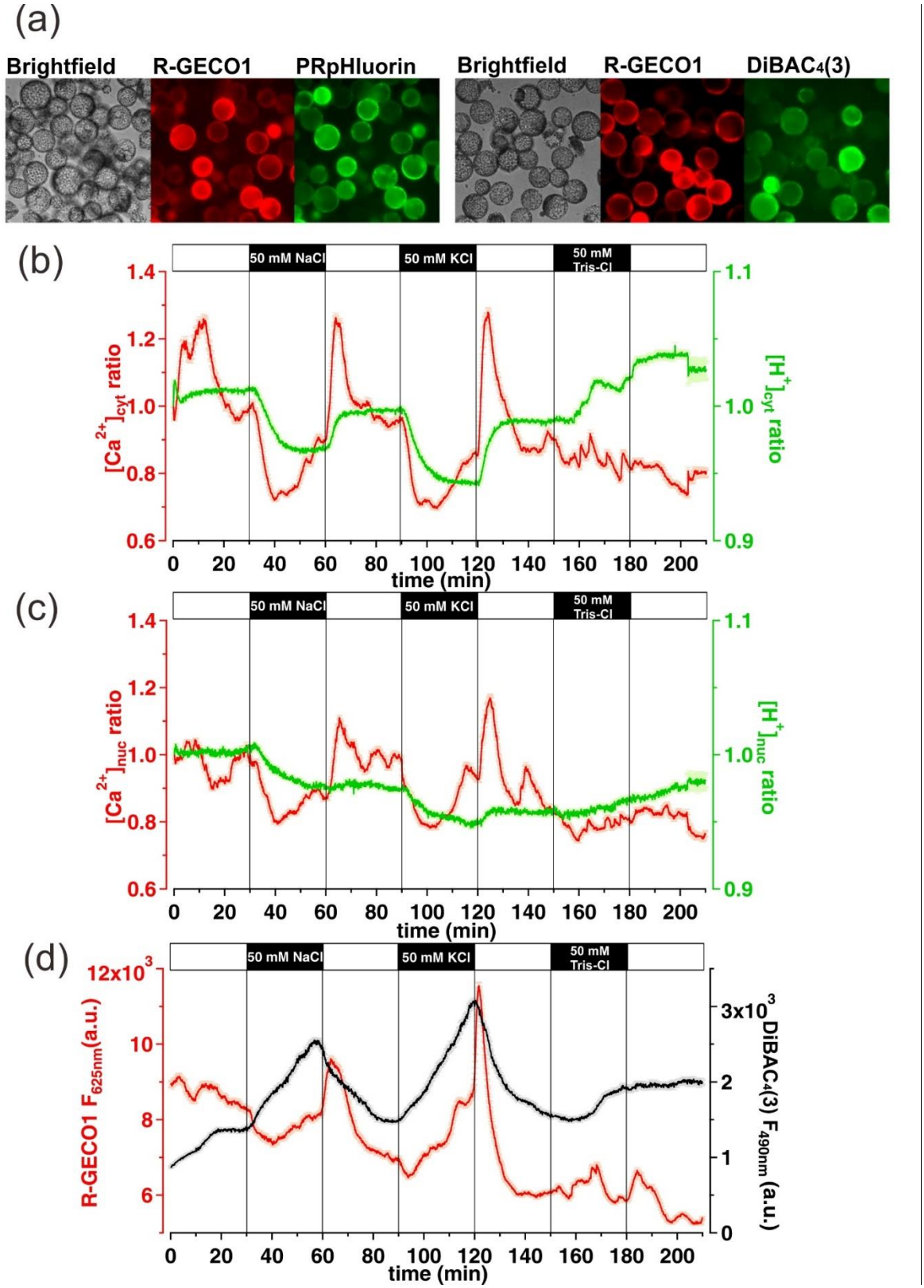

Figure 33. Ca^{2+}, H^{+} and membrane potential induced by salt attribute to cations not anions.

(a) Brightfield and fluorescent images of protoplasts from *N. benthamiana* mesophyll tissues transiently expressing the cytosolic version of CapHensor (left), or expressing only R-GECO1 in the cytosol but co-staining with the membrane voltage dye $DiBAC_4(3)$ (right). Red and green color represent fluorescence of R-GECO1 and PRpHluorin (left) or R-GECO1 and $DiBAC_4(3)$ (right), respectively. (b, c) Mean Ca^{2+} ratio (red) and H^+ (green) ratio in the cytosol (b, n = 85) and nuclei (c, n = 66) in response to 50 mM NaCl, KCl and Tris-Cl buffered with Tris to pH 5.8. (c) Mean fluorescence intensity of R-GECO1 (red) and $DiBAC_4(3)$ (black) of mesophyll protoplasts (n = 90) upon NaCl, KCl and Tris-Cl (both 50 mM) treatment. Error bars = SE.

To make sure that no artifacts with respect to cell viability occurred because of the long time treatment on cells and overall long recordings, I switched the sequence of treatments within the experiment and perfused with 50 mM Tris-Cl first, followed by 50 mM NaCl and KCl treatment (Fig. 34a, c). Within this sequence of applications, very similar responses were monitored, which further confirmed Na^+ or K^+ is the main ion in salt stress to cause the changes in Ca^{2+} and pH in the cytosol or nucleus of mesophyll cells (Fig. 34a-c).

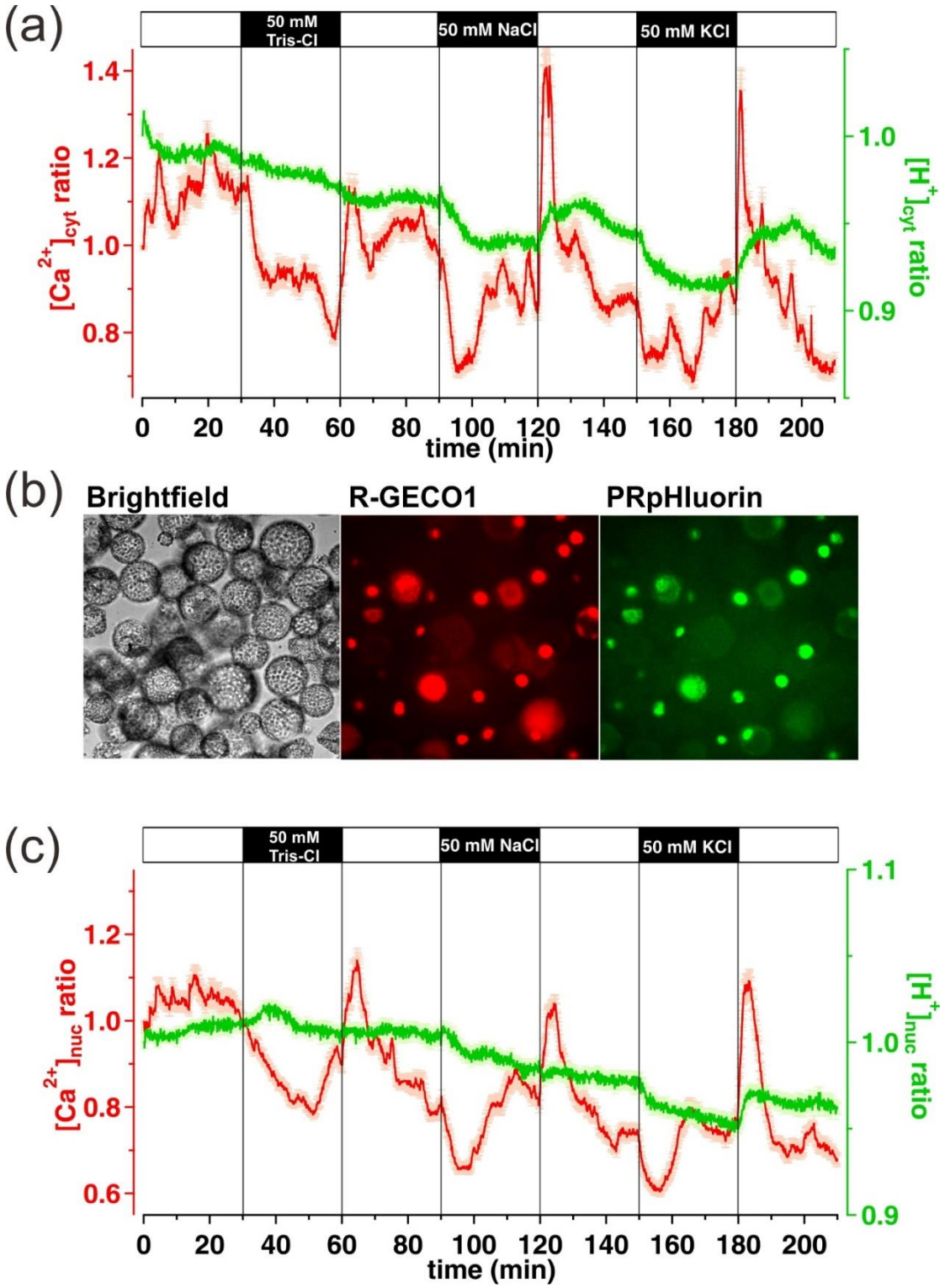

Figure 34. Cytosolic and nuclear alkalization attributes to cations, not Cl^-.

Ca^{2+} and H^+ ratio of *N. benthamiana* leaves protoplasts transiently expressing CapHensor in the cytosol or nucleus upon different treatments. (a, c) Mean Ca^{2+} (red) and H^+ (green) in the cytosol (a) or in the nuclei (c) of protoplasts upon 50 mM Tris-Cl, NaCl and KCl. Cytosolic or nuclear alkalization is triggered by

cations (Na^+, K^+), but not by Cl^-. (b) Brightfield image (left), fluorescent R-GECO1 (red, middle) and PRpHluorin (green, right) images of protoplasts transiently expressing the nuclear version of CapHensor. Error bars = SE.

4.8.2 AtNHX1 overexpression functions in mesophyll cells by regulation of $[Ca^{2+}]_{cyt}$, $[H^+]_{cyt}$ and membrane potential under salt stress

To investigate the response to saline administration at the tissue level, I again used the transient expression system of *N. benthamiana* leaves to accomplish direct membrane potential recordings simultaneously with CapHensor imaging. I applied 50 mM NaCl on the intact leaves and compared $[Ca^{2+}]_{cyt}$, $[H^+]_{cyt}$ and membrane potential between leaves only expressing CapHensor (Fig. 35a) and leaves co-expressed AtNHX1 (Fig. 35b). Removing the lower epidermal layer allowed to administer different buffers to the leaf tissue that was glued with the adaxial side to the cover slip of the recording chamber. Under control conditions stable $[Ca^{2+}]_{cyt}$, $[H^+]_{cyt}$ and membrane potential states were simultaneously recorded and showed no changes (Fig. 35c).

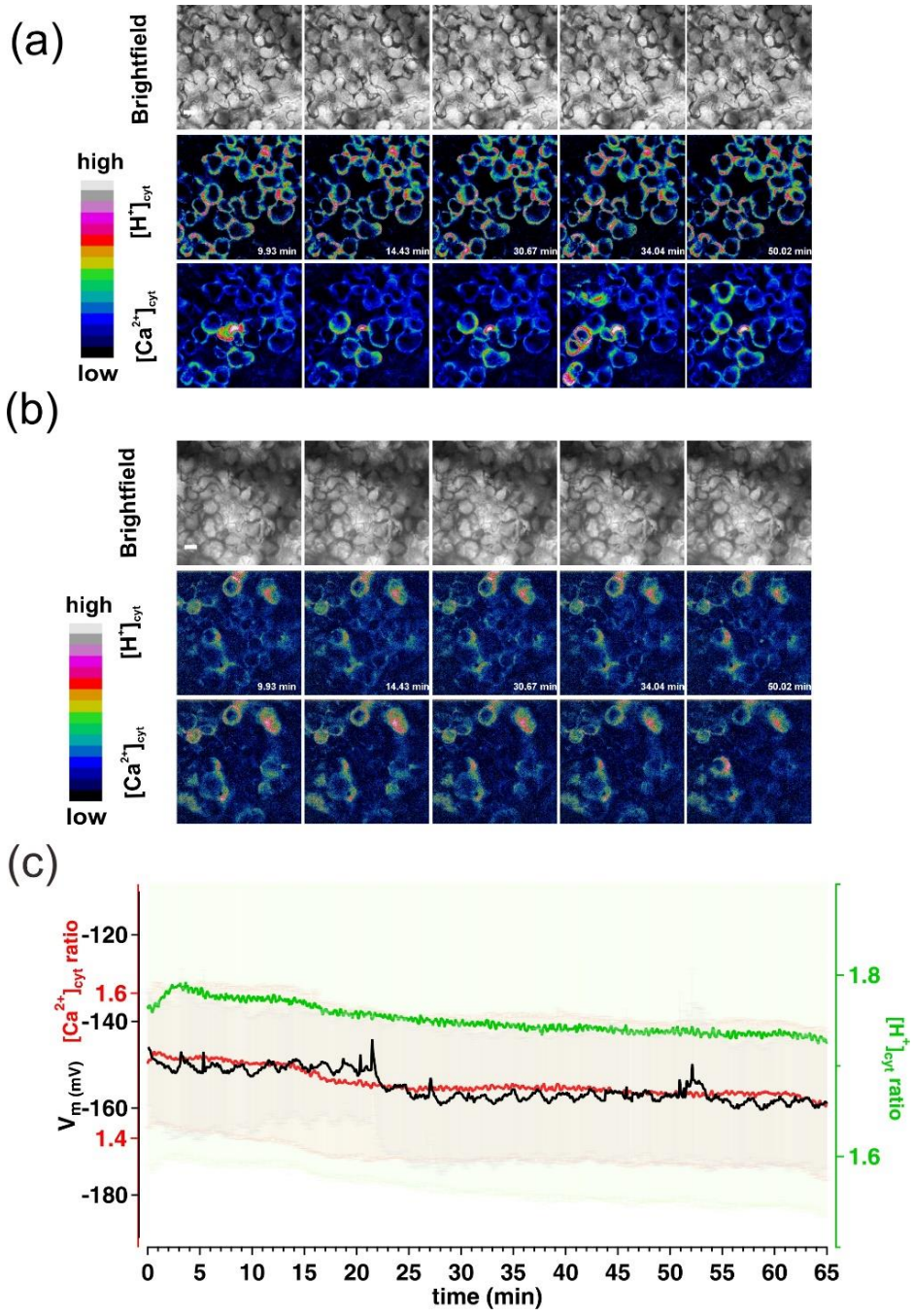

Figure 35. CapHensor imaging of $[Ca^{2+}]_{cyt}$- and $[H^+]_{cyt}$- ratio combined with voltage recordings upon NaCl treatment in mesophyll cells co-expressing or not AtNHX1.

(a, b) Time-lapses brightfield images (upper) and false colored images of $[H^+]_{cyt}$ ratio (middle) and $[Ca^{2+}]_{cyt}$ ratio (bottom) of *N. benthamiana* mesophyll cells transiently expressing CapHensor (a) and co-expressiong CapHensor and AtNHX1 (b). 50 mM NaCl is perfused during 10 min to 30 min and then washed out. The mean data of $[Ca^{2+}]_{cyt}$- and $[H^+]_{cyt}$- ratio from these fluorescent images are shown in Fig. 36. (c) Simultaneous live-cell imaging of $[Ca^{2+}]_{cyt}$- and $[H^+]_{cyt}$- ratio together with membrane potential (V_m) recordings in mesophyll cells of *N. benthamiana* leaves transiently expressing CapHensor without any

treatment. Mean $[Ca^{2+}]_{cyt}$- (red) and $[H^+]_{cyt}$- ratio (green) and membrane potential (V_m, black) values under control conditions (c, n = 3). Error bars = SE.

Similar to the protoplast responses to salt, $[Ca^{2+}]_{cyt}$ and $[H^+]_{cyt}$ both decreased and simultaneously a depolarization was measured by means of glass microelectrode in response to 50 mM NaCl (Fig. 36a). After removing 50 mM NaCl, the membrane potential repolarized and $[Ca^{2+}]_{cyt}$ increases and cytosolic acidification were induced, that reached steady state in leaves again after a pronounced overshoot response (Fig. 36a, b). The changes of membrane potential before (white circle), during maximum depolarization (black diamond) induced by 50 mM NaCl, at the end of the treatment (black circle) and when repolarized after salt wash-out (black square) showed a depolarization of 38.30 mV by NaCl (Fig. 36a, b). In roots, $[Ca^{2+}]_{cyt}$ was reported to increase in salt stress and Na^+ is thought to be detoxified via Na^+/H^+ antiporters at the plasma membrane and vacuolar membrane in a Ca^{2+}-dependent manner [14,308,388]. For example, the vacuolar localized NHX1 antiporter functions to sequester Na^+ into the vacuole, thereby using the proton motive force at the tonoplast [95,322,331,389]. Despite the difference in $[Ca^{2+}]_{cyt}$ responses between roots and leaves, by all means I never observed a $[Ca^{2+}]_{cyt}$ rise in leaves, but rather the opposite (Fig. 33, 34, 36a). I thus aimed to study the role of a Na^+/H^+ antiport mechanism at the tonoplast, which has been described to confer salt tolerance in many species [290,322,389-391]. I co-expressed *Arabidopsis thaliana* NHX1 (AtNHX1) and CapHensor in *N. benthamiana* leaves and repeated the salt-administration experiments to see if an increase of NHX1 function feeds-back on the $[Ca^{2+}]_{cyt}$ and $[H^+]_{cyt}$ signaling when cells cope with the salt load. Interestingly, $[Ca^{2+}]_{cyt}$ and $[H^+]_{cyt}$ decreases which I observed in wild-type leaves were diminished when AtNHX1 was overexpressed although the depolarization still occurred (Fig. 36c). However, the depolarization range upon 50 mM NaCl was approximately 28.29 mV (Fig. 36c, d), which was significantly smaller than that in wild-type ($p < 0.05$) (Fig. 36b, d). These results suggested NHX1 to function in modulating $[Ca^{2+}]_{cyt}$ and buffering $[H^+]_{cyt}$ homeostasis by enhancing the efficiency of antiporter mechanism that Na^+ is transported into the vacuole to accomplish sodium detoxicification.

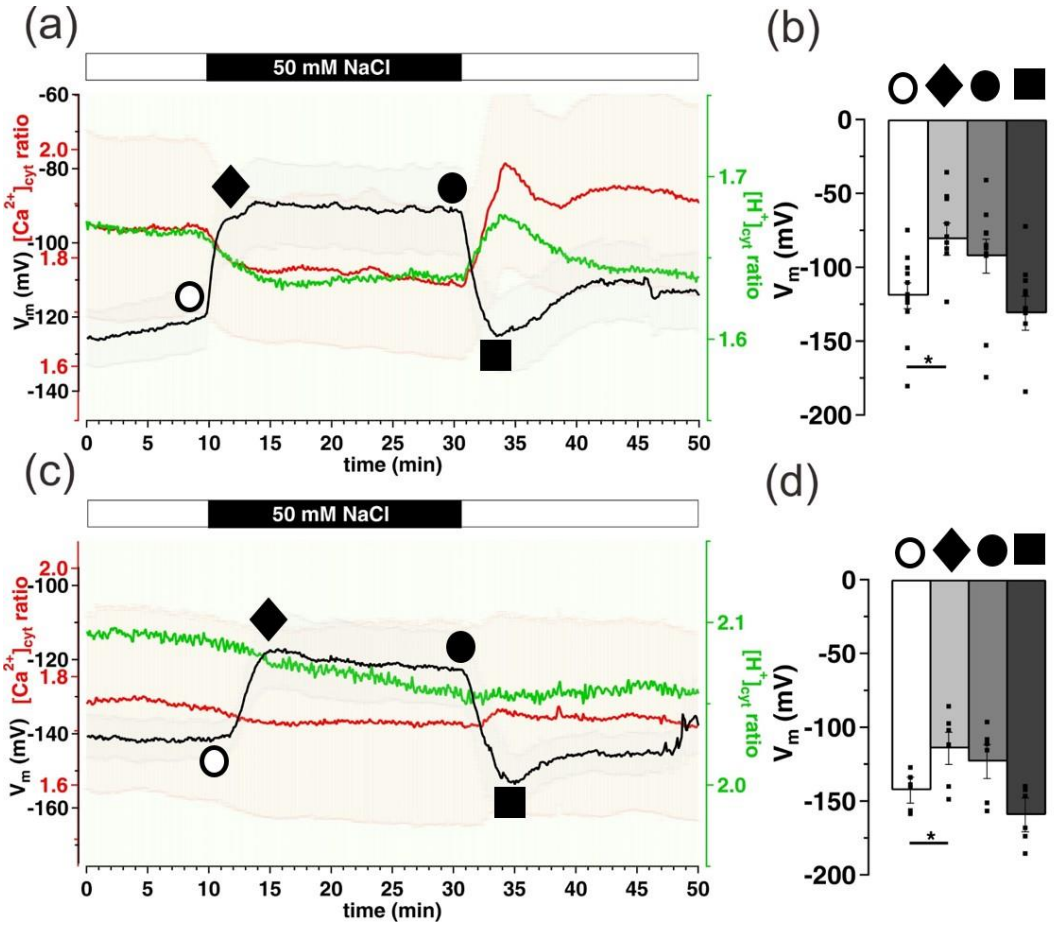

Figure 36. Overexpression of AtNHX1 diminishes $[Ca^{2+}]_{cyt}$ and $[H^+]_{cyt}$ reductions and suppresses depolarization in mesophyll cells upon NaCl application.

Simultaneous live-cell imaging of $[Ca^{2+}]_{cyt}$, $[H^+]_{cyt}$ and membrane potential recording in *N. benthamiana* leaves. (a, c) Mean $[Ca^{2+}]_{cyt}$- (red), $[H^+]_{cyt}$- ratio (green) and membrane potential recording (V_m, black) are induced in mesophyll cells only transiently expressing CapHensor (a, WT, n = 11) and co-expressing *Arabidopsis thaliana* NHX1 (b, +AtNHX1, n = 6). (b, d) Bar diagrams of mean values of membrane potential (V_m) before (○), maximum responses (♦), at the end (●) of 50 mM NaCl or after washout to reach the maximum repolarization (■) in wild type (WT) leaves (b, n = 11) or leaves transiently overexpressing AtNHX1 (d, n = 6). Error bars = SE. Dots are individual measurements. *, $p < 0.05$.

4.8.3 $[Ca^{2+}]_{cyt}$ signals are different between leaves and roots under salt stress

When plants suffer from high concentration of NaCl around 200 mM, $[Ca^{2+}]_{cyt}$ transients were part of the salt response in roots [306-308,392]. Based on my results gathered so far with different leaf cells did not show any $[Ca^{2+}]_{cyt}$ elevation in leaves upon salt administration, but rather the opposite, $[Ca^{2+}]_{cyt}$ transients were seen only when salt was washed out. Does salt detoxification in leaves not rely on $[Ca^{2+}]_{cyt}$- dependent mechanisms? Given that $[Ca^{2+}]_{cyt}$ increases were not observed

under balanced 50 mM NaCl treatment in leaves (Fig. 33b, 34a, 36a), higher concentration NaCl up to 200 mM was applied to the leaf discs expressing the Ca^{2+} sensor GCaMP3 (Fig. 37a-c). This green fluorescent Ca^{2+} sensor allows to observe $[Ca^{2+}]_{cyt}$ dynamics at lower optical magnification where R-GECO1 with its lower quantum efficiency is not able to perform well. This allowed me to observe $[Ca^{2+}]_{cyt}$ dynamics of a bigger field of view which would possibly monitor $[Ca^{2+}]_{cyt}$ waves having been described to occur in roots upon salt stress [307]. The intact leaf disc with epidermis was glued with the adaxial side down and salt solutions were perfused from the side of the leaf where the cut end of the leaf resided. When perfusing with 200 mM NaCl, the leaf tissue did shrink and very small $[Ca^{2+}]_{cyt}$ elevations were recorded whereas pronounced $[Ca^{2+}]_{cyt}$ transients and waves occurred when washing 200 mM NaCl out (Fig. 37a-c). Given that the slight $[Ca^{2+}]_{cyt}$ increases in leaves (Fig. 37a-c) and even reduction of $[Ca^{2+}]_{cyt}$ in the single protoplast and leaf experiments occurred (Fig. 33b, 34a, 36a), I applied 200 mM NaCl directly on tobacco roots stably expressing CapHensor (Fig. 37d) to test my experimental conditions there and to verify cell type specific differences upon the same stimuli. Surprisingly, and in contrast to all my results on leaves and cells therof, $[Ca^{2+}]_{cyt}$ increases were observed in the roots which were accompanied with cytosolic alkalization (Fig. 37d). Therefore, a lack of the $[Ca^{2+}]_{cyt}$ increases in leaves but a pronounced response in roots to high NaCl suggested that the mechanisms for salt detoxification in both tissues are regulated by different signaling pathways.

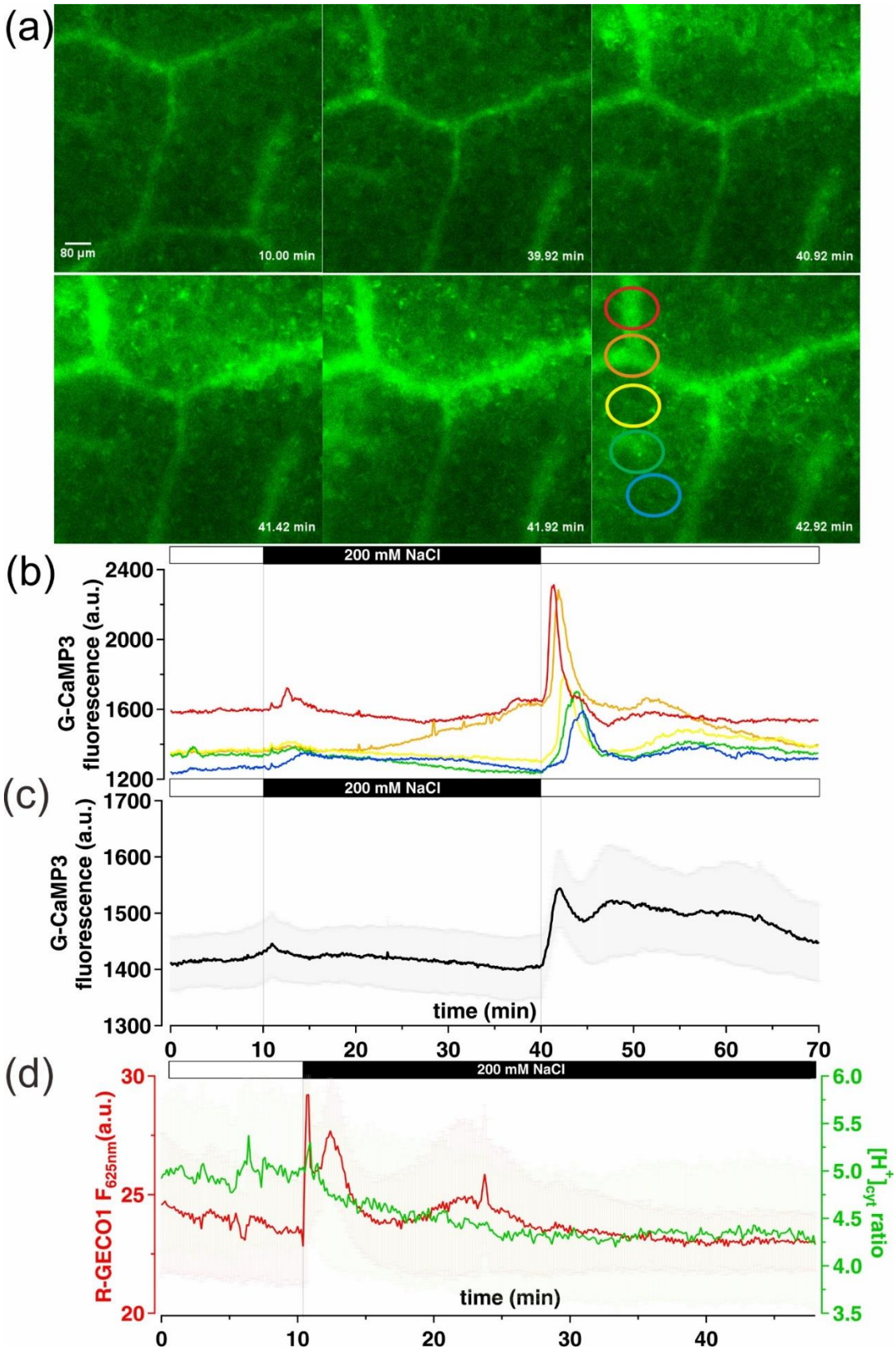
(a)
80 µm
10.00 min
39.92 min
40.92 min
41.42 min
41.92 min
42.92 min
(b)
200 mM NaCl
G-CaMP3 fluorescence (a.u.)
2400
2000
1600
1200
(c)
200 mM NaCl
G-CaMP3 fluorescence (a.u.)
1700
1600
1500
1400
1300
time (min)
0
10
20
30
40
50
60
70
(d)
200 mM NaCl
R-GECO1 F625nm(a.u.)
30
25
20
[H+]cyt ratio
6.0
5.5
5.0
4.5
4.0
3.5
time (min)
0
10
20
30
40

Figure 37. $[Ca^{2+}]_{cyt}$ dynamics differ between leaves and roots under 200 mM NaCl treatment.
(a, b) False colored fluorescent images (a) and the time-course recording (b) of $[Ca^{2+}]_{cyt}$ dynamics showing $[Ca^{2+}]_{cyt}$ waves from the top to the bottom marked by circles with different colors (bottom) during or after 200 mM NaCl in *N. benthamiana* leaves stably epressing GCaMP3. (c) Mean $[Ca^{2+}]_{cyt}$ in *N. benthamiana* leaves stably expressing GCaMP3 (n = 6) upon 200 mM NaCl application by the perfusion system. (d) Mean $[Ca^{2+}]_{cyt}$ and $[H^+]_{cyt}$ in *N. tabacum* roots stably expressing CapHensor (n = 5) upon application of 200 mM NaCl. Error bars = SE.

4.8.4 $[Ca^{2+}]_{cyt}$ and $[H^+]_{cyt}$ responses in guard cells under different salt concentrations

In addition to salt shocks on mesophyll cells or epidermal cells, which have been demonstrated in this thesis, I aimed to study $[Ca^{2+}]_{cyt}$ and $[H^+]_{cyt}$ signaling upon salt shocks in guard cells, which have been reported to react upon acute salt stress to close the stomata [298,307,387]. High salt stress has two ways to trigger its effects, which include an osmotic component in addition to the toxic effect of Na^+ and Cl^-, besides the effect on ion transport. Therefore, I performed live-cell imaging in *N. tabacum* guard cells stably expressing CapHensor and recorded aperture changes in parallel (Fig. 38). To discriminate the osmotic effects and effects from the membrane transport alterations, I chose to apply three different experiments. One set of measurements where 200 mM NaCl was applied and osmolality was imbalanced (Fig. 38a). Another one providing osmotic pressure by approximately 400 mM mannitol (Fig. 38b) with equal osmolality as the 200 mM NaCl treatment and a third one where osmolality matched 50 mM NaCl (Fig. 38c). The time-lapse fluorescent images and aperture area changes are shown in Fig. 38.

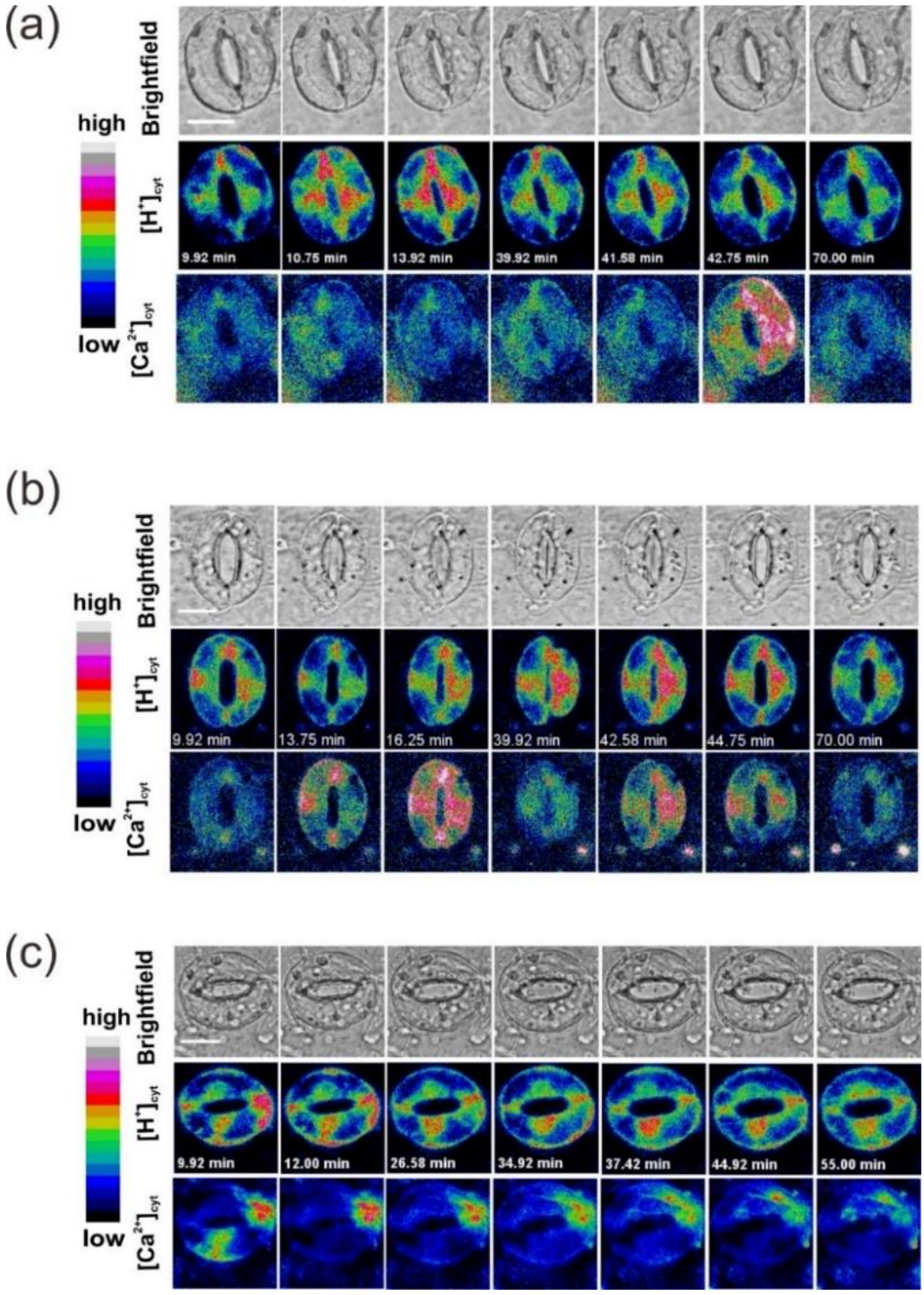

Figure 38. Images of $[Ca^{2+}]_{cyt}$-, $[H^+]_{cyt}$- ratio and stomatal movement upon salt application.

(a-c) Time-lapse brightfield images (upper) and false colored images of $[H^+]_{cyt}$ ratio (middle) and $[Ca^{2+}]_{cyt}$ ratio (bottom) of guard cells in *N. tabacum* epidermal strips stably expressing CapHensor upon 200 mM NaCl (a), 400 mM mannitol (b) and osmolality-balanced control solution equal to 50 mM NaCl (c). The mean data of $[Ca^{2+}]_{cyt}$- and $[H^+]_{cyt}$- ratio from these fluorescent images and stomatal aperture is shown in Fig. 39.

Rapid stomatal closure and pronounced cytoslic alkalization and surprisingly almost no $[Ca^{2+}]_{cyt}$ changes were triggered by 200 mM NaCl (Fig. 38a, 39a), which was similar to leaf responses to 200 mM NaCl (Fig. 37a-c). However, a $[Ca^{2+}]_{cyt}$ peak was evident when 200 mM NaCl was washed out and stomata re-opened (Fig. 38a, 39a). To investigate whether stomatal movement upon 200 mM NaCl administration resulted from osmotic effects, 400 mM mannitol was applied displaying basically the same aperture movement as with 200 mM NaCl (Fig. 38b, 39b). Upon 400 mM mannitol application pronounced $[Ca^{2+}]_{cyt}$ elevations were observed, which might be due to the strong mechanical forces induced by the hyperosmotic treatment (Fig. 38b, 39b), which could address mechano-sensitive Ca^{2+}-permeable channels such as OSCA1 [4]. In contrast to the 200 mM NaCl treatment, 400 mM mannitol only induced a transient small cytoslic alkalization (Fig. 38b, 39b). This is in line with previous results on the cation induced cytosolic alkalization responses in guard cells, which were characterized to depend on cation transport into guard cells (Fig. 28b, 29a, 33b, 34a, 36). Such an import of cations, be it Na^+ or K^+, is compatible with results of stomatal opening, when I treated guard cells with 50 mM NaCl while balancing osmolality of the control solution since 50 mM NaCl induced a reduction of $[H^+]_{cyt}$ and a transient reduction in $[Ca^{2+}]_{cyt}$ (Fig. 38c, 39c). This result well demonstrated that Na^+ and Cl^- are uptaken by guard cells to generate turgor for stomatal opening, thereby causing a cytosolic alkalization (Fig. 39c). The results of the experiments with the osmolality imbalanced solution pointed out it is crucial to interprete the results of $[Ca^{2+}]_{cyt}$ and $[H^+]_{cyt}$ changes with caution with respect to the effects to regulate stomatal aperture as the osmotic strength has a huge impact on stomatal movement. In general, I concluded that salt stress to guard cells was not associated with Ca^{2+} signaling and guard cells were able to transport Na^+ and Cl^- very rapidly**.**

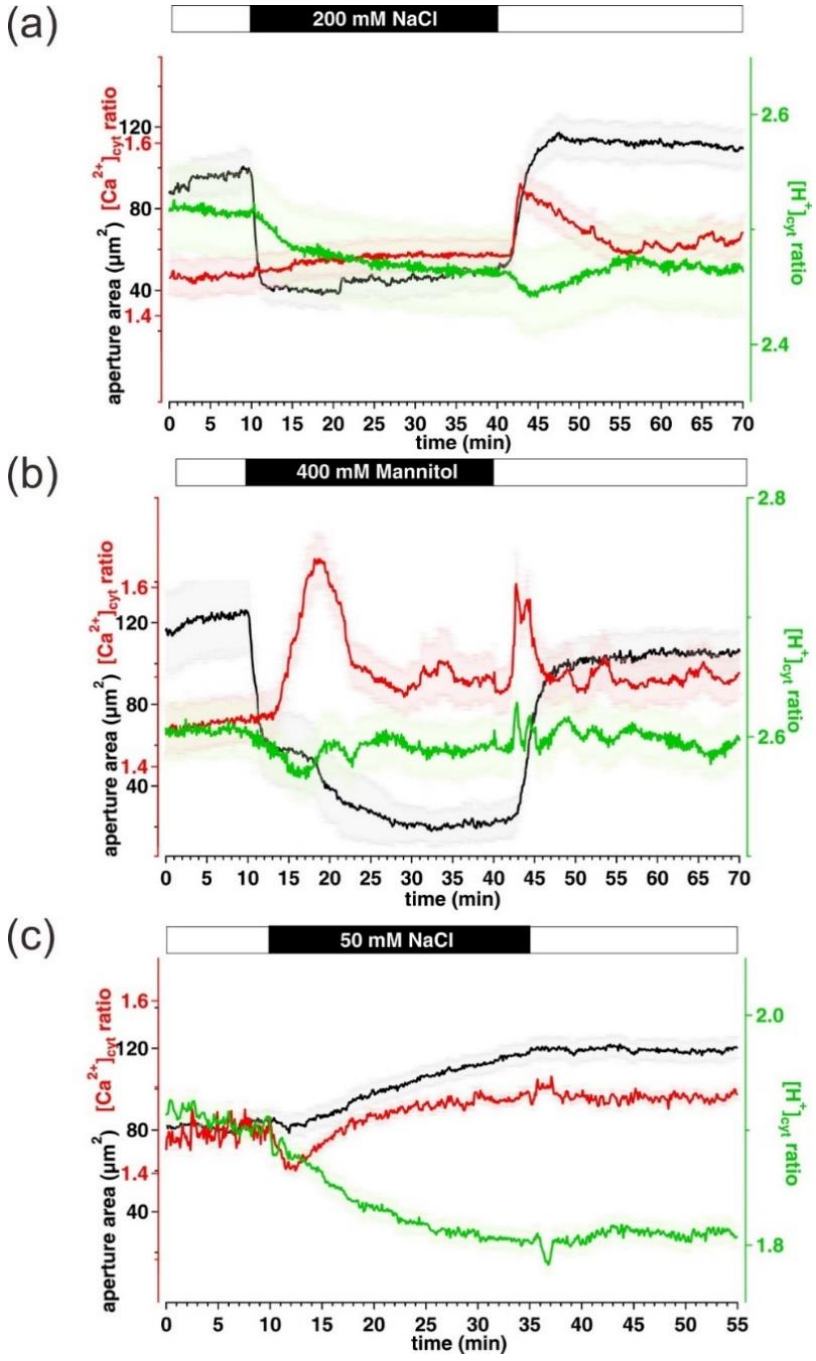

Figure 39. Stomatal closure under salt attributes to osmolality and not $[Ca^{2+}]_{cyt}$ signals.

Simultaneous $[Ca^{2+}]_{cyt}$ (red) and $[H^+]_{cyt}$ (green) imaging together with monitoring aperture area (black) over time in guard cells of *N. tabacum* epidermal strips stably expressing CapHensor under different stimuli. (a-b) Mean $[Ca^{2+}]_{cyt}$ ratio (red), $[H^+]_{cyt}$ ratio (green) and aperature area (black) in response to perfusion from low osmolality control solution (1 mM $CaCl_2$, 1 mM KCl, 10 mM MES, adjust pH to 5.8 with BTP) to 200 mM NaCl (a, n = 24) or 400 mM mannitol (b, n = 18). (c) Effects of 50 mM NaCl from osmolality-balanced control solution (1 mM $CaCl_2$, 75 mM MES, adjust pH to 5.8 with Tris) on $[Ca^{2+}]_{cyt}$-, $[H^+]_{cyt}$- ratio and aperture area (n = 18). Error bars = SE. Note stomata rapidly close in (a, b) while stomatal opening is observed upon 50 mM NaCl application when osmolality of the control solution is iso-osmotic.

4.8.5 Summary of salt detoxification mechanisms in leaves

Combined monitoring Ca^{2+} and H^+ changes side-by-side in different compartments such as the cytosol and the nucleus, the results in leaves upon salt adminstration were integrated in a scheme (Fig. 40). In this scheme the transport processes related to Ca^{2+} dynamics and pH changes have been highlightened which were demonstarted to occur in tobacco leaves upon salt stress (Fig. 40). Under salt stress, Na^+ enters the cell via non-selective cation channels (NSCCs) or HKTs [44,393] (Fig. 40), which induces a plasma membrane depolarization, and Ca^{2+} and H^+ decreases in the cytosol and the nucleus in wild type (Fig. 40, left side). Contrary to salt effects on roots, $[Ca^{2+}]_{cyt}$ did not increase in leaves neither in mesophyll tissue or protoplasts therof nor in guard cells of epidermal strips (Fig. 33, 34, 36a, 37a-b, 38-40). When the vacuolar AtNHX1 cation/H^+ antiporter was overexpressed in *N. benthamiana* leaves, pronounced reductions in $[Ca^{2+}]_{cyt}$ and $[H^+]_{cyt}$ were absent and NaCl induced depolarization was reduced (Fig. 40, right side) compared with responses in wildtype. This means salt triggered $[Ca^{2+}]_{cyt}$ and $[H^+]_{cyt}$ reductions are regulated by AtNHX1 which was shown to also feed-back on membrane potential changes. The diminished $[H^+]_{cyt}$ changes by AtNHX1 overexpression upon salt was likely attributed to sequestering Na^+ into the vacuole and thereby shutteling H^+ to the cytosol to detoxify the salt load. Therefore, NHX1 functions in leaves by transport of Na^+ into the vacuoles thereby buffering the pH changes occurred in the cytosol, which is independent on $[Ca^{2+}]_{cyt}$ increases.

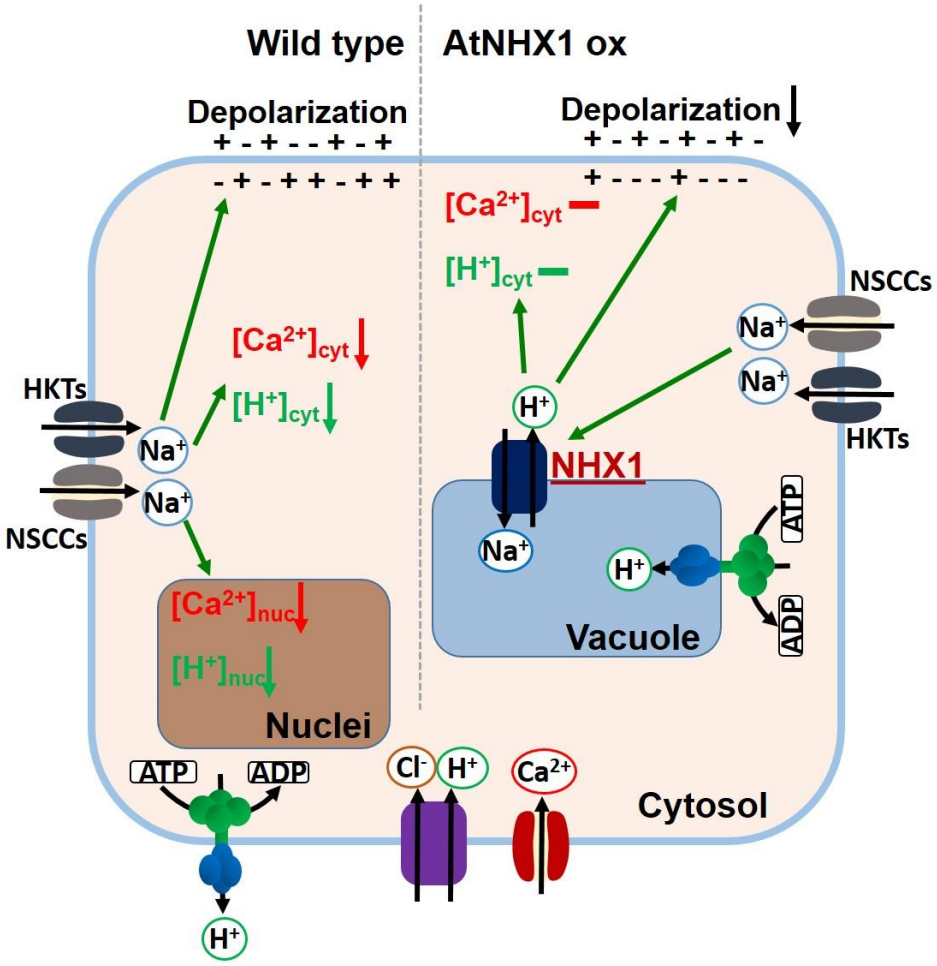

Figure 40. Scheme of salt detoxification in leaves.

Ca^{2+}, H^+ changes in wild type and AtNHX1 overexpression leaves upon salt stress. Na^+ can enter the cell via non-selective cation channels (NSCCs, grey) and others such as HKTs (dark blue). The transport of Na^+ into the cell triggers a depolarization and causes a Ca^{2+} and H^+ reduction in the cytosol and nucleus in widetype (left side) leaf cells. When overexpressing AtNHX1 (AtNHX1 ox) in leaves, intracellular increased Na^+ stimulates AtNHX1 acitivity to pump H^+ into the cytosol and sequester Na^+ into the vacuole. This mechanism buffers $[H^+]_{cyt}$ and prevents cytosolic alkalization while the vacuole alkalizes. These transport events do not depend on $[Ca^{2+}]_{cyt}$ increases. The depolarization upon salt stress does occur even when AtNHX1 is overexpressed, however it is much less pronounced compared to wild type. H^+-ATPases at the plasma membrane and vacuolar membrane likely contribute to the H^+ homeostasis and pump H^+ out of the cytosol.

5 Discussion

5.1 Advantages of CapHensor for dual imaging of Ca^{2+} and pH

To perform ratiometric imaging of Ca^{2+} and H^+ simultaneously, I developed a sophisticated dual sensor named CapHensor. Simultaneous live-cell imaging of intracellular Ca^{2+} and H^+ was achieved by fusing a pH-dependent GFP (PRpHluorin) and a red fluorescent Ca^{2+} sensor (R-GECO1) via a self-cleavage sequence P2A in one multicistronic vector (Fig. 5, 6e, 6f). Our CapHensor has several advantages over existing biosensors which were recently developed to measure Ca^{2+} and pH either simultaneously or individually [115,116]. In detail, the low quantum yield of red fluorescence from R-GECO1 was overcome by fusing two R-GECO1 in tandem which increased the Ca^{2+} signal-to-noise ratio and improved the quality of Ca^{2+}-imaging in living cells substantially (Fig. 6e-g). Additionally, the use of the P2A sequence circumvented undesired FRET events, that will occur between PRpHluorin and R-GECO1 when these are translationally fusion. Since GFP proteins without any tag can localize in the cytosol and nuclei [364] and different cellular compartments such as the nuclei and the cytosol could generate their own Ca^{2+} signals [31,394,395], I chose to tag both biosensors with localization sequences. To prevent mixed signals from different subcellular compartments in plants, different versions of CapHensor were designed to target exclusively either in the cytosol or in the nucleus (Fig. 5).

R-GECO1 was reported to be pH sensitive *in vitro* in the pH range from 6.8 to 8.0, with increasing R-GECO1 fluorescence through cellular alkalization [101,108]. The range of intracellular pH changes was reported to be approximately 0.1-0.4 pH unit in plants [112,128] which was in line with no noticeable pH effects on R-GECO1 fluorescence in pollen tubes (Fig. 7a-c) or guard cells (Fig. 18a-c, 19b, 28c) during natural or imposed pH changes. Moreover, different temporal relationships between Ca^{2+} and H^+ signals were observed in pollen tubes, guard cells and mesophyll cells (Fig. 7, 8, 14, 19, 20, 23, 33), all pointing towards negligible pH effects on the R-GECO1 fluorescence *in planta*. A blue light dependent photoswitching problem with R-GECO1 imaging was recently reported to cause imaging artifacts [396]. Transient increases of R-GECO1 fluorescence by blue-light could last up to 940 ms [396]. However, this photoactivation only influences Ca^{2+} imaging when it is faster than 1 Hz. This problem can be ignored in the data presented here since I performed the live-cell imaging with sequential excitation light with the time interval of 2, 3 or 5 seconds. Moreover, in my study R-GECO1 was firstly excited and followed by PRpHluorin excitation at different

wavelengths, which enabled to leave enough time for possible photoswitching effects on R-GECO1 to be reversed during an imaging series.

The isosbestic point of PRpHluorin was quantified for calculations of ratiometric Ca^{2+} in different cell types *in vivo* (Fig. 6a-d, S1) to avoid artifacts such as focus changes or differences in expression level. Albeit a laser with 415 nm excitation wavelength does not exist on conventional confocal laser microscopes that required for ratiometric Ca^{2+} imaging (Fig. 6a-d), illuminating the isosbestic point was achieved by using a polychromator system. Alternatively, one would be able to use a setup equipped with a light-emitting diode-based excitation system. At a conventional confocal system simultaneous Ca^{2+} and H^+ imaging with our CapHensor could be accomplished by monitoring pH ratiometrically using the 405 nm laser diode and the 476 nm argon laser line while intensiometrically recording Ca^{2+} by excitation at 561 nm ($\Delta F/F0$) with all mentioned advantages.

5.2 The role of $[H^+]_{cyt}$ gradients and its interaction with $[Ca^{2+}]_{cyt}$ in pollen tube growth

Previous studies showed $[Ca^{2+}]_{cyt}$ and $[H^+]_{cyt}$ gradients were of great significance for apical pollen tube growth [131,156,366]. The role of pH gradients in pollen tubes growth was described to be not important at all by some groups [397,398] but was thought to be more important than Ca^{2+} signal by others [75,366,399]. Here, I made use of CapHensor expressed in *N. tabacum* pollen tubes to monitor $[Ca^{2+}]_{cyt}$ and $[H^+]_{cyt}$ gradients together with growth using sophisticated quantitative data analysis with algorithms specifically designed to perform coherence analysis. Compared with pollen tubes of *Lilium longiflorum*, tobacco plants are easily cultivated in greenhouse and accessible for stable transformation. Moreover, tobacco pollen grains can be collected, stored in the freezer and easily cultivated with high germination rate compared with *Arabidopsis*. Therefore, tobacco is an appropriate model for studying sexual reproduction in plants [128].

My results demonstrated that high $[H^+]_{cyt}$ levels at the tip stimulated growth rate while low tip $[H^+]_{cyt}$ was associated with suppressed growth when pollen tubes were challenged with an extracellular medium pH from optimal pH 5.8 to pH 5 or pH 6.8, respectively (Fig. 7a-c). The correlation coefficient analysis between growth and $[H^+]_{cyt}$ or growth and $[Ca^{2+}]_{cyt}$, indicating a more important role of $[H^+]_{cyt}$ in regulation of growth speed (Fig. 7f) as the cross correlation values

were significantly higher with $[H^+]_{cyt}$ compared to $[Ca^{2+}]_{cyt}$. This matched with recent results, where plasma membrane H^+-ATPases (AHAs) were proven genetically to contribute to $[H^+]_{cyt}$ gradients and growth in pollen tubes [75]. Mechanisms of H^+ entry at the tip of pollen tubes are still unknown, however, from the magnitude of H^+ fluxes a channel driven transport seems possible, but H^+ channels in higher plants have not been identified, but only found in animals or phytoplankton [400,401]. H^+ efflux at the shank through H^+ pumps generates a proton motive force that serves to drive secondary active transport mechanisms at the plasma membrane in pollen tubes [146] (Fig. 2). Other factors such as cell wall or membrane trafficking are also involved in pollen tubes growth and associated with H^+ and/or Ca^{2+} regime [402]. In contrast to most other plant cell types, pectin is the major cell wall component in pollen tubes and can be deesterified by pectin methylesterase (PME) [150,403]. PME activity observed in the cell wall at the tip of growing pollen tubes was deactivated by increased acidity which links protons with apical growth [117,131,404]. The 'acid-growth theory' was related to H^+ stimulated processes and resulted in cell wall loosening to accomplish cell extension [147]. I investigated the effect of extracellular acidification or alkalization on growth rate (Fig. 7a, b), however growth rate promotion was also observed by exclusively acidifying the cytosol without changing the apoplastic pH (Fig. 7c). This provided evidence that cellular pH not only apoplastic pH changes play a role in controlling pollen tube growth. To investigate the role of $[Ca^{2+}]_{cyt}$ in pollen tubes growth, caffeine was applied (Fig. 7d, e) since it was regarded to diminish $[Ca^{2+}]_{cyt}$ gradients and as a consequence to inhibit growth [129,131,133]. My results showed not only tip $[Ca^{2+}]_{cyt}$ and growth but even more pronounced inhibition of tip $[H^+]_{cyt}$ by caffeine (Fig. 7d, e), indicative for an effect which has previously been overlooked. After washout of caffeine, growth rate recovered in parallel with tip $[H^+]_{cyt}$ gradients, but tip $[Ca^{2+}]_{cyt}$ dynamics seemed to be independent on the growth recovery timeline (Fig. 7d-f). Quantitative analysis indicated better correlation between increased growth rate and elevated $[H^+]_{cyt}$ at the tip compared with tip $[Ca^{2+}]_{cyt}$ (Fig. 7f). These results suggested tip $[H^+]_{cyt}$ gradients to steer growth more effectively than $[Ca^{2+}]_{cyt}$ gradients (Fig. 7), which has not been compared simultaneously in the same cell before. $[Ca^{2+}]_{cyt}$ and $[H^+]_{cyt}$ oscillations were considered to control oscillatory growth in pollen tubes [119,131,160], but both second messengers actually lagged behind the growth rate as determined by sophisticated bioinformatics algorithm in my study (Fig. 8e, f) co-developed by our collaborators Dr. Daniel S.C. Damineli and Dr. Juan Prada. The growth event during oscillations preceded tip $[H^+]_{cyt}$ increases by approximately 18 s and tip $[Ca^{2+}]_{cyt}$ signal by 34 s (Fig. 8e, f)

matching a similar sequence of events observed in lily pollen tubes recently [366]. Due to the lagging $[Ca^{2+}]_{cyt}$ signal of several dozens of seconds, it is hard to argue that a $[Ca^{2+}]_{cyt}$ signal initiates the growth process in spite of genetic evidence that Ca^{2+} permeable channels at the tip play an essential role in pollen tubes [143,144] (Fig. 2). My results also matched previous reports that when increasing extracellular Ca^{2+} concentration, the growth speed was reduced, against the expectation that increased tip $[Ca^{2+}]_{cyt}$ signals would enhance cell protrusion [117,140]. However, Ca^{2+} contribution in pollen tubes growth can not be excluded since many other factors can be regulated by Ca^{2+} signals. For example, there is a positive feedback loop between ROS and Ca^{2+} while ROS dampens oscillations of growth speed [135,405]. However, how Ca^{2+} regulates ROS to control pollen tube growth is still largely unknown [406]. $[Ca^{2+}]_{cyt}$ gradients were assumed to participate in exocytosis to promote tip growth [138,139] for almost three decades, however, the growth rate of pollen tubes was not stimulated although the exocytosis was enhanced by imposed $[Ca^{2+}]_{cyt}$ increases [402]. The molecular mechanisms of Ca^{2+}-related membrane trafficking for cell expansion remain to be characterized [407,408]. Hence, my results point to a re-consideration of the Ca^{2+}-dependent mechanisms for pollen tubes growth and more importantly suggest tip $[H^+]_{cyt}$ gradient to be an important determinant for growth (Fig. 7, 8).

Remarkably, tip $[H^+]_{cyt}$ signals preceded tip $[Ca^{2+}]_{cyt}$ dynamics in oscillating growing pollen tubes whereas this relationship was reversed when growth was abrogated (Fig. 8e, f). The term of leading or lagging sequences is used to compare the shortest interval time or the best cross-correlations between two oscillatory signals during the whole period, but it did not suggest causation between the signals [120]. In my study, it suggested tip $[Ca^{2+}]_{cyt}$ and $[H^+]_{cyt}$ regimes are interchangeable (Fig. 8e, f), which is partially different from the concept that others brought out that defined pH signatures are induced by Ca^{2+} signals [115]. The interchangeable temporal sequence of $[Ca^{2+}]_{cyt}$ and $[H^+]_{cyt}$ dynamics in pollen tubes demonstrated the link between the two second messengers to be not fixed, but probably their relationship to control different cell states. During the process of fertilization, pollen tubes grow in an oscillatory manner into the ovule and stop growth before entering the ovule and finally releasing the sperms [129,141]. It is still unclear why growth sometimes arrests also in *in vitro* experiments, since live-cell imaging showed cytoplasmic streaming (data not shown) and tip-focused $[Ca^{2+}]_{cyt}$ and $[H^+]_{cyt}$ both remained prominent (Fig. 8a-b, 9a-b, 10d-e). A growth arrest as triggered by different stimuli such as extracellular alkalization or impalement, showed the frequency of $[Ca^{2+}]_{cyt}$ and $[H^+]_{cyt}$ oscillations was significantly increased, compared to

growing pollen tubes (Fig. 8a-d, 9, 10). Similar to other studies, high frequency and high amplitude tip $[Ca^{2+}]_{cyt}$ oscillations were observed [129,141] upon spontaneous or imposed growth arrests while $[H^+]_{cyt}$ oscillations monitored with CapHensor have not been observed before in non-growing pollen tubes. Monitoring $[Ca^{2+}]_{cyt}$ and $[H^+]_{cyt}$ oscillations in different growth states would help to understand ion signalings in non-growing pollen tubes in the last steps of fertilization.

A phenomenon described here for the first time was that $[Ca^{2+}]_{cyt}$ oscillations between the tip and the shank were in antiphase to one another whereas $[H^+]_{cyt}$ oscillations were in phase (Fig. 10a, b). Given that protons have higher mobility than Ca^{2+}, the different traveling speeds of Ca^{2+} and pH from the tip to the shank might result from around 12-fold faster diffusion of H^+ [409]. The spatio-temporal $[Ca^{2+}]_{cyt}$ dynamics between the tip and the shank might be differentially regulated by Ca^{2+}-dependent proteins such as CPKs in pollen tubes with distinct subcellular localization [19,410]. $[H^+]_{cyt}$ gradients between the tip and the shank are necessary for pollen tubes growth and maintained by plasma membrane H^+-ATPases [75,146]. For example, synchronized $[H^+]_{cyt}$ and growth oscillations were slower in the *aha6/8/9* mutant [75]. Even though pollen tubes growth in the *aha6/8/9* mutant was impaired, turgor pressure was not significantly different compared with turgor pressure in wild type [75]. $[H^+]_{cyt}$ influx at the tip could form a current loop with Cl^- efflux but at the shank H^+ and Cl^- efflux occurs in a steady manner [117]. In contrast, $[H^+]_{cyt}$ oscillations at the shank exist in my study (Fig. 10a, b). The inphase $[H^+]_{cyt}$ oscillations between the tip and the shank (Fig. 10a, b) might function in actin or cytoplasmic streaming [117] since reduced pollen tubes growth in the *aha6/8/9* mutant was involved in the absence of actin organization at the tip influenced by protons [75]. In agreement with both Ca^{2+} and H^+ regimes to lag behind growth oscillations (Fig. 8), other ions such as K^+ and anions were reported to regulate pollen tube growth as well and directly or indirectly to be controlled by Ca^{2+} and/or H^+ [117,130,152,156]. Ion transport is integrated into membrane potential changes via charges movement, while the membrane potential functions simultaneously as the driving force for ion fluxes across membranes. The impalement in *N. tabacum* pollen tubes at the shank showed oscillatory membrane potential values correlated better with tip $[H^+]_{cyt}$ oscillations than tip $[Ca^{2+}]_{cyt}$ oscillations (Fig. 10e-g). Unfortunately, these three parameters could not be linked to growth since pollen tube growth was arrested even with gentle electrode insertion in almost all cases. However, membrane potential in pollen tubes lagged behind tip $[Ca^{2+}]_{cyt}$ and $[H^+]_{cyt}$ by temporal resolution on these three parameters in parallel (Fig. 10c-f). Cl^- might act as a central regulator in pollen tube growth in a Ca^{2+}-dependent pattern [125]. Anion

channel SLAH3 is activated by CPK2/20 [125] and K^+ inward currents could be inhibited by increased $[Ca^{2+}]_{cyt}$ via CPK11/24 [155], which might explain $[Ca^{2+}]_{cyt}$ preceding V_m (Fig. 10e, f). However, I found tip $[H^+]_{cyt}$ rather than $[Ca^{2+}]_{cyt}$ oscillations to better correlate with V_m (Fig. 10g). This phenomenon might be related to H^+-ATPases and/or channels regulation by H^+. Pollen tube growth reduction in the *aha6/8/9* mutant was associated with reduced anion efflux at the tip and thus the membrane potential was less hyperpolarized in the *aha6/8/9* mutant compared to wild type [75]. Moreover, cytosolic acidification can activate SLAH3 channel to increase anion efflux resulting in membrane depolarization [411]. The K^+-inward currents were inhibited by extracellular alkalization but not by acidification while outward K^+ channels were activated by external acidification to control apical growth [412,413], which fits my findings on the roles of $[H^+]_{cyt}$ in pollen tube growth (Fig. 7, 10g). Even though I could not exclude the coupling of $[Ca^{2+}]_{cyt}$ and V_m in pollen tubes, the method of combining live-cell imaging of $[Ca^{2+}]_{cyt}$ and $[H^+]_{cyt}$ with V_m recordings indicate $[Ca^{2+}]_{cyt}$ and $[H^+]_{cyt}$ oscillations possibly modulate ion transport during apical growth [123]. In conclusion, through observing the $[Ca^{2+}]_{cyt}$ and $[H^+]_{cyt}$ and growth dynamics with high temporal and spatial resolution, I could uncover that apical $[H^+]_{cyt}$ correlates with pollen tube growth speed and much better than tip $[Ca^{2+}]_{cyt}$ gradients. This implies $[H^+]_{cyt}$ to play a prominent role in the regulation of pollen tube growth. I could provide a precise description of the sequences of events in pollen tubes, emphasizing on the importance of $[H^+]_{cyt}$ in apical growth, and the relationship between $[Ca^{2+}]_{cyt}$ signals and growth to be revisited. Furthermore, the interchangeable $[Ca^{2+}]_{cyt}$ and $[H^+]_{cyt}$ regimes I observed point to distinct roles of $[Ca^{2+}]_{cyt}$ and $[H^+]_{cyt}$ in the process of pollen tube guidance or during communication with the ovule in case the tubes stop growing. Therefore, in the future, combining our method with reverse genetics approaches in *Arabidopsis* will shed light on the molecular components responsible for $[Ca^{2+}]_{cyt}$ and $[H^+]_{cyt}$ oscillations and on the potential regulatory network in pollen tube growth.

5.3 Guard cell pH changes play an important role to control stomatal movement

I made use of *N. tabacum* guard cells to investigate the role of $[Ca^{2+}]_{cyt}$ and $[H^+]_{cyt}$ in regulation of stomatal movement because tobacco guard cells are an ideal system, which outperform *Arabidopsis* guard cells due to their size. Tobacco guard cells are comparably big and the aperture

change recordings over time were possible to be monitored automatically via a custom-made macro in Fiji (Table 10). Different $[Ca^{2+}]_{cyt}$ and $[H^+]_{cyt}$ regimes were monitored in *N. tabacum* guard cells upon ABA, flg22, H_2O_2 and extracellular changes in pH or $CaCl_2$ concentration (Fig. 14, 16, 19, 27, 32). $[Ca^{2+}]_{cyt}$ transients and cytosolic alkalization were triggered by ABA (Fig. 14a-b), which has been observed before in separate experiments having a low signal-to-noise ratio but without such a temporal resolution [68,112,372,414]. Making use of CapHensor, I precisely quantified the temporal relationship between $[Ca^{2+}]_{cyt}$, $[H^+]_{cyt}$ and aperture changes in the same cell and identified cytosolic alkalization to precede Ca^{2+} transients by 33 s in ABA induced stomatal closure (Fig. 14c). In flg22 induced stomatal closure, pronounced $[Ca^{2+}]_{cyt}$ signals seemed to be more important to induce stomatal closure and only minor $[H^+]_{cyt}$ changes were seen (Fig. 14d, e). $[Ca^{2+}]_{cyt}$ elevations upon flg22 were reported many times [170,269,301] whereas $[H^+]_{cyt}$ changes were rarely reported. The temporal resolution during CapHensor imaging uncovered $[Ca^{2+}]_{cyt}$ and $[H^+]_{cyt}$ changes to occur very rapidly after exposure to the stomata closing stimuli. In earlier reports, cytosolic alkalization was observed ca. 2-8 min [112,227] and $[Ca^{2+}]_{cyt}$ increases more than 10 min [33,174,415] after ABA application, whereas stomatal immunity could be detected within minutes upon pathogen infection [246]. In those earlier reports, however, the timing of these events was investigated separately and stomatal movement was monitored several hours after stimuli application. In my study, simultaneous $[Ca^{2+}]_{cyt}$ and $[H^+]_{cyt}$ during stomatal movement were visualized with time-lapse imaging in the same cell under different stimuli. My approach is superior to quantify the sequence of the signaling events (Fig. 14) and to conclude the role of $[Ca^{2+}]_{cyt}$ and $[H^+]_{cyt}$ changes in controlling stomatal movement. I observed stomata started to close ca. 3-4 min after ABA or flg22 application, obviously lagging behind $[Ca^{2+}]_{cyt}$ and $[H^+]_{cyt}$ responses (Fig. 14b-e), indicating $[Ca^{2+}]_{cyt}$ and $[H^+]_{cyt}$ could possibly initiate stomatal closure. $[H^+]_{cyt}$ responses set off first in ABA induced stomatal closure indicated Ca^{2+}-independent regulatory mechanisms were initiated at a very early time point of the response and the pH changes could control the $[Ca^{2+}]_{cyt}$ response. In my experiments, stomatal closure induced by ABA or flg22 could be completely blocked by clamping the cytosol to more acid pH with 3 mM BTA (Fig. 18a, c) which was used before [227,337] indicating the ABA and flg22 core pathway to be pH dependent (Fig. 18). Similar effects were also reported by others [173,243,416]. However, Islam et al claimed that increased $[Ca^{2+}]_{cyt}$ was the initial signals followed by cytosolic alkalization in ABA induced stomatal closure in *Arabidopsis* using low temporal and imaging resolution [173] whereas I found cytosolic alkalization is the initial

signal in tobacco guard cells upon ABA treatment (Fig. 14b, c). $[Ca^{2+}]_{cyt}$ increases triggered by ABA could be largely inhibited by BTA whereas $[Ca^{2+}]_{cyt}$ elevations triggered by flg22 were less suppressed (Fig. 18a-c). These results indicated stomatal closure induced by flg22 depends more on pronounced $[Ca^{2+}]_{cyt}$ increases (Fig. 14d, e, S2c) than ABA does, while the latter one is more associated with a cytosolic alkalization (Fig. 14b, c, S2b). This is in line with the finding of CPKs and ROS function in the flg22 pathway [264]. However, it should be mentioned that the quadruple *cpk3/5/6/11* mutant displayed normal stomatal closure upon ABA and flg22 [261], suggesting Ca^{2+}-independent or other Ca^{2+}-sensing mechanisms to exist. Even though mild cytosolic alkalization upon flg22 was observed (Fig. 14d), cytosolic acidification by applying BTA interrupted flg22 induced stomatal closure (Fig. 18b). The pathogen signaling pathway might be connected by cytosolic acidification since crucial components of immunity in plants like MPKs were found to be activated by decreased cytosolic pH [417,418]. In the flg22 signaling pathway, MPKs might be important factors of a Ca^{2+}-independent mechanism [419,420] by modifying anion channel activity [419,421], which remains to be identified in the future combined with reverse genetic studies. Combined with others' findings (shown in Fig. 3), ABA can be recognized by ABA receptors to inhibit the activity of PP2C family like ABI1 in 5 min in *Arabidopsis* and OST1 activity is suppressed by PP2C [5,198,372,422] (Fig. 3), which is regarded as an early step in ABA signaling. One of the key regulator in ABA pathway in guard cells is ABI1, and its activity can be increased by ABA by the pH shift from around 7.2 to 7.5 [423]. ABA induced cytosolic alkalization and stomatal closure were both impaired in the *abi1-1*, *abi2-1* and *ost1-2* loss-of-function mutant [173]. The cytosolic alkalization observed in ABA induced stomatal closure was less likely to attribute to plasma membrane H^+-ATPases since they were inhibited by ABA in biochemical experiments *in vivo* and moreover the apoplast in sub-stomata upon ABA became more alkalized as well [68,229]. Therefore, the inhibited plasma membrane H^+-ATPases by ABA should be interpreted with caution [84,279,424]. Although Ca^{2+} and ROS could influence plasma membrane H^+-ATPases activity [5,275] and $[Ca^{2+}]_{cyt}$ increases and ROS production were important in flg22 induced stomatal closure [266,342], roles of plasma membrane H^+-ATPases in guard cells upon flg22 still remain to be characterized. Apoplastic alkalization has also been reported in leaves under flg22 treatment [259] but not in guard cells. Thereby the question arises where the cytosolic alkalization come from? A potential contributor for cytosolic alkalization might be H^+ accumulation in the tonoplast [243]. ABA activated vacuolar H^+-ATPases (V-ATPases) activity in *Mesembryanthemum crystallinum* [244], for

instance. The central vacuole usually occupies more than 90 % of the cell volume and vacuolar osmolyte changes are of great importance for regulating guard cells turgor pressure [290,425,426]. Vacuolar pH monitored by BCECF dye was visualized here in *N. tabacum* guard cells during ABA and flg22 treatment (Fig. 15). I observed ABA induced a sustained vacuolar acidification while a transient vacuolar acidification was observed upon flg22 application (Fig. 15). This vacuolar pH regimes matched with ABA induced sustained cytosolic alkalization and flg22 triggered mild transient cytosolic alkalization (Fig. 14) and fitted previous reports on vacuolar acidification [243]. Vacuolar H^+-ATPases and vacuolar H^+-PPases constantly pump H^+ from the cytosol into the vacuole [62]. The double vacuolar H^+-ATPases (*vhaa2/a3*) mutant displayed more alkalized vacuole [241]. ABA induced stomatal closure and vacuolar acidification were delayed in the double *vhaa2/a3* mutant and vacuolar H^+-PPases (*vhp1*) mutant [243]. Its functions in flg22 induced stomatal movement remains to be revealed.

Common events reported for ABA and flg22 triggered stomatal closure in *Arabidopsis* are ROS production, anion channels activation and membrane depolarization [6,45,209,215,249,261] (Fig. 3). Some studies reported ROS production is the earliest event in the ABA pathway after 1 min [48,375]. However, this is controversial because others found cytosolic alkalization to start 5 min after ABA application whereas ROS production started 10 min later and reached a maximum around 30 min [197,416]. ROS production was found to be mainly produced by NADPH oxidases RbohD/F in ABA and flg22 triggered stomatal closure [211,249,294,427,428] (Fig. 3). However, the initial $[H^+]_{cyt}$ responses and lagging $[Ca^{2+}]_{cyt}$ signal in guard cells under ABA treatment could not be observed with flg22 or H_2O_2 (Fig. 14, 16, S2), suggesting distinct interactions between $[Ca^{2+}]_{cyt}$ and $[H^+]_{cyt}$ upon specific stimuli. Early studies in *Arabidopsis* showed Ca^{2+} channel activation by ROS increase to induce stomata closure [48,376,429]. In contrast, neither stomatal closure nor $[Ca^{2+}]_{cyt}$ increases in tobacco guard cells were observed upon physiological H_2O_2 concentration ($\leq$ 200 μM) (Fig. 16a, b), probably indicating a different effect of ROS to be present in tobacco guard cells. Only mild stomatal closure and slow $[Ca^{2+}]_{cyt}$ increases were observed in high H_2O_2 concentration of 1 mM when cell integrity was lost after 15–30 min treatment (Fig. 16c, 17c). Interestingly and very reproducibly, cytosolic acidification was induced by H_2O_2 in a dose-dependent manner (Fig. 16a-c) which is in conflict with an earlier report showing H_2O_2 triggered cytosolic alkalization and vacuolar acidification in *Vicia faba* guard cells [375]. However, similar to my results of cytosolic acidification blocked ABA and flg22 induced stomatal closure (Fig. 18a-c), butyrate also inhibited

ABA, MeJA and high external Ca^{2+} or H_2O_2 induced stomatal closure in *Arabidopsis* or in *Vicia faba* by suppression cytosolic alkalization [173,375]. Similarly, they found cytosolic alkalization through H^+ efflux from the cytosol into the vacuole is important for stomatal closure [375]. My observation that H_2O_2 triggered $[H^+]_{cyt}$ elevations in *N. tabacum* guard cells (Fig. 16) might explain the phenomenon that stomata open upon H_2O_2 at physiological concentration [284]. Combing with other studies (Fig. 3), these distinct observations of $[Ca^{2+}]_{cyt}$, $[H^+]_{cyt}$ and stomatal movement upon ABA, flg22 and H_2O_2 application indicate these different stimuli to merge at the level of anion and potassium channels regulation via the demonstrated CPK- and OST1-dependent mechanisms. CPKs and OST1 were found to phosphorylate SLAC1 channel at different sites [191], which could account for Ca^{2+}-dependent and -independent mechanisms in the ABA pathway (Fig. 3). Ca^{2+}-dependent mechanisms in ABA and flg22 induced stomatal closure could be achieved by CPKs or CBL/CIPK to control anion channels activity [191,430,431] whereas cytosolic acidification induced by H_2O_2 in *N. tabacum* guard cells might contribute to stomatal movement by activation anion channels [432] (Fig. 16). Especially, anion channels SLAH3 was recently found to be directly activated by cytosolic acidification [411].

The triggering of $[Ca^{2+}]_{cyt}$ elevations by increased extracellular Ca^{2+} concentration was used in the past to argue for a Ca^{2+} dependent step in stomatal closure across species [169,173,186]. However, only very slow stomatal closure with the speed of 0.8186 μm^2/min in *N. tabacum* was observed upon extracellular Ca^{2+} increases accompanied by strong $[Ca^{2+}]_{cyt}$ increases and initial cytosolic alkalization (Fig. 19b). In addition to $[Ca^{2+}]_{cyt}$ increases, however, $[H^+]_{cyt}$ changes upon extracellular pH changes were observed to control stomatal movement much more efficiently (Fig. 19). Especially when I compared $[Ca^{2+}]_{cyt}$ and $[H^+]_{cyt}$ responses in *N. tabacum* guard cells and quantified the ratio between these two signals, the speed of stomata closing depended on the magnitude of the cytosolic alkalization (Fig. 19c-g). Another strong argument for pH to affect stomata behavior effectively is the stomata opening speed, it was stimulated by cytosolic acidification when changing the normal solution with pH 5.8 (0.8143 μm^2/min) to one with pH 4.8 (1.190 μm^2/min) (Fig. 19b, f). Stomatal closure occurred upon external Ca^{2+} application in a dose-dependent manner meaning the higher extracellular Ca^{2+} concentration, more pronounced closure was observed [173,186]. Contrary to these findings, significant stomatal closure upon high extracellular Ca^{2+} concentration was not observed in *N. tabacum* (Fig. 19b). During stomatal closure, the required membrane depolarization occurs ~ 2 min [187,207] after ABA treatment through

activation of anion channels [187]. Therefore the initial cytosolic alkalization might be a very early regulatory step to control stomatal movement via changing ion channels' activities and subsequently the membrane potential. This potential signaling step remains to be studied in detail in the future and it has to be compared using different species to understand universal and distinct signaling mechanisms across species.

Generally, I concluded that stomatal closure or opening in *N. tabacum* was more effectively regulated by cytosolic alkalization or acidification than by $[Ca^{2+}]_{cyt}$ increases, however, Ca^{2+} responses were always accompanied with stomatal closure (Fig. 14, 18, 19, S2). Whether Ca^{2+}-independent pathway in regulations of stomatal closure depends on pH changes and whether pH-dependent mechanism exists in stomatal movement can not finally be claimed here, but I uncovered that ABA and flg22 signaling pathways triggered stomatal closure depend on pH via visualizing cytosolic and vacuolar pH dynamics (Fig. 14, 15). In guard cells, OST1 is a central regulator in ABA and flg22 pathways [246,251,261] (Fig. 3). OST1 activates NADPH oxidase RbohD/F in HEK cells to produce ROS and this mechanism is proposed to activate downstream events such as channels activity even though OST1 is reported to be suppressed by ABI1, pointing out the complexity of the signaling networks in stomatal movement [191,433,434]. I provided a detailed time-resolution of $[Ca^{2+}]_{cyt}$ and $[H^+]_{cyt}$ and stomatal movement events and demonstrated pH to be a major regulator for stomatal movement (Fig. 14, 16, 18, 19, S2). In the future, reverse genetic studies and biochemical approaches to study protein-protein interactions upon pH changes combining with CapHensor imaging could contribute to understand the balance and interaction between Ca^{2+}-dependent or pH-dependent mechanisms in stomatal movement.

5.4 A distinct set of Ca^{2+}, H^+ and electric responses in mesophyll cells upon different stimuli

Mesophyll physiology related to ion signaling is much less studied compared to guard cells, however leaves are well known to respond fast to salt, drought stress or wounding, which were shown to induce chemo-electric systemic signals [230,259,435,436]. $[Ca^{2+}]_{cyt}$ rises and plasma membrane H^+-ATPases both participated in the electric signals in leaves upon different stresses but the sequence of chemo-electric signaling events has not been studied in detail [107,234,259,344,437-439].

To characterize the temporal dynamics of Ca^{2+}, H^+ and V_m in mesophyll cells to different stimuli and to compare them with the ones from guard cells, I here combined live-cell CapHensor imaging with V_m recording upon flg22, ABA and H_2O_2 treatment (Fig. 20). The electrode was placed in the same area as monitoring fluorescence from CapHensor to simultaneously record membrane potential and Ca^{2+} and H^+ changes. A rapid $[Ca^{2+}]_{cyt}$ transient occurred approximately 4 min after flg22 application and preceded a cytosolic acidification transient around 24 s, but both of them significantly lagged behind V_m depolarization around 2 min (Fig. 20b, i). This was in line with other studies showing $[Ca^{2+}]_{cyt}$ increases are essential for membrane depolarization in leaves upon flg22 [107,259] or wounding [437]. $[Ca^{2+}]_{cyt}$ increases induced by flg22 are thought to be dependent on ROS bursts and membrane potential depolarization is likely to result from the activation of anion channels [45,259,336]. Because apoplastic alkalization in leaves and plasma membrane H^+-ATPases have been proved to participate in systemic signaling [94,438,439], cytosolic acidification I observed here (Fig. 20b, f) might be related to apoplastic alkalization in leaves in response to flg22 [259,440]. Transcriptional reprogramming takes place after pathogen invasion [257,264,265] and defense genes in tobacco were influenced by cytosolic acidification [441,442]. Apoplastic pH changes upon pathogen attack are linked to Ca^{2+} signaling but pH changes alone are able to regulate genes expression [443]. However, H^+ signals in the nucleus upon stresses are rarely reported [71]. The spatio-temporal imaging of Ca^{2+} and H^+ with high resolution in the nuclei in my study uncovered $[Ca^{2+}]_{nuc}$ and $[H^+]_{nuc}$ increases, very similar to the responses in the cytosol (Fig. 20f, j), pointing out these two messengers could lead to the genetic reprogramming. Ca^{2+} permeable channels existed in the nuclear envelope and were required for cytosolic and nuclear Ca^{2+} [444], which might be responsible for the Ca^{2+} transients upon flg22 application I could monitor.

The interesting observation is the membrane depolarization started 2 min after flg22 application to mesophyll cells and both preceded Ca^{2+} and H^+ by approximately 1-2 min (Fig. 20b, f, i, j). The fast electric signal preceding the Ca^{2+} signal (Fig. 20b, f, i, j) was also reported by others, but hypothesis for lagging chemical signals has not been presented so far [259,349,439]. The high buffering capacity for Ca^{2+} and H^+ in the cytosol can not be responsible for the time delay between the electric and chemical signals since the diffusion of Ca^{2+} within a cell is expected to be accomplished in the millisecond to second range [445]. The flg22 triggered fast depolarization in mesophyll cells can not be explained by Ca^{2+}- or H^+- dependent mechanisms for anion channel activation [218,446] based on my results. In *Arabidopsis*, due to lagging $[Ca^{2+}]_{cyt}$ increases (Fig. 20b,

f, i, j), fast and initial membrane depolarization likely does not involve CPKs [264,265], but mitogen-activated protein kinase (MAPK) cascades such as MPK3, MPK6 could be triggered in minutes by pathogens [447]. Because depolarization in mesophyll cells upon flg22 treatement was not interrupted in the quadruple *cpk3/5/6/11* mutant [261] although CPK3, 5, 6 and 11 are essential for flg22 induced ROS production [261,262,264]. The depolarization but also the V_m repolarization after the maximum depolarization accompanied by coordinated $[Ca^{2+}]_{cyt}$ and $[H^+]_{cyt}$ decline might be regulated by H^+-dependent activation of plasma membrane H^+-ATPases, but which molecular components are involved in these chemo-electric transient signal remains to be genetically identified [343,448-450].

Except Ca^{2+} and H^+, ROS waves were also important for systemic electrical signals in leaves upon wounding [345,451,452]. Moreover, ABA synthesis in guard cells [246,249] or ROS production in leaves [259] were observed under pathogen stress. The re-distribution of proteins such as CPK32 from the cytosol into the nucleus was reported in an ABA-dependent manner [453,454]. However, I observed no Ca^{2+}, H^+ and V_m changes within the mesophyll after ABA or H_2O_2 treatment neither in the cytosol nor in the nucleus (Fig. 20c, d, g, h). This indicates no fast chemo-electric signals in the cytosol or the nucleus of mesophyll cells by ABA and ROS, at least not in the time scale I investigated here, which matches with a recent report no $[Ca^{2+}]_{cyt}$ and $[H^+]_{cyt}$ changes were observed upon ABA or H_2O_2 treatment in roots [116]. An unchanged V_m response upon H_2O_2 treatment (Fig. 20d, h) might be in line with a previous study showing flg22 induced membrane depolarization is more likely to be ROS-independent since depolarizations still occurred in the NADPH oxidase loss-of-function mutant [259]. Therefore, other mechanisms independent on Ca^{2+} or pH changes upon ABA or H_2O_2 application in mesophyll cells must exist and remain to be shown.

The $[Ca^{2+}]_{cyt}$ increases in guard cells and mesophyll cells differed significantly with respect to their temporal dynamics (Fig. 14, 16, 20). While only one Ca^{2+} peak was induced in mesophyll cells under flg22 (Fig. 20), the guard cells displayed often pronounced Ca^{2+} oscillations with repetitive Ca^{2+} increases (Fig. 14d). In spite of distinct Ca^{2+} signals between mesophyll cells and guard cells upon flg22 treatment, mesophyll cells and guard cells are likely to share signaling pathways for flg22, but not for ABA and H_2O_2. A pronounced cytosolic acidification in mesophyll cells (Fig. 20b, f) but slight alkalization in guard cells under flg22 treatment (Fig. 14d, S2c) observed in my study indicate distinct $[H^+]_{cyt}$ signals in different cell types by the same stimulus.

The combination of live-cell imaging via CapHensor and electrophysiology uncovered novel aspects on the spatio-temporal interconnection between intracellular Ca^{2+}, H^+ and membrane potential. Different Ca^{2+} reactions of different cell types were reported previously [455-457]. I could also demonstrate that distinct $[Ca^{2+}]_{cyt}$ and $[H^+]_{cyt}$ regimes with different interrelationships exist in different cell types even of the same organ, the leaf (Fig. 22). Therefore, one should not generalize and assume that the response of one cell type to a stimulus means that other cell types react in the same way. In addition, the simultaneous approach of CapHensor imaging and electrophysiological recording of membrane voltage has shown that this approach is suitable to uncover missing or existing correlations between chemical- and electrical signals.

5.5 Spontaneous $[Ca^{2+}]_{cyt}$ and $[H^+]_{cyt}$ oscillations are linked, but correlated differently within a population of guard cells

Compared with imposed $[Ca^{2+}]_{cyt}$ oscillations induced by ABA, flg22 or high external Ca^{2+} (Fig. 14, 19b), spontaneous $[Ca^{2+}]_{cyt}$ and $[H^+]_{cyt}$ oscillations were observed in 38.31 % of all the measured guard cells, in the absence of any treatment via time-lapse live-cell imaging of $[Ca^{2+}]_{cyt}$ and $[H^+]_{cyt}$ via CapHensor (Fig. 23a, b). In fact, natural $[Ca^{2+}]_{cyt}$ oscillations were observed previously [5,175,277,415,458] but are commonly neglected and only the responses of non-oscillating cells are considered [459]. Time-resolved imaging of $[H^+]_{cyt}$ dynamics was not reported in guard cells and spontaneous $[H^+]_{cyt}$ oscillations were not described before. I found two populations of oscillatory guard cells with in phase or antiphase relationship, in other words negative or positive correlation between $[Ca^{2+}]_{cyt}$ and $[H^+]_{cyt}$ (Fig. 23). $[H^+]_{cyt}$ regimes preceded $[Ca^{2+}]_{cyt}$ oscillations in inphase guard cells whereas $[Ca^{2+}]_{cyt}$ dynamics preceded $[H^+]_{cyt}$ oscillations in antiphase guard cells (Fig. 23, 24). It is possible that these oscillatory guard cells are in different states, which probably can be explained by the phenomenon of stomatal patchiness which is not at all understood. Stomatal patchiness stands for stomata in different states that respond quite differently to a defined treatment which is thought to optimize the response network in leaves [460,461]. The guard cells with $[Ca^{2+}]_{cyt}$ and $[H^+]_{cyt}$ dynamics in phase showed cytosolic acidification preceded $[Ca^{2+}]_{cyt}$ increases ca. 13 s (Fig. 23a), which is indicative of cytosolic acidification to promote Ca^{2+} influx [462]. The antiphase guard cells displayed $[Ca^{2+}]_{cyt}$ increases preceded cytosolic alkalization (Fig. 23b), suggesting Ca^{2+}-stimulation of H^+-ATPases or H^+-coupled transporters [40,463-465] to be potential components for synchronized $[Ca^{2+}]_{cyt}$ and $[H^+]_{cyt}$ homeostasis [66,96,465,466]. But high Ca^{2+} was found

to inhibit plasma membrane H^+-ATPases [275,348]. Activation of H^+-ATPases is known to induce hyperpolarization [88], which might stimulate hyperpolarization activated Ca^{2+}-permeable channels [48,49], however, this would imply that voltage changes would precede $[Ca^{2+}]_{cyt}$ changes, which was not shown here but is helpful to understand the sequence of events in chemo-electric signalling networks. It should be noted that the phase analysis does indicate leading and lagging signals but does not represent proof for causality [120].

It was proposed that $[Ca^{2+}]_{cyt}$ oscillations are rather associated with a sustained stomatal closure mechanism instead of triggering stomatal closure per se [33]. This might explain the phenomenon that closed stomata are likely to display spontaneous $[Ca^{2+}]_{cyt}$ oscillations [414] (Fig. 25a, b, e, f). Guard cells exhibiting spontaneous $[Ca^{2+}]_{cyt}$ oscillations did not always lead to stomatal closure [175,337], which was proposed to result from shorter periods of spontaneous $[Ca^{2+}]_{cyt}$ oscillations than ABA-imposed $[Ca^{2+}]_{cyt}$ oscillations [34,175]. However, this assumption was hardly explained since similar period of spontaneous $[Ca^{2+}]_{cyt}$ oscillations was observed in 10 mM external Ca^{2+} induced $[Ca^{2+}]_{cyt}$ oscillations but stomata closed [34,172,174]. Moreover, spontaneous $[Ca^{2+}]_{cyt}$ oscillations seem to be contrary to the view of Ca^{2+}-dependent stomatal closure [467]. These studies have suggested a more complex picture of guard cells signaling network than previously thought [384]. I found natural oscillations in guard cells having $[Ca^{2+}]_{cyt}$ and $[H^+]_{cyt}$ regimes in phase to harbor a higher frequency than guard cells having antiphase regime (Fig. 23, 24d). To investigate the physiological role of these spontaneous oscillations to influence stomatal movement, ABA or flg22 was applied on these oscillatory guard cells (Fig. 25). Stomatal closure on oscillatory guard cells induced by ABA or flg22 was much less pronounced (Fig. 25) compared with guard cells with stable resting $[Ca^{2+}]_{cyt}$ (Fig. 14b, d). Whether these oscillatory guard cells are less reactive to external stimuli still remains to be investigated in detail though. However, the interesting phenomenon was that natural $[H^+]_{cyt}$ oscillations, but not $[Ca^{2+}]_{cyt}$ oscillations were blocked by ABA but not by flg22 (Fig. 25) and naturally coupled $[Ca^{2+}]_{cyt}$ and $[H^+]_{cyt}$ oscillations were uncoupled by ABA (Fig. 25g, h). In contrast, spontaneous $[Ca^{2+}]_{cyt}$ or membrane potential oscillations were diminished by ABA [175,468], but the underlying mechanisms are unknown. The dampened natural $[Ca^{2+}]_{cyt}$ oscillations by ABA could use Ca^{2+} sensitivity priming mechanisms in stomatal closing, which was proposed in guard cell responses to ABA and high external Ca^{2+} [467,469,470]. This Ca^{2+} sensitivity priming model was proposed to display not only different modes of $[Ca^{2+}]_{cyt}$ elevations, but is also based on Ca^{2+} sensors reacting to Ca^{2+} increases differently [35,277]. This might explain the less-opened stomata

with spontaneous $[Ca^{2+}]_{cyt}$ and $[H^+]_{cyt}$ oscillations (Fig. 25a, b, e, f). The role of spontaneous $[H^+]_{cyt}$ oscillations carrying information in guard cells was not even speculated or discussed in the past. In line with inhibited natural $[H^+]_{cyt}$ oscillations upon ABA but not by flg22, vacuolar pH regime in guard cells visualized by BCECF showed oscillations in vacuolar pH was dampened by ABA but not by flg22 (Fig. 26). It indicates natural $[H^+]_{cyt}$ oscillations actually originate from vacuolar H^+ oscillations, since the central vacuole is regarded as the pH buffering organ. Although many ion channels, pumps and H^+-coupled transporters have been well described, factors contributing to $[Ca^{2+}]_{cyt}$ and $[H^+]_{cyt}$ interrelationship still remain to be unravelled. My CapHensor approach combined with sophisticated bioinformatics analysis not only uncover two distinct interconnections between spontaneous $[Ca^{2+}]_{cyt}$ and $[H^+]_{cyt}$ oscillations, but question whether guard cells having spontaneous oscillations are less responsive upon stimuli. The interrupted natural $[H^+]_{cyt}$ oscillations likely result from vaculoar H^+ regimes which are altered by ABA but not by flg22, representing a specific ABA signalling mechanism in guard cells distinct from the one of flg22.

5.6 Imposed $[Ca^{2+}]_{cyt}$ oscillations are negatively correlated with $[H^+]_{cyt}$ in guard cells

Ca^{2+} is a well-known second messenger to function in stomatal movement. Ca^{2+} oscillations with defined amplitudes, duration and frequency were suggested to control stomatal closure [171,172]. However, when using a similar approach to evoke defined Ca^{2+} oscillations by alternating the extracellular solution from high to low KCl concentration, stomatal movement turned out to depend more on the osmotic effects rather than depend on the evoked Ca^{2+} transients (Fig. 27, 29). To solely study the role of $[Ca^{2+}]_{cyt}$ changes, I used an approach avoiding osmotic effects by changing external $CaCl_2$ concentration from 0.01 mM to 1 mM (Fig. 27a, 27b, S3). High external Ca^{2+} concentration induced $[Ca^{2+}]_{cyt}$ transients might originate from activation of Ca^{2+}-permeable channels such as GLRs in guard cells [53], as high external Ca^{2+} induced stomatal closure was impaired in the double *glr3.1/glr3.5* mutant [459,471]. $[Ca^{2+}]_{cyt}$ transients were accompanied by cytosolic alkalization but obvious stomatal closure in *N. tabacum* was not observed (Fig. 27a, 27b, S3). It is worth noting that a similarly negative relationship between $[Ca^{2+}]_{cyt}$ and $[H^+]_{cyt}$ has been observed in my previous experiments using ABA and extracellular alkalization (Fig. 14b-e, S2b-d, 19b). To identify possible components in this negative correlation between $[Ca^{2+}]_{cyt}$ and $[H^+]_{cyt}$

in stomatal closure, vanadate was used to block plasma membrane H^+-ATPases (Fig. 27a, 27b, S3). Strikingly, quantitative cross-correlation analysis showed the negative correlation between $[Ca^{2+}]_{cyt}$ and $[H^+]_{cyt}$ (Fig. 27a-c) depended on plasma membrane H^+-ATPases activity when $[Ca^{2+}]_{cyt}$ signals were triggered by high external $CaCl_2$ treatment (Fig. 27a-c). Based on the time of the onset or peak response of $[Ca^{2+}]_{cyt}$ significantly preceding the timing of $[H^+]_{cyt}$ during the negative correlation (Fig. 27d), $[Ca^{2+}]_{cyt}$ might trigger a H^+-translocating process. My pharmacological approach indicated plasma membrane H^+-ATPases could be stimulated by a Ca^{2+} increase (Fig. 27b, c) which is in contrast to earlier work [315]. To date, only a calcium stimulated protein kinase, PKS5 (CIPK11) was reported to negatively regulate H^+-ATPases [315]. In addition to plasma membrane H^+-ATPases contribution to this negative $[Ca^{2+}]_{cyt}$ and $[H^+]_{cyt}$ correlation, Ca^{2+} channel activity regulation via pH or H^+-coupled Ca^{2+} transporters (CAXs) could participate in the homeostasis of these two ions. In fact, GLRs activity was assumed to be inhibited by extracellular alkalization [344], which did not fit my results of $[Ca^{2+}]_{cyt}$ increases accompanied by cytosolic alkalization (Fig. 27b, S3). Plasma membrane and vacuolar membrane localized CAXs in guard cells could transport Ca^{2+} out of the cytosol in exchange for H^+ [40,42,472], a possible transport mode for the occurring negative correlation observed in my studies (Fig. 14a-e, 19b, 27b, 32). For example, CAX1 and CAX3 localized in the tonoplast of guard cells are suggested to participate in Ca^{2+} homeostasis [42,473] and might contribute to apoplastic pH regulation in stomatal closure [463]. CAXs might function by mediating cytosolic 'Ca^{2+} signature' or regulating pH signal in various abiotic stresses [42,384,463,474]. Up to now, Ca^{2+} transporters at the plasma membrane are poorly characterized to contribute to $[Ca^{2+}]_{cyt}$ homeostasis in guard cells. Monitoring $[Ca^{2+}]_{cyt}$ and $[H^+]_{cyt}$ changes via CapHensor combined with reverse genetic studies including loss-of-function mutants of CAXs, ACAs, etc. could significantly help to unravel the functional interrelation and the contribution of $[Ca^{2+}]_{cyt}$ and $[H^+]_{cyt}$ signaling in stomatal movement.

Against the common view that Ca^{2+} is the main second messenger to promote stomatal closure, pronounced $[Ca^{2+}]_{cyt}$ oscillations imposed by increased external Ca^{2+} concentration did not induce stomatal closure in *N. tabacum* (Fig. 19b, 27a-b, S3). This fits my other results that $[Ca^{2+}]_{cyt}$ dynamics were observed in stomatal opening and closure (Fig. 14, 19b, 27b, 28-30) and spontaneous $[Ca^{2+}]_{cyt}$ oscillations did not show pronounced stomatal closure upon ABA and flg22 (Fig. 25a, b, e, f). Moreover, stomatal closure occurred in the absence of $[Ca^{2+}]_{cyt}$ increases in others studies [112,173,187,188,192,277,455,469]. I observed stomatal closure in the presence of vanadate upon

high external $CaCl_2$ (Fig. 27b), which might explained the observation that increased $[Ca^{2+}]_{cyt}$ promoted H^+-ATPases activation in stomatal opening under blue light [475]. While the knowledge on stomatal closure mechanisms mostly results from researches on *Arabidopsis*, Ca^{2+}-dependent anion channels activation was reported in tobacco [188], and this is known to represent the initial step in stomatal closure [187,476]. But pH-dependent regulation of anion channels like the recently described acid-activation of SLAH3 or pH effects on R- and S-type anion channels were also reported [477]. While I can not exclude different stomata regulation mechanisms in different species, Ca^{2+} dependent and independent mechanisms for stomatal closure were also reported in *N. tabacum* [188]. Based on the high/low KCl washings induced stomatal movements, $[Ca^{2+}]_{cyt}$ transients were observed in stomatal opening (Fig. 29a-c), which fits some previous observations [112,277]. In case $[Ca^{2+}]_{cyt}$ was the strongest signal of all, stomatal closure would have occurred even during the alternating high/low KCl washings, because $[Ca^{2+}]_{cyt}$ increases from this treatment were massive (Fig. 28, 29a-c). However, arguments for the prominent role of $[Ca^{2+}]_{cyt}$ to reduce stomatal aperture in my study could not be well formulated. Cytosolic acidification could regulate stomatal opening while cytosolic alkalization induced stomatal closure very effectively (Fig. 19b). In line with my findings of butyrate blocking ABA and flg22 induced $[Ca^{2+}]_{cyt}$ oscillations and stomatal closure (Fig. 18), external Ca^{2+} induced $[Ca^{2+}]_{cyt}$ oscillations and stomatal closure could be inhibited by butyrate [173]. However, when I applied 3 mM BTA on guard cells showing spontaneous $[Ca^{2+}]_{cyt}$ and $[H^+]_{cyt}$ oscillations (Fig. 27e), pronounced stomatal opening was observed while $[Ca^{2+}]_{cyt}$ oscillations were not blocked (Fig. 27e). These results also showed cytosolic acidification could induce stomatal opening even in the presence of pronounced $[Ca^{2+}]_{cyt}$ oscillations, pointing out that pH changes are able to override the effect of strong $[Ca^{2+}]_{cyt}$ increases on stomatal movement.

Hence, the interconnection between imposed $[Ca^{2+}]_{cyt}$ and $[H^+]_{cyt}$ oscillations in guard cells was distinct upon different stimuli, but generally in a negative correlation (Fig. 14, 19, 27, 32). In high/low KCl experiments, a positive correlation between $[Ca^{2+}]_{cyt}$ and $[H^+]_{cyt}$ homeostasis was based on the effects of K^+ influx in the cell which influenced the net H^+ fluxes (Fig. 28b, 29). In detail, $[Ca^{2+}]_{cyt}$ transients resulted from osmolality while $[H^+]_{cyt}$ homeostasis was regulated by ions and plasma membrane H^+-ATPases (Fig. 28, 29, 30). Therefore, cytosolic pH changes and Ca^{2+} increases depended on the approach used to induce $[Ca^{2+}]_{cyt}$ increases (Fig. 14b, 19b, 27b, 29). However, stomatal closure in my study did not rely on increased $[Ca^{2+}]_{cyt}$, despite of the Ca^{2+}-

dependent signaling in guard cells in tobacco [188,339]. My results fit previous studies of a Ca^{2+}-independent pathway in stomatal closure [173,186-188,414,469] and a recent report demonstrating $[Ca^{2+}]_{cyt}$ elevations to promote stomatal closure but not to be essential [192]. My results provide evidence of H^+ to play a prominent role in stomatal movement (Fig. 14-16, 18, 19) and more importantly the live-cell imaging tool provides the real-time responses of $[Ca^{2+}]_{cyt}$ and $[H^+]_{cyt}$, proving these second messengers to correlate with each other in stomatal movement upon different stimuli.

5.7 Interactions between K^+ and H^+ homeostasis in guard cells

Potassium and chloride are the main ions to regulate guard cell turgor pressure and to modulate stomatal movement (Fig. 3). To monitor the interconnected network of H^+, Ca^{2+} and K^+, I challenged guard cells with alternating exchanges between 50.1 mM KCl and 0.1 mM KCl (Fig. 28, 29a). Stomatal closure and opening was induced by high KCl and low KCl solutions, respectively (Fig. 28, 29a), which was different from previous reports arguing that K^+ enters guard cells to increase turgor pressure for stomatal opening [239,291,478]. With the protocol mentioned above, based on the protocol by others [171], stomatal closure was observed at high KCl conditions, which was accompanied by a reduction in $[H^+]_{cyt}$ (Fig. 28b, 29a). Washing out the high KCl solution resulted in stomatal opening, accompanied by a $[H^+]_{cyt}$ increase and a strong $[Ca^{2+}]_{cyt}$ increase (Fig. 28b, 29a). Contrary to the generally prevailing opinion that long lasting or repetitive $[Ca^{2+}]_{cyt}$ spikes lead to stomatal closure, an increased $[Ca^{2+}]_{cyt}$ signal was detected during stoma opening (Fig. 27e, 28b, 29a) and repetitive $[Ca^{2+}]_{cyt}$ increases did not result in significant stomatal closure (Fig. 19b, 27b). $[Ca^{2+}]_{cyt}$ transients were originally proposed to result from hyperpolarization triggered Ca^{2+} channels by altering high and low KCl solution [171]. However, $[Ca^{2+}]_{cyt}$ transients triggered by this way in my experiments were attributed to differences in osmolality since the application of mannitol generated basically the same $[Ca^{2+}]_{cyt}$ transients, but had no impact on $[H^+]_{cyt}$ homeostasis (Fig. 29a-b, 29e). Therefore, $[Ca^{2+}]_{cyt}$ transients in stomatal opening (Fig. 29, 30) were a result of turgor pressure changes caused by osmotic effects by altering solutions in guard cells, likely addressing OSCA-type Ca^{2+} channels [4]. Because CAXs were proposed to mediate $[Ca^{2+}]_{cyt}$ concentration reduction to micromolar range after $[Ca^{2+}]_{cyt}$ increases which show a pronounced overshoot while ACAs were more likely to sustain the resting $[Ca^{2+}]_{cyt}$ to be low [479]. Thereby, the overshoot of $[Ca^{2+}]_{cyt}$ when changing the medium from low KCl to high KCl observed

(Fig. 29a), might be explained by the action of CAXs transporters and their high-affinity and low-capacity Ca^{2+} shuttling whereas ACAs have low-affinity and high capacity for cation efflux [479]. Cytosolic alkalization and acidification were triggered by high and low KCl, respectively, and this effect was more pronounced in the presence of BTA (Fig. 29a, d), but to a minor extent in Cl^- based medium (Fig. 30b, c). My experiments thus did provide evidence for K^+ channels to control K^+ homeostasis and subsequently to regulate $[H^+]_{cyt}$ homeostasis in *N. tabacum* guard cells (Fig. 29-32). However, a large part of the K^+-dependent change in $[H^+]_{cyt}$ homeostasis does not depend on shaker K^+ channels. When blocking plasma membrane shaker K^+-channels with Cs^+, a strong alteration of $[H^+]_{cyt}$ (Fig. 29c, d) was still observed, suggesting a K^+-dependent impact on $[H^+]_{cyt}$ homeostasis likely by K^+/H^+ antiporters at the plasma membrane or tonoplast. It is worth noting other K^+-transporting mechanisms could still function under Cs^+ conditions such as HAK5 even transporting Cs^+ [480]. Many putative cation/H^+ transporters in plants participate in $[H^+]_{cyt}$ homeostasis such as Ca^{2+}/H^+ transporters (CAXs) and K^+/H^+ transporters (NHXs) [40,42,95,291] (Fig. 1, 32). Moreover, the activity of K^+/H^+ antiporters might be stimulated by the acid intracellular environment in the presence of BTA due to higher $[H^+]_{cyt}$ (Fig. 28b, 29a). The contribution of H^+-pumps to $[H^+]_{cyt}$ homeostasis by P-type H^+-ATPases was tested by the application of the P-type ATPase inhibitor Na_3VO_4. Cytosolic acidification and alkalization induced by low and high KCl were partially reduced by Na_3VO_4, indicating that plasma membrane H^+-ATPases contributed to $[H^+]_{cyt}$ homeostasis, despite the prominent role of K^+ in $[H^+]_{cyt}$ changes (Fig. 30a, c). Stomatal movement was not influenced by Na_3VO_4, but $[Ca^{2+}]_{cyt}$ peaks induced by osmotic effects were interrupted (Fig. 30a, b), which might be due to unexpected effects of vanadate on Ca^{2+}-ATPases [481,482]. How $[H^+]_{cyt}$ homeostasis is related to K^+-homeostasis and K^+ channels can not be conclusively stated from my studies and was not studied in detail yet. However, K^+ transport at the vacuole seems crucial for stomatal movement, K^+ channels and K^+/H^+ transporters such as NHXs at the tonoplast function in guard cells [95,96,291]. H^+ gradients between the cytosol and the vacuole enable K^+ import into the vacuole via NHXs [95,290,293]. Vacuolar acidification and alkalization by using BCECF dye were visualized by low and high KCl, respectively (Fig. 31). It suggested not only vacuolar H^+ homeostasis is likely to be regulated by K^+/H^+ transporters at the vacuolar membrane (Fig. 31b), but is also consistent with previous results showing high external K^+ led to vacuolar alkalization via NHX1 and NHX2 to regulate K^+ and H^+ homeostasis [290,293]. But, K^+/H^+ transporters at the tonoplast could be excluded to contribute to high/low KCl induced

cytosolic pH homeostasis because vacuolar H^+ responses were in accordance with $[H^+]_{cyt}$ induced by the same buffer exchanges (Fig. 29a, 29d, 31, 32).

I can thus conclude that K^+ transport in *N. tabacum* guard cells participates in cytosolic and vacuolar pH homeostasis, a similar scenario as in *Arabidopsis* guard cells [293,483]. I found vacuolar H^+ to be regulated by external KCl (Fig. 31), which is a nice starting point to study further the K^+-dependent cellular pH homeostasis via several putative K^+/H^+ co-transporters like CAXs and NHXs or CHXs at the tonoplast using CapHensor expressing lines. Even though here my direct experimental evidence suggested K^+ homeostasis and plasma membrane H^+-ATPases to function in $[H^+]_{cyt}$ homeostasis by different concentrations of external KCl application (Fig. 28-31), it is also possible that a combination of K^+/H^+ antiporters and K^+/H^+ symporters as well as K^+ channels contributes in a coordinated way [98]. This could be identified by combining experimental and theoretical approaches [98] based on CapHensor imaging.

In addition to K^+ regulations on $[H^+]_{cyt}$ homeostasis, my data also provided good evidence for the existence of H^+/Cl^- symporters at the plasma membrane [9,82,484] since the application of high Cl^- concenrations evoked a cytosolic acidification (Fig. 30b). However, in contrast to the effect on $[H^+]_{cyt}$ homeostasis by K^+, the transport resulting from Cl^- application was much less pronounced, pointing out the important role of K^+-transport to set cellular pH dynamics.

5.8 Cytosolic alkalization is a general feature of salt stress in leaves and salt detoxification in leaves is independent of Ca^{2+}-signaling

The mechanisms in leaves to cope with salt stress have not yet been resolved and the signaling mechanisms proposed to play a role in salt stress mainly originate from researches on roots and young seedlings. Salt detoxification mechanisms were investigated extensively in roots and salt can be transported from the root to the shoot which resulted in the accumulation of salt in leaves via sequestering it into the vacuole [9,10,307,485]. Salt treatment must initiate distinct leaf reactions and this underlines the importance for unravelling salt detoxification mechanisms in leaves.

My results demonstrated novel aspects of the Ca^{2+} and H^+ dependent mechanisms for leaves to cope with salt stress. However, I have to consider separating the effects of ion transport and osmotic effects involved in salinity stress. To investigate ion signaling with Ca^{2+} and H^+ under salinity in leaves, I firstly balanced the control solution with the same osmolality as the salt concentration (Fig. 33-36). In the osmolality-balanced system, CapHensor imaging was combined

with electrophysiology with minimal osmotic effects. Cytosolic alkalization and pronounced depolarization were observed in response to both 50 mM NaCl and KCl (Fig. 33b, 33d, 34a), indicating cation influx either by cation channels or transporters [486] (Fig. 4) to cause the depolarization, while the depolarization-activated plasma membrane H^+-ATPases [236] could play a role in the cytosolic alkalization. This is consistent with H^+-efflux under NaCl treatment [487]. In roots, Na^+ can enter into the cell and trigger a membrane depolarization while K^+ efflux is induced via the depolarization-activated GORK channel or other K^+ transporters in *Arabidopsis* [44,488-490]. K^+/H^+ transporters were proven to function in guard cells to regulate K^+ and H^+ homeostasis [96,239,291] (Fig. 32), which is in line with the more pronounced pH effects in protoplasts upon 50 mM KCl treatment (Fig. 33, 34). Differently, slightly cytosolic acidification and minor depolarization was induced by 50 mM Tris-Cl in protoplasts (Fig. 33b, 33d, 34a), which might be explained by a ≥ 1 H^+/Cl^- symporter mechanism [9,82,484]. ABA synthesis was observed under salt stress [230,303,491,492] to initiate transcriptional reprogramming [1,493]. If this transcriptional reprogramming is associated with Ca^{2+} or pH signaling in the nucleus in leaf cells upon salt stress was unknown. I found $[Ca^{2+}]_{nuc}$ and $[H^+]_{nuc}$ changes upon salt stress are similar to $[Ca^{2+}]_{cyt}$ and $[H^+]_{cyt}$ (Fig. 33c, 34c). However, in my previous results, ABA itself didn't induce any effects on Ca^{2+}, H^+ and membrane potential in mesophyll cells (Fig. 20c, g). During salt stress in leaves, membrane depolarization and intracellular alkalization tend to regulate the detoxification process in leaves and the transcriptional regulation known to occur when ABA rises [1,493] are mediated in a Ca^{2+}-independent signaling mechanism (Fig. 33-36).

Under salt stress, ABA levels could be re-distributed to trigger stomatal closure by pH dependent mechanisms since salt could be transported from the root to the shoot [230,231,491]. Similar to the salt-induced H^+ dynamics in mesophyll cells and protoplasts thereof, cytosolic alkalization was observed in guard cells upon salt treatment while only slight $[H^+]_{cyt}$ reduction was observed upon mannitol despite the strong osmotic effects (Fig. 38a-b, 39a-b). In experiments where the osmolality was not balanced between control and salt solution, leaf cells did shrink visibly and guard cells closed unnaturally fast upon 200 mM NaCl (Fig. 37a-c, 38a, 39a). Application of a mannitol solution with the same osmolality indicated the stomatal closure upon high salt resulted from osmotic effects rather than a toxic salt effect (Fig. 38a-b, 39a-b). However, $[Ca^{2+}]_{cyt}$ was not changed under 200 mM NaCl induced stomatal closure (Fig. 38a, 39a), indicating the existence of Ca^{2+}-dependent and -independent mechanisms in tobacco guard cells to close stomata [188,339].

Pronounced $[Ca^{2+}]_{cyt}$ transient induced by 400 mM mannitol (Fig. 38b, 39b) might be attributed to hyperosmotic effects on Ca^{2+}-permeable channels such as OSCA1 [4]. Interestingly, stomatal closure upon 400 mM mannitol was even more pronounced compared with 200 mM NaCl, indicative for an ion uptake event during 200 mM NaCl administration to compensate for the strong osmotic effects. This fast Na^+ and Cl^- uptake mechanism was observed in experiments where the osmotic effects were compensated and equimolar concentrated solutions were used (Fig. 38c). Then, stomata opened upon 50 mM NaCl application, which was accompanied by a cytosolic alkalization and a $[Ca^{2+}]_{cyt}$ reduction in the first 5 min (Fig. 38c, 39c). It suggests that Na^+ and Cl^- ions are taken up and used as "cheap osmoticum" by leaf cells.

The SOS pathway is well established in roots under salt stress and is thought to depend on $[Ca^{2+}]_{cyt}$ increases [11]. In contrast to salt induced $[Ca^{2+}]_{cyt}$ transients in roots [306-308,392] (Fig. 37d), no or only slight $[Ca^{2+}]_{cyt}$ increases were observed in intact leaves or guard cells in epidermal strips upon 200 mM NaCl application (Fig. 37a-c, 38-39) and even decreased $[Ca^{2+}]_{cyt}$ was observed in mesophyll cells and protoplasts upon 50 mM NaCl application (Fig. 33-34, 36a). The salt tolerance mechanism in leaves seems to be different from the Ca^{2+}-dependent salt detoxification mechanisms in roots as I confirmed a steep $[Ca^{2+}]_{cyt}$ rise right after salt-shock treatment in roots which was sometimes accompanied by a second $[Ca^{2+}]_{cyt}$ peak minutes later (Fig. 37d). In contrast to the root response with a NaCl-treatment induced $[Ca^{2+}]_{cyt}$ rise, pronounced $[Ca^{2+}]_{cyt}$ peaks were only visualized in intact leaves or protoplasts thereof after washing salt out (Fig. 33, 34, 36a, 37a-c), which is consistent with previous reports [494-496]. This observation could be explained by activation of mechanosensitive Ca^{2+}-permeable channels due to osmotic changes [497] and/or Na^+ uptake dependent depolarization and in turn a hyperpolarization when washing the salt out, since Ca^{2+}-permeable channels could be activated by hyperpolarization [49,498]. Osmotic effects by salt application can be ruled out in protoplasts and mesophyll cells since osmolality has been balanced there (Fig. 33b-c, 34, 36a). To monitor membrane potential in leaves upon salt stress in parallel, I did CapHensor imaging and V_m recording in intact mesophyll cells removing the lower epidermis (Fig. 35, 36). Similar to protoplasts responses to 50 mM NaCl (Fig. 33b, 33d), cytosolic alkalization and a depolarization were observed upon 50 mM NaCl application (Fig. 36a, b). This is not likely to result from H^+-translocation via plasma membrane H^+-ATPases pumping H^+ out of the cytosol into the apoplast or Na^+/H^+ antiporters at the plasma membrane because the apoplast became more alkalized in leaves upon salt stress [231,300]. Moreover, in roots, Na^+ could be

transported out of the cytosol from Na^+/H^+ antiporter (SOS1) at the plasma membrane and Na^+/H^+ antiporters (NHX1) at the tonoplast via SOS pathway [499]. Given that I previously observed cytosolic alkalization in guard cells under ABA and flg22 was coordinated with vacuolar acidification (Fig. 14, 15), the cytosolic alkalization in leaves under salt stress might be also regulated by H^+-translocation at the tonoplast. AtNHX1 has been characterized to function in salinity tolerance mechanisms [322,500]. When co-expressing AtNHX1 with CapHensor in *N. benthamiana* leaves, salt induced $[Ca^{2+}]_{cyt}$ and $[H^+]_{cyt}$ decreases did not occur anymore and the depolarization was significantly lower in AtNHX1 overexpressing leaves compared with wild type (Fig. 35, 36). Although AtNHX1 activity was negatively regulated by Ca^{2+} [391], my results indicated the $[Ca^{2+}]_{cyt}$ responses regulated by AtNHX1 during salt stress in leaves and not the other way around (Fig. 36). Moreover, AtNHX1 did compensate the NaCl induced cytosolic alkalization (Fig. 36). Consistently, AtNHX1 overexpression improved salt tolerance in many plants such as *Arabidopsis* or tomato [322,500]. Vacuolar alkalization upon salt in roots has been reported based on its Na^+/H^+ antiporter property to achieve salt detoxification [501]. AtNHX1 overexpression in tobacco improved salt tolerance upon 200 mM NaCl and the AtNHX1 activity was associated with activated V-ATPases activity [319]. These studies might explain my results of missing cytosolic alkalization upon salt when overexpressing AtNHX1 in tobacco leaves (Fig. 36c). When AtNHX1 (Na^+/H^+ antiporter) at the tonoplast sequesters Na^+ into the vacuole and exports H^+ into the cytosol to maintain cytosolic pH to accomplish salt detoxification, it acts against the observed cytosolic alkalization which can be detected without NHX1 overexpression.

Taken together, in guard cells and mesophyll cells, Ca^{2+} rather decreased during salt stress which is the opposite response in roots (Fig. 37d), while cytosolic H^+ was reduced in both tissues (Fig. 33b-c, 34, 36a, 37a-c, 38, 39). Although substantial progress has been made in the salt stress field, many questions remain to be solved including the mechanism for salt detoxification in leaves and the role of Ca^{2+} and H^+ to control the transport mechanisms. Putative osmotic sensors and NHXs and their underlying mechanisms in leaves still remain to be characterized in detail. My results demonstrated Ca^{2+}-independent mechanism in leaves exist during salt stress which is distinct from root reactions relying on Ca^{2+} increases. AtNHX1 function in salt tolerance in leaves did act against the deflections in $[Ca^{2+}]_{cyt}$, $[H^+]_{cyt}$ and depolarization that salt may cause to leaf cells. Therefore AtNHX1 helps the detoxification of salt by sequestering salt into vacuoles (Fig. 40) and suggests a role in helping to maintain $[H^+]_{cyt}$ homeostasis in leaves upon salt stress.

6 Tables list

7 Figures list

8 References

1 Gong, Z. *et al.* **Plant abiotic stress response and nutrient use efficiency**. *Sci China Life Sci* 63, 635-674, doi:10.1007/s11427-020-1683-x (2020).

2 Zhu, J. K. **Salt and drought stress signal transduction in plants**. *Annu Rev Plant Biol* 53, 247-273, doi:10.1146/annurev.arplant.53.091401.143329 (2002).

3 Monshausen, G. B. & Gilroy, S. **Feeling green: mechanosensing in plants**. *Trends Cell Biol* 19, 228-235, doi:10.1016/j.tcb.2009.02.005 (2009).

4 Yuan, F. *et al.* **OSCA1 mediates osmotic-stress-evoked Ca^{2+} increases vital for osmosensing in *Arabidopsis***. *Nature* 514, 367-371, doi:10.1038/nature13593 (2014).

5 Kim, T. H. *et al.* **Guard cell signal transduction network: advances in understanding abscisic acid, CO2, and Ca^{2+} signaling**. *Annu Rev Plant Biol* 61, 561-591, doi:10.1146/annurev-arplant-042809-112226 (2010).

6 Kollist, H. *et al.* **Closing gaps: linking elements that control stomatal movement**. *New Phytol* 203, 44-62, doi:10.1111/nph.12832 (2014).

7 Kudla, J. *et al.* **Advances and current challenges in calcium signaling**. *New Phytol* 218, 414-431, doi:10.1111/nph.14966 (2018).

8 Zorb, C. *et al.* **Salinity and crop yield**. *Plant Biol (Stuttg)* 21 Suppl 1, 31-38, doi:10.1111/plb.12884 (2019).

9 Munns, R. & Tester, M. **Mechanisms of salinity tolerance**. *Annu Rev Plant Biol* 59, 651-681, doi:10.1146/annurev.arplant.59.032607.092911 (2008).

10 Morton, M. J. L. *et al.* **Salt stress under the scalpel - dissecting the genetics of salt tolerance**. *Plant J* 97, 148-163, doi:10.1111/tpj.14189 (2019).

11 Zhu, J. K. **Abiotic stress signaling and responses in plants**. *Cell* 167, 313-324, doi:10.1016/j.cell.2016.08.029 (2016).

12 Munns, R. **Comparative physiology of salt and water stress**. *Plant Cell Environ* 25, 239-250, doi:10.1046/j.0016-8025.2001.00808.x (2002).

13 Pommerrenig, B. *et al.* **Differential regulation of sorbitol and sucrose loading into the phloem of Plantago major in response to salt stress**. *Plant Physiol* 144, 1029-1038, doi:10.1104/pp.106.089151 (2007).

14 Ji, H. *et al.* **The Salt Overly Sensitive (SOS) pathway: established and emerging roles**. *Mol Plant* 6, 275-286, doi:10.1093/mp/sst017 (2013).

15 Jones, J. D. & Dangl, J. L. **The plant immune system**. *Nature* 444, 323-329, doi:10.1038/nature05286 (2006).

16 Boller, T. & Felix, G. **A renaissance of elicitors: perception of microbe-associated molecular patterns and danger signals by pattern-recognition receptors**. *Annu Rev Plant Biol* 60, 379-406, doi:10.1146/annurev.arplant.57.032905.105346 (2009).

17 Fujita, Y. *et al.* **Transcription Factors Involved in the Crosstalk between Abiotic and Biotic Stress-Signaling Networks**. *transcription factors* (2009).

18 Zhang, J. *et al.* **Plant Immune Mechanisms: From Reductionistic to Holistic Points of View**. *Mol Plant* 13, 1358-1378, doi:10.1016/j.molp.2020.09.007 (2020).

19 Konrad, K. R. *et al.* **Spatio-temporal Aspects of Ca^{2+} Signalling: Lessons from Guard Cells and Pollen Tubes**. *J Exp Bot*, doi:10.1093/jxb/ery154 (2018).

20 Stael, S. *et al.* **Plant organellar calcium signalling: an emerging field**. *J Exp Bot* 63, 1525-1542, doi:10.1093/jxb/err394 (2012).

21 Himschoot, E. *et al.* **The ins and outs of Ca^{2+} in plant endomembrane trafficking**. *Curr Opin Plant Biol* 40, 131-137, doi:10.1016/j.pbi.2017.09.003 (2017).

22 Sheen, J. **Ca^{2+}-dependent protein kinases and stress signal transduction in plants**. *Science* 274, 1900-1902, doi:10.1126/science.274.5294.1900 (1996).

23 Luan, S. *et al.* **Calmodulins and calcineurin B-like proteins: calcium sensors for specific signal response coupling in plants**. *Plant Cell* 14 Suppl, S389-400, doi:10.1105/tpc.001115 (2002).

24 Hrabak, E. M. *et al.* **The *Arabidopsis* CDPK-SnRK superfamily of protein kinases**. *Plant Physiol* 132, 666-680, doi:10.1104/pp.102.011999 (2003).

25 McCormack, E. *et al.* **Handling calcium signaling: *Arabidopsis* CaMs and CMLs**. *Trends Plant Sci* 10, 383-389, doi:10.1016/j.tplants.2005.07.001 (2005).

26 Luan, S. **The CBL-CIPK network in plant calcium signaling**. *Trends Plant Sci* 14, 37-42, doi:10.1016/j.tplants.2008.10.005 (2009).

27 DeFalco, T. A. *et al.* **Breaking the code: Ca^{2+} sensors in plant signalling**. *Biochem J* 425, 27-40, doi:10.1042/BJ20091147 (2009).

28 Bender, K. W. *et al.* **Revisiting paradigms of Ca^{2+} signaling protein kinase regulation in plants**. *Biochem J* 475, 207-223, doi:10.1042/BCJ20170022 (2018).

29 McAinsh, M. R. & Hetherington, A. M. **Encoding specificity in Ca^{2+} signalling systems**. *Trends in Plant Science* 3, 32-36, doi:10.1016/s1360-1385(97)01150-3 (1998).

30 Ng, C. K. & McAinsh, M. R. **Encoding specificity in plant calcium signalling: hot-spotting the ups and downs and waves**. *Ann Bot* 92, 477-485, doi:10.1093/aob/mcg173 (2003).

31 Resentini, F. *et al.* **The signatures of organellar calcium**. *Plant Physiol*, doi:10.1093/plphys/kiab189 (2021).

32 Webb, A. A. R. *et al.* **Calcium Ions as Intracellular Second Messengers in Higher Plants** Vol. Volume 22 Advances in Botanical Research (ed J. A. Callow) 45-96 (Academic Press, 1996).

33 Staxen, I. *et al.* **Abscisic acid induces oscillations in guard-cell cytosolic free calcium that involve phosphoinositide-specific phospholipase C**. *Proc. Natl. Acad. Sci. USA* 96, 1779–1784 (1999).

34 Hetherington, A. M. & Brownlee, C. **The Generation of Ca^{2+} signals in plants**. *Annu Rev Plant Physiol Plant Mol Biol* 55, 401-427 (2004).

35 Kudla, J. *et al.* **Calcium signals: the lead currency of plant information processing**. *Plant Cell* 22, 541-563, doi:10.1105/tpc.109.072686 (2010).

36 Dodd, A. N. *et al.* **The language of calcium signaling**. *Annu Rev Plant Biol* 61, 593-620, doi:10.1146/annurev-arplant-070109-104628 (2010).

37 Demidchik, V. *et al.* **Calcium transport across plant membranes: mechanisms and functions**. *New Phytol* 220, 49-69, doi:10.1111/nph.15266 (2018).

38 Swarbreck, S. M. *et al.* **Plant calcium-permeable channels**. *Plant Physiol* 163, 514-522, doi:10.1104/pp.113.220855 (2013).

39 Pottosin, I. & Schonknecht, G. **Vacuolar calcium channels**. *J Exp Bot* 58, 1559-1569, doi:10.1093/jxb/erm035 (2007).

40 Manohar, M. *et al.* **Plant cation/H^+ exchangers (CAXs): biological functions and genetic manipulations**. *Plant Biol (Stuttg)* 13, 561-569, doi:10.1111/j.1438-8677.2011.00466.x (2011).

41 Demidchik, V. *et al.* **Nonselective cation channels in plants**. *Annu Rev Plant Biol* 53, 67-107, doi:10.1146/annurev.arplant.53.091901.161540 (2002).

42 Pittman, J. K. & Hirschi, K. D. **CAX-ing a wide net: Cation/H^+ transporters in metal remediation and abiotic stress signalling**. *Plant Biol (Stuttg)* 18, 741-749, doi:10.1111/plb.12460 (2016).

43 White, P. J. & Broadley, M. R. **Calcium in plants**. *Ann Bot* 92, 487-511, doi:10.1093/aob/mcg164 (2003).

44 Demidchik, V. & Maathuis, F. J. M. **Physiological roles of nonselective cation channels in plants: from salt stress to signalling and development**. *New Phytol* 175, 387-404, doi:10.1111/j.1469-8137.2007.02128.x (2007).

45 Hedrich, R. **Ion channels in plants**. *Physiol Rev* 92, 1777-1811, doi:10.1152/physrev.00038.2011 (2012).

46 Miedema, H. *et al.* **Two voltage-dependent calcium channels co-exist in the apical plasma membrane of *Arabidopsis thaliana* root hairs**. *New Phytol* 179, 378-385, doi:10.1111/j.1469-8137.2008.02465.x (2008).

47 Grabov, A. & Blatt, M. R. **Membrane voltage initiates Ca^{2+} waves and potentiates Ca^{2+} increases with abscisic acid in stomatal guard cells**. *Proc Natl Acad Sci U S A* 95, 4778-4783, doi:10.1073/pnas.95.8.4778 (1998).
48 Pei, Z. M. *et al.* **Calcium channels activated by hydrogen peroxide mediate abscisic acid signalling in guard cells**. *Nature* 406, 731-734, doi:10.1038/35021067 (2000).
49 Hamilton, D. W. *et al.* **Ca^{2+} channels at the plasma membrane of stomatal guard cells are activated by hyperpolarization and abscisic acid**. *Proc Natl Acad Sci U S A* 97, 4967-4972, doi:10.1073/pnas.080068897 (2000).
50 Frietsch, S. *et al.* **A cyclic nucleotide-gated channel is essential for polarized tip growth of pollen**. *Proc Natl Acad Sci U S A* 104, 14531-14536, doi:10.1073/pnas.0701781104 (2007).
51 Balague, C. *et al.* **HLM1, an essential signaling component in the hypersensitive response, is a member of the cyclic nucleotide-gated channel ion channel family**. *Plant Cell* 15, 365-379, doi:10.1105/tpc.006999 (2003).
52 Yoshioka, K. *et al.* **The chimeric *Arabidopsis* CYCLIC NUCLEOTIDE-GATED ION CHANNEL11/12 activates multiple pathogen resistance responses**. *Plant Cell* 18, 747-763, doi:10.1105/tpc.105.038786 (2006).
53 Kang, J. *et al.* **The putative glutamate receptor 1.1 (AtGLR1.1) in *Arabidopsis thaliana* regulates abscisic acid biosynthesis and signaling to control development and water loss**. *Plant Cell Physiol* 45, 1380-1389, doi:10.1093/pcp/pch159 (2004).
54 Cosgrove, D. J. & Hedrich, R. **Stretch-activated chloride, potassium, and calcium channels coexisting in plasma membranes of guard cells of Vicia faba L**. *Planta* 186, 143-153, doi:10.1007/BF00201510 (1991).
55 Dutta, R. & Robinson, K. R. **Identification and characterization of stretch-activated ion channels in pollen protoplasts**. *Plant Physiol* 135, 1398-1406, doi:10.1104/pp.104.041483 (2004).
56 Hamilton, E. S. *et al.* **Mechanosensitive channel MSL8 regulates osmotic forces during pollen hydration and germination**. *Science* 350, 438-441, doi:10.1126/science.aac6014 (2015).
57 Garcia Bossi, J. *et al.* **The role of P-type IIA and P-type IIB Ca^{2+}-ATPases in plant development and growth**. *J Exp Bot* 71, 1239-1248, doi:10.1093/jxb/erz521 (2020).
58 Cheng, N. H. *et al.* **The *Arabidopsis* cax1 mutant exhibits impaired ion homeostasis, development, and hormonal responses and reveals interplay among vacuolar transporters**. *Plant Cell* 15, 347-364, doi:10.1105/tpc.007385 (2003).
59 Shigaki, T. *et al.* **Identification of three distinct phylogenetic groups of CAX cation/proton antiporters**. *J Mol Evol* 63, 815-825, doi:10.1007/s00239-006-0048-4 (2006).
60 Zhao, J. *et al.* **The *Arabidopsis* cax3 mutants display altered salt tolerance, pH sensitivity and reduced plasma membrane H^+-ATPase activity**. *Planta* 227, 659-669, doi:10.1007/s00425-007-0648-2 (2008).
61 Fuglsang, A. T. a. P., M. **Proton and calcium pumping P-type ATPases and their regulation of plant responses to the environment**. *Plant Physiology*, doi:10.1093/plphys/kiab330/6328787 (2021).
62 Sze, H. *et al.* **A simple nomenclature for a complex proton pump:VHAgenes encode the vacuolar H^+-ATPase**. *Trends Plant Sci.* 7, 157–161 (2002).
63 Harper, J. F. *et al.* **A novel calmodulin-regulated Ca^{2+}-ATPase (ACA2) from *Arabidopsis* with an N-terminal autoinhibitory domain**. *J Biol Chem* 273, 1099-1106, doi:10.1074/jbc.273.2.1099 (1998).
64 Boursiac, Y. *et al.* **Disruption of the vacuolar calcium-ATPases in *Arabidopsis* results in the activation of a salicylic acid-dependent programmed cell death pathway**. *Plant Physiol* 154, 1158-1171, doi:10.1104/pp.110.159038 (2010).
65 Schiøtt, M. *et al.* **A plant plasma membrane Ca^{2+} pump is required for normal pollen tube growth and fertilization**. *Proc Natl Acad Sci* 101, 9502–9507 (2004).

66 Frei dit Frey, N. *et al.* **Plasma membrane calcium ATPases are important components of receptor-mediated signaling in plant immune responses and development**. *Plant Physiol* 159, 798-809, doi:10.1104/pp.111.192575 (2012).
67 Kadota, Y. *et al.* **Quantitative phosphoproteomic analysis reveals common regulatory mechanisms between effector- and PAMP-triggered immunity in plants**. *New Phytol* 221, 2160-2175, doi:10.1111/nph.15523 (2019).
68 Felle, H. H. **pH: Signal and Messenger in Plant Cells**. *Plant Biology* 3, 577-591, doi:10.1055/s-2001-19372 (2001).
69 Martiniere, A. *et al.* **In vivo intracellular pH measurements in tobacco and *Arabidopsis* reveal an unexpected pH gradient in the endomembrane system**. *Plant Cell* 25, 4028-4043, doi:10.1105/tpc.113.116897 (2013).
70 Martiniere, A. *et al.* **Uncovering pH at both sides of the root plasma membrane interface using noninvasive imaging**. *Proc Natl Acad Sci U S A* 115, 6488-6493, doi:10.1073/pnas.1721769115 (2018).
71 Tsai, H. H. & Schmidt, W. **The enigma of environmental pH sensing in plants**. *Nat Plants* 7, 106-115, doi:10.1038/s41477-020-00831-8 (2021).
72 Bibikova, T. N. *et al.* **Ca^{2+} AND PH AS INTEGRATING SIGNALS IN TRANSPORT CONTROL**. *Annual Plant Reviews* 15, 282-312, doi:10.1002/9781119312994.apr0149 (2004).
73 Sakano, K. **Metabolic regulation of pH in plant cells: role of cytoplasmic pH in defense reaction and secondary metabolism**. *Int Rev Cytol* 206, 1-44, doi:10.1016/s0074-7696(01)06018-1 (2001).
74 Shabala, S. N. *et al.* **Oscillations in H^+ and Ca^{2+} lon Fluxes around the Elongation Region of Corn Roots and Effects of External pH**. *Plant Physiol.* 113, 111-118 (1997).
75 Hoffmann, R. D. *et al.* **Plasma membrane H^+-ATPases sustain pollen tube growth and fertilization**. *Nat Commun* 11, 2395, doi:10.1038/s41467-020-16253-1 (2020).
76 Feijo, J. A. *et al.* **Growing pollen tubes possess a constitutive alkaline band in the clear zone and a growth-dependent acidic tip**. *J Cell Biol* 144, 483-496, doi:10.1083/jcb.144.3.483 (1999).
77 Mangano, S. *et al.* **How Does pH Fit in with Oscillating Polar Growth?** *Trends Plant Sci* 23, 479-489, doi:10.1016/j.tplants.2018.02.008 (2018).
78 Cosse, M. & Seidel, T. **Plant Proton Pumps and Cytosolic pH-Homeostasis**. *Front Plant Sci* 12, 672873, doi:10.3389/fpls.2021.672873 (2021).
79 Fuglsang, A. T. *et al.* **Plant Proton Pumps: Regulatory Circuits Involving H^+-ATPase and H^+-PPase** Signaling and Communication in Plants (eds Markus Geisler & Kees Venema) Ch. Chapter 2, 39-64 (Springer Berlin Heidelberg, 2011).
80 Luo, G. Z. *et al.* **A putative plasma membrane cation/proton antiporter from soybean confers salt tolerance in *Arabidopsis***. *Plant Mol Biol* 59, 809-820, doi:10.1007/s11103-005-1386-0 (2005).
81 Reguera, M. *et al.* **Intracellular NHX-type cation/H^+ antiporters in plants**. *Mol Plant* 7, 261-263, doi:10.1093/mp/sst091 (2014).
82 Felle, H. H. **The H^+/Cl^- symporter in root-Hair cells of Sinapis alba (an electrophysiological study using ion-selective microelectrodes)**. *Plant Physiol* 106, 1131-1136, doi:10.1104/pp.106.3.1131 (1994).
83 Gaxiola, R. A. *et al.* **Plant proton pumps**. *FEBS Lett* 581, 2204-2214, doi:10.1016/j.febslet.2007.03.050 (2007).
84 Falhof, J. *et al.* **Plasma membrane H^+-ATPase regulation in the center of plant physiology**. *Mol Plant* 9, 323-337, doi:10.1016/j.molp.2015.11.002 (2016).
85 Duby, G. *et al.* **AtKC1, a conditionally targeted Shaker-type subunit, regulates the activity of plant K^+ channels**. *Plant J* 53, 115-123, doi:10.1111/j.1365-313X.2007.03324.x (2008).
86 Morsomme, P. & Boutry, M. **The plant plasma membrane H^+-ATPase: structure, function and regulation**. *Biochim Biophys Acta* 1465, 1-16, doi:10.1016/s0005-2736(00)00128-0 (2000).
87 Morth, J. P. *et al.* **A structural overview of the plasma membrane Na^+,K^+-ATPase and H^+-ATPase ion pumps**. *Nat Rev Mol Cell Biol* 12, 60-70, doi:10.1038/nrm3031 (2011).

88 Palmgren, M. G. **PLANT PLASMA MEMBRANE H^+-ATPases: Powerhouses for Nutrient Uptake**. *Annu Rev Plant Physiol Plant Mol Biol* 52, 817-845, doi:10.1146/annurev.arplant.52.1.817 (2001).
89 Sondergaard, T. E. *et al.* **Energization of transport processes in plants. roles of the plasma membrane H^+-ATPase**. *Plant Physiol* 136, 2475-2482, doi:10.1104/pp.104.048231 (2004).
90 Bock, K. W. *et al.* **Integrating membrane transport with male gametophyte development and function through transcriptomics**. *Plant Physiol* 140, 1151-1168, doi:10.1104/pp.105.074708 (2006).
91 Haruta, M. *et al.* **Molecular characterization of mutant *Arabidopsis* plants with reduced plasma membrane proton pump activity**. *J Biol Chem* 285, 17918-17929, doi:10.1074/jbc.M110.101733 (2010).
92 Haruta, M. *et al.* **Regulation of the plasma membrane proton pump (H^+-ATPase) by phosphorylation**. *Curr Opin Plant Biol* 28, 68-75, doi:10.1016/j.pbi.2015.09.005 (2015).
93 Rodrigues, R. B. *et al.* **Expression of a translationally fused TAP-tagged plasma membrane proton pump in *Arabidopsis thaliana***. *Biochemistry* 53, 566-578, doi:10.1021/bi401096m (2014).
94 Geilfus, C. M. **The pH of the Apoplast: Dynamic Factor with Functional Impact Under Stress**. *Mol Plant* 10, 1371-1386, doi:10.1016/j.molp.2017.09.018 (2017).
95 Bassil, E. & Blumwald, E. **The ins and outs of intracellular ion homeostasis: NHX-type cation/H^+ transporters**. *Curr Opin Plant Biol* 22, 1-6, doi:10.1016/j.pbi.2014.08.002 (2014).
96 Sze, H. & Chanroj, S. **Plant endomembrane dynamics: Studies of K^+/H^+ antiporters provide insights on the effects of pH and ion homeostasis**. *Plant Physiol* 177, 875-895, doi:10.1104/pp.18.00142 (2018).
97 Blatt, M. R. **Ion transport at the plant plasma membrane** (2008).
98 Dreyer, I. **Nutrient cycling is an important mechanism for homeostasis in plant cells**. *Plant Physiology*, doi:10.1093/plphys/kiab217 (2021).
99 Swanson, S. J. *et al.* **In vivo imaging of Ca^{2+}, pH, and reactive oxygen species using fluorescent probes in plants**. *Annu Rev Plant Biol* 62, 273-297, doi:10.1146/annurev-arplant-042110-103832 (2011).
100 Germond, A. *et al.* **Design and development of genetically encoded fluorescent sensors to monitor intracellular chemical and physical parameters**. *Biophys Rev* 8, 121-138, doi:10.1007/s12551-016-0195-9 (2016).
101 Zhao, Y. *et al.* **An expanded palette of genetically encoded Ca^{2+} indicators**. *Science* 333, 1888-1891 (2011).
102 Walia, A. *et al.* **Genetically encoded biosensors in plants: pathways to discovery**. *Annu Rev Plant Biol* 69, 497-524, doi:10.1146/annurev-arplant-042817-040104 (2018).
103 Schulte, A. *et al.* **A novel fluorescent pH probe for expression in plants**. *Plant Methods* 2, 7, doi:10.1186/1746-4811-2-7 (2006).
104 Chudakov, D. M. *et al.* **Fluorescent proteins as a toolkit for in vivo imaging**. *Trends Biotechnol* 23, 605-613, doi:10.1016/j.tibtech.2005.10.005 (2005).
105 Souslova, E. A. & Chudakov, D. M. **Genetically encoded intracellular sensors based on fluorescent proteins**. *Biochemistry (Mosc)* 72, 683-697, doi:10.1134/s0006297907070012 (2007).
106 Nakai, J. *et al.* **A high signal-to-noise Ca^{2+} probe composed of a single green fluorescent protein**. *Nat Biotechnol* 19, 137-141, doi:10.1038/84397 (2001).
107 DeFalco, T. A. *et al.* **Using GCaMP3 to study Ca^{2+} signaling in *Nicotiana* species**. *Plant Cell Physiol* 58, 1173-1184, doi:10.1093/pcp/pcx053 (2017).
108 Keinath, N. F. *et al.* **Live cell imaging with R-GECO1 sheds light on flg22- and Chitin-induced transient $[Ca^{2+}]_{cyt}$ patterns in *Arabidopsis***. *Mol Plant* 8, 1188-1200, doi:10.1016/j.molp.2015.05.006 (2015).
109 Carlson, H. J. & Campbell, R. E. **Circular permutated red fluorescent proteins and calcium ion indicators based on mCherry**. *Protein Eng Des Sel* 26, 763-772, doi:10.1093/protein/gzt052 (2013).

110 Carlson, H. J. & Campbell, R. E. **Mutational analysis of a red fluorescent protein-based calcium ion indicator**. *Sensors (Basel)* 13, 11507-11521, doi:10.3390/s130911507 (2013).
111 James-kracke, M. R. **Quick and accurate method to convert BCECF fluorescence to pH: Calibration in three different types of cell preparations**. *JOURNAL OF CELLULAR PHYSIOLOGY* 151, 596-603 (1992).
112 Irving, H. R. *et al.* **Changes in cytosolic pH and calcium of guard cells precede stomatal movements**. *Proc Natl Acad Sci U S A* 89, 1790-1794, doi:10.1073/pnas.89.5.1790 (1992).
113 Miesenböck, G. *et al.* **Visualizing secretion and synaptic transmission with pH-sensitive green fluorescent proteins**. *Nature* 394, 192-195 (1998).
114 Reifenrath, M. & Boles, E. **A superfolder variant of pH-sensitive pHluorin for in vivo pH measurements in the endoplasmic reticulum**. *Sci Rep* 8, 11985, doi:10.1038/s41598-018-30367-z (2018).
115 Behera, S. *et al.* **Cellular Ca^{2+} Signals Generate Defined pH Signatures in Plants**. *Plant Cell* 30, 2704-2719, doi:10.1105/tpc.18.00655 (2018).
116 Waadt, R. *et al.* **Dual-Reporting transcriptionally linked genetically encoded fluorescent indicators resolve the spatiotemporal coordination of cytosolic abscisic acid and second messenger dynamics in *Arabidopsis***. *Plant Cell* 32, 2582-2601, doi:10.1105/tpc.19.00892 (2020).
117 Holdaway-Clarke, T. L. & Hepler, P. K. **Control of pollen tube growth: role of ion gradients and fluxes**. *New Phytol* 159, 539-563, doi:10.1046/j.1469-8137.2003.00847.x (2003).
118 Cheung, A. Y. & Wu, H. M. **Structural and signaling networks for the polar cell growth machinery in pollen tubes**. *Annu Rev Plant Biol* 59, 547-572, doi:10.1146/annurev.arplant.59.032607.092921 (2008).
119 Feijó, J. A. *et al.* **Cellular oscillations and the regulation of growth: the pollen tube paradigm**. *Bioessays* 23, 86-94 (2001).
120 Damineli, D. S. C. *et al.* **One thousand and one oscillators at the pollen tube tip: The quest for a central pacemaker revisited** (eds Gerhard Obermeyer & José Feijó) Ch. Chapter 15, 391-413 (Springer International Publishing, 2017).
121 Hepler, P. K. *et al.* **Polarized cell growth in higher plants**. *Annu Rev Cell Dev Biol* 17, 159-187, doi:10.1146/annurev.cellbio.17.1.159 (2001).
122 Konrad, K. R. *et al.* **Calcium regulation of tip growth: new genes for old mechanisms**. *Curr Opin Plant Biol* 14, 721-730, doi:10.1016/j.pbi.2011.09.005 (2011).
123 Michard, E. *et al.* **Signaling with ions: The keystone for apical cell growth and morphogenesis in pollen tubes**. *Plant Physiol* 173, 91-111, doi:10.1104/pp.16.01561 (2017).
124 Steinhorst, L. & Kudla, J. **Calcium - a central regulator of pollen germination and tube growth**. *Biochim Biophys Acta* 1833, 1573-1581, doi:10.1016/j.bbamcr.2012.10.009 (2013).
125 Gutermuth, T. *et al.* **Pollen tube growth regulation by free anions depends on the interaction between the anion channel SLAH3 and calcium-dependent protein kinases CPK2 and CPK20**. *Plant Cell* 25, 4525-4543, doi:10.1105/tpc.113.118463 (2013).
126 Rathore, K. S. *et al.* **A cytoplasmic gradient of Ca^{2+} is correlated with the growth of lily pollen tubes**. *Developmental Biology* 148, 612-619, doi:10.1016/0012-1606(91)90278-b (1991).
127 Pierson, E. S. *et al.* **Pollen tube growth is coupled to the extracellular calcium ion flux and the intracellular calcium gradient: effect of BAPTA-type buffers and hypertonic media**. *Plant Cell* 6, 1815-1828, doi:10.1105/tpc.6.12.1815 (1994).
128 Michard, E. *et al.* **Tobacco pollen tubes as cellular models for ion dynamics: improved spatial and temporal resolution of extracellular flux and free cytosolic concentration of calcium and protons using pHluorin and YC3.1 CaMeleon**. *Sexual Plant Reproduction* 21, 169-181 (2008).
129 Diao, M. *et al.* **Calcium imaging in *Arabidopsis* pollen cells using G-CaMP5**. *J Integr Plant Biol* 60, 897-906, doi:10.1111/jipb.12642 (2018).
130 Gutermuth, T. *et al.* **Tip-localized Ca^{2+}-permeable channels control pollen tube growth via kinase-dependent R- and S-type anion channel regulation**. *New Phytol* 218, 1089-1105, doi:10.1111/nph.15067 (2018).

131 Holdaway-Clarke, T. L. *et al.* **Pollen tube growth and the intracellular cytosolic calcium gradient oscillate in phase while extracellular calcium influx is delayed**. *Plant Cell* 9, 1999-2010, doi:10.1105/tpc.9.11.1999 (1997).
132 Iwano, M. *et al.* **Ca^{2+} dynamics in a pollen grain and papilla cell during pollination of *Arabidopsis***. *Plant Physiol* 136, 3562-3571, doi:10.1104/pp.104.046961 (2004).
133 Pierson, E. S. *et al.* **Tip-localized calcium entry fluctuates during pollen tube growth**. *Dev Biol* 174, 160-173, doi:10.1006/dbio.1996.0060 (1996).
134 Messerli, M. A. *et al.* **Periodic increases in elongation rate precede increases in cytosolic Ca^{2+} during pollen tube growth**. *Dev Biol* 222, 84-98, doi:10.1006/dbio.2000.9709 (2000).
135 Lassig, R. *et al.* **Pollen tube NAD(P)H oxidases act as a speed control to dampen growth rate oscillations during polarized cell growth**. *Plant J* 78, 94-106, doi:10.1111/tpj.12452 (2014).
136 Parton, R. M. *et al.* **Dynamics of the apical vesicle accumulation and the rate of growth are related in individual pollen tubes**. *J Cell Sci* 114, 2685-2695 (2001).
137 McKenna, S. T. *et al.* **Exocytosis precedes and predicts the increase in growth in oscillating pollen tubes**. *Plant Cell* 21, 3026-3040, doi:10.1105/tpc.109.069260 (2009).
138 Roy, S. J. *et al.* **Uncoupling secretion and tip growth in lily pollen tubes: evidence for the role of calcium in exocytosis**. *Plant J* 19, 379-386, doi:10.1046/j.1365-313x.1999.00515.x (1999).
139 Sutter, J. U. *et al.* **Synthesis of vesicle cargo determines amplitude of Ca^{2+}-sensitive exocytosis**. *Cell Calcium* 52, 283-288, doi:10.1016/j.ceca.2012.05.011 (2012).
140 Messerli, M. A. & Robinson, K. R. **Ionic and osmotic disruptions of the lily pollen tube oscillator: testing proposed models**. *Planta* 217, 147-157, doi:10.1007/s00425-003-0972-0 (2003).
141 Iwano, M. *et al.* **Cytoplasmic Ca^{2+} changes dynamically during the interaction of the pollen tube with synergid cells**. *Development* 139, 4202-4209, doi:10.1242/dev.081208 (2012).
142 Duan, Q. *et al.* **Reactive oxygen species mediate pollen tube rupture to release sperm for fertilization in *Arabidopsis***. *Nat Commun* 5, 3129, doi:10.1038/ncomms4129 (2014).
143 Michard, E. *et al.* **Glutamate receptor-like genes form Ca^{2+} channels in pollen tubes and are regulated by pistil D-serine**. *Science* 332, 434-437, doi:10.1126/science.1201101 (2011).
144 Gao, Q. F. *et al.* **Cyclic nucleotide-gated channel 18 is an essential Ca^{2+} channel in pollen tube tips for pollen tube guidance to ovules in *Arabidopsis***. *Proc Natl Acad Sci U S A* 113, 3096-3101, doi:10.1073/pnas.1524629113 (2016).
145 Hamilton, E. S. & Haswell, E. S. **The Tension-sensitive Ion Transport Activity of MSL8 is Critical for its Function in Pollen Hydration and Germination**. *Plant Cell Physiol* 58, 1222-1237, doi:10.1093/pcp/pcw230 (2017).
146 Certal, A. C. *et al.* **Exclusion of a proton ATPase from the apical membrane is associated with cell polarity and tip growth in *Nicotiana tabacum* pollen tubes**. *Plant Cell* 20, 614-634 (2008).
147 Kutschera, U. & Schopfer, P. **Evidence for the acid-growth theory of fusicoccin action**. *Planta* 163, 494-499, doi:10.1007/BF00392706 (1985).
148 Fu, Y. *et al.* **Rop GTPase-dependent dynamics of tip-localized F-actin controls tip growth in pollen tubes**. *J Cell Biol* 152, 1019-1032, doi:10.1083/jcb.152.5.1019 (2001).
149 Campanoni, P. & Blatt, M. R. **Membrane trafficking and polar growth in root hairs and pollen tubes**. *J Exp Bot* 58, 65-74, doi:10.1093/jxb/erl059 (2007).
150 Chebli, Y. *et al.* **The cell wall of the *Arabidopsis* pollen tube--spatial distribution, recycling, and network formation of polysaccharides**. *Plant Physiol* 160, 1940-1955, doi:10.1104/pp.112.199729 (2012).
151 Zhou, Y. *et al.* **Advances and prospects of rhodopsin-based optogenetics in plant research**. *Plant Physiology* 187, 572-589, doi:10.1093/plphys/kiab338 (2021).
152 Mouline, K. *et al.* **Pollen tube development and competitive ability are impaired by disruption of a Shaker K^+ channel in *Arabidopsis***. *Genes Dev* 16, 339-350, doi:10.1101/gad.213902 (2002).

153 Fan, L. M. *et al.* ***In vitro Arabidopsis*** **pollen germination and characterization of the inward potassium currents in *Arabidopsis* pollen grain protoplasts**. *J Exp Bot* 52, 1603-1614, doi:10.1093/jexbot/52.361.1603 (2001).
154 Lacombe, B. *et al.* **pH control of the plant outwardly-rectifying potassium channel SKOR**. *FEBS Lett* 466, 351-354, doi:10.1016/s0014-5793(00)01093-0 (2000).
155 Zhao, L. N. *et al.* **Ca^{2+}-dependent protein kinase11 and 24 modulate the activity of the inward rectifying K^+ channels in *Arabidopsis* pollen tubes**. *Plant Cell* 25, 649-661, doi:10.1105/tpc.112.103184 (2013).
156 Messerli, M. A. *et al.* **Pulsatile influxes of H^+, K^+ and Ca^{2+} lag growth pulses of *Lilium longiflorum* pollen tubes**. *J Cell Sci* 112 (Pt 10), 1497-1509 (1999).
157 Weisenseel, M. H. & Wenisch, H. H. **The membrane potential of growing Lily pollen**. *Zeitschrift Fur Pflanzenphysiologie* 99, 313-323 (1980).
158 Malhó, R. *et al.* **Calcium channel activity during pollen tube growth and reorientation**. *Plant Cell* 7, 1173-1184 (1995).
159 Hepler, P. K. *et al.* **Control of cell wall extensibility during pollen tube growth**. *Mol Plant* 6, 998-1017, doi:10.1093/mp/sst103 (2013).
160 Damineli, D. S. C. *et al.* **Oscillatory signatures underlie growth regimes in *Arabidopsis* pollen tubes: computational methods to estimate tip location, periodicity, and synchronization in growing cells**. *J Exp Bot* 68, 3267-3281, doi:10.1093/jxb/erx032 (2017).
161 Lang, V. *et al.* **Pump up the volume - a central role for the plasma membrane H^+ pump in pollen germination and tube growth**. *Protoplasma* 251, 477-488, doi:10.1007/s00709-013-0555-2 (2014).
162 Choi, W. G. *et al.* **High-resolution imaging of Ca^{2+}, redox status, ROS and pH using GFP biosensors**. *Plant J* 70, 118-128, doi:10.1111/j.1365-313X.2012.04917.x (2012).
163 Hetherington, A. M. **Guard cell signalling**. *Cell* 107, 711-714 (2001).
164 Schroeder, J. I. *et al.* **Guard Cell Signal Transduction**. *Annu Rev Plant Physiol Plant Mol Biol* 52, 627-658, doi:10.1146/annurev.arplant.52.1.627 (2001).
165 MacRobbie, E. A. **Control of volume and turgor in stomatal guard cells**. *J Membr Biol* 210, 131-142, doi:10.1007/s00232-005-0851-7 (2006).
166 Ache, P. *et al.* **Stomatal action directly feeds back on leaf turgor: new insights into the regulation of the plant water status from non-invasive pressure probe measurements**. *Plant J* 62, 1072-1082, doi:10.1111/j.1365-313X.2010.04213.x (2010).
167 Murata, Y. *et al.* **Diverse stomatal signaling and the signal integration mechanism**. *Annu Rev Plant Biol* 66, 369-392, doi:10.1146/annurev-arplant-043014-114707 (2015).
168 McAinsh, M. R. *et al.* **Abscisic acid induced elevation of guard cell cytosolic Ca^{2+} precedes stomatal closure**. *Nature* 343, 186-188 (1990).
169 McAinsh, M. R. *et al.* **Stimulus-induced oscillations in guard cell cytosolic free calcium**. *Plant Cell* 7, 1207-1219, doi:10.1105/tpc.7.8.1207 (1995).
170 Thor, K. & Peiter, E. **Cytosolic calcium signals elicited by the pathogen-associated molecular pattern flg22 in stomatal guard cells are of an oscillatory nature**. *New Phytol* 204, 873-881, doi:10.1111/nph.13064 (2014).
171 Allen, G. J. *et al.* **A defined range of guard cell calcium oscillation parameters encodes stomatal movements**. *Nature* 411, 1053-1057, doi:10.1038/35082575 (2001).
172 Allen, G. J. *et al.* **Alteration of stimulus-specific guard cell calcium oscillations and stomatal closing in *Arabidopsis* det3 mutant**. *Science* 289, 2338-2342, doi:10.1126/science.289.5488.2338 (2000).
173 Islam, M. M. *et al.* **Cytosolic alkalization and cytosolic calcium oscillation in *Arabidopsis* guard cells response to ABA and MeJA**. *Plant Cell Physiol* 51, 1721-1730, doi:10.1093/pcp/pcq131 (2010).

174 Allen, G. J. *et al.* ***Arabidopsis*** **abi1-1 and abi2-1 phosphatase mutations reduce abscisic acid-induced cytoplasmic calcium rises in guard cells**. *Plant Cell* 11, 1785-1798, doi:10.1105/tpc.11.9.1785 (1999).
175 Klusener, B. *et al.* **Convergence of calcium signaling pathways of pathogenic elicitors and abscisic acid in** ***Arabidopsis*** **guard cells**. *Plant Physiol* 130, 2152-2163, doi:10.1104/pp.012187 (2002).
176 Nambara, E. & Marion-Poll, A. **Abscisic acid biosynthesis and catabolism**. *Annu Rev Plant Biol* 56, 165-185, doi:10.1146/annurev.arplant.56.032604.144046 (2005).
177 Wang, X. F. & Zhang, D. P. **Abscisic acid receptors: multiple signal-perception sites**. *Ann Bot* 101, 311-317, doi:10.1093/aob/mcm284 (2008).
178 Park, S. Y. *et al.* **Abscisic acid inhibits type 2C protein phosphatases via the PYR/PYL family of START proteins**. *Science* 324, 1068-1071, doi:10.1126/science.1173041 (2009).
179 Ma, Y. *et al.* **Regulators of PP2C phosphatase activity function as abscisic acid sensors**. *Science* 324, 1064-1068, doi:10.1126/science.1172408 (2009).
180 Wang, Y. *et al.* **PYR/PYL/RCAR abscisic acid receptors regulate K^+ and Cl^- channels through reactive oxygen species-mediated activation of Ca^{2+} channels at the plasma membrane of intact Arabidopsis guard cells**. *Plant Physiol* 163, 566-577, doi:10.1104/pp.113.219758 (2013).
181 Castillo, M. C. *et al.* **Inactivation of PYR/PYL/RCAR ABA receptors by tyrosine nitration may enable rapid inhibition of ABA signaling by nitric oxide in plants**. *Sci. Signal.* 8, ra89 (2015).
182 Dittrich, M. *et al.* **The role of** ***Arabidopsis*** **ABA receptors from the PYR/PYL/RCAR family in stomatal acclimation and closure signal integration**. *Nat Plants* 5, 1002-1011, doi:10.1038/s41477-019-0490-0 (2019).
183 MacRobbie, E. A. C. **ABA activates multiple Ca^{2+} fluxes in stomatal guard cells, triggering vacuolar K^+(Rb^+) release**. *Proceedings of the National Academy of Sciences of the United States of America* 97, 12361-12368 (2000).
184 Mori, I. C. *et al.* **CDPKs CPK6 and CPK3 function in ABA regulation of guard cell S-type anion- and Ca^{2+}-permeable channels and stomatal closure**. *PLoS Biol* 4, e327, doi:10.1371/journal.pbio.0040327 (2006).
185 Zhu, S. Y. *et al.* **Two calcium-dependent protein kinases, CPK4 and CPK11, regulate abscisic acid signal transduction in** ***Arabidopsis***. *Plant Cell* 19, 3019-3036, doi:10.1105/tpc.107.050666 (2007).
186 Gilroy, S. *et al.* **Role of Calcium in Signal Transduction of Commelina Guard Cells**. *Plant Cell* 3, 333-344, doi:10.1105/tpc.3.4.333 (1991).
187 Levchenko, V. *et al.* **Cytosolic abscisic acid activates guard cell anion channels without preceding Ca^{2+} signals**. *Proceedings of the National Academy of Sciences of the United States of America* 102, 4203-4208 (2005).
188 Marten, H. *et al.* **Ca^{2+}-dependent and -independent abscisic acid activation of plasma membrane anion channels in guard cells of** ***Nicotiana tabacum***. *Plant Physiol* 143, 28-37, doi:10.1104/pp.106.092643 (2007).
189 Allan, A. C. *et al.* **Two transduction pathways mediate rapid effects of abscisic acid in** ***Commelina*** **guard cells**. *Plant Cell* 6, 1319-1328, doi:10.1105/tpc.6.9.1319 (1994).
190 Schroeder, J. I. & Hagiwara, S. **Repetitive increases in cytosolic Ca^{2+} of guard cells by abscisic acid activation of nonselective Ca^{2+} permeable channels**. *Proc Natl Acad Sci U S A* 87, 9305-9309, doi:10.1073/pnas.87.23.9305 (1990).
191 Brandt, B. *et al.* **Calcium specificity signaling mechanisms in abscisic acid signal transduction in** ***Arabidopsis*** **guard cells**. *Elife* 4, doi:10.7554/eLife.03599 (2015).
192 Huang, S. *et al.* **Calcium signals in guard cells enhance the efficiency by which abscisic acid triggers stomatal closure**. *New Phytol* 224, 177-187, doi:10.1111/nph.15985 (2019).
193 Melcher, K. *et al.* **A gate-latch-lock mechanism for hormone signalling by abscisic acid receptors**. *Nature* 462, 602-608, doi:10.1038/nature08613 (2009).

194 Hao, Q. *et al.* **The molecular basis of ABA-independent inhibition of PP2Cs by a subclass of PYL proteins**. *Mol Cell* 42, 662-672, doi:10.1016/j.molcel.2011.05.011 (2011).
195 Soon, F. F. *et al.* **Molecular mimicry regulates ABA signaling by SnRK2 kinases and PP2C phosphatases**. *Science* 335, 85-88, doi:10.1126/science.1215106 (2012).
196 Grabov, A. *et al.* **Alteration of anion channel kinetics in wild-type and *abi1-1* transgenic *Nicotiana benthamiana* guard cells by abscisic acid**. *Plant J* 12, 203-213, doi:10.1046/j.1365-313x.1997.12010203.x (1997).
197 Murata, Y. *et al.* **Abscisic acid activation of plasma membrane Ca^{2+} channels in guard cells requires cytosolic NAD(P)H and is differentially disrupted upstream and downstream of reactive oxygen species production in abi1-1 and abi2-1 protein phosphatase 2C mutants**. *Plant Cell* 13, 2513-2523, doi:10.1105/tpc.010210 (2001).
198 Mustilli, A. C. *et al.* ***Arabidopsis* OST1 protein kinase mediates the regulation of stomatal aperture by abscisic acid and acts upstream of reactive oxygen species production**. *Plant Cell* 14, 3089-3099, doi:10.1105/tpc.007906 (2002).
199 Yoshida, R. *et al.* **The regulatory domain of SRK2E/OST1/SnRK2.6 interacts with ABI1 and integrates abscisic acid (ABA) and osmotic stress signals controlling stomatal closure in *Arabidopsis***. *J Biol Chem* 281, 5310-5318, doi:10.1074/jbc.M509820200 (2006).
200 Fujii, H. & Zhu, J. K. ***Arabidopsis* mutant deficient in 3 abscisic acid-activated protein kinases reveals critical roles in growth, reproduction, and stress**. *Proc Natl Acad Sci U S A* 106, 8380-8385, doi:10.1073/pnas.0903144106 (2009).
201 Nakashima, K. *et al.* **Three *Arabidopsis* SnRK2 protein kinases, SRK2D/SnRK2.2, SRK2E/SnRK2.6/OST1 and SRK2I/SnRK2.3, involved in ABA signaling are essential for the control of seed development and dormancy**. *Plant Cell Physiol* 50, 1345-1363, doi:10.1093/pcp/pcp083 (2009).
202 Agurla, S. & Raghavendra, A. S. **Convergence and Divergence of Signaling Events in Guard Cells during Stomatal Closure by Plant Hormones or Microbial Elicitors**. *Frontiers in plant science* 7, 1332 (2016).
203 Kwak, J. M. *et al.* **NADPH oxidase AtrbohD and AtrbohF genes function in ROS-dependent ABA signaling in *Arabidopsis***. *EMBO J* 22, 2623-2633, doi:10.1093/emboj/cdg277 (2003).
204 Brault, M. *et al.* **Plasma membrane depolarization induced by abscisic acid in *Arabidopsis* suspension cells involves reduction of proton pumping in addition to anion channel activation, which are both Ca^{2+} dependent**. *Plant Physiol* 135, 231-243, doi:10.1104/pp.104.039255 (2004).
205 Bright, J. *et al.* **ABA-induced NO generation and stomatal closure in *Arabidopsis* are dependent on H_2O_2 synthesis**. *Plant Journal* 45, 113-122 (2006).
206 Pottosin, I. & Zepeda-Jazo, I. **Powering the plasma membrane Ca^{2+}-ROS self-amplifying loop**. *J Exp Bot* 69, 3317-3320, doi:10.1093/jxb/ery179 (2018).
207 Roelfsema, M. R. *et al.* **ABA depolarizes guard cells in intact plants, through a transient activation of R- and S-type anion channels**. *Plant J* 37, 578-588, doi:10.1111/j.1365-313x.2003.01985.x (2004).
208 Saxena, I. *et al.* **Cross talk between H_2O_2 and interacting signal molecules under plant stress response**. *Front Plant Sci* 7, 570, doi:10.3389/fpls.2016.00570 (2016).
209 Sierla, M. *et al.* **Reactive oxygen species in the regulation of stomatal movements**. *Plant Physiol* 171, 1569-1580, doi:10.1104/pp.16.00328 (2016).
210 Sirichandra, C. *et al.* **Phosphorylation of the *Arabidopsis* AtrbohF NADPH oxidase by OST1 protein kinase**. *FEBS Lett* 583, 2982-2986, doi:10.1016/j.febslet.2009.08.033 (2009).
211 Wang, P. & Song, C. P. **Guard-cell signalling for hydrogen peroxide and abscisic acid**. *New Phytol* 178, 703-718, doi:10.1111/j.1469-8137.2008.02431.x (2008).
212 Watkins, J. M. *et al.* **Abscisic acid-induced reactive xxygen species are modulated by flavonols to control stomata aperture**. *Plant Physiol* 175, 1807-1825, doi:10.1104/pp.17.01010 (2017).
213 Hedrich, R. *et al.* **Ca^{2+} and nucleotide dependent regulation of voltage dependent anion channels in the plasma membrane of guard cells**. *EMBO J* 9, 3889-3892 (1990).

214 Schroeder, J. I. & Keller, B. U. **Two types of anion channel currents in guard cells with distinct voltage regulation**. *Proc Natl Acad Sci U S A* 89, 5025-5029, doi:10.1073/pnas.89.11.5025 (1992).
215 Vahisalu, T. *et al.* **SLAC1 is required for plant guard cell S-type anion channel function in stomatal signalling**. *Nature* 452, 487-491 (2008).
216 MacRobbie, E. A. **Signal transduction and ion channels in guard cells**. *Philos Trans R Soc Lond B Biol Sci* 353, 1475-1488, doi:10.1098/rstb.1998.0303 (1998).
217 Ache, P. *et al.* **GORK, a delayed outward rectifier expressed in guard cells of *Arabidopsis thaliana*, is a K^+-selective, K^+-sensing ion channel**. *FEBS Letters* 486, 93-98 (2000).
218 Geiger, D. *et al.* **Stomatal closure by fast abscisic acid signaling is mediated by the guard cell anion channel SLAH3 and the receptor RCAR1**. *Sci Signal* 4, ra32, doi:10.1126/scisignal.2001346 (2011).
219 Dreyer, I. *et al.* **Molecular Evolution of Slow and Quick Anion Channels (SLACs and QUACs/ALMTs)**. *Front Plant Sci* 3, 263, doi:10.3389/fpls.2012.00263 (2012).
220 Belin, C. *et al.* **Identification of features regulating OST1 kinase activity and OST1 function in guard cells**. *Plant Physiol* 141, 1316-1327, doi:10.1104/pp.106.079327 (2006).
221 Lee, S. C. *et al.* **A protein kinase-phosphatase pair interacts with an ion channel to regulate ABA signaling in plant guard cells**. *Proc Natl Acad Sci U S A* 106, 21419-21424, doi:10.1073/pnas.0910601106 (2009).
222 Umezawa, T. *et al.* **Type 2C protein phosphatases directly regulate abscisic acid-activated protein kinases in *Arabidopsis***. *Proc Natl Acad Sci U S A* 106, 17588-17593, doi:10.1073/pnas.0907095106 (2009).
223 Brandt, B. *et al.* **Reconstitution of abscisic acid activation of SLAC1 anion channel by CPK6 and OST1 kinases and branched ABI1 PP2C phosphatase action**. *Proc Natl Acad Sci U S A* 109, 10593-10598, doi:10.1073/pnas.1116590109 (2012).
224 Imes, D. *et al.* **Open stomata 1 (OST1) kinase controls R-type anion channel QUAC1 in *Arabidopsis* guard cells**. *Plant J* 74, 372-382, doi:10.1111/tpj.12133 (2013).
225 Acharya, B. R. *et al.* **Open Stomata 1 (OST1) is limiting in abscisic acid responses of *Arabidopsis* guard cells**. *New Phytol* 200, 1049-1063, doi:10.1111/nph.12469 (2013).
226 Goh, C. H. *et al.* **Inhibition of Blue Light-Dependent H^+ Pumping by Abscisic Acid in Vicia Guard-Cell Protoplasts**. *Plant Physiol* 111, 433-440, doi:10.1104/pp.111.2.433 (1996).
227 Blatt, M. R. & Armstrong, F. **K^+ channels of stomatal guard cells: Abscisic-acid-evoked control of the outward rectifier mediated by cytoplasmic pH**. *Planta*, 330-341 (1993).
228 Miedema, H. & Assmann, S. M. **Effect of cytosolic pH on the *Vicia faba* guard cell K^+ outward rectifier: A single channel study**. *Plant Physiology* 111, 695-695 (1996).
229 Felle, H. H. *et al.* **Dynamics of ionic activities in the apoplast of the sub-stomatal cavity of intact *Vicia faba* leaves during stomatal closure evoked by ABA and darkness**. *Plant J* 24, 297-304, doi:10.1046/j.1365-313x.2000.00878.x (2000).
230 Geilfus, C. M. *et al.* **Chloride-inducible transient apoplastic alkalinizations induce stomata closure by controlling abscisic acid distribution between leaf apoplast and guard cells in salt-stressed Vicia faba**. *New Phytol* 208, 803-816, doi:10.1111/nph.13507 (2015).
231 Geilfus, C. M. *et al.* **Leaf apoplastic alkalization promotes transcription of the ABA-synthesizing enzyme Vp14 and stomatal closure in *Zea mays***. *J Exp Bot* 72, 2686-2695, doi:10.1093/jxb/eraa589 (2021).
232 Palmgren, M. G. & Nissen, P. **P-type ATPases**. *Annu Rev Biophys* 40, 243-266, doi:10.1146/annurev.biophys.093008.131331 (2011).
233 Macara, I. G. **Vanadium- an element in search of a role**. *Trends in Biochemical Sciences* 5, 92–94 (1980).
234 Geilfus, C. M. & Muhling, K. H. **Ratiometric monitoring of transient apoplastic alkalinizations in the leaf apoplast of living Vicia faba plants: chloride primes and PM-H^+-ATPase shapes NaCl-induced systemic alkalinizations**. *New Phytol* 197, 1117-1129, doi:10.1111/nph.12046 (2013).

235 Yan, S. *et al.* **The role of plasma membrane H^+-ATPase in jasmonate-induced ion fluxes and stomatal closure in *Arabidopsis thaliana***. *Plant J* 83, 638-649, doi:10.1111/tpj.12915 (2015).
236 Reyera, A. *et al.* **Channelrhodopsin-mediated optogenetics highlights a central role of depolarization-dependent plant proton pumps**. *Proc Natl Acad Sci U S A* 117, 24004, doi:10.1073/pnas.2017782117 (2020).
237 Assmann, S. M. & Schwartz, A. **Synergistic effect of light and fusicoccin on stomatal opening : epidermal peel and patch clamp experiments**. *Plant Physiol* 98, 1349-1355, doi:10.1104/pp.98.4.1349 (1992).
238 Kinoshita, T. & Shimazaki, K. **Analysis of the phosphorylation level in guard-cell plasma membrane H^+-ATPase in response to fusicoccin**. *Plant Cell Physiol* 42, 424-432, doi:10.1093/pcp/pce055 (2001).
239 Roux, B. & Leonhardt, N. **The Regulation of Ion Channels and Transporters in the Guard Cell** Advances in Botanical Research 171-214 (2018).
240 Merlot, S. *et al.* **Constitutive activation of a plasma membrane H^+-ATPase prevents abscisic acid-mediated stomatal closure**. *EMBO J* 26, 3216-3226, doi:10.1038/sj.emboj.7601750 (2007).
241 Krebs, M. *et al.* ***Arabidopsis* V-ATPase activity at the tonoplast is required for efficient nutrient storage but not for sodium accumulation**. *Proc Natl Acad Sci U S A* 107, 3251-3256, doi:10.1073/pnas.0913035107 (2010).
242 Darley, C. P. *et al.* **Tonoplast inorganic pyrophosphatase in Vicia faba guard cells**. *Planta* 206, 272–277 (1998).
243 Bak, G. *et al.* **Rapid structural changes and acidification of guard cell vacuoles during stomatal closure require phosphatidylinositol 3,5-bisphosphate**. *Plant Cell* 25, 2202-2216, doi:10.1105/tpc.113.110411 (2013).
244 Barkla, B. J. *et al.* **Abscisic acid induction of vacuolar H^+-ATPase activity in Mesembryanthemum crystallinum is developmentally regulated**. *Plant Physiol.* 120, 811 – 819 (1999).
245 Gonugunta, V. K. *et al.* **Nitric oxide production occurs after cytosolic alkalinization during stomatal closure induced by abscisic acid**. *Plant Cell Environ* 31, 1717-1724, doi:10.1111/j.1365-3040.2008.01872.x (2008).
246 Melotto, M. *et al.* **Plant stomata function in innate immunity against bacterial invasion**. *Cell* 126, 969-980, doi:10.1016/j.cell.2006.06.054 (2006).
247 McLachlan, D. H. *et al.* **Gate control: guard cell regulation by microbial stress**. *New Phytol* 203, 1049-1063, doi:10.1111/nph.12916 (2014).
248 Sawinski, K. *et al.* **Guarding the green: pathways to stomatal immunity**. *Mol Plant Microbe Interact* 26, 626-632, doi:10.1094/MPMI-12-12-0288-CR (2013).
249 Arnaud, D. & Hwang, I. **A sophisticated network of signaling pathways regulates stomatal defenses to bacterial pathogens**. *Mol Plant* 8, 566-581, doi:10.1016/j.molp.2014.10.012 (2015).
250 Felix, G. *et al.* **Plants have a sensitive perception system for the most conserved domain of bacterial flagellin**. *Plant Journal* 18, 265-276 (1999).
251 Gomez-Gomez, L., and Boller, T. . **FLS2: An LRR Receptor–like Kinase Involved in the Perception of the Bacterial Elicitor Flagellin in *Arabidopsis***. *Molecular Cell* 5, 1003-1011 (2000).
252 Kunze, G. *et al.* **The N terminus of bacterial elongation factor Tu elicits innate immunity in *Arabidopsis* plants**. *Plant Cell* 16, 3496-3507, doi:10.1105/tpc.104.026765 (2004).
253 Mersmann, S. *et al.* **Ethylene signaling regulates accumulation of the FLS2 receptor and is required for the oxidative burst contributing to plant immunity**. *Plant Physiol* 154, 391-400, doi:10.1104/pp.110.154567 (2010).
254 Sun, Y. *et al.* **Structural basis for flg22-induced activation of the *Arabidopsis* FLS2-BAK1 immune complex**. *Science* 342, 624-628, doi:10.1126/science.1243825 (2013).
255 Chinchilla, D. *et al.* **A flagellin-induced complex of the receptor FLS2 and BAK1 initiates plant defence**. *Nature* 448, 497-500, doi:10.1038/nature05999 (2007).

256 Shang, Y. *et al.* **BRI1-Associated Receptor Kinase 1 Regulates Guard Cell ABA Signaling Mediated by Open Stomata 1 in *Arabidopsis***. *Mol Plant* 9, 447-460, doi:10.1016/j.molp.2015.12.014 (2016).
257 Asai, T. *et al.* **MAP kinase signalling cascade in *Arabidopsis* innate immunity**. *Nature* 415, 977-983, doi:10.1038/415977a (2002).
258 Zhang, W. *et al.* **The plant innate immunity response in stomatal guard cells invokes G-protein-dependent ion channel regulation**. *Plant J* 56, 984-996, doi:10.1111/j.1365-313X.2008.03657.x (2008).
259 Jeworutzki, E. *et al.* **Early signaling through the *Arabidopsis* pattern recognition receptors FLS2 and EFR involves Ca-associated opening of plasma membrane anion channels**. *Plant J* 62, 367-378, doi:10.1111/j.1365-313X.2010.04155.x (2010).
260 Macho, A. P. *et al.* **Aspartate oxidase plays an important role in *Arabidopsis* stomatal immunity**. *Plant Physiol* 159, 1845-1856, doi:10.1104/pp.112.199810 (2012).
261 Guzel Deger, A. *et al.* **Guard cell SLAC1-type anion channels mediate flagellin-induced stomatal closure**. *New Phytol* 208, 162-173, doi:10.1111/nph.13435 (2015).
262 Dubiella, U. *et al.* **Calcium-dependent protein kinase/NADPH oxidase activation circuit is required for rapid defense signal propagation**. *Proc Natl Acad Sci U S A* 110, 8744-8749, doi:10.1073/pnas.1221294110 (2013).
263 Gao, J. *et al.* **Saccharomyces cerevisiae-induced stomatal closure mainly mediated by salicylhydroxamic acid-sensitive peroxidases in Vicia faba**. *Plant Physiol Biochem* 65, 27-31, doi:10.1016/j.plaphy.2013.01.008 (2013).
264 Boudsocq, M. *et al.* **Differential innate immune signalling via Ca^{2+} sensor protein kinases**. *Nature* 464, 418-422, doi:10.1038/nature08794 (2010).
265 Boudsocq, M. & Sheen, J. **CDPKs in immune and stress signaling**. *Trends Plant Sci* 18, 30-40, doi:10.1016/j.tplants.2012.08.008 (2013).
266 Li, L. *et al.* **The FLS2-associated kinase BIK1 directly phosphorylates the NADPH oxidase RbohD to control plant immunity**. *Cell Host Microbe* 15, 329-338, doi:10.1016/j.chom.2014.02.009 (2014).
267 Ogasawara, Y. *et al.* **Synergistic activation of the *Arabidopsis* NADPH oxidase AtrbohD by Ca^{2+} and phosphorylation**. *J Biol Chem* 283, 8885-8892, doi:10.1074/jbc.M708106200 (2008).
268 Kimura, S. *et al.* **Protein phosphorylation is a prerequisite for the Ca^{2+}-dependent activation of *Arabidopsis* NADPH oxidases and may function as a trigger for the positive feedback regulation of Ca^{2+} and reactive oxygen species**. *Biochim Biophys Acta* 1823, 398-405, doi:10.1016/j.bbamcr.2011.09.011 (2012).
269 Seybold, H. *et al.* **Ca^{2+} signalling in plant immune response: from pattern recognition receptors to Ca^{2+} decoding mechanisms**. *New Phytol* 204, 782-790, doi:10.1111/nph.13031 (2014).
270 Suarez-Rodriguez, M. C. *et al.* **MEKK1 is required for flg22-induced MPK4 activation in *Arabidopsis* plants**. *Plant Physiol* 143, 661-669, doi:10.1104/pp.106.091389 (2007).
271 Rodriguez, M. C. *et al.* **Mitogen-activated protein kinase signaling in plants**. *Annu Rev Plant Biol* 61, 621-649, doi:10.1146/annurev-arplant-042809-112252 (2010).
272 Krol, E. **Ways of Ion Channel Gating in Plant Cells**. *Annals of Botany* 86, 449-469, doi:10.1006/anbo.2000.1226 (2000).
273 Nuhse, T. S. *et al.* **Quantitative phosphoproteomic analysis of plasma membrane proteins reveals regulatory mechanisms of plant innate immune responses**. *Plant J* 51, 931-940, doi:10.1111/j.1365-313X.2007.03192.x (2007).
274 Keinath, N. F. *et al.* **PAMP (pathogen-associated molecular pattern)-induced changes in plasma membrane compartmentalization reveal novel components of plant immunity**. *J Biol Chem* 285, 39140-39149, doi:10.1074/jbc.M110.160531 (2010).
275 Elmore, J. M. & Coaker, G. **The role of the plasma membrane H^+-ATPase in plant-microbe interactions**. *Mol Plant* 4, 416-427, doi:10.1093/mp/ssq083 (2011).

276 Liu, J. *et al.* **RIN4 functions with plasma membrane H^+-ATPases to regulate stomatal apertures during pathogen attack**. *PLoS Biol* 7, e1000139, doi:10.1371/journal.pbio.1000139 (2009).
277 Young, J. J. *et al.* **CO(2) signaling in guard cells: calcium sensitivity response modulation, a Ca^{2+}-independent phase, and CO(2) insensitivity of the gca2 mutant**. *Proc Natl Acad Sci U S A* 103, 7506-7511, doi:10.1073/pnas.0602225103 (2006).
278 Dietrich, P. *et al.* **The role of ion channels in light-dependent stomatal opening**. *J Exp Bot* 52, 1959-1967, doi:10.1093/jexbot/52.363.1959 (2001).
279 Zhao, R. *et al.* **Cosuppression of a plasma membrane H^+-ATPase isoform impairs sucrose translocation, stomatal opening, plant growth, and male fertility**. *Plant Cell* 12, 535-546, doi:10.1105/tpc.12.4.535 (2000).
280 Hoth, S. *et al.* **Molecular basis of plant-specific acid activation of K^+ uptake channels**. *Proc Natl Acad Sci U S A* 94, 4806-4810, doi:10.1073/pnas.94.9.4806 (1997).
281 Hoth, S. *et al.* **The pore of plant K^+ channels is involved in voltage and pH sensing: domain-swapping between different K^+ channel alpha-subunits**. *Plant Cell* 13, 943-952 (2001).
282 Kwak, J. M. *et al.* **Dominant negative guard cell K^+ channel mutants reduce inward-rectifying K^+ currents and light-induced stomatal opening in *Arabidopsis***. *Plant Physiol* 127, 473-485, doi:10.1104/pp.010428 (2001).
283 Daloso, D. M. *et al.* **Roles of sucrose in guard cell regulation**. *New Phytol* 211, 809-818, doi:10.1111/nph.13950 (2016).
284 Li, J. G. *et al.* **Brassinosteroid and hydrogen peroxide interdependently induce stomatal opening by promoting guard cell starch degradation**. *Plant Cell* 32, 984-999, doi:10.1105/tpc.19.00587 (2020).
285 Becker, D. *et al.* **Regulation of the ABA-sensitive *Arabidopsis* potassium channel gene GORK in response to water stress**. *FEBS Lett* 554, 119-126, doi:10.1016/s0014-5793(03)01118-9 (2003).
286 Hosy, E. *et al.* **The *Arabidopsis* outward K^+ channel GORK is involved in regulation of stomatal movements and plant transpiration**. *Proceedings of the National Academy of Sciences of the United States of America* 100, 7418-7418 (2003).
287 Osakabe, Y. *et al.* **Osmotic stress responses and plant growth controlled by potassium transporters in *Arabidopsis***. *Plant Cell* 25, 609-624, doi:10.1105/tpc.112.105700 (2013).
288 Corratge-Faillie, C. *et al.* **The *Arabidopsis* guard cell outward potassium channel GORK is regulated by CPK33**. *FEBS Lett* 591, 1982-1992, doi:10.1002/1873-3468.12687 (2017).
289 Roelfsema, M. R. G. & Hedrich, R. **In the light of stomatal opening: new insights into 'the Watergate'**. *New Phytologist* 167, 665-691 (2005).
290 Barragan, V. *et al.* **Ion exchangers NHX1 and NHX2 mediate active potassium uptake into vacuoles to regulate cell turgor and stomatal function in *Arabidopsis***. *Plant Cell* 24, 1127-1142, doi:10.1105/tpc.111.095273 (2012).
291 Wang, Y. & Wu, W. H. **Potassium transport and signaling in higher plants**. *Annu Rev Plant Biol* 64, 451-476, doi:10.1146/annurev-arplant-050312-120153 (2013).
292 Nieves-Cordones, M. *et al.* **Roles and transport of sodium and potassium in plants**. *Met Ions Life Sci* 16, 291-324, doi:10.1007/978-3-319-21756-7_9 (2016).
293 Andres, Z. *et al.* **Control of vacuolar dynamics and regulation of stomatal aperture by tonoplast potassium uptake**. *Proc Natl Acad Sci U S A* 111, E1806-1814, doi:10.1073/pnas.1320421111 (2014).
294 Qi, J. *et al.* **Apoplastic ROS signaling in plant immunity**. *Curr Opin Plant Biol* 38, 92-100, doi:10.1016/j.pbi.2017.04.022 (2017).
295 Wilkinson, S. & Davies, W. J. **ABA-based chemical signalling: the co-ordination of responses to stress in plants**. *Plant Cell Environ* 25, 195-210, doi:10.1046/j.0016-8025.2001.00824.x (2002).
296 Todaka, D. *et al.* **Temporal and spatial changes in gene expression, metabolite accumulation and phytohormone content in rice seedlings grown under drought stress conditions**. *Plant J* 90, 61-78, doi:10.1111/tpj.13468 (2017).

297 Bauer, H. *et al.* **The stomatal response to reduced relative humidity requires guard cell-autonomous ABA synthesis**. *Curr Biol* 23, 53-57, doi:10.1016/j.cub.2012.11.022 (2013).
298 Karimi, S. M. *et al.* **Under salt stress guard cells rewire ion transport and abscisic acid signaling**. *New Phytol* 231, 1040-1055, doi:10.1111/nph.17376 (2021).
299 Schachtman, D. P. & Shin, R. **Nutrient sensing and signaling: NPKS**. *Annu Rev Plant Biol* 58, 47-69, doi:10.1146/annurev.arplant.58.032806.103750 (2007).
300 Geilfus, C. M. & Muhling, K. H. **Transient alkalinization in the leaf apoplast of Vicia faba L. depends on NaCl stress intensity: an in situ ratio imaging study**. *Plant Cell Environ* 35, 578-587, doi:10.1111/j.1365-3040.2011.02437.x (2012).
301 Ma, Y. *et al.* **Intracellular Ca^{2+} is important for flagellin-triggered defense in *Arabidopsis* and involves inositol polyphosphate signaling**. *J Exp Bot* 68, 3617-3628, doi:10.1093/jxb/erx176 (2017).
302 Rus, A. *et al.* **Natural variants of AtHKT1 enhance Na+ accumulation in two wild populations of *Arabidopsis***. *PLoS Genet* 2, e210, doi:10.1371/journal.pgen.0020210 (2006).
303 Carillo, P. *et al.* **Salinity Stress and Salt Tolerance**. (2015).
304 Yang, Y. & Guo, Y. **Unraveling salt stress signaling in plants**. *J Integr Plant Biol* 60, 796-804, doi:10.1111/jipb.12689 (2018).
305 Liu, J. & Zhu, J. K. **A calcium sensor homolog required for plant salt tolerance**. *Science* 280, 1943-1945, doi:10.1126/science.280.5371.1943 (1998).
306 Kiegle, E. *et al.* **Cell-type-speci®c calcium responses to drought, salt and cold in the *Arabidopsis* root**. *Plant Journal* 23, 267-278 (2000).
307 Choi, W. G. *et al.* **Salt stress-induced Ca^{2+} waves are associated with rapid, long-distance root-to-shoot signaling in plants**. *Proc Natl Acad Sci U S A* 111, 6497-6502, doi:10.1073/pnas.1319955111 (2014).
308 Manishankar, P. *et al.* **Calcium Signaling during Salt Stress and in the Regulation of Ion Homeostasis**. *J Exp Bot*, doi:10.1093/jxb/ery201 (2018).
309 Shi, H. *et al.* **The *Arabidopsis thaliana* salt tolerance gene *SOS1* encodes a putative Na^+/H^+ antiporter**. *Proc Natl Acad Sci U S A* 97, 6896-6901, doi:10.1073/pnas.120170197 (2000).
310 Liu, J. *et al.* **The *Arabidopsis thaliana SOS2* gene encodes a protein kinase that is required for salt tolerance**. *Proceedings of the National Academy of Sciences* 97, 3730-3734, doi:10.1073/pnas.97.7.3730 (2000).
311 Batelli, G. *et al.* **SOS2 promotes salt tolerance in part by interacting with the vacuolar H^+-ATPase and upregulating its transport activity**. *Mol Cell Biol* 27, 7781-7790, doi:10.1128/MCB.00430-07 (2007).
312 Janicka-Russak, M. & Klobus, G. **Modification of plasma membrane and vacuolar H^+-ATPases in response to NaCl and ABA**. *J Plant Physiol* 164, 295-302, doi:10.1016/j.jplph.2006.01.014 (2007).
313 Bose, J. *et al.* **Rapid regulation of the plasma membrane H^+-ATPase activity is essential to salinity tolerance in two halophyte species, Atriplex lentiformis and Chenopodium quinoa**. *Ann Bot* 115, 481-494, doi:10.1093/aob/mcu219 (2015).
314 Małgorzata, J. & Kabała, K. **The role of plasma membrane H^+-ATPase in salinity stress of plants**. *Progress in Botany* 76, 77-92, doi:10.1007/978-3-319-08807-5_3 (2015).
315 Fuglsang, A. T. *et al.* ***Arabidopsis* protein kinase PKS5 inhibits the plasma membrane H^+-ATPase by preventing interaction with 14-3-3 protein**. *Plant Cell* 19, 1617-1634, doi:10.1105/tpc.105.035626 (2007).
316 Gevaudant, F. *et al.* **Expression of a constitutively activated plasma membrane H^+-ATPase alters plant development and increases salt tolerance**. *Plant Physiol* 144, 1763-1776, doi:10.1104/pp.107.103762 (2007).
317 Wang, M. *et al.* **Overexpression of PeHA1 enhances hydrogen peroxide signaling in salt-stressed *Arabidopsis***. *Plant Physiol Biochem* 71, 37-48, doi:10.1016/j.plaphy.2013.06.020 (2013).

318 Silva, P. & Geros, H. **Regulation by salt of vacuolar H^+-ATPase and H^+-pyrophosphatase activities and Na^+/H^+ exchange**. *Plant Signal Behav* 4, 718-726, doi:10.4161/psb.4.8.9236 (2009).
319 Zhou, S. *et al.* **Enhanced V-ATPase activity contributes to the improved salt tolerance of transgenic tobacco plants overexpressing vacuolar Na^+/H^+ antiporter AtNHX1**. *Biotechnol Lett* 33, 375-380, doi:10.1007/s10529-010-0418-2 (2011).
320 Gaxiola, R. A. *et al.* **Drought- and salt-tolerant plants result from overexpression of the AVP1 H^+-pump.** . *Proc. Natl. Acad. Sci. USA* 98, 11444–11449 (2001).
321 Graus, D. *et al.* **High V-PPase activity is beneficial under high salt loads, but detrimental without salinity**. *New Phytol* 219, 1421-1432, doi:10.1111/nph.15280 (2018).
322 Apse, M. P. *et al.* **Salt tolerance conferred by overexpression of a vacuolar Na^+/H^+ antiport in *Arabidopsis***. *Science* 285, 1256-1258, doi:10.1126/science.285.5431.1256 (1999).
323 Quan, R. *et al.* **SCABP8/CBL10, a putative calcium sensor, interacts with the protein kinase SOS2 to protect *Arabidopsis* shoots from salt stress**. *Plant Cell* 19, 1415-1431, doi:10.1105/tpc.106.042291 (2007).
324 Weinl, S. & Kudla, J. **The CBL-CIPK Ca^{2+}-decoding signaling network: function and perspectives**. *New Phytologist* 184, 517-528 (2009).
325 Bassil, E. *et al.* **The *Arabidopsis* Na^+/H^+ antiporters NHX1 and NHX2 control vacuolar pH and K^+ homeostasis to regulate growth, flower development, and reproduction**. *Plant Cell* 23, 3482-3497, doi:10.1105/tpc.111.089581 (2011).
326 Yin, X. *et al.* **The protein kinase complex CBL10-CIPK8-SOS1 functions in *Arabidopsis* to regulate salt tolerance**. *J Exp Bot* 71, 1801-1814, doi:10.1093/jxb/erz549 (2020).
327 Robinson, M. F. *et al.* **How can stomata contribute to salt tolerance?** . *Annals of Botany* 80, 387–393 (1997).
328 Yue, Y. *et al.* **SOS1 gene overexpression increased salt tolerance in transgenic tobacco by maintaining a higher K^+/Na^+ ratio**. *J Plant Physiol* 169, 255-261, doi:10.1016/j.jplph.2011.10.007 (2012).
329 Deng, Y. Q. *et al.* **Exogenous hydrogen sulfide alleviates salt stress in wheat seedlings by decreasing Na+ content**. *Plant Growth Regulation* 79, 391-399, doi:10.1007/s10725-015-0143-x (2015).
330 Sun, T. J. *et al.* **A Glycine max sodium/hydrogen exchanger enhances salt tolerance through maintaining higher Na^+ efflux rate and K^+/Na^+ ratio in *Arabidopsis***. *BMC Plant Biol* 19, 469, doi:10.1186/s12870-019-2084-4 (2019).
331 Sun, H. *et al.* **Advances in salt tolerance molecular mechanism in tobacco plants**. *Hereditas* 157, 5, doi:10.1186/s41065-020-00118-0 (2020).
332 Maathuis, F. J. *et al.* **Regulation of Na^+ fluxes in plants**. *Front Plant Sci* 5, 467, doi:10.3389/fpls.2014.00467 (2014).
333 Franco-Navarro, J. D. *et al.* **Chloride as a macronutrient increases water-use efficiency by anatomically driven reduced stomatal conductance and increased mesophyll diffusion to CO2**. *Plant J* 99, 815-831, doi:10.1111/tpj.14423 (2019).
334 Storey, R. & Walker, R. R. **Citrus and salinity**. *Scientia Horticulturae* 78, 39-81 (1999).
335 Kuchitsu, K. *et al.* **Transient Cytoplasmic pH Change and Ion Fluxes through the Plasma Membrane in Suspension-Cultured Rice Cells Triggered by NAcetylchitooligosaccharide Elicitor**. *Plant Cell Physiol.* 38, 1012-1018 (1997).
336 Blume, B. *et al.* **Receptor-mediated increase in cytoplasmic free calcium required for activation of pathogen defense in parsley**. *Plant Cell* 12, 1425-1440, doi:10.1105/tpc.12.8.1425 (2000).
337 Grabov, A. & Blatt, M. R. **Co-ordination of signalling elements in guard cell ion channel control**. *Journal of Experimental Botany* 49, 351–360 (1998).
338 Blatt, M. R. **HORMONAL CONTROL OF ION CHAN L GATING**. *Annu. Rev. Plant Physiol. Plant Mol. BioI.* 44, 543--567 (1993).

339 Li, K. *et al.* **An optimized genetically encoded dual reporter for simultaneous ratio imaging of Ca^{2+} and H^{+} reveals new insights into ion signaling in plants**. *New Phytol* 230, 2292-2310, doi:10.1111/nph.17202 (2021).
340 Hepler, P. K. **The Cytoskeleton and Its Regulation by Calcium and Protons**. *Plant Physiol* 170, 3-22, doi:10.1104/pp.15.01506 (2016).
341 Choi, W. G. *et al.* **Orchestrating rapid long-distance signaling in plants with Ca^{2+} , ROS and electrical signals**. *Plant J* 90, 698-707, doi:10.1111/tpj.13492 (2017).
342 Marcec, M. J. *et al.* **Mutual interplay of Ca^{2+} and ROS signaling in plant immune response**. *Plant Sci* 283, 343-354, doi:10.1016/j.plantsci.2019.03.004 (2019).
343 Kumari, A. *et al.* ***Arabidopsis*** **H^{+}-ATPase AHA1 controls slow wave potential duration and wound-response jasmonate pathway activation**. *Proc Natl Acad Sci U S A* 116, 20226-20231, doi:10.1073/pnas.1907379116 (2019).
344 Shao, Q. *et al.* **Two glutamate- and pH-regulated Ca^{2+} channels are required for systemic wound signaling in *Arabidopsis***. *Sci Signal* 13, eaba1453, doi:10.1126/scisignal.aba1453 (2020).
345 Gilroy, S. *et al.* **ROS, Calcium, and Electric Signals: Key Mediators of Rapid Systemic Signaling in Plants**. *Plant Physiol* 171, 1606-1615, doi:10.1104/pp.16.00434 (2016).
346 Choi, W. G. *et al.* **Rapid, Long-Distance Electrical and Calcium Signaling in Plants**. *Annu Rev Plant Biol* 67, 287-307, doi:10.1146/annurev-arplant-043015-112130 (2016).
347 Westphal, L. *et al.* **pH effects on plant calcium fluxes: lessons from acidification-mediated calcium elevation induced by the gamma-glutamyl-leucine dipeptide identified from Phytophthora infestans**. *Sci Rep* 9, 4733, doi:10.1038/s41598-019-41276-0 (2019).
348 Kinoshita, T. *et al.* **Cytosolic concentration of Ca^{2+} regulates the plasma membrane H^{+}-ATPase in guard cells of *Fava Bean***. *Plant Cell* 7, 1333-1342, doi:10.1105/tpc.7.8.1333 (1995).
349 Nguyen, C. T. *et al.* **Identification of cell populations necessary for leaf-to-leaf electrical signaling in a wounded plant**. *Proc Natl Acad Sci U S A* 115, 10178-10183, doi:10.1073/pnas.1807049115 (2018).
350 Nour-Eldin, H. H. *et al.* **Advancing uracil-excision based cloning towards an ideal technique for cloning PCR fragments**. *Nucleic Acids Res* 34, e122, doi:10.1093/nar/gkl635 (2006).
351 Wen, W. *et al.* **Identification of a signal for rapid export of proteins from the nucleus**. *Cell* 82, 463-473, doi:10.1016/0092-8674(95)90435-2 (1995).
352 Matsushita, T. *et al.* **Dimers of the N-terminal domain of phytochrome B are functional in the nucleus**. *Nature* 424, 571-574, doi:10.1038/nature01837 (2003).
353 Fukuda, M. *et al.* **Cytoplasmic localization of mitogen-activated protein kinase kinase directed by its NH2-terminal, leucine-rich short amino acid sequence, which acts as a nuclear export signal**. *J Biol Chem* 271, 20024-20028, doi:10.1074/jbc.271.33.20024 (1996).
354 Kim, J. H. *et al.* **High cleavage efficiency of a 2A peptide derived from porcine teschovirus-1 in human cell lines, zebrafish and mice**. *PLoS One* 6, e18556, doi:10.1371/journal.pone.0018556 (2011).
355 Krylova, I. *et al.* **A versatile, bar-coded nuclear marker/reporter for live cell fluorescent and multiplexed high content imaging**. *PLoS One* 8, e63286, doi:10.1371/journal.pone.0063286 (2013).
356 Twell, D. *et al.* **Promoter analysis of genes that are coordinately expressed during pollen development reveals pollen-specific enhancer sequences and shared regulatory elements**. *Genes Dev* 5, 496-507, doi:10.1101/gad.5.3.496 (1991).
357 Clough, S. J. & Bent, A. F. **Floral dip: a simplified method for Agrobacterium-mediated transformation of *Arabidopsis thaliana***. *Plant J* 16, 735-743, doi:10.1046/j.1365-313x.1998.00343.x (1998).
358 Becker, D. *et al.* **AtTPK4, an *Arabidopsis* tandem-pore K^{+} channel, poised to control the pollen membrane voltage in a pH- and Ca^{2+}-dependent manner**. *Proc Natl Acad Sci U S A* 101, 15621-15626, doi:10.1073/pnas.0401502101 (2004).

359 Liland, K. H. *et al.* **Optimal choice of baseline correction for multivariate calibration of spectra**. *Appl Spectrosc* 64, 1007-1016, doi:10.1366/000370210792434350 (2010).
360 Roesch, A. & Schmidbauer, H. **WaveletComp: Computational Wavelet Analysis. R package version 1.1**. *https://CRAN.R-project.org/package=WaveletComp* (2018).
361 Shen, J. *et al.* **Organelle pH in the *Arabidopsis* endomembrane system**. *Mol Plant* 6, 1419-1437, doi:10.1093/mp/sst079 (2013).
362 Brummer, B. *et al.* **Evidence that acid solutions induce plant cell elongation by acidifying the cytosol and stimulating the proton pump**. *FEBS Letters* 174, 223-227, doi:10.1016/0014-5793(84)81162-x (1984).
363 Wall, K. P. *et al.* **Fluorescence quantum yield measurements of fluorescent proteins: a laboratory experiment for a biochemistry or molecular biophysics laboratory course**. *Biochem Mol Biol Educ* 43, 52-59, doi:10.1002/bmb.20837 (2015).
364 Hanson, R. M. & Koehler, H. R. **GFP imaging: methodology and application to investigate cellular compartmentation in plants**. *Journal of Experimental Botany* 52, 529-539 (2001).
365 Holdaway-Clarke, T. L. *et al.* **Effect of extracellular calcium, pH and borate on growth oscillations in Lilium formosanum pollen tubes**. *J Exp Bot* 54, 65-72, doi:10.1093/jxb/erg004 (2003).
366 Winship, L. J. *et al.* **Perturbation Analysis of Calcium, Alkalinity and Secretion during Growth of Lily Pollen Tubes**. *Plants (Basel)* 6, 3, doi:10.3390/plants6010003 (2016).
367 Torrence, C. & Compo, G. P. **A Practical Guide to Wavelet Analysis**. *Bulletin of the American Meteorological Society* 79, 61-78 (1998).
368 Weisenseel, M. H. & Jaffe, L. F. **Major growth current through Lily pollen tubes enters as K^+ and leaves as H^+**. *Planta* 133, 1-7 (1977).
369 Zhou, Y. *et al.* **Optogenetic control of plant growth by a microbial rhodopsin**. *Nat Plants* 7, 144-151, doi:10.1038/s41477-021-00853-w (2021).
370 Waadt, R. *et al.* **Multiparameter imaging of calcium and abscisic acid and high-resolution quantitative calcium measurements using R-GECO1-mTurquoise in *Arabidopsis***. *New Phytol* 216, 303-320, doi:10.1111/nph.14706 (2017).
371 Lind, C. *et al.* **Stomatal guard cells co-opted an ancient ABA-dependent desiccation survival system to regulate stomatal closure**. *Curr Biol* 25, 928-935, doi:10.1016/j.cub.2015.01.067 (2015).
372 Pei, Z. M. & Kuchitsu, K. **Early ABA Signaling Events in Guard Cells**. *Journal of Plant Growth Regulation* 24, 296-307, doi:10.1007/s00344-005-0095-x (2005).
373 Pantin, F. *et al.* **The dual effect of abscisic acid on stomata**. *New Phytol* 197, 65-72, doi:10.1111/nph.12013 (2013).
374 Brauer, D. *et al.* **Selective accumulation of the fluorescent pH indicator,BCECF, in vacuoles of *Maize* root-hair cells**. *Journal of Plant Physiology* 145, 57-61, doi:10.1016/s0176-1617(11)81846-8 (1995).
375 Zhang, X. *et al.* **Hydrogen peroxide-induced changes in intracellular pH of guard cells precede stomatal closure**. *Cell Res* 11, 37-43, doi:10.1038/sj.cr.7290064 (2001).
376 Wu, F. *et al.* **Hydrogen peroxide sensor HPCA1 is an LRR receptor kinase in *Arabidopsis***. *Nature* 578, 577-581, doi:10.1038/s41586-020-2032-3 (2020).
377 Rea, A. C. **Say "Ah!" The right amounts of brassinosteroids and hydrogen peroxide open the "Mouths" of plant leaves**. *Plant Cell* 32, 795-796, doi:10.1105/tpc.20.00125 (2020).
378 Xue, S. *et al.* **Central functions of bicarbonate in S-type anion channel activation and OST1 protein kinase in CO2 signal transduction in guard cell**. *EMBO J* 30, 1645-1658, doi:10.1038/emboj.2011.68 (2011).
379 Li, B. *et al.* **Transcriptional regulation of pattern-triggered immunity in plants**. *Cell Host Microbe* 19, 641-650, doi:10.1016/j.chom.2016.04.011 (2016).
380 Song, L. *et al.* **A transcription factor hierarchy defines an environmental stress response network**. *Science* 354, doi:10.1126/science.aag1550 (2016).

381 Tsuda, K. & Somssich, I. E. **Transcriptional networks in plant immunity**. *New Phytol* 206, 932-947, doi:10.1111/nph.13286 (2015).
382 Minguet-Parramona, C. *et al.* **An optimal frequency in Ca^{2+} oscillations for stomatal closure is an emergent property of ion transport in guard cells**. *Plant Physiol* 170, 33-42, doi:10.1104/pp.15.01607 (2016).
383 Kosuta, S. *et al.* **Differential and chaotic calcium signatures in the symbiosis signaling pathway of legumes**. *Proc Natl Acad Sci U S A* 105, 9823-9828, doi:10.1073/pnas.0803499105 (2008).
384 McAinsh, M. R. & Pittman, J. K. **Shaping the calcium signature**. *New Phytol* 181, 275-294, doi:10.1111/j.1469-8137.2008.02682.x (2009).
385 White, P. J. & Broadley, M. R. **Mechanisms of caesium uptake by plants.** . *New Phytologist* 147, 241–256 (2000).
386 Zhu, Y. G. & Smolders, E. **Plant uptake of radiocaesium: a review of mechanisms, regulation and application**. *J Exp Bot* 51, 1635-1645, doi:10.1093/jexbot/51.351.1635 (2000).
387 Xiong, T. C. *et al.* **Imaging long distance propagating calcium signals in intact plant leaves with the BRET-based GFP-aequorin reporter**. *Front Plant Sci* 5, 43, doi:10.3389/fpls.2014.00043 (2014).
388 Mahajan, S. *et al.* **Calcium- and salt-stress signaling in plants: shedding light on SOS pathway**. *Arch Biochem Biophys* 471, 146-158, doi:10.1016/j.abb.2008.01.010 (2008).
389 Duan, X. *et al.* **The transgene pyramiding tobacco with betaine synthesis and heterologous expression of AtNHX1 is more tolerant to salt stress than either of the tobacco lines with betaine synthesis or AtNHX1**. *Physiol Plant* 135, 281-295, doi:10.1111/j.1399-3054.2008.01194.x (2009).
390 Wang, H. *et al.* **A new Na^+/H^+ antiporter gene *Kv*NHX1 isolated from the halophyte *Kosteletzkya virginica* improves salt tolerance in transgenic tobacco**. *Biotechnology & Biotechnological Equipment* 32, 1378-1386, doi:10.1080/13102818.2018.1522972 (2018).
391 Yamaguchi, T. *et al.* **Vacuolar Na^+/H^+ antiporter cation selectivity is regulated by calmodulin from within the vacuole in a Ca^{2+}- and pH-dependent manner**. *Proc Natl Acad Sci U S A* 102, 16107-16112, doi:10.1073/pnas.0504437102 (2005).
392 Huang, F. *et al.* **Cytosolic and nucleosolic calcium signaling in response to osmotic and salt stresses are independent of each other in roots of *Arabidopsis* seedlings**. *Front Plant Sci* 8, 1648, doi:10.3389/fpls.2017.01648 (2017).
393 Hamamoto, S. *et al.* **HKT transporters mediate salt stress resistance in plants: from structure and function to the field**. *Current opinion in biotechnology* 32, 113-120, doi:10.1016/j.copbio.2014.11.025 (2015).
394 Charpentier, M. **Calcium Signals in the Plant Nucleus: Origin and Function**. *J Exp Bot* 69, 4165-4173, doi:10.1093/jxb/ery160 (2018).
395 Kelner, A. *et al.* **Dual color sensors for simultaneous analysis of calcium signal dynamics in the nuclear and cytoplasmic compartments of plant cells**. *Front Plant Sci* 9, 245, doi:10.3389/fpls.2018.00245 (2018).
396 Akerboom, J. *et al.* **Genetically encoded calcium indicators for multi-color neural activity imaging and combination with optogenetics**. *Front Mol Neurosci* 6, 2, doi:10.3389/fnmol.2013.00002 (2013).
397 Fricker, M. D. *et al.* **pH gradients are not associated with tip growth in pollen tubes of Lilium longiflorum**. *Journal of Cell Science* 110, 1729-1740 (1997).
398 Parton, R. M. *et al.* **Pronounced cytoplasmic pH gradients are not required for tip growth in plant and fungal cells**. *Journal of Cell Science* 110, 1187-1198 (1997).
399 Monshausen, G. B. *et al.* **Oscillations in extracellular pH and reactive oxygen species modulate tip growth of *Arabidopsis* root hairs**. *Proc Natl Acad Sci U S A* 104, 20996-21001, doi:10.1073/pnas.0708586104 (2007).
400 Taylor, A. R. *et al.* **A voltage-gated H^+ channel underlying pH homeostasis in calcifying coccolithophores**. *PLoS Biol* 9, e1001085, doi:10.1371/journal.pbio.1001085 (2011).

401 Taylor, A. R. *et al.* **Proton channels in algae: reasons to be excited**. *Trends Plant Sci* 17, 675-684, doi:10.1016/j.tplants.2012.06.009 (2012).
402 Camacho, L. & Malho, R. **Endo/exocytosis in the pollen tube apex is differentially regulated by Ca^{2+} and GTPases**. *Journal of Experimental Botany* 54, 83-92, doi:10.1093/jxb/erg043 (2003).
403 Jauh, G. Y. & Lord, E. M. **Localization of pectins and arabinogalactanproteins in lily (Lilium longiflorum L.) pollen tube and style, and their possible roles in pollination**. *Planta* 199 (1996).
404 Moustacas, A. M. *et al.* **Electrostatic effects and the dynamics of enzyme reactions at the surface of plant cells. 2. The role of pectin methyl esterase in the modulation of electrostatic effects in soybean cell walls.** *Eur. J. Biochem. 1* 155, 191–197 (1986).
405 Kaya, H. *et al.* **Ca^{2+}-activated reactive oxygen species production by *Arabidopsis* RbohH and RbohJ is essential for proper pollen tube tip growth**. *Plant Cell* 26, 1069-1080, doi:10.1105/tpc.113.120642 (2014).
406 Wudick, M. M. & Feijo, J. A. **At the intersection: merging Ca^{2+} and ROS signaling pathways in pollen**. *Mol Plant* 7, 1595-1597, doi:10.1093/mp/ssu096 (2014).
407 Homann, U. & Tester, M. **Ca^{2+}-independent and Ca^{2+}/GTP-binding protein-controlled exocytosis in a plant cell**. *Proc Natl Acad Sci U S A* 94, 6565-6570, doi:10.1073/pnas.94.12.6565 (1997).
408 Battey, N. H. *et al.* **Exocytosis and endocytosis**. *Plant Cell* 11, 643-660, doi:10.1105/tpc.11.4.643 (1999).
409 Vanýsek, P. **Ionic Conductivity and Diffusion at Infinite Dilution**. *CRC Hand Book of Chemistry and Physics*, 5-92 (1993).
410 Boudsocq, M. *et al.* **Characterization of *Arabidopsis* calcium-dependent protein kinases: activated or not by calcium?** *Biochem J* 447, 291-299, doi:10.1042/BJ20112072 (2012).
411 Lehmann, J. *et al.* **Acidosis-induced activation of anion channel SLAH3 in the flooding-related stress response of *Arabidopsis***. *Curr Biol* 31, 3575-3585 e3579, doi:10.1016/j.cub.2021.06.018 (2021).
412 Fan, L. M. *et al.* **Outward K^+ channels in Brassica chinensis pollen protoplasts are regulated by external and internal pH**. *Protoplasma* 220, 143-152, doi:10.1007/s00709-002-0037-4 (2003).
413 Fan, L. M. & Wu, W. H. **External pH regulates the inward K^+ channels in Brassica pollen protoplasts**. *Progress in Natural Science* 10, 68-73 (2000).
414 McAinsh, M. R. *et al.* **Visualizing Changes in Cytosolic-Free Ca^{2+} during the Response of Stomatal Guard Cells to Abscisic Acid**. *Plant Cell* 4, 1113-1122, doi:10.1105/tpc.4.9.1113 (1992).
415 Allen, G. J. *et al.* **Cameleon calcium indicator reports cytoplasmic calcium dynamics in *Arabidopsis* guard cells**. *Plant J* 19, 735-747, doi:10.1046/j.1365-313x.1999.00574.x (1999).
416 Suhita, D. *et al.* **Cytoplasmic alkalization precedes reactive oxygen species production during methyl jasmonate- and abscisic acid-induced stomatal closure**. *Plant Physiol* 134, 1536-1545, doi:10.1104/pp.103.032250 (2004).
417 Bigeard, J. & Hirt, H. **Nuclear Signaling of Plant MAPKs**. *Front Plant Sci* 9, 469, doi:10.3389/fpls.2018.00469 (2018).
418 Lee, J. *et al.* **Cellular reprogramming through mitogen-activated protein kinases**. *Front Plant Sci* 6, 940, doi:10.3389/fpls.2015.00940 (2015).
419 Toldsepp, K. *et al.* **Mitogen-activated protein kinases MPK4 and MPK12 are key components mediating CO2 -induced stomatal movements**. *Plant J* 96, 1018-1035, doi:10.1111/tpj.14087 (2018).
420 Lin, C. & Chen, S. **New functions of an old kinase MPK4 in guard cells**. *Plant Signal Behav* 13, e1477908, doi:10.1080/15592324.2018.1477908 (2018).
421 Marten, H. *et al.* **Silencing of NtMPK4 impairs CO-induced stomatal closure, activation of anion channels and cytosolic Casignals in Nicotiana tabacum guard cells**. *Plant J* 55, 698-708, doi:10.1111/j.1365-313X.2008.03542.x (2008).

422 Nishimura, N. *et al.* **PYR/PYL/RCAR family members are major in-vivo ABI1 protein phosphatase 2C-interacting proteins in *Arabidopsis***. *Plant J* 61, 290-299, doi:10.1111/j.1365-313X.2009.04054.x (2010).
423 Leube, M. P. *et al.* **ABI1 of *Arabidopsisis* a protein serine/threonine phosphatase highly regulated by the proton and magnesium ion concentration1**. *FEBS Letters* 424, 100-104, doi:10.1016/s0014-5793(98)00149-5 (1998).
424 Planes, M. D. *et al.* **A mechanism of growth inhibition by abscisic acid in germinating seeds of *Arabidopsis thaliana* based on inhibition of plasma membrane H^+-ATPase and decreased cytosolic pH, K^+, and anions**. *J Exp Bot* 66, 813-825, doi:10.1093/jxb/eru442 (2015).
425 Gao, X. Q. *et al.* **The dynamic changes of tonoplasts in guard cells are important for stomatal movement in *Vicia faba***. *Plant Physiol* 139, 1207-1216, doi:10.1104/pp.105.067520 (2005).
426 Baetz, U. *et al.* **Vacuolar Chloride Fluxes Impact Ion Content and Distribution during Early Salinity Stress**. *Plant Physiol* 172, 1167-1181, doi:10.1104/pp.16.00183 (2016).
427 Song, Y. *et al.* **Behind the scenes: the roles of reactive oxygen species in guard cells**. *New Phytol* 201, 1121-1140, doi:10.1111/nph.12565 (2014).
428 Kimura, S. *et al.* **Bound by Fate: The Role of Reactive Oxygen Species in Receptor-Like Kinase Signaling**. *Plant Cell* 29, 638-654, doi:10.1105/tpc.16.00947 (2017).
429 Demidchik, V. & Shabala, S. **Mechanisms of cytosolic calcium elevation in plants: the role of ion channels, calcium extrusion systems and NADPH oxidase-mediated 'ROS- Ca^{2+} Hub'**. *Funct Plant Biol* 45, 9-27, doi:10.1071/FP16420 (2018).
430 Geiger, D. *et al.* **Activity of guard cell anion channel SLAC1 is controlled by drought-stress signaling kinase-phosphatase pair**. *Proceedings of the National Academy of Sciences of the United States of America* 106, 21425-21430 (2009).
431 Maierhofer, T. *et al.* **Site- and kinase-specific phosphorylation-mediated activation of SLAC1, a guard cell anion channel stimulated by abscisic acid**. *Sci Signal* 7, ra86, doi:10.1126/scisignal.2005703 (2014).
432 Schulz-Lessdorf, B. *et al.* **GCAC1 recognizes the pH gradient across the plasma membrane: a pH-sensitive and ATP-dependent anion channel links guard cell membrane potential to acid and energy metabolism**. *The Plant Journal* 10 (6), 993-1004 (1996).
433 Takahashi, Y. *et al.* **MAP3Kinase-dependent SnRK2-kinase activation is required for abscisic acid signal transduction and rapid osmotic stress response**. *Nat Commun* 11, 12, doi:10.1038/s41467-019-13875-y (2020).
434 Han, J. P. *et al.* **Fine-tuning of RBOHF activity is achieved by differential phosphorylation and Ca^{2+} binding**. *New Phytol* 221, 1935-1949, doi:10.1111/nph.15543 (2019).
435 Okamoto, M. *et al.* **Activation of dimeric ABA receptors elicits guard cell closure, ABA-regulated gene expression, and drought tolerance**. *Proc Natl Acad Sci U S A* 110, 12132-12137, doi:10.1073/pnas.1305919110 (2013).
436 Mousavi, S. A. *et al.* **GLUTAMATE RECEPTOR-LIKE genes mediate leaf-to-leaf wound signalling**. *Nature* 500, 422-426, doi:10.1038/nature12478 (2013).
437 Toyota, M. *et al.* **Glutamate triggers long-distance, calcium-based plant defense signaling**. *Science* 361, 1112-1115, doi:10.1126/science.aat7744 (2018).
438 Felle, H. H. *et al.* **Root-to-shoot signalling: apoplastic alkalinization, a general stress response and defence factor in barley (*Hordeum vulgare*)**. *Protoplasma* 227, 17-24, doi:10.1007/s00709-005-0131-5 (2005).
439 Zimmermann, M. R. *et al.* **System potentials, a novel electrical long-distance apoplastic signal in plants, induced by wounding**. *Plant Physiol* 149, 1593-1600, doi:10.1104/pp.108.133884 (2009).
440 Gust, A. A. *et al.* **Bacteria-derived peptidoglycans constitute pathogen-associated molecular patterns triggering innate immunity in *Arabidopsis***. *J Biol Chem* 282, 32338-32348, doi:10.1074/jbc.M704886200 (2007).

441 Mathieu, Y. *et al.* **Cytoplasmic acidification as an early phosphorylation-dependent response of tobacco cells to elicitors**. *Planta* 199, 416-424, doi:10.1007/bf00195734 (1996).
442 Lapous, D. *et al.* **Increase of defense gene transcripts by cytoplasmic acidification in tobacco cell suspensions**. *Planta* 205, 452-458, doi:10.1007/s004250050343 (1998).
443 Lager, I. *et al.* **Changes in external pH rapidly alter plant gene expression and modulate auxin and elicitor responses**. *Plant Cell Environ* 33, 1513-1528, doi:10.1111/j.1365-3040.2010.02161.x (2010).
444 Kim, S. *et al.* **Ca^{2+}-regulated Ca^{2+} channels with an RCK gating ring control plant symbiotic associations**. *Nat Commun* 10, 3703, doi:10.1038/s41467-019-11698-5 (2019).
445 Donahue, B. S. & Abercrombie, R. F. **Free diffusion coefficient of ionic calcium in cytoplasm**. *Cell Calcium* 8, 437-448, doi:10.1016/0143-4160(87)90027-3 (1987).
446 Geiger, D. *et al.* **Guard cell anion channel SLAC1 is regulated by CDPK protein kinases with distinct Ca^{2+} affinities**. *Proc Natl Acad Sci U S A* 107, 8023-8028, doi:10.1073/pnas.0912030107 (2010).
447 Tena, G. *et al.* **Protein kinase signaling networks in plant innate immunity**. *Curr Opin Plant Biol* 14, 519-529, doi:10.1016/j.pbi.2011.05.006 (2011).
448 Sze, H. **H^+-translocating ATPases of the plasma membrane and tonoplast of plant cells**. *Physiologia Plantarum* 61, 683-691, doi:10.1111/j.1399-3054.1984.tb05191.x (1984).
449 Luo, H. *et al.* **The two major types of plant plasma membrane H^+-ATPases show different enzymatic properties and confer differential pH sensitivity of yeast growth**. *Plant Physiology* 119, 627-634, doi:10.1104/pp.119.2.627 (1999).
450 Viotti, C. *et al.* **Characterization of the interaction between the plasma membrane H-ATPase of *Arabidopsis thaliana* and a novel interactor (PPI1)**. *FEBS J* 272, 5864-5871, doi:10.1111/j.1742-4658.2005.04985.x (2005).
451 Steinhorst, L. & Kudla, J. **Calcium and reactive oxygen species rule the waves of signaling**. *Plant Physiol* 163, 471-485, doi:10.1104/pp.113.222950 (2013).
452 Evans, M. J. *et al.* **A ROS-Assisted Calcium Wave Dependent on the AtRBOHD NADPH Oxidase and TPC1 Cation Channel Propagates the Systemic Response to Salt Stress**. *Plant Physiol* 171, 1771-1784, doi:10.1104/pp.16.00215 (2016).
453 Choi, H. I. *et al.* ***Arabidopsis* calcium-dependent protein kinase AtCPK32 interacts with ABF4, a transcriptional regulator of abscisic acid-responsive gene expression, and modulates its activity**. *Plant Physiol* 139, 1750-1761, doi:10.1104/pp.105.069757 (2005).
454 Rucha, K. **Functional characterization of calcium dependent protein kinase 32 from *Arabidopsis***. *All Dissertations* Paper 455 (2009).
455 Harada, A. & Shimazaki, K. **Measurement of changes in cytosolic Ca^{2+} in *Arabidopsis* guard cells and mesophyll cells in response to blue light**. *Plant Cell Physiol* 50, 360-373, doi:10.1093/pcp/pcn203 (2009).
456 Martí, M. C. *et al.* **Cell- and stimulus type-specific intracellular free Ca^{2+} signals in *Arabidopsis***. *Plant Physiology* 163, 625-634, doi:10.1104/pp.113.222901 (2013).
457 Ranf, S. *et al.* **Interplay between calcium signalling and early signalling elements during defence responses to microbe- or damage-associated molecular patterns**. *Plant J* 68, 100-113, doi:10.1111/j.1365-313X.2011.04671.x (2011).
458 Yang, Y. *et al.* **Isolation of a strong *Arabidopsis* guard cell promoter and its potential as a research tool**. *Plant Methods* 4, 6, doi:10.1186/1746-4811-4-6 (2008).
459 Cho, D. *et al.* **De-regulated expression of the plant glutamate receptor homolog AtGLR3.1 impairs long-term Ca^{2+}-programmed stomatal closure**. *Plant J* 58, 437-449, doi:10.1111/j.1365-313X.2009.03789.x (2009).
460 Mott, K. A. & Buckley, T. N. **Patchy stomatal conductance: emergent collective behaviour of stomata**. *Trends Plant Sci* 5, 258-262, doi:10.1016/s1360-1385(00)01648-4 (2000).
461 Mott, K. A. & Peak, D. **Stomatal patchiness and task-performing networks**. *Ann Bot* 99, 219-226, doi:10.1093/aob/mcl234 (2007).

462 Felle, H. **Cytoplasmic free calcium in Riccia fluitans L. and Zea mays L.: Interaction of Ca^{2+} and pH?** *Planta* 176, 248-255, doi:10.1007/BF00392452 (1988).
463 Cho, D. *et al.* **Vacuolar CAX1 and CAX3 influence auxin transport in guard cells via regulation of apoplastic pH**. *Plant Physiol* 160, 1293-1302, doi:10.1104/pp.112.201442 (2012).
464 Costa, A. *et al.* **The contribution of organelles to plant intracellular Calcium signalling**. *J Exp Bot* 69, 4175-4193, doi:10.1093/jxb/ery185 (2018).
465 Hocking, B. *et al.* **Heterodimerization of *Arabidopsis* calcium/proton exchangers contributes to regulation of guard cell dynamics and plant defense responses**. *J Exp Bot* 68, 4171-4183, doi:10.1093/jxb/erx209 (2017).
466 Eisenach, C. & De Angeli, A. **Ion transport at the vacuole during stomatal movements**. *Plant Physiol* 174, 520-530, doi:10.1104/pp.17.00130 (2017).
467 Siegel, R. S. *et al.* **Calcium elevation-dependent and attenuated resting calcium-dependent abscisic acid induction of stomatal closure and abscisic acid-induced enhancement of calcium sensitivities of S-type anion and inward-rectifying K channels in *Arabidopsis* guard cells**. *Plant J* 59, 207-220, doi:10.1111/j.1365-313X.2009.03872.x (2009).
468 Konrad, K. R. a. H., R. **The use of voltage-sensitive dyes to monitor signal-induced changes in membrane potential - ABA triggered membrane depolarization in guard cells**. *Plant Journal* 55, 161-173 (2008).
469 Hubbard, K. E. *et al.* **Abscisic acid and CO2 signalling via calcium sensitivity priming in guard cells, new CDPK mutant phenotypes and a method for improved resolution of stomatal stimulus-response analyses**. *Ann Bot* 109, 5-17, doi:10.1093/aob/mcr252 (2012).
470 Laanemets, K. *et al.* **Calcium-dependent and -independent stomatal signaling network and compensatory feedback control of stomatal opening via Ca^{2+} sensitivity priming**. *Plant Physiol* 163, 504-513, doi:10.1104/pp.113.220343 (2013).
471 Kong, D. *et al.* **L-Met Activates *Arabidopsis* GLR Ca^{2+} Channels Upstream of ROS Production and Regulates Stomatal Movement**. *Cell reports* 17, 2553-2561, doi:10.1016/j.celrep.2016.11.015 (2016).
472 Zhai, J. *et al.* **Ca^{2+}/H^{+} exchange in the plasma membrane of *Arabidopsis thaliana* leaves**. *Acta Physiologiae Plantarum* 35, 161-173, doi:10.1007/s11738-012-1059-y (2012).
473 Conn, S. J. *et al.* **Cell-specific vacuolar calcium storage mediated by CAX1 regulates apoplastic calcium concentration, gas exchange, and plant productivity in *Arabidopsis***. *Plant Cell* 23, 240-257, doi:10.1105/tpc.109.072769 (2011).
474 Pittman, J. K. *et al.* **Evidence of differential pH regulation of the *Arabidopsis* vacuolar Ca^{2+}/H+ antiporters CAX1 and CAX2**. *FEBS Lett* 579, 2648-2656, doi:10.1016/j.febslet.2005.03.085 (2005).
475 Shimazaki, K. *et al.* **Involvement of calmodulin and calmodulin-dependent myosin light chain kinase in blue light-dependent H^{+} pumping by guard cell protoplasts from *Vicia faba* L**. *Plant Physiol* 99, 1416-1421, doi:10.1104/pp.99.4.1416 (1992).
476 Huang, S. *et al.* **Optogenetic control of the guard cell membrane potential and stomatal movement by the light-gated anion channel *Gt*ACR1**. *Sci Adv* 7, doi:10.1126/sciadv.abg4619 (2021).
477 Colcombet, J. *et al.* **Distinct pH regulation of slow and rapid anion channels at the plasma membrane of *Arabidopsis thaliana* hypocotyl cells**. *J Exp Bot* 56, 1897-1903, doi:10.1093/jxb/eri184 (2005).
478 Wang, Y. & Wu, W. H. **Regulation of potassium transport and signaling in plants**. *Curr Opin Plant Biol* 39, 123-128, doi:10.1016/j.pbi.2017.06.006 (2017).
479 Hirschi, K. D. **Expression of *Arabidopsis* CAX1 in tobacco: altered calcium homeostasis and increased stress sensitivity**. *Plant Cell* 11, 2113-2122, doi:10.1105/tpc.11.11.2113 (1999).
480 Qi, Z. *et al.* **The high affinity K^{+} transporter AtHAK5 plays a physiological role in planta at very low K^{+} concentrations and provides a caesium uptake pathway in *Arabidopsis***. *J Exp Bot* 59, 595-607, doi:10.1093/jxb/erm330 (2008).

481 Pick, U. **The interaction of vanadate ions with the Ca-ATPase from sarcoplasmic reticulum**. *J Biol Chem* 257, 6111-6119, doi:10.1016/s0021-9258(20)65113-4 (1982).
482 Holzheu, P. *et al.* **An integrative view on vacuolar pH homeostasis in *Arabidopsis thaliana*: Combining mathematical modeling and experimentation**. *Plant J* 106, 1541-1556, doi:10.1111/tpj.15251 (2021).
483 Bassil, E. *et al.* **Cation Specificity of Vacuolar NHX-Type Cation/H^+ Antiporters**. *Plant Physiol* 179, 616-629, doi:10.1104/pp.18.01103 (2019).
484 Sanders, D. **The mechanism of Cl^- transport at the plasma membrane of *Chara corallina*.1. Cotransport with H^+**. *Journal of Membrane Biology* 53, 129-141 (1980).
485 Razavizadeh, R. *et al.* **Proteome analysis of tobacco leaves under salt stress**. *Peptides* 30, 1651-1659, doi:10.1016/j.peptides.2009.06.023 (2009).
486 Very, A. A. *et al.* **Molecular biology of K^+ transport across the plant cell membrane: what do we learn from comparison between plant species?** *J Plant Physiol* 171, 748-769, doi:10.1016/j.jplph.2014.01.011 (2014).
487 Shabala, S. **Ionic and osmotic components of salt stress specifically modulate net ion fluxes from bean leaf mesophyll**. *Plant, Cell & Environment* 23, 825-837, doi:10.1046/j.1365-3040.2000.00606.x (2001).
488 Jayakannan, M. *et al.* **Salicylic acid improves salinity tolerance in *Arabidopsis* by restoring membrane potential and preventing salt-induced K^+ loss via a GORK channel**. *J Exp Bot* 64, 2255-2268, doi:10.1093/jxb/ert085 (2013).
489 Nieves-Cordones, M. *et al.* **Uneven HAK/KUP/KT Protein Diversity Among Angiosperms: Species Distribution and Perspectives**. *Front Plant Sci* 7, 127, doi:10.3389/fpls.2016.00127 (2016).
490 Cherel, I. & Gaillard, I. **The Complex Fine-Tuning of K^+ Fluxes in Plants in Relation to Osmotic and Ionic Abiotic Stresses**. *Int J Mol Sci* 20, doi:10.3390/ijms20030715 (2019).
491 Fricke, W. *et al.* **Rapid and tissue-specific changes in ABA and in growth rate in response to salinity in barley leaves**. *J Exp Bot* 55, 1115-1123, doi:10.1093/jxb/erh117 (2004).
492 Duan, L. *et al.* **Endodermal ABA signaling promotes lateral root quiescence during salt stress in *Arabidopsis* seedlings**. *Plant Cell* 25, 324-341, doi:10.1105/tpc.112.107227 (2013).
493 Li, H. *et al.* **The plant ESCRT component FREE1 shuttles to the nucleus to attenuate abscisic acid signalling**. *Nat Plants* 5, 512-524, doi:10.1038/s41477-019-0400-5 (2019).
494 Behera, S. *et al.* **Analyses of Ca^{2+} dynamics using a ubiquitin-10 promoter-driven Yellow Cameleon 3.6 indicator reveal reliable transgene expression and differences in cytoplasmic Ca^{2+} responses in *Arabidopsis* and rice (*Oryza sativa*) roots**. *New Phytol* 206, 751-760, doi:10.1111/nph.13250 (2015).
495 Corso, M. *et al.* **Endoplasmic reticulum-localized CCX2 is required for osmotolerance by regulating ER and cytosolic Ca^{2+} dynamics in *Arabidopsis***. *Proc Natl Acad Sci U S A* 115, 3966-3971, doi:10.1073/pnas.1720422115 (2018).
496 Jeon, B. W. *et al.* **The *Arabidopsis* heterotrimeric G-protein beta subunit, AGB1, is required for guard cell calcium sensing and calcium-induced calcium release**. *Plant J*, doi:10.1111/tpj.14318 (2019).
497 Jiang, Z. *et al.* **Plant cell-surface GIPC sphingolipids sense salt to trigger Ca^{2+} influx**. *Nature* 572, 341-346, doi:10.1038/s41586-019-1449-z (2019).
498 Véry, A. A. & Davies, J. M. **Hyperpolarization-activated calcium channels at the tip of *Arabidopsis* root hairs.** . *Proc Natl Acad Sci USA* 97, 9801–9806 (2000).
499 Seifikalhor, M. *et al.* **Calcium signaling and salt tolerance are diversely entwined in plants**. *Plant Signal Behav* 14, 1665455, doi:10.1080/15592324.2019.1665455 (2019).
500 Zhang, H. X. & Blumwald, E. **Transgenic salt-tolerant tomato plants accumulate salt in foliage but not in fruit**. *Nat Biotechnol* 19, 765-768, doi:10.1038/90824 (2001).

501 Leshem, Y. *et al.* **Suppression of *Arabidopsis* vesicle-SNARE expression inhibited fusion of H_2O_2-containing vesicles with tonoplast and increased salt tolerance**. *Proc Natl Acad Sci U S A* 103, 18008-18013, doi:10.1073/pnas.0604421103 (2006).

9 Appendix

9.1 Supplement Figures

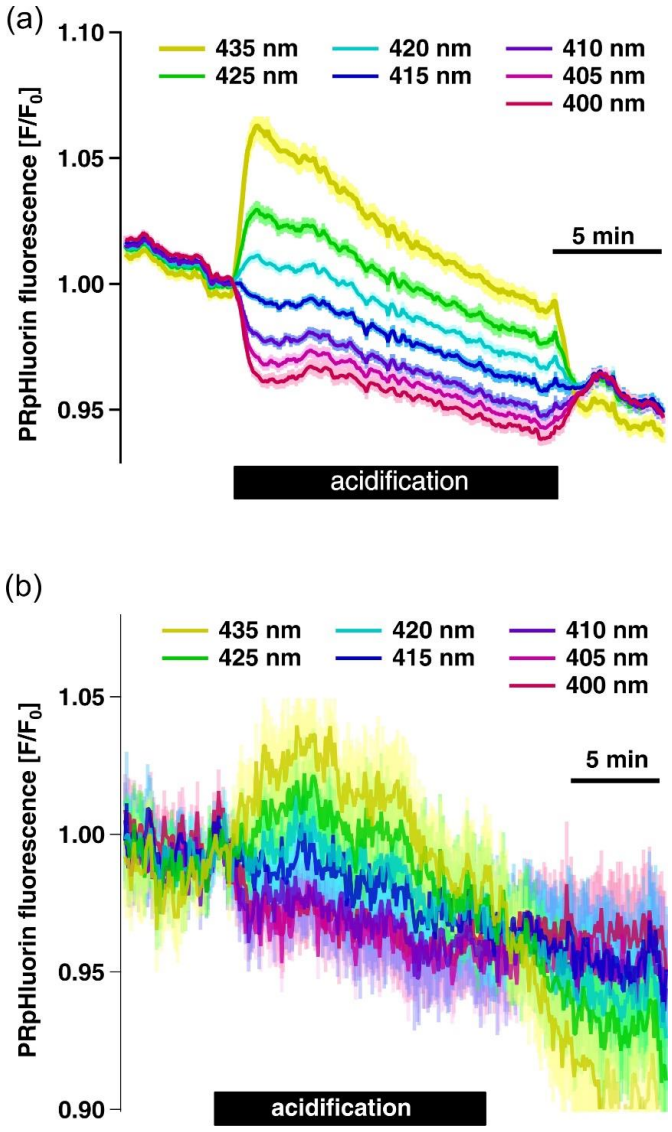

Figure S1. PRpHluorin isosbesitc point verification in guard cells and pollen tubes stably expressing CapHensor.

The fluorescence of PRpHluorin is shown in guard cells (a, n = 50) and pollen tubes (b, n = 16) in response to acidification induced by 5 mM or 2 mM HAc, respectively when excited at different wavelengths shown by colors. Error bars = SE.

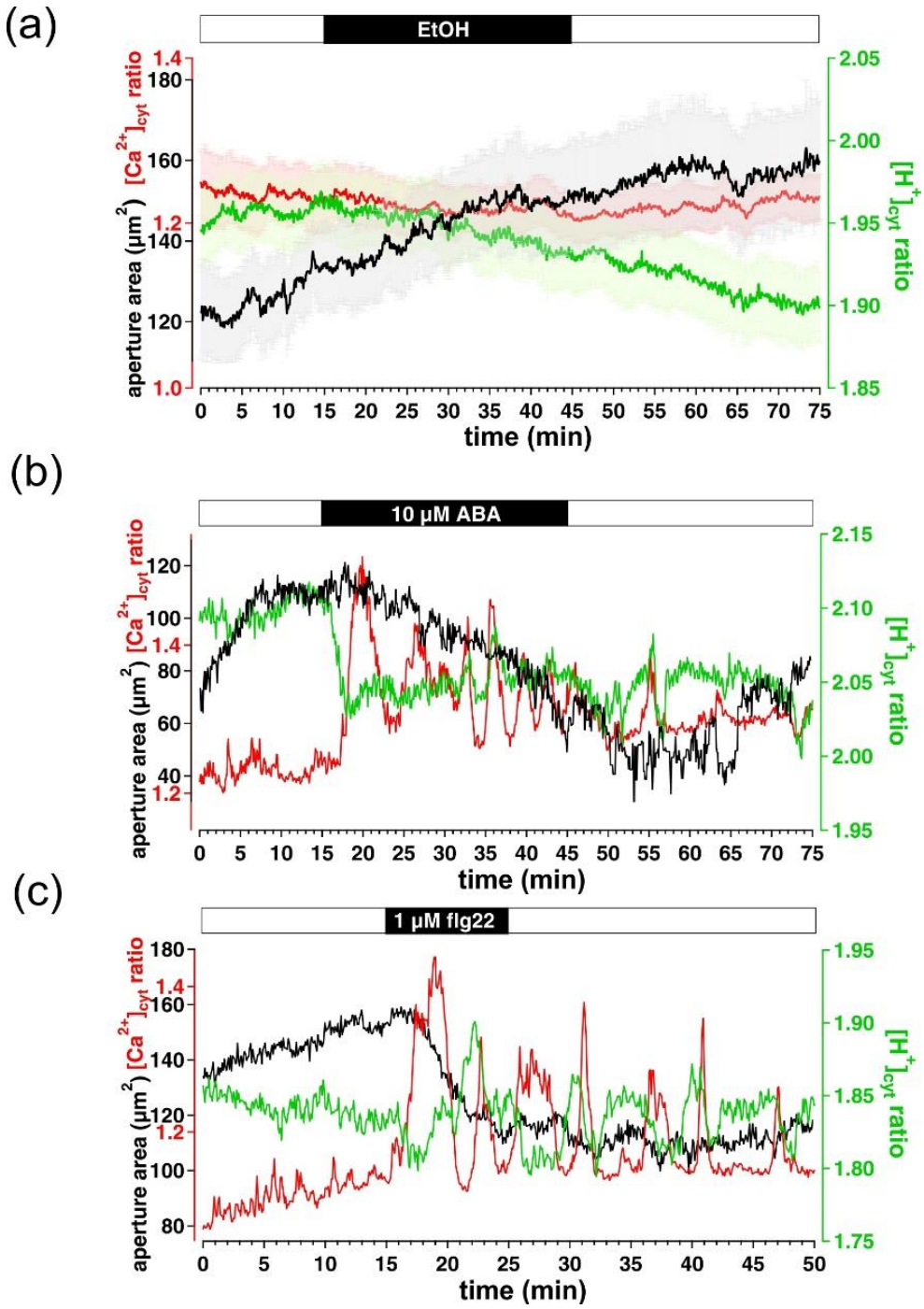

Figure S2. $[Ca^{2+}]_{cyt}$, $[H^+]_{cyt}$ regimes and stomatal movement in individual guard cells in response to EtOH, ABA and flg22.

Live-cell imaging of $[Ca^{2+}]_{cyt}$ and $[H^+]_{cyt}$ over time together with stomata aperture monitoring in guard cells stably expressing CapHensor in the cytosol. (a) Mean $[Ca^{2+}]_{cyt}$ ratio (red), $[H^+]_{cyt}$ ratio (green) and stomatal aperture area (black) in response to 0.005 % EtOH (n = 16), corresponding to the amount when applied 10 µM ABA. (b-c) Mean $[Ca^{2+}]_{cyt}$ ratio (red), $[H^+]_{cyt}$ ratio (green) and stomatal aperture area (black) in single representative guard cell when challenged with (b) 10 µM ABA, (c) 1 µM flg22.

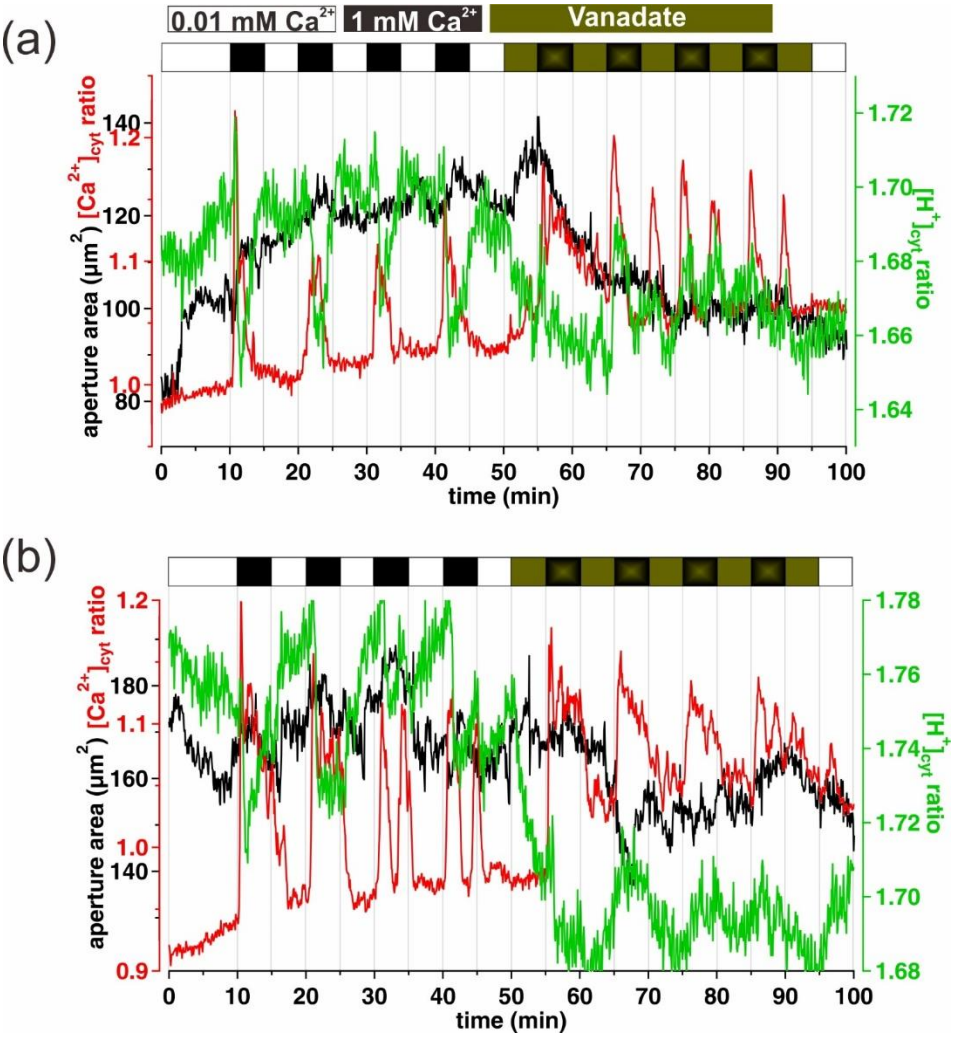

Figure S3. $[Ca^{2+}]_{cyt}$ and $[H^+]_{cyt}$ interactions in individual guard cells induced by high $CaCl_2$ are reversed in the presense of vanadate.

(a, b) $[Ca^{2+}]_{cyt}$ ratio (red), $[H^+]_{cyt}$ ratio (green) and aperture area (black) of two representative *N. tabacum* guard cells stably expressing CapHensor in the cytosol perfused from 10 μM $CaCl_2$ to 1 mM $CaCl_2$ without and with 100 μM vanadate (Na_3VO_4). The negative correlated $[Ca^{2+}]_{cyt}$ and $[H^+]_{cyt}$ relationship triggered by external increased $CaCl_2$ concentration are converted to be positive relations and stomata close when 100 μM vanadate exists. The bars upon the graph are treatments marked by relative colors.

9.3 Abbreviations

HAc	Acetic acid
ABA	Abscisic acid
AtNHX1	*Aradibopsis thaliana* Na^+/H^+ antiporter at the tonoplast
BAS	Bovine serum albumin
BTA	Butyric acid
BTP	Bis-tris propane, or 1,3-bis(tris(hydroxymethyl)methylamino)propane
Ca^{2+}	Calcium ion
$[Ca^{2+}]_{cyt}$	Cytosolic Ca^{2+} concentration
$[Ca^{2+}]_{nuc}$	Nuclear Ca^{2+} concentration
Cs^+	Cesium ion
CsCl	Cesium chloride
dNTP	Deoxynucleotide triphosphate
EDTA	Ethylenediaminetetraacetic acid
EtOH	Ethanol
flg22	Flagellin 22
GFP	Green fluorescent protein
H_2O_2	Hydrogen peroxide
H^+	Proton ion
$[H^+]_{cyt}$	Cytosolic H^+ concentration
$[H^+]_{nuc}$	Nuclear H^+ concentration
$[H^+]_{vac}$	Vaculoar H^+ concentration
H_3BO_4	Boric acid
KOH	Potassium hydroxide
KH_2PO_4	Monopotassium phosphate
LB	Lysogeny Broth
MES	2-(N-morpholino)ethanesulfonic acid
mM	Milli mole

MS medium	Murashige and Skoog medium
MΩ	Mega ohm
NaAc	Sodium acetate
NaClO	Sodium hypochloride
NaOH	Sodium hydroxide
Na_3VO_4	Sodium vanadate
NES	Nuclear export sequence
NLS	Nuclear localization sequence
SDS	Sodium dodecyl sulfate
SOC medium	Super Optimal broth with Catabolite repression
Tris	Tris(hydroxymethyl)aminomethane
µl min^{-1}	Micro liter per minute
µM	Micro mole
μm^2	square micrometers
μm^2/min	square micrometers per minute
V_m	Membrane potential
YEB	Yeast Extract Beef
YFP	Yellow fluorescent protein

Acknowledgements

Four years have passed by so fast. I am very happy here. During my PhD study, I am very grateful to the people who have been in my life and who have made me grow.

First of all, I would like to show my great appreciation to my supervisor, Dr. Kai Robert Konrad, who gave me a lot of guidance on science and helped me solve problems related to experiments and writing. With lots of discussions regardless of experimental results, problems or papers, he always gave me suggestive help. I appreciate that he gave me lots of freedom to explore science and always to be open to discussions. Also, I am very grateful for his help and revision on my writing, which has improved my English writing skills a lot.

I am very grateful to my supervisors Prof. Dr. Dirk Becker and PD. Dr. Frank Waller, who were tutors of my defense committee. Thanks to them for participating in my start-up report and annual presentations during my PhD study. I appreciate their brilliant scientific research advice, which made my research running more smoothly. I am also grateful for their revision and guidance of my doctoral dissertation.

Thanks to Prof. Dr. Rainer Hedrich for providing the lab space and equipment. Thanks to our collaborators Dr. Juan Prada for writing R-scripts and helping me understand how to use them. Thanks to my colleagues in Botany I for their support and help in research and life.

Thanks to the friends I met in Würzburg. I am so happy to have met them and thanks to enrich my life here. I felt very happy and warm to spend time with them. Thanks to them to encourage and support me.

Thanks so much to my best friends, Yun Zhao and Weiqi Dong. They have been my joy and supporters. I have heard from them every day during my study, sharing the happiness and sadness in each other's lives. One of the lucky things in my life is that I met them. They have given me encouragement and support, and they have grown up with me, so thank you for being there all the time, and the thousands of mountains and rivers have never separated our feelings.

Thank you very much to my boyfriend Ke Yao, with whom I am in love for seven years, including almost four years in a foreign country. We both are very busy, separated by the time lag, normally only talked in a hurry for a while. I remembered for the first year we often had arguments, but the

good thing is that we have been supporting, encouraging and loving each other, to become a better version of ourselves and the future.

There are no words to express my gratitude to my family. I am very grateful to my family for their unconditional love and support. They have told me that they are my eternal backing forever. During the process of growing up, I know my mom and dad have always had a hard time, but they tried their best to never let me worry about things all the time. I am grateful for their deep love, tolerance and support, which made me grow up in happiness. They are my greatest motivation during my doctoral studies. Thanks to my siblings for their support, love and sharing, so that I can live and take care of myself without worries. Thanks for the love my family has given me, I feel very lucky and blessed to be their daughter and their siblings. Thanks for the joy that my little nephew and niece, born during my doctoral studies, have brought me. I love you.

I would like to appreciate the financial support from the China Scholarship Council and DAAD scholarship to support me to finish my PhD study.

22 years of study are coming to an end. I am very grateful for this long journey of study, for the fact that I can explore the path of science, and for my family, teachers and friends who have helped me along the way. I hope I could become a useful person to the society.

Kunkun Li

Written in Würzburg, Germany, September 2021

Education and publications

Education

2017/10-now University of Wuerzburg	Molecular Plant-Physiology and Biophysics	PhD
2014/09-2017/07 Zhejiang University	Horticulture	Master
2010/09-2014/07 Anhui Normal University	Horticulture	Bachelor

Publication lists:

1. Tobacco leaves rapidly detoxify acute salt loads without Ca^{2+}-elevations and transcriptional regulation of the SOS pathway. Dorothea Graus*, Kunkun Li*, Jan M. Rathje, Meiqi Ding, Markus Krischke, Martin J. Müller, M. Rob G. Roelfsema, Sönke Scherzer, Irene Marten, Kai R. Konrad, Rainer Hedrich. (*in preparation*). *, co-first author.
2. Transporter networks can serve plant cells as nutrient sensors and mimic a transceptor-like behaviour. Ingo Dreyer*, Kunkun Li*, Janin Riedelsberger, Rainer Hedrich, Kai Robert Konrad, Erwan Michard. (*submitted*). *, co-first author.
3. An optimized genetically encoded dual reporter for simultaneous ratio imaging of Ca^{2+} and H^{+} reveals new insights into ion signaling in plant. Kunkun Li, Juan Prada, Daniel S. C. Damineli, Anja Liese, Tina Romeis, Thomas Dandekar, Jose A. Feijo, Rainer Hedrich and Kai Robert Konrad. *New phytologist*, 2021, 230: 2292-2310.
4. Effects of Cultivar and Ethanol Disinfection on Aseptic Germination of Loquat (*Eriobotrya japonica*) Seeds. Kunkun Li, Weiqi Dong, Yun Zhao, Hongxia Xu, Junwei Chen, Changjie Xu. *Hortscience*, 2017, 52(7): 941-945.
5. Effects of Fruit Maturity and Storage Conditions on Aseptic Germination of Loquat Seeds. Kunkun Li and Changjie Xu. *Journal of Tropical and Subtropical Botany*, 2017, 44(9): 1633-1644. (in Chinese)
6. Advances in Regeneration and Genetic Transformation of *Rosaceae* Fruit Trees. Kunkun Li and Changjie Xu. *Acta Horticulturae Sinica*. 2017, 25(5): 510-516. (in Chinese)

Declaration of independence

I hereby declare that my thesis entitled: „Dissecting the interconnection of Ca^{2+} and pH signaling in plants with a novel biosensor for dual imaging" is the result of my own work. I did not receive any help or support from commercial consultants. All sources and / or materials applied are listed and specified in the thesis.

Furthermore I verify that the thesis has not been submitted as part of another examination process neither in identical nor in similar form.

Würzburg, den_____

_____

Signature PhD-student